THE EXTRUSION OF ATOMISED POWDERS OF SOME ALUMINIUM ALLOYS

by

PETER JOHN MICHAEL CHARE, B.Sc(Eng), A.R.S.M.

A thesis submitted for the Doctor of Philosophy degree,
London University.

October, 1972

John Percy Research Group
Department of Metallurgy
Imperial College of Science
and Technology
London, S.W.7

ABSTRACT

An extensive research programme has been carried out to investigate the mechanism involved and the effect of the extrusion process variables on the structure, sub structure, and mechanical properties of the extruded product when processing atomised aluminium powders. Powder variables, such as the size and type of aluminium powder particles (commercial Al, Al-Mn, Al-Fe, Al-Mg-Zn) used, have been investigated, together with manufacturing variables, such as temperature of extrusion billet, reduction ratio in extrusion, ram speed, and heat treatment after extrusion. It is demonstrated that the strength and ductility of the product may be controlled by the process variables. Major variables are the size of the aluminium particles, the alloy content, and temperature, and it has been found that the strength increases and the elongation decreases for decreasing size of aluminium particles.

It is also demonstrated that the extrusion pressure is largely independent of the final properties. A mechanism is proposed, using an upper bound analogue, to explain the extrusion mechanism, and the relatively low pressures recorded that agrees with experimental observations.

Cold compaction results obtained indicated that the powders compacted according to equations derived by previous workers.

Hirst and Ursell type limit diagrams have been constructed theoretically, using a theoretical equation, to determine the temperature rise, thus improving the accuracy of the diagram.

The microstructure of the extruded aluminium product has been examined by optical and transmission electron microscopy and the mechanical properties have been determined at room temperature and elevated temperature by tensile testing. Yield strengths have been related to sub grain size, particle size, and oxide fraction using a Petch type equation.

ACKNOWLEDGEMENTS

The author wishes to express his sincere appreciation to Mr. T. E. Sheppard for his constant encouragement, advice, and supervision during the course of this work.

Thanks are due to Alcan International, and to the British Aluminium Company Limited, for the provision of the powders used in the experimental work.

Thanks are also due to Mr. A. J. Haynes, his colleagues, and to the members of the John Percy Research Group, past and present, for many helpful discussions, and without whose help the experimental work would not have been possible.

Grateful acknowledgement is made to the Science Research Council for their financial support.

Finally, the author would like to thank Miss Sharon Long for typing this thesis, and his wife for her constant encouragement and devotion throughout the duration of his research.

CONTENTS

LIST OF FIGURES

CHAPTER 1

Introduction

1.1 Development of dispersion strengthened alloys

Following the discovery of sintered aluminium products of high strength at elevated temperatures, subsequently known as S.A.P., a whole new field was opened up of dispersion hardening. This has since been applied to many other metals for high temperature applications. The development of dispersion strengthened alloys with a more stable phase at elevated temperatures has been primarily, although not exclusively, an accomplishment of powder metallurgy[1,2]. It seems that in order to obtain useful properties from dispersion strengthened materials produced by powder metallurgy, consolidation by hot working, usually extrusion, is essential.

Many materials have been investigated, including lead, tin, silver, copper, nickel, stainless steels, and various refractory metals. The stable oxides such as alumina, silica, magnesia, or thoria usually provide the dispersed phase. In aluminium the dispersed phase, aluminia Al_2O_3, is completely insoluble in the matrix at all temperatures even above the melting point of the latter.

S.A.P. has been produced commercially, the first production by A.I.A.G., Switzerland, and products ranging from 6% Al_2O_3 to 15% Al_2O_3 were fabricated. Problems have been encountered during the mechanical working of the high oxide content material due to its lack of ductility. In an attempt to improve the ductility without losing strength, pre alloyed powders have been hot pressed containing such elements as iron, nickel, and chromium, which form finely divided

intermetallic compounds in the original atomized powder. However, as might be expected, overageing occurs at elevated temperatures of the pre-alloyed powders and improvement is lost.

1.2 Atomized Powders

The advantage of atomizing a pre alloyed material into fine particulate form is that a rapid quench is applied to the material without the use of elaborate casting dies or moulds. Materials, such as Al-Fe, have a very limited solid solubility in aluminium and quenching rapidly from a melt produces extremely finely dispersed precipitates and a super saturated solid solution. The same alloy conventionally cast will result in large primary precipitates in the aluminium matrix, usually present at grain boundaries, producing a very weak and brittle material. Therefore, production by atomization enables a high strength material to be manufactured from an alloy that presents problems during conventional casting. The cost of producing a material using this technique is also competitive compared to casting, heat treatment, and fabrication of an alloy.

Materials, such as Al-Fe, where the iron has a very limited solid solubility in aluminium can be quenched from a melt in a supersaturated form. Conventionally cast Al-Fe alloy will result in large precipitates of $Fe\,Al_3$ in an aluminium matrix, usually at grain boundaries, producing a very weak and brittle material. Intergranular fracture will result during tensile testing. Atomized powders will produce extremely fine dispersed precipitates throughout the material giving it strength in the form of precipitation hardening. Fabrication of the atomized alloys, compared to an equivalent strengthened oxide material, is easier because it has better ductility thus lending itself to some form of plastic deformation.

1.3 Present work

Previous detailed work on the extrusion parameters is lacking, in the literature available, and the scope of the present work was to carry out a detailed analysis of the various extrusion variables on the final product. This analysis has been carried out on two atomized aluminium powders and reported in a published paper[3].

Having completed the first stage of the research programme attention was then turned to the fabrication, by extrusion, of some aluminium alloys produced by atomization. Two of these alloys, Al-4% Mn, and Al-3% Fe, present considerable practical difficulties in casting and fabrication and the aim of the work was to show the feasibility of working these materials. Their strength at room and elevated temperatures and structure were studied as in the preliminary work.

CHAPTER 2

Literature Survey

2.1 Introduction

In powder metallurgy, the extrusion process is often used to produce components, as it easily combines the effects of hot compacting and mechanical working into one operation. After extrusion, the material produced has acquired the properties that are useful for practical purposes, i.e. controlled orientation and dispersion hardening. The density of the end product after extrusion has been found to be dependent upon the temperature of working and reduction in area, and it has been stated that a theoretical density of 99% can be obtained by extrusion at a homologous temperature of 0.67 and a reduction of area, 6:1. However, this statement was further qualified by saying that the reduction of area required to achieve complete densification was a function of the initial density and the plasticity of the powder at the extrusion temperature. Nevertheless a fairly low reduction ratio will be required to give a high theoretical density as the material will experience a very high percentage deformation through a die even of a relatively low reduction ratio.

2.1.1 Historical progress

The first reference to a metal being extruded in powder form was that by Von Wehbach in 1870 who produced osmium filaments by extruding osmium oxide with a sugar syrup binder. The fine threads produced were then fired to carbonize and volatilize the binder, reduce the oxide, and sinter the metal. From this date until the 1940's many ideas for the extrusion of various metallic powders were tried and some patented. A review of the early patents has been carried out by

Jones[6]. An example of an early patent taken out on the extrusion of a sintered metal powder is that of Carl Heinrich Fischer[7] in 1924. He patented a system for extruding sintered powder by pressing the material with a ram so that it passed through a die. The compressed material, as it passed through the die, was simultaneously heated to the sintering temperature to produce a solid part to a required diameter.

Sufficient experience had been gained in the field of powder extrusion by the year 1940 for the Carboloy Company[8], Detroit, to make a serious commercial use of extrusion. Sintered carbide materials in the form of tubing, round or shaped bars, or spirals of various lengths were produced.

Just after the end of the second World War, S.A.P., sintered aluminium products, was accidently discovered during experiments involving the preparation of Al-C extruded wires[9]. The remarkable room temperature properties of extruded aluminium powder were also noted by Von Zeerleder[10] who attributed the increase in strength over conventionally extruded aluminium to small dispersed vacant lattice sites or pores. After the discovery of S.A.P., R Irmann[11-13] then initiated research on the creep resistance and high temperature properties of extruded aluminium powder and this initial interest sparked off a widespread activity in the field of dispersion hardened material. An extensive review of the early work carried out the this field during the 1950's is given in a review by E. A. Block[14] which contains many useful references.

Following this interest in dispersion hardened aluminium, research work has been carried out on a variety of metal powders to produce

high strength materials after extrusion. Examples of the preliminary nature in which the work was carried out can be seen in the reported research on lead[15,16], tin[17,18], magnesium[19-22], copper[4], aluminium alloys[20,23-25], nickel alloys, and stainless steel[26]. In all these papers the work has been of an exploratory nature with the end product as the main consideration thus usually neglecting the details of the extrusion process.

After the initial enthusiasm on the product S.A.P. had subsided, interest was again revived in the possible development of S.A.P. for nuclear applications. This has been carried out by Euratom since 1960 as part of the 'Orgel' reactor project and similar work has also been reported from the Oak Ridge National Laboratory, U.S.A., the Canadian Atomic En ergy Commission, and the Danish Atomic Energy Commission. The most accessible of the published research work is that of the Danish Atomic Energy Commission in papers submitted by N. Hansen. In a report[27] published in 1971 the work carried out and published since 1959 is dealt with in detail and includes details of the extensive bibliography[28] in the field. The research started with the objective to examine whether commercial S.A.P. was applicable as a standard material in the case of an organic coolant reactor, operating at a temperature 400 - 500°C. It has been found that it is acceptable as pressure tubes and canning material.

The recent research programme carried out at the Riso research establishment in Denmark has dealt with the process variables in extrusion in a little more detail than previously reported work, and under more reproducible conditions. However, the most recent published work in the field by Sheppard and Chare[3] considers the variables in greater detail and under satisfactorily reproducible conditions.

2.2 Compaction

The process of compaction is a method usually used before metal powders are consolidated by hot working, the most convenient technique for product of dispersion strengthened materials being hot extrusion.

Cold compaction enables metal powders to be compressed and shaped into a useful form and the billets manufactured will have sufficient strength to facilitate handling. This process has a wide commercial application in shaping metal powders and so has been extensively studied both theoretically and experimentally. A short review of this field is given in the following section.

Hot compaction, when pressure and heat are applied simultaneously, is usually used for large or heavy parts as well as in cases where satisfactory results cannot be obtained by cold compaction and sintering. This process has not been so well developed as the cold pressing field and satisfactory literature is lacking but a review of the relevant literature is given.

2.2.1 Cold Compaction

Many experimental and empirical equations have been proposed and these have been reviewed by Jones[29] and Kawakita[30] in some detail.

The deformation mechanisms of the particles during compaction have been studied in some detail[31,32] and it is now well established that there are the following stages, although often stages (ii) and (iii) occur concurrently.

(i) packing

(ii) elastic and plastic deformation

(iii) cold working with or without deformation

The first small application of load to a die filled with loose powder will cause particles to rearrange themselves to provide better packing. The extent of the re-arrangement depends mainly upon the characteristics of the particles in an open ended compression die. Fine powders, having poor flow properties, are liable to form bridges and the first slight pressure will cause their collapse[33]. Further pressure increase will cause point to point contact and where the oxide films have been broken cold welding takes place. Increasing the pressure further will increase the contact areas and individual particle deformation at contact points[34].

The compaction phenomenon has been well documented but a rigorous theoretical analysis has proved difficult. Empirical formulae have often been proposed after a detailed observation of the relationship between pressure and volume.

One of the earliest equations proposed, relating density and pressure was that by Athy[35].

$$C_{10} P = \ln n_o^* - \ln n^* \qquad (2.1)$$

n_o^* = initial porosity

n^* = porosity at applied pressure, P.

The equation was fitted to data on the density of sedimentary rocks at various depths. The results, however, showed a considerable scatter and it is doubtful if there was any justification in choosing this particular equation to fit the experimental data.

In a relationship between the pressure and the relative volume

of the compact Bal'shin[36] found that:

$$\ln P = -LV + C_{11} \qquad (2.2)$$

P is the applied pressure

V is the relative volume of the compact

L is a constant described as the modulus of pressing

C is a constant

The argument for the relationship was based on an elastic analogy with Hookes' Law which cannot possibly be valid. The equation was found to be applicable over a limited range, but is relatively insensitive to variations in pressure values at high ranges of pressures.

In more recent well documented work, Heckel[37,38] proposed a density pressure relationship in powder compaction similar to that of Athy. Experimental results confirmed the relationship derived theoretically. The compaction of powders was considered to be analogous to a first order chemical reaction with the pores being the reactant so that the ratio of change in density with change in pressure was proportional to pore fraction. The equation was derived in terms of relative density that can easily be changed to a particular pore fraction and was of the form:

$$\ln \left(\frac{1}{1 - D}\right) = C_{12} P + \ln \left(1/1 - D_o\right) \qquad (2.3)$$

where D_o is the relative apparent density of the powder. Deviations from linearity of the plot of $\ln (1/1-D)$ against pressure were attributed to inter particle motion, i.e. packing or rearrangement of particles.

The most recent empirical equation has been proposed by Kawakita[39] based upon observations of the volume change with pressure. The following piston compression equation was derived:

$$C^* = \frac{Vo - V}{Vo} = \frac{ab\,P}{1 + bP}$$

$$\text{or } \frac{P}{C^*} = \frac{1}{ab} + \frac{P}{a} \qquad (2.4)$$

where C^* = degree of volume reduction

Vo = initial apparent volume

V = powder volume under applied pressure

a,b = constants

The linear relationship between P/C^* and P allowed constants a and b to be evaluated graphically, deviations from linearity at low pressures were again attributed to the rearrangement of packing of particles. This equation was found[30] to have a wide application in the field of compaction and Kawakita[30] examined the validity of this and various other equations with respect to the porosity n^*. For zero pressure the value of n should be n_o, the initial porosity, and for infinite pressure the value of n should be zero. In the equations considered only those of Athy and Kawakita were valid. From the above it can also be seen that Heckels' equation would also be valid. Therefore, it can be seen that the experimental equations, such as Bal'shin although not really valid over the whole range of pressure do have some practical value over a limited range.

2.2.2 Hot Compaction

The theoretical treatment of hot pressing is still relatively new and the older research work was aimed at the attainment of high density products. A review of the subject of hot pressing and theories presented has been carried out by Ramqvist[40] and to a lesser extent by Thummler and Thomma[41] in their review of the sintering process.

The theories of hot pressing have been derived theoretically and

empirically of the form:

$$\frac{dQ}{dt} = -\frac{3}{4} P \frac{Q}{\eta} \qquad (2.5)$$

Q = porosity

t = time

P = applied pressure

η = viscosity

This equation was derived theoretically by Murray, Rodgers, and Williams[42] from the Shuttleworth and MacKenzie[43] theory of sintering and verified by studies on refractory oxides. The sintering theory of Shuttleworth and MacKenzie, is based upon hydrostatic pressure on spherical pores and this pressure decays with increasing distance from the pore. The pressure leads to viscous or plastic flow under the action of surface tension. For free sintering, the action of surface tension alone is not sufficient to exceed the yield point, however, the theory used in conjunction with an applied pressure produces creditable results.

A similar equation has been found by Kovalchenko and Samsonov[44] using a rheological method according to the continuum theory of the elastic, plastic, and viscous behaviour of the solid bodies and their dispersions in each other.

Equation (2.5) has been satisfactorily confirmed by work on alumina by Mangsen, Lambertson and Best[45], and Vasilos[46].

A correction to equation (2.5) was given by Kovalchenko and

Samsonov, that took into account grain growth. The Nabarro-Herring mechanism was used, that connects the viscosity coefficient with the diffusion coefficient, Dv, and the grain size, d. The viscosity has the relationship:

$$= \frac{k^* T d^2}{10 Dv Vo} \qquad (2.6)$$

k^* = Boltzmann's constant

d = average grain diameter

Dv = coefficient of self diffusion

Vo = atomic volume

in which grain size, d, increases with time; of the form

$$d^2 = do^2 (1 + C_{13} t) \qquad (2.6a)$$

The pressure can then be written in the form:

$$P = Po (1 + C_{13} t)^{-k'\sigma} \qquad (2.7)$$

where $k' = \frac{15}{2} \frac{Dv Vo}{d.^2 k^* T C_{13}}$ (2.7a)

This equation is considered to be applicable where the pores are few in number and the density is approaching the theoretical density.

Deviations from the equations formulated were attributed by McClelland[47] to three different stages

(i) densification by re-ordering of powder particles

(ii) Densification by plastic flow according to equation (2.5)

(iii) Diffusion controlled approach to limiting density by Nabarro-Herring mechanism

Empirical relationships have been obtained[40] which show a trend towards a hyperbolic equation for the densification process with respect

to time and can be connected to the previous theories. However, differences found, suggest complex mechanisms for hot pressing similar to those suggested by McClelland.

Garber and Polyakov[48] performed experiments to study the resistance to tearing of massive aluminium blocks pressed together at 300 to 600°C and found that the initial increase in strength was controlled by plastic deformation.

There is no doubt from the experimental work, that hot pressing takes place by plastic deformation in the first stages of densification. Under the temperature and pressure employed in practice, and when the 'supporting cross section' in the porous compacts is considered, the yield strength is easily exceeded in the material and plastic deformation takes place. The later stages are, however, dominated by the diffusion processes probably in accordance with the Nabarro-Herring mechanism. The first stage, controlled by plastic deformation, is more rapid than the later slow one by diffusion processes.

2.3 Conventional Extrusion

2.3.1 Introduction

Extrusion is the process by which a block of metal is reduced in cross section by forcing it to flow through a die orifice under high pressure. The practical advantages and details of the process have been reviewed by several authors[49-52], but no really satisfactory theory of extrusion has been presented. Estimation of the forces and deformation existing during extrusion, is difficult due to the axially symmetrical rather than plane strain conditions present. However, as a very precise specification of the forces is unnecessary, a simplified solution can be used, usually a plane strain limitation,

which is sufficient to enable the extrusion pressure to be predicted.

To determine the behaviour of the deforming metal during extrusion, an exact theory would be required that includes both macroscopic and microscopic metallurgical effects. Alexander[53] described some of the problems involved in deriving a theory of extrusion that must be overcome to establish a complete theory. He came to the conclusion that an exact theoretical treatment was virtually impossible. This is not surprising as the extrusion process has not been studied as extensively as other mechanical working processes, for example rolling and forging, and the present state of knowledge is based mainly upon practical observations.

2.3.2 Flow stress determination

There are several methods for calculating the flow stress from the load recorded during extrusion using both empirical and theoretical formulae.

For plane strain conditions, square dies, and direct extrusion, empirical formulae generally take the form[54]:

$$\frac{P}{Y_m} = A + B \ln R + C_{14}\, l \qquad (2.8)$$

where A is the redundant deformation

R is the reduction ratio

$C_{14}\, l$ is the frictional term for billet length l

B, C_{14} are constants

Y_m is the mean yield stress of the material

To overcome the need for estimating the frictional term, formulae have been derived for inverted extrusion, so that:

$$\frac{P}{\bar{Y}m} = A + B \ln R \qquad (2.9)$$

These formulae only compensate for the variation of the yield stress in the material during extrusion by the use of a mean yield stress. To estimate the degree of work hardening Dodeja and Johnson[55] used the fact that the extrusion pressure equals the work done per unit volume, this is also given by the product of stress and strain. Thus the stress operating is the same as that acting in plane strain compression and the value A + BlnR is regarded as the effective strain. Values of A and B were then determined from work on lead extruded at room temperature so that it could be assumed that the rate of recovery equalled the rate of work hardening. The equations obtained were:

$$\frac{P}{\bar{Y}m} = 0.8 + 1.5 \ln R \qquad (2.10)$$

(for extrusion through square dies with a graphite and tallow lubricant)
P, the pressure, was taken as the pressure at the coring point which is equivalent to the pressure in inverted extrusion for identical conditions

$$\frac{P}{\bar{Y}m} = 0.6 + 1.8 \ln R \qquad (2.11)$$

(for extrusion through square dies without lubrication)
Wilcox and Whitton[56] assumed that A and B were dependent upon the frictional force on the die surface, resovled in the direction of the applied load, and therefore should be a function of the die angle, ϕ. They derived an empirical equation for inverted extrusion for die angles from 30° to 90° and for extrusion ratios from 5:1 to 150:1.

$$\frac{P}{\bar{Y}m} = (0.9 - 1.6 \cot\phi) + (1.5 + 0.8 \cot\phi)\ln R \qquad (2.12)$$

The yield stress values were obtained from uni-axial compression tests using a mean strain rate for the reduction ratio considered, and corresponding to the mean natural strain imparted to the extrusion,

measured by ln R. However, the yield stress values obtained by this method will not be the same as that for extrusion, as the temperature rise during uni-axial deformation will be different. The restraint conditions imposed by the container and die for extrusion compared to those of compression will give rise to a different deformation flow for the same strain and therefore different temperature rises.

The formulae derived for inverted extrusion, apply only to flow of type A[49] whereas flow of lubricated direct extrusion has been found to be of type B[49]. In the formula derived by Wilcox and Whitton, the value of α can be regarded as the angle formed by the dead metal zone, i.e. the deformation zone cone angle.

Hirst and Ursell[57] using Johnsons[58] equation for the extrusion pressure

$$\frac{P}{\bar{Y}m} = 0.47 + 1.2 \ln R \qquad (2.13)$$

modified it to allow for the frictional effect of larger billets and obtained:

$$\frac{P}{\bar{Y}m} = (0.47 + 1.2 \ln R) \exp \frac{4\mu l}{Dc} \qquad (2.14)$$

Hirst and Ursell in fact considered extrusion of tubes so that instead of Dc, Dc-d was considered where d was the diameter of the mandrel. The correction factor for container wall friction was derived by considering a cylindrical element of the billet and the forces acting at equilibrium upon it. Upon integration the frictional force was determined as the initial ram pressure required on the billet. It was assumed that the pressure acting in any plane, distance l from the die face, was hydrostatic and the boundary condition at l = 0, i.e. at the die face, was that $\frac{P}{\bar{Y}m} = 0.47 + 1.2 \ln R$ (2.15)

Wilcox and Whitton[56] also considered the effect of friction on extrusion pressure, but dismissed the effect as negligible, provided the coefficient of friction on the die face was small ($\mu < 0.05$). If the value of μ was greater than 0.05 the extrusion pressure was multiplied by a factor $(1/1-4\frac{\mu l}{Dc})$ so that:

$$P_L = P(1/1 - 4\mu l/Dc) \qquad (2.16)$$

where P is the maximum inverted extrusion pressure
and P_L the maximum direct extrusion pressure
This analysis assumed hydrostatic conditions existed throughout the billet. If the pressure dependence on friction is compared to the analysis by Hirst and Ursell, there is a smaller dependence on friction at high values of μ than the Hirst and Ursell relationship would predict.

The value of μ, the coefficient of friction, was shown by Hirst and Ursell to be determined from two extrusions using two billets of upset lengths l_1 and l_2 with the same process variables and conditions. The two pressures corresponding to billet lengths l_1 and l_2 were then used in the equation form below to give a value for μ.

$$\mu = \frac{0.575\ Dc}{l_1 - l_2} \log_{10} \left(\frac{Pl_1}{Pl_2}\right) \qquad (2.17)$$

Similarly the value of μ can be determined by comparing loads at different points on one autographic diagram.

The values of the coefficient friction will, however, be dependent upon the frictional conditions at the container billet interface which vary with temperature and ram speed, thus influencing the flow stress at the interface. Therefore care must be used in the

determination of the value μ to ensure fairly uniform frictional conditions for comparison of different extrusions.

2.3.3 Theoretical background

The theoretical approaches for the estimation of the extrusion process are

(i) The slip-line field solution[61]

(ii) The upper bound solution[62,63]

The slip line field solution is the more rigorous of the two solutions and if the slip line pattern is known, the stress and velocity equation can be readily applied in determining the pressure and direction of flow. A slip line field solution satisfies both stress and velocity equations and solutions and well established for steady state extrusion through symmetrically placed single hole dies. It has been shown by Dodeja and Johnson[55], that extrusion pressures estimated in plane strain correspond closely to those in axial symmetry, so a theory does exist although it is empirical being based mainly on experiments.

The second solution considered is based upon the principle that the material being extruded is assumed to consist of a number of rigid parallelpiped blocks of uniform quasi static zones. Their zones, of unit thickness normal to the plane of the paper, are bordered by straight line velocity discontinuities and are built up around the deformation zone. This is the upper bound solution. It is possible to construct the solutions without comparison with slip line field and provide a method towards finding good approximate solutions. The over estimation to the load required to perform an extrusion is only

around 20% for the most basic fields and more sophisticated solutions give loads equal to those given by corresponding slip line field[64].

2.3.4 Extrusion process

The direct extrusion process can be divided into three principal phases[59,60]

(i) the coining phase

(ii) the steady state

(iii) the unsteady state

The first phase, called the coining phase, is the upsetting period when there is a rapid pressure build up so that the billet is forced to exactly fill the container. There is only a small amount of extrusion of relatively unstrained material during this period.

The steady state phase usually commences at the point of maximum load and continues until the type of deformation is changed. As the ram moves over this range, extrusion proceeds steadily, and the total load decreases as the frictional load due to the relative motion of billet and container wall is decreasing.

The unsteady state phase occurs after a certain point when the deformation zone changes due to the close proximity of the ram to the die. Beyond a certain point, the extrusion load decreases fairly rapidly; this point is called the coning point and is due to the back-end extrusion defect. Continued extrusion beyond the coring point increases the size of the defect and as the original billet decreases in length to almost nothing, the load rapidly increases.

The transition from steady to post steady state has been found fairly difficult to pin point. Johnson and Kudo[62,64] found that the transition point was dependent on reduction ratio and the frictional conditions between the billet and the tooling. Several combinations of frictional conditions for the container, die, and ram were investigated and it was found that the post steady stage commenced as soon as the rough ram face touched the bottom of the steadily deforming zone. However, with a smooth ram face the transition occurred before contact with the deforming zone.

2.3.5 Limit diagrams

The limit of an extrusion occurs when either the load required to extrude a material at a certain temperature, reduction ratio, and strain rate exceeds the capacity of the press or the temperature of the extruded rod passing through the die exceeds the solidus temperature of the material.

Hirst and Ursell[57] were the first workers in the extrusion field to consider the limits of extrusion on a particular press and used their equation (2.14) for hot lubricated extrusion. They produced a useful limit diagram (fig. 2.1) to represent the extrusion variable R, the reduction ratio, as a function of pre heat temperature of the billet. The range of extrusion conditions was then bounded by two lines; one, the constant pressure line, and the other, the incipient melting condition. The incipient melting condition was then dependent upon the extrusion rate and degree of adiabatic conditions.

To the right hand side of the diagram is included the isothemal condition, for extremely slow extrusion, when the heat of deformation is dissipated without raising the billet temperature. This line can

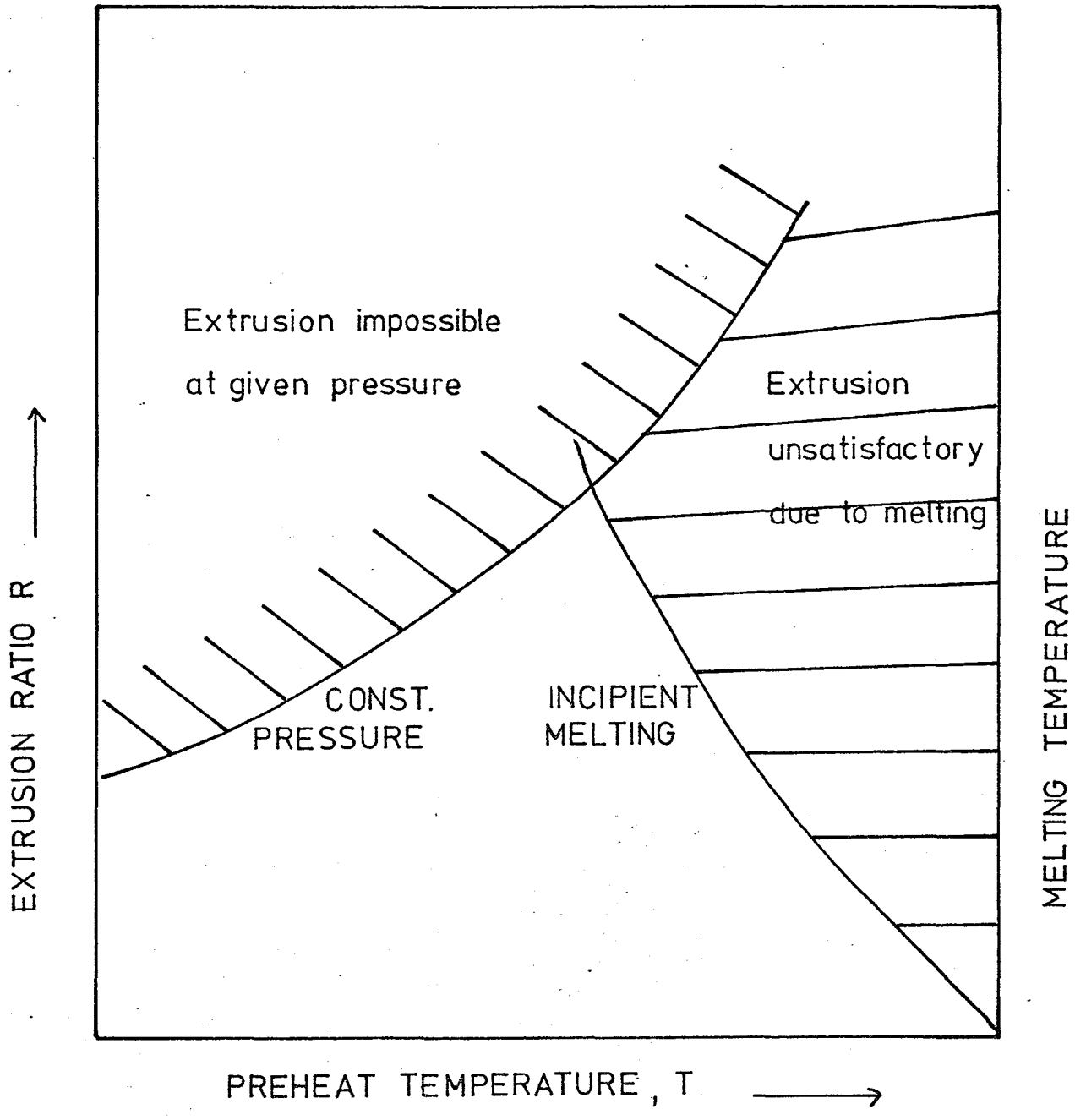

FIG: 2.1 HIRST-URSELL LIMIT DIAGRAM

be drawn through either the melting point of the material or the solidus temperature of the alloy. For very high strain rates, the condition is adiabatic, all the heat of deformation goes into the billet and raises its temperature thus requiring a lower pre-heat temperature for an increased reduction ratio. For practical strain rates the incipient melting line lies between the two extremes mentioned.

The limit imposed by adiabatic extrusion was calculated using the equation

$$\ln R = \frac{(Tm - T)\rho C_H}{4.43\ Ym\ (1-2\frac{\mu l}{Dc})} - 0.39 \qquad (2.18)$$

This gave the maximum reduction ratio for a particular initial pre-heat temperature.

The values of Ym, the mean yield stress, for the maximum load determination were obtained from cam plastometer work where the initial temperature was the same as for extrusion. The values of Ym to avoid hot shortness were the mean yield stress values of the initial and final temperatures involved. However, both methods of determining Ym are in error due to the variation of yield stress during extrusion caused by temperature rise which will not be the same on the cam plastometer at the same initial temperature and strain rate. Strain rate is another factor not considered in great detail, the authors took the yield stress values at an arbitrary strain rate value of 30 sec^{-1} and assumed an infinitely fast strain rate for their melting line.

Although the diagram produced represented only a very simple picture of limiting conditions, it was the first attempt to describe

the process in technological terms. The theoretically developed limit curves were compared with experimental results from extrusion of an aluminium alloy BSL64 using an unspecified ram speed.

Ashcroft and Lawson[65] produced a similar diagram for an Al-Zn-Mg-Cu alloy based on experimental determinations on one ram speed. There again arises the limitation that the work applies to the particular alloy investigated and the extrusion press used.

In order to provide results that could be universally applicable, Meadows and Cutler[66], in work on Al-Mg-Si alloy, derived an improved method for the determination of the limit diagram using as a basis equation (2.14). To determine the incipient melting line, the temperature rise was predicated using a modification of Singers[67] equation to include the effect of ram speed. The equation then used to calculate the limit of incipient melting was of the form:

$$\ln R = \frac{F\,(Tm - T)\rho C_H}{4.43\ Ym\ (1 + 2\frac{\mu 1}{Dc})} - 0.39 \qquad (2.19)$$

where $$F = 1 + \frac{\alpha_1 kal}{(\rho_{AL} \cdot C_{AL} \cdot S)^2 Ao} + \frac{\alpha_2}{(\rho_{St.} \cdot C_{St} \cdot S)} \qquad (2.19a)$$

The rate of heat flow was time dependent and values of α_1 and α_2 representing the heat loss to the container and die, were graphically determined.

The value of the mean yield stress was determined from cam plastometer work using an equation that included the effects of strain rate, temperature, and reduction ratio but whether the value calculated can be used for the extrusion process is doubtful.

In more recent work by Raybould[68] limit diagrams were constructed for super pure aluminium and an Al-Zn-Mg alloy. In this work the temperature rise was considered using a model based upon the integral profile technique. The mean yield stress was then determined using the upper bound solution to find the flow stress at the initial temperature, final temperature, and deformation temperature during steady rate extrusion. The limiting reduction ratios were calculated using an empirically adjusted form of the Hirst and Ursell equation. The logarithmic value of the reduction ratio was plotted against both the initial billet temperature and deformation temperature and the load limit line was constructed for different strain rates for both temperatures considered. Strain rate effects had not previously been considered for the load limit side of the diagram. It was found that the limit diagram of log R against deformation temperature showed that decreased strain rate was beneficial to the load limit line. In comparison decreased strain rate was slightly detrimental to the load line when initial temperatures were considered; i.e. the maximum value of reduction ratio was reduced with decreasing strain rate. This latter effect was explained by the fact that once the load started to reduce the ram speed extrusion became impossible. However, this is not strictly true as the ram speed is always reduced on the application of the initial load and increases again until steady state deformation occurs; steady ram speed is usually observed over this region.

The constructed limit diagrams were also used in conjunction with final structure results, i.e. recovered, or recrystallised and single or two phase products. He considered the Al-Zn-Mg alloy which has a high susceptibility to stress corrosion especially with the presence of a second phase at the grain boundaries. The onset of

recrystallisation was thought to be as important as the start of hot shortness. Recrystallisation was shown to occur below a certain z, Zener Holloman value, dependent upon the type of cooling after extrusion, and so for a particular strain rate a recrystallisation temperature was determined. This type of diagram would be considered useful if a second phase or recrystallised structure was to be avoided knowing the particular strain rate and temperature.

The limit diagrams constructed in the past have been rather limited in nature as no account has been taken of strain rate during extrusion and the yield stress values estimated from cam plastometer results. The yield stress results do not give good agreement because of the variable strain rate of the extrusion process. The exception to these criticisms is the work by Raybould who calculated the yield stress from upper bound theory. Prediction of temperature rise during extrusion is the main difference in the work carried out by previous investigators and its dependence on strain rate has been found difficult to estimate accurately. Raybould used his own theory and experimental results to predict the rise.

2.3.6 Structure

Previous work on the extrusion of aluminium and its alloys has shown that the products are recrystallised, partially recrystallised, or non recrystallised. The non recrystallised structures have received considerable attention as they were produced by hot working above the normal recrystallisation temperature and yet had the appearance of a cold worked structure. The structures have been found not to recrystallise on further annealing. In 1944, Hardy[69], using optical microscopy, discovered that the inside of the fibrous grains were again further sub divided into sub grains. Jonas et al[70], with the

aid of an electron microscope, proved the existence of these sub grains in much later work, and found that the sub grains with dislocation walls of low orientation increased in size and internal perfection as the temperature of extrusion was increased. The sub grain formation was suggested to be the result of concurrent action of the externally applied shear stress and temperature on the dislocations, which increase the mobility of dislocations and thus the recovery rate.

The recrystallised and non recrystallised microstructures represent the end products of two different softening processes, i.e. dynamic recovery and recrystallisation.

The process of recovery during hot working results in a polygonised structure, composed of sub grains. During deformation dislocation tangles formed by combination of forest and glide dislocations arrange themselves into cells by the mobility of dislocations. This process is similar to polygonisation during annealing where dislocations rearrange themselves by glide, cross glide, and climb under stress fields of dislocation tangles. The cells formed become sub grains as dislocations move to walls and the walls change to less dense and regular networks. The configuration is then a stable low energy configuration and sub grains increase in size by coalescence.

This process of dynamic recovery is found in metals of high stacking fault energy where the dislocations are not extended and if partial dislocations are formed they are only about one atom wide. At the temperatures and strain rates experienced in extrusion, the ability of climb and cross slip is activated by stress as well as temperature. Experimental verification of the importance of stacking

fault energy on recovery has been determined by Swann[71] and Tegart[72].

It has also been shown by Li[73] and Hu[74] that recrystallised grains can be nucleated by the growth of sub grains to form stable high angle boundaries.

Recrystallisation has been sub divided by Stuwe[75] into three types depending upon relative time of initiation. They are

(a) after deformation before metal cooled to room temperature

(b) during deformation by recovery process (in situ recrystallisation)

(c) recrystallisation during deformation.

Type (b) is that proposed by Li[73] and Hu[74]. Type (c) is often called dynamic recrystallisation and the possibility of its occurrence during hot deformation has been argued by Jonas et al[76,77]. Doubt as to the likelihood of this process occurring still remains as highly mobile boundaries are required to form recrystallised structures and the presence of any small impurities will be sufficient to restrict the motion.

2.3.7 Deformation mode

Various theories have been proposed based upon dynamic recovery particularly for the creep range of strain rates. The models have the common characteristic that the activation enthal py is the same as that for self diffusion and differences arise in the terms comprising the structure factor and activation volume. The following equation was derived by Jonas et al[76] from rate theory:

$$\dot{\varepsilon} = \phi_f \exp\left(\frac{v\tau}{k^*T}\right) \exp\left(-\frac{\Delta H_o}{k^*T}\right) \qquad (2.20)$$

ϕ_f - structure factor

ΔH_o - activation enthal py

τ - shear stress

υ - activation volume

(volume swept out by dislocation as it moves from one metactable position to another)

The three models that the theories are based upon are

(a) Jogged screw dislocation

(b) Climb

(c) Network

The jogged screw dislocation model, has been shown to be consistent for creep at low strain rates and its applicability to high strain rate deformation in the hot working range has only been qualitatively shown by Jonas[77]. The jog is formed when a screw dislocation does not lie in a slip plane and the application of a shear stress will move the screw dislocation, while the jog maintains its position on the dislocation by leaving a trail of vacancies behind. The value of the stress will depend on the vacancy concentration and its affect on the jog. Alloying is difficult to assess and its effect is overcome by the use of a rather unsatisfactory back stress factor.

A theory of steady state creep has been presented by Barrett and Nix[140] based on the diffusion controlled motion of jogged screw dislocations. Steady state creep is assumed to exist when the chemical force on the jogs is balanced by the force on the dislocation due to the applied stress and the expression found is:

$$\dot{\varepsilon} = 2\pi\rho_s D_v x' \left(\frac{b}{a_o}\right)^3 \sinh\left(\frac{\sigma b^2 \lambda'}{2k^*T}\right) \qquad (2.21)$$

where ρ_s is mobile screw dislocation density, D_v the self diffusion coefficient, x' the number of atoms per unit cell, a_o the lattice parameter, λ' is the average spacing between jogs. Experimental results showed that

$$\rho_s = C_9 \sigma^3 \tag{2.21a}$$

The equation (2.21) bears some resemblance to Garofalo's empirical equation for creep.

The main criticism to this model is common to models that have the strain rate relationship of the form

$$\dot{\epsilon} = \rho_d b \bar{v} = \rho_d b f(\sigma, T) \tag{2.21b}$$

where ρ_d is the mobile dislocation density, and $\bar{v}$ is the average dislocation velocity. Specimen of increasing ρ_d at a given temperature, then subjected to an equal stress, should show higher initial strain rates for specimens with higher initial density. Experimentally, the opposite dependence is observed[141].

To explain the power stress dependence observed at low stresses, models have been proposed dependent upon the rate at which edge dislocations climb. In theories proposed by Weertman[78,79] the model is highly idealised and therefore cannot be expected to fit closely to experimental data over a wide range of conditions. The effect of alloying can only be allowed for by a stress concentration factor, another unsatisfactory factor.

The steady state creep model proposed by Weertman[78,79] assumes that the dislocation sources are distributed throughout the material and by the action of an applied shear stress, their sources emit loops. The loops expand until they are blocked from further expansion by the stress fields of loops on parallel slip planes.

Steady state creep is assumed to be controlled by the rate at which the piled up dislocation segments are able to climb out of the slip plane. The following relationship has been proposed:

$$K' = \frac{C_{15}\,\sigma^{4.5}\,Dv}{b^{\frac{1}{2}}\,M^{\frac{1}{2}}\,\mu^{3.5}\,k^{*}T} \qquad (2.22)$$

where C_{15} is a constant, σ is the applied stress, Dv is the self diffusion coefficient, b is the Burgers vector, M is the dislocation source density, μ is the shear modulus.

Objections to this model have been raised because the predicted sub structure is not generally seen in metals that have undergone creep strain[83].

The steady state creep of solid solution alloys has also been treated by Weertman[79] and the original model was modified by replacing the self diffusion coefficient by the chemical diffusivity $\tilde{D}$, given by:

$$\tilde{D} = \frac{D_A\,D_B}{C_B\,D_A + C_A\,D_B} \qquad (2.22a)$$

where D_A is the diffusivity of component A and C_A its concentration. At higher solute concentrations, the rate controlling process of viscous dislocation glide rather than dislocation climb was proposed and this led to the following relationship:

$$K' = \frac{\sigma^3\,b^2}{\mu\,\bar{A}\,\bar{B}} \qquad (2.23)$$

where $\overline{B}$ is equal to $b^2/2\ (1-\nu)$ and $\overline{A}$ is a constant dependent upon the particular viscous drag mechanism.

Thus the creep models of Weertman suggest that the stress dependence of steady state creep in single phase solid solution of Al-Mg or Al-Cu should decrease from a value of 4.5 for pure aluminium to 3 for concentrated alloys.

The network model was proposed by McLean[80] who argued that the sub grains or grains were filled with a regular three dimensional dislocation network. Their presence forces moving dislocations to form junctions and the portion of the dislocations not pinned bow out under the applied stress and thus decrease the size of the network. The growth of the network during recovery involves the climb of edge dislocations and migration of jogs along the dislocation so that recovery rate depends upon the diffusion coefficient.

The effect of alloying addition on the dislocation network has been dealt with by McLean[81]. There is anticipated a dislocation network anchored by particles of a dispersed phase so that a slip plane can intersect both network and particles. Consequently, the particles are not the only barriers to slip. Results of this theory are partly experimental so are applicable to one set of conditions.

The theories mentioned have all been proposed for creep results and their application to high strain rates must be difficult due to the increased scale of activity of the dislocations and vacancies.

2.4 Z parameter

Zener and Holloman[82] showed that for creep,

$$\sigma \propto Z \quad \text{where} \quad Z = f(\dot{\varepsilon})$$

$$Z = \dot{\varepsilon}\, e^{\Delta Q/RT} \tag{2.24}$$

The value of ΔQ, the activation energy for plastic deformation, was found to be the same as the energy for self diffusion. Garofalo[83] found the equations for creep could be divided into two main relationships.

$$\dot{\varepsilon} = A_2 \sigma^{n_1} \qquad \text{at low stress values}$$

and $\dot{\varepsilon} = A_3 \exp(B\sigma)$ at high stress values

these could be replaced by

$$\dot{\varepsilon} = A_4 (\sinh \alpha\sigma)^n \tag{2.25}$$

The constants A_2, A_3, A_4 apply to a particular temperature and the parameter $\alpha = \beta/n$

Sellars and Mc G. Tegart[84] combined the above equations to obtain an empirical relationship valid for torsion.

$$\dot{\varepsilon} = F^* (\sinh \alpha\sigma)^n \exp^{-\Delta Q/RT} \tag{2.26}$$

F^*, α, and n are independent of temperature and strain rate, ΔQ the activation energy. The equation has been shown to be valid for hot extrusion of aluminium[77].

2.5 Powder extrusions

The different methods for the extrusion of metals that have been tried can be listed thus:

(a) fill extrusion container with loose powder and extrude

(b) cold compact, then extrude

(c) cold compact, sinter, then extrude

(d) cold compact, sinter, hot press, extrude

(e) cold press in a can, extrude the canned material

(f) isostatic compaction, can, hot extrusion

The method for extruding low melting point metal powders has nearly always included the cold pressing of the powder to give a compact that can easily be handled. For the higher melting point temperature metals, the canning method has been used to facilitate handling at elevated temperatures.

The use of a can and its deformation characteristics compared to that of the consolidated powder has been well discussed by Williams, who concluded that for the best results the deformation characteristics of the can and consolidated material should be as close as possible. The main disadvantage in using a canning method is the lack of uniformity after extrusion and the machining operation required to remove the extruded can. However, the main advantages of the canning method override this. The can protects the consolidated material from oxidation at elevated temperatures and acts as a lubricant, reducing the effect of friction, during the extrusion of the material. An example of the advantage of canning on the effect of friction is that reported by Chadwick[85]. A. Von Zeerleder[10] had reported a specific pressure of 1,080 MNm^{-2} for extruding an aluminium powder compact at a ratio of 15:1 and temperature 500-600°C. In a British Patent this pressure was reported to be reduced to 540 MNm^{-2} if the cylindrical compacts were wrapped in aluminium strip, as the aluminium strip acted as a lubricant during extrusion.

The extrusion of metal powders has concentrated mainly on pure metals although some preliminary work has been carried out on alloy powders. Previous work[24,25] to combine the oxide dispersion strengthening and precipitation hardening, has proved fairly inconclusive as the strength due to the precipitate phase is lost when the products are exposed at elevated temperatures. There has

been no evidence found of an inter action between solute elements and the dispersed particles. The effect of alloying additions on the corrosion resistance of S.A.P. has been considered. Elements such as iron and nickel, or silicon, nickel, and titanium[86], have been added but results, although promising, were only indicative as the products were manufactured on a small scale.

2.6 Powder extrusion variables

The variables involved in the extrusion process for powders, in previous work, have not been considered in any great detail. Only Hansen[87], in work concerning the extrusion of powder blended products, covered the variables in any detail and some of these only superficially. The variable of ram speed was not considered at all. He considered the variables in two distinct groups, those concerning the product, and those concerning the process. Using these two groups the variables will be divided and considered in some detail separately.

The process variables can be separated thus:

(a) temperature of extrusion billet

(b) reduction ratio in extrusion

(c) ram speed, i.e. strain rate

(d) heat treatment of extruded products

The product variables considered are

(a) size of powder particles

(b) alloy powder type

The separation of the variables is not easy, as each variable must be considered in terms of the others, e.g. temperature of the billet with reduction ratio and speed.

In early work by Cole[20] the factor of ram speed was considered with temperature and found to be closely related. Smooth extrusions were found to be produced at any speed provided that the initial billet temperature exceeded a particular temperature. For the particular material considered, this was in contradiction to the solid billet material where the defect of hot shortness would have been experienced under the same conditions.

2.6.1 Initial billet temperature

In most of the work reported, a temperature is usually quoted as the initial billet temperature which could easily be that of the furnace pre-heat temperature. The temperature measurement technique is not often mentioned and one must take the temperature quoted as the pre-heat temperature. However, in most of the earlier work reported, the temperature was important only in so much that it facilitated hot working and enabled extrusion to be performed on a particular press. This criterion led to a range of temperature values being quoted in which the extrusion was carried out. The effect of temperature of billet on final properties was not investigated in any great detail.

In early work on magnesium powder, Brown[19] reported obtaining good extrusions at temperatures as low as 300°C, using a speed of 50.8 mm/sec, and as high as 450°C, using a speed of 508 mm/sec. With increasing temperature and speed, it was found that the tensile properties of the product improved; this is contrary to subsequent work. The results cannot be satisfactorily explained as the powder was cold pressed, sintered, and hot pressed resulting in a dense billet prior to extrusion. However, the tensile test results quoted were based on one test only so some doubt can be cast upon the

published results.

Also working with magnesium powders Cole[20] obtained smooth extrusions of good mechanical properties at low extrusion speeds provided the initial billet temperature exceeded 470°C. The reduction ratio used was 25:1, and the ram speed varied from 0.015 to 0.905 mm/sec. In relating his work to that of Brown[19], Cole suggested that good extrusions were feasible provided a certain speed was used. The reason proposed was that there was sufficient heat generated at high speeds to raise the temperature at the die beyond the minimum satisfactory temperature. Experience in conventional extrusion of magnesium is contrary to this; a cast billet experiences hot shortness if the temperature exceeds about 420°C. However, no satisfactory explanation has been given to explain this enigma and as if to emphasise the difference between solid and powder, R. Biais[89] found no difficulty in extruding magnesium granules at 500°C through a 30:1 die, 330 mm/sec.

Research on aluminium powder in its various forms has been extensive and extrusion usually carried out in the range of 500°C after initial hot pressing. The temperature used for working has been high to enable the material to be worked easily and thus the load required for deformation within the capacity of the press. There has been little work on the effect of billet temperature on the extrusion process and the work reported is lacking in detail.

Schwartzwelder[88] reported the results of extruding large aluminium powder compacts using a commercial extrusion press to prove the feasibility of performing powder extrusions on a large scale. The billets were of two sizes: 276 mm in diameter, approx. 550 mm long,

and 517 mm in diameter, approx. 550 mm long. Low compact temperatures were again found to be detrimental to surface finish and overcome by increasing the speed. Temperatures as low as 410°C, with a ram speed of 28 mm/sec, were used but temperatures quoted in this paper must be regarded with some caution. Billets for extrusion were transferred from a nearby furnace and the subsequent drop in temperature considered to be less than 30°C. Conditions of the press and furnace would be such that exact measurement of billet temperature would be impossible and the figures quoted regarded as rough approximations.

In more detailed controlled experimental work, Hansen[87] showed the effect of extrusion billet temperature on the microstructure and tensile properties of the product in terms of sub grain size. It was shown that a decrease in the initial billet temperature of the compacted aluminium powder reduced the sub grain size, and by reducing the sub grain size the tensile strength was increased at the expense of ductility. The presence of a sub structure had been revealed in a previous paper[86] and its effect on tensile strength shown in the form of a Petch type equation. High temperature tensile tests performed at 400°C revealed little dependence of the product on the initial billet temperature, indicating that the matrix sub structure was ineffective at that temperature. Two temperatures were considered; 500°C and 300°C, and an external speed of extrusion of 8.35 mm/sec was used. There are no details of the extrusion press so the validity of the 500°C temperature is in some doubt as this could be the pre-heat temperature. The micrographs shown in the paper reveal high angle sub grain boundaries with little evidence of recrystallisation, but this would not necessarily be a product of a lower temperature than 500°C. However, this does not detract from the results of sub grain size dependence on temperature, and the tensile strength

properties in terms of a Petch type sub grain size equation.

Unfortunately the reported work on this variable is very sketchy and a thorough appraisal has not been carried out. However it has been found that, in connection with surface finish, the parameter of temperature is closely allied to the speed of extrusion. In more recent work the matrix sub structure of the extruded product has been found to be similar to that of worked commercially pure aluminium. The subsequent measurements of the sub grain size have shown a dependence on temperature and the size on the product strength at room temperature.

2.6.2 Reduction ratio

The main criterion for selecting a particular ratio has been to ensure sufficient working to produce a dense product and not exceed the capacity of the press. Several investigators have examined the effect of reduction ratio on the extruded products, but the results were inconclusive.

The only analysis of loads obtained from differing reduction ratios has been that by Schwartzwelder[88], who found a linear relationship between the maximum pressure and the natural logarithm of extrusion ratio. In a preliminary report[3] of the present work, a similar relationship to that of Schwartzwelder was found between pressure and reduction ratio.

The results of Schwartzwelder's[88] work show that up to a reduction of about 15:1 both strength and ductility are increased, but at higher reductions the variations are scattered. It would seem that up to 15:1 the product has been insufficiently worked so that the density

of the product is not quite the theoretical and pores from the original compact were still present in the product. Variations of the properties above the 15:1 ratio are within experimental error, involved in extrusion, especially on the massive scale it was carried out with all the accompanying inaccuracies. The results do indicate, however, that at high reduction ratios the longitudinal tensile properties improve due to the better degree of dispersion of the oxide within the matrix.

This last observation has been confirmed by Nilsson, who measured the transverse properties of an extruded S.A.P. type alloy. There was an increase in strength and uniform elongation with increasing reduction in area. The results shown in graphical form hide the errors and reveal quite a wide scatter. Some of the specimens for the higher reductions were produced by transverse extrusion and swaging to re align the structure. These further deformation processes must to some extent invalidate the results as the position from which results were compared was not specified and it is well known that the tensile properties of the product vary along the extruded length[49].

Eastwood and Robins[17,18] discovered that the tensile strength and elongation of the products from extruded tin powder, decreased at room temperature and 150°C for reductions of 80:1 when compared to those of 20:1 and 40:1. The results of the tensile properties of the 20:1 and 40:1 ratios showed little variation. This decrease was not explained.

Dispersion strengthened aluminium products manufactured by powder blending, as reported by Hansen, showed that increasing the reduction ratio had little effect, if any, on the tensile properties of the product. It was noted that the sub grain size stayed the same but with

increasing reduction ratio there was a slightly more uniform distribution of the oxide phase. Although only two ratios were used, 15:1 and 75:1, the work by Hansen was generally found to be reliable so the results can be viewed with a certain amount of confidence.

Included in the reported work of Euratorm are the results[91] of the effect of reduction ratio on the product of S.A.P. 7 and 10 wt pct. Al_2O_3. It was found that only elongation was influenced; with increasing reduction ratio the elongation at room temperature and 400°C increased slightly.

Looking at the various reported papers, it can be seen that a rather confusing picture emerges as to the effect of reduction ratio on the product properties. It seems, however, that increasing the extent of reduction improves the distribution of the oxide.

2.6.3 Extrusion speed

As discussed previously under section 2.6.1, the variables of temperature and speed were found to be closely related when considering the production of a smooth extrusion. Cole[20] has also shown that for a high temperature, a greater increase in speed is required for a given increase in pressure when compared to an extrusion of a conventional solid billet. The explanation given for this phenomenon was that a high proportion of the work was required to break up the oxide film and once broken the material was easily deformed. This reason has not been questioned as little documented work on the subject exists. However, in the more recent work by Sheppard and Chare[3], the powder material was also found to exhibit small strain rate dependence, smaller than that of the solid billet. This indicated that the powder behaved in a different manner from the solid during deformation through

and into the die. During the process of extrusion, as the material approaches the die, there is extensive particle sliding and increase of the areaof particulate contact by welding and rewelding of the contact. There is not full intimate contact between the particles until the material emerges through into the die so that the process of deformation occurs over a smaller area than expected while in the container. This will lead to a lower strain rate dependence.

The tensile properties of the product seem little affected by the speed of extrusion.

2.6.4 Heat treatment

The effect of heat treatment on the subsequent room temperature properties of an extruded product is a softening process. Observation of electron micrographs, as did Hansen[87], show that the sub grain size slightly increase by heat treatment at an elevated temperature thus decreasing the tensile strength accordingly.

The oxide distribution in the extruded product can be more uniformily distributed by cold work and recrystallisation or by double extrusion. Recrystallisation reduces the tensile strength whereas double extrusion was found to have little effect on the tensile properties. Dromsky and Lenel[92] produced a coarse grained structure of a product manufactured from atomised powder (2 - 4 μm in diameter) by cold rolling at least 70 pct. and annealing 2 hours at 540°C. This reduced the yield stress from 113.5 MNm^{-2} to 92 MNm^{-2} and the grains were elongated in the direction of rolling. Flake powders above a certain percentage oxide, were unsuccessfully cold worked and annealed. Similar results had been previously reported on alloys containing 1.75 and 3.0 pct. Al_2O_3 by weight[93]. It was also noted in this earlier

work that these alloys preferentially recrystallise at the centres of the cold worked rod and the new grains grow most readily in the direction of cold working.

A detailed analysis of the recovery phenomena of S.A.P. has been carried out by Nobili and his co workers.[149-151] They showed that there was no fundamental difference between S.A.P. and pure aluminium except that recovery could occur over a wide temperature range due to increase of recrystallisation temperature. It was also found in the research programme that there was no recrystallisation up to 360°C.

2.6.5 Powder particle size

This parameter can be easily measured by a variety of techniques, the most popular and easiest being that of sieving. Usually the compacted billets used in powder extrusions are of a known particle size distribution, e.g. Shakespere and Oliver[26] used compacts of particle size distribution varying in the range from - 60 mesh to - 300 mesh. However, some workers have separated the metal powder particles into various separate sieve mesh fractions which cover a range of sizes from minus one sieve to plus the next sieve size. This allows a relatively good determination for a mean size value.

During extrusion the load required to extrude the billet can be recorded with suitable instrumentation and the values obtained compared. Lenel et al[94] noted that the load varied according to the powder used; the conditions for extrusion, temperature 540°C, reduction ratio 16:1, speed 31.8 - 42.3 mm/sec, being the same for all extrusions. The load recorded for a 25.4 mm diameter billet of the thinnest flake powder, (0.17 μ in thickness with 12 wt pct oxide), was 400 KN decreasing to 100 KN for a coarse atomised powder billet,

(178 μ average diameter with 0.2 wt pct. oxide). These are figures quoted from the experimental section of the paper and their accuracy can be questioned but the trend is obvious.

In a preliminary investigation Roberts[15] observed a dependence of tensile strength on powder particle size in extruded atomised lead powder alloys.

More detailed work, on atomised tin powders, has been carried out by Eastwood and Robins[17,18] who separated the powder in the range from 53 to 8 μm into sieve fractions. The extruded product consisted of an extremely fine grain sized microstructure with the oxide from the particles visible as banded stringers. Room temperature tensile strength was found to increase with decreasing powder particle size and this increase was accompanied by a marked reduction in ductility. Although no measurements were taken of grain size, it was noted that the grain size of the extruded material decreased with decreasing particle size, a factor that is of some importance considering the tensile properties. This last observation was confirmed by Hansen[95,96], who did measure the sub grain size of extruded atomised aluminium powders of varying particle sizes. The sub grain size was observed to decrease from 3.2 μm for the coarse powder (average particle diameter 110 μ) to 1.6 μm for the finest powder (average particle diameter 8 μ). The measurements of sub grain size were based on a large number of measurements with a standard deviation estimated at less than 10 pct. In this work it was also noted that as the powder particle size decreased the oxide agglomerates decreased as the surface area increased. The tensile strength was increased with decreasing aluminium particle size but the tensile elongation at room temperature was practically unaffected, whereas at 400°C a decrease was observed. However, it

should be noted that in the preliminary report on this work[86] only a few tensile test results were reported, and in subsequent papers[95,96] the elongation values were not quoted therefore comparison was difficult.

Previous work on aluminium powder, concentrated upon the flake type powder, showed that the tensile strength of the product was related to the flake thickness[99,97,98]. This was shown by a linear relationship between tensile strength and logarithmic value of flake thickness[99], measured from electron micrographs. The ductility of the extruded specimen tested at room temperature and 400°C was found to decrease rapidly with decrease flake thickness of powder. The oxide content was noted to only affect the mechanical properties if it was related to particle size. Similarly, Wiseman et al[100] found that a relationship existed between the reciprocal square root of aluminium flake and yield strength and that the weight of oxide was not as important as flake thickness. Thus the tensile and yield strength depended on flake thickness and particle size which can be related to oxide content in the extruded product.

Included in the work by Hansen[87] is an equation based upon the Petch equation to relate yield stress with particle size. It is of the form and found valid at room temperature and 400°C.

$$\sigma = \sigma_o + C_{18}\, dp^{-\frac{1}{2}} \qquad (2.27)$$

dp is the diameter of the aluminium powder particles

σ is the yield stress

σ_o is the yield stress of a coarse grained aluminium (99.5% purity)

This equation has been confirmed in the preliminary report of this

research[3] using a larger number of results.

2.6.6 Alloy powder type

To improve the properties of powder products, alloying has been tried to combine dispersion strengthening and precipitation hardening. Reasonably good results have been obtained with iron and nickel[24] as additions up to about 300°C, but at higher temperatures the strength is less than conventional S.A.P. due to the loss of the precipitated phase. There was found no interaction between the solute atoms and dispersed phase, so increasing the temperature will coarsen the precipitated structure and le en the yield strength. However, room temperature tensile strength is greater than pure aluminium powder due to the appreciable fine precipitation hardening within the particles. Decreasing the size of the atomised powder particles increases the strength of the extruded product due to the decreasing dendrite size, because of the greater cooling and solidification.

Production of aluminium powder metallurgy parts has been considered by Dudas and Dean[101] on a commercial scale in which precipitation hardened alloys were discussed. This is not a detailed paper and must be regarded as a technological feasibility study rather than a piece of research. The paper concludes that powder metallurgy aluminium alloys can be produced in useful components using the presses available and the strength enhanced by sintering and heat treatment.

More detailed work on pre alloyed powders has been carried out on aluminium-silicon[102] and aluminium-tin[103]. The hypereutectic aluminium silicon casting alloy was investigated, becuase of its use in the motor industry, and atomised to refine the primary phase. Results were few in number and little detail was given of the fabrication

technique but the results presented did show a refined structure and useful tensile properties. The same criticisms apply to the work on aluminium-tin in which a total of six experiments were performed.

Details of the effect of adding copper on the strength of sintered aluminium copper alloys have been studied in some detail by two Japanese workers[104]. They found that using a mixed powder had advantage over a pre alloyed aluminium copper alloy. In the green compact using mixed powders, the aluminium and copper powders have metallic contact through the fractured oxide layer and upon sintering alloy starts at this point. Above the eutectic temperature the alloy becomes liquid and forms a large quantity of liquid phase in which the oxide is scattered. This will result in an increase in the strength of the compact. Further sintering will disperse the copper atoms by diffusion into the aluminium matrix to form a solid solution alloy. However, no details are given of the final strength of the product so it is difficult to judge the advantages of one method over the other, i.e. pre-alloying over mixed powder or vice versa. It would be unwise to take too much notice of this work at present as the results are far from convincing and few in number.

2.6.7 Extruded structure

In powder extrusions, the extrusion process works the material through a die and the particles become coalesced into a solid form. This was first shown in work on electrolytic copper by Stout[105] and Tynowski[106]. The particles were found to coalesce, not just to adhere to one another, so that the grain boundaries separating the particles no longer existed as clear cut dividing lines.

Metallographic examination of extruded bars from metal powders

has revealed a fine structure with the oxide present as banded stringers[17,18,26]. Due to this fine structure, electron microscopy has had to be used to enable a more thorough investigation. An extruded specimen of aluminium powder or S.A.P. type alloy shows no significant microstructural detail upon examination by conventional optical techniques, but the lines of extrusion flow can be seen in a deeply etched longitudinal section[99]. For a more detailed look, electron microscopy is required and there is considerable amount of literature concerning the extruded structure. The product S.A.P. has been subjected to many theoretical and experimental analysis with results that supported the dispersion hardening theory as seen in the review by Bloch[14].

The production of S.A.P. depends upon the oxide film present on the flakes of aluminium or the addition of an oxide in the form of powder blended with the aluminium powder[107]. In the case of flake powder, the oxide film is about 100A° thick and during grinding the oxide content is increased by partial welding and exposure of new surfaces to the atmosphere. During extrusion the oxide particles become aligned in the extrusion direction and often the distribution of them is non uniform. The extruded condition of the oxide has been reported as platelets[108] and estimated to be 50-100A° thick. Having identified the structure form it was then found that these platelets were partially or completely spheroidized[86,99] depending on the method of preparation. In some detailed microscopy work using carbon replicas, Dromsky and Lenel[92], reported a non uniform dispersion of oxide particles segregated near grain boundaries and suggested that these particles were fragments of the original oxide film on the powder particles that acted to restrict grain boundary movement. It was also put forward that the parallel oxide particle platelets retain the shape

of the oxide coating and that vacuum sintering caused the break up of the oxide. This break up was confirmed by Goodrich and Ansell[109] who found irregular oxide platelets strung out along grain boundaries. The size and distribution of the oxide particles was found to depend upon the initial powders and the degree of deformation.

In more recent work by Hansen[86,87,110,111] using transmission electron microscopy, showed that the aluminium particles deformed into cylindrical shapes during extrusion with the oxide phase being distributed as agglomerates of varying size along the aluminium cylinders. Close examination of the extruded product, revealed smaller sub grains with few dislocations in the interior formed during extrusion similar to the deformation of pure aluminium at elevated temperatures by extrusion[70]. The sub grains were thought to be formed by the effect of high temperature and large plastic strain during extrusion. It was then shown[86,87] that the matrix sub structure contributed largeley to the strength at room temperature by comparing as extruded and recrystallised products from the same material. The sub grain boundaries formed by high temperature extrusion were as effective as slip barriers at room temperature as grain boundaries formed by recrystallisation. The hard particles of oxide were found to be distributed throughout the metal matrix and did not directly govern the sub grain boundaries[95]. Dislocation density between the sub grain boundaries was low, but found to be higher around the dispersed phase particles where they were pinned[112]. The strengthening factor of the material was thought to be the energy of the structure which depended on the interfacial relationship between the oxide and matrix phase. In the case of aluminium and alumina, there was a favourable relationship between the oxide and matrix to form a stable alloy.

The more recent extensively reported work by Hansen is the most reliable on the microstructure of aluminium powder products. The results can be viewed with some confidence although often lacking in number. Interest was concentrated on the dispersion strengthening properties and relation of tensile test results to microstructural details, sub grain size and oxide dispersion.

There has been a school of thought[113-115] that has considered the distribution of alumina within the aluminium matrix as a continuous, inter penetrating, and three dimensional cell network. The experiments carried out to prove the existence of a honeycomb structure of alumina have been based on the dissolution of the aluminium matrix to leave a thin skeleton of alumina. It is, in fact, difficult to conceive how a honeycomb structure could exist after the process of extrusion and the results presented are far from convincing. The action of the dissolving agent on the remaining alumina was not investigated so this gives rise to the speculation that during the dissolution of aluminium precipitation could occur on the original oxide leaving a skeleton behind. The existence of a continuous cell-like structure is difficult to prove using transmission electron microscopy, as very thin specimens are required. However, Hansen[87] did find a cell pattern of oxide particles in a transverse section for very fine powder particles but the uniformity in the longitudinal section was such that a regular continuous network was unlikely.

The formation of a solid solution and precipitation from it, is also a strengthening mechanism for a metal and the combination of this with dispersion hardening has been tried by Towner[24] and more recently by Jones and Thursfield[116-118]. Towner prepared a solid solution alloy by extruding pre alloyed aluminium powders, Al-8%Fe.

The extruded product was found to have superior strength and structure stability in the temperature range 200-400°C. The Al-Fe powders were found to have an internal structure of a supersaturated solid solution containing a fine inter dendritic network of intermediate phases. During the hot deformation of the powder in extrusion, the oxide was dispersed and the insoluble elements in the supersaturated solid solution were precipitated. The precipitate was fine and uniformly distributed and increasing the extrusion temperature 450-500°C resulted in a slight coarsening of the precipitates.

Jones and Thursfield have been concerned with a splat cooled Al-8%Fe alloy having a higher strength than powders produced by atomisation. Results for a high strength room temperature material, unable to be produced by conventional means, are promising but large scale use seems limited.

2.7 Mechanical Properties

Products made from atomised aluminium powder in which the dispersion strengthening constituent is the alumina present on the surface of the original powder, show a distinct improvement in mechanical properties as compared with cast and wrought material. The strength at room temperature is higher than for extruded pure aluminium and at 400°C is more marked. With increasing oxide content of the aluminium powder, the tensile strength increases at room and elevated temperatures until the oxide content reaches 10-13%[14]. Correspondingly the elongation decreases with increasing oxide content.

The dependence of tensile strength on powder particle size for atomised powder alloys has been observed by Eastwood and Robins[17,18], Roberts[15], and Hansen[87]. The room temperature strength was increased

with decreasing powder particle size and with this increase there was a marked reduction in ductility. For the tin powder work by Eastwood and Robins, the fine fraction, -8μm, had an elongation of 6% compared with 30% for the coarse fraction, -52 + 30 μm particle size. However, increasing the oxide content without changing the particle size had little effect on the properties.

A similar dependence on powder particle size has been found by Hansen[87], who proposed a relationship based on the Petch relation. Yield strength was equated to particle size both at room temperature and 400°C values of the former.

$$\sigma = \sigma_o + C_{19}\, dp^{-\frac{1}{2}} \qquad (2.28)$$

Values of σ_o were obtained by extrapolation of lines on the plot of yield stress against reciprocal square root of particle diameter; these were found to agree with the flow stress values of coarse grained pure aluminium at room temperature and 400°C.

In an earlier paper, Hansen[86] showed the effect of matrix substructure on the mechanical properties by comparing extruded and recrystallised materials. Flow stress was found to be:

$$\sigma\ (\text{extruded}) = \sigma\ (\text{recrystallised}) + C_{20}\ (de^{-\frac{1}{2}} - dr^{-\frac{1}{2}}) \qquad (2.29)$$

where de and dr are the extruded and the recrystallised grain size. This was found to be valid for products containing up to 1wt% oxide but for larger oxide contents the cold work required to effect recrystallisation redistributes the oxide, forming a stronger structure on recrystallisation, thus not corresponding to the equation.

The powder alloys of aluminium investigated by Towner[24] contained up to 7.6% of iron which gave the extruded product yield strength values comparable to an S.A.P. alloy up to about 300°C; above this temperature they were slightly lower. The greatest difference of these alloys with respect to S.A.P. alloys is the trend of elongation, which, for the atomised alloys increases with rising temperature, whereas it decreases for S.A.P.

2.8 Dispersion Hardened Theories

There is a general lack of agreement as to the precise nature of the dislocation particle interaction during deformation of a dispersion hardened metal, despite the widespread application of dispersion hardening.

Empirical relationships have been suggested[119] to relate the mean free path between particles and the yield strength. However, to identify the particle/dislocation interaction, the quantitive theories of Orowan[120] and Ansell and Lenel[121] have received considerable attention.

The yield strength in a precipitation hardened alloy is determined by the stress required to bow out dislocations between precipitates, and is given by the Orowan relationship.

$$\tau = \tau_s + \frac{2T'}{b\lambda} \qquad (2.30)$$

where τ = flow stress; τ_s = yield strength of the matrix; T' = line tension of the dislocation; b = Burgess vector of the dislocation; λ = mean planar spacing of particles on the slip plane. The relevant value of T' in the Orowan equation must be the line tension of a

dislocation in the shape of a semi-circular loop. This problem has not yet been treated exactly. Kelly and Nicholson[122] have suggested a good approximation of the value of T';

$$T' = \frac{Gb^2}{4} \theta^* \ln \frac{\lambda}{2b} \qquad (2.31)$$

where $\theta^* = \frac{1}{2}\left(1 + \frac{1}{1-V}\right)$ is an averaging term for screw and edge dislocations and G = shear modulus.

Ansell and Lenel[121] devised a model for yielding in dispersion hardened material based on the accumulation of dislocations at the dispersed particles. According to this model, yielding occurs when the shear stress due to the pile up of dislocations is sufficient to deform the particles plastically or to fracture them, thus reducing the back pressure on the dislocation sources. They proposed a relationship.

$$\tau = \tau_s + C_{21} \lambda^{-\frac{1}{2}} \qquad (2.32)$$

However considerable objections have been raised on theoretical grounds by Kelly and Nicholson and there has been no conclusive evidence that particles are sheared at the yield point.

In both the models proposed, the particles are considered to be spherical, non coherent with the matrix, and uniformly distributed, no consideration being given to particle shape. To test the equations (2.30, 2.32), annealed single crystals or polycrystals of constant grain size should be used.

Fisher, Hart, and Pry[123] proposed a theory to account for the

variation with strain of the increment of flow stress of dispersion hardened crystals over that of the precipitate free matrix. This increment was attributed to the accumulation of dislocation loops left around the particles by a repeated Orowan mechanism. The possibility of cross slip of the moving dislocations was neglected and the increase in flow stress was expressed in terms of a back stress imposed on glide dislocations by the loops around the particles. The main defect of this theory is the back stress which is thought to affect the Frank-Read sources in the slip plane. These Frank-Read sources are considered to determine the matrix flow stress. The back stress exerted by the loops is given by

$$\tau_h = C_{22} f^{3/2} \frac{NGb}{r} \qquad (2.33)$$

where C_{22} = constant; f = volume fraction of second phase; N = number of dislocation loops; G = shear modulus; b = Burgers vector of dislocations forming the loops; r = radius of second phase particles.

Experimental electron microscopy observations of dispersion hardened alloys show that, on deformation, the dislocation particle interactions are quite complex and tangles of dislocations form as cells in the vicinity of the particles. Thus the dispersed phase has a controlling influence on the dislocation sub structure resulting in much larger dislocation densities for a given strain.

Another flow stress theory has been proposed by Ashby[124] assuming that the increment in stress caused by the particles in a metal is due to an increased number of dislocation loops impeding the movement of glide dislocations. A relationship between the tensile

flow stress and strain can be derived, e.g. assuming forest hardening mechanism, and the following equation obtained.

$$\sigma - \sigma_{oy} = C_{23}\, G \quad \frac{2bf\varepsilon}{da} \tag{2.34}$$

where C_{23} is a constant; ε is the tensile strain; f the volume fraction of particle of diameter da, in the slip plane. Experimental evidence to support the model was provided from work on the Al-Cu, Cu-Al_2O_3, and Cu-SiO_2 systems.

More recently in the work by Hansen[128] the strengthening of aluminium was considered to be by a three dimensional network of aluminium-oxide particles. Considering the transverse section the oxide was seen as a mesh network and the proof stress proposed as a function of the mesh size, tm.

$$\sigma = \sigma_0 + C_{24}\, tm^{-\frac{1}{2}} \tag{2.35}$$

This equation is similar to that proposed by Ansell. Results were presented to agree with the equation, but there was little theoretical background to back this model.

In a later paper on the same work, the results were found to agree with Ashby's[129] equation. This equation was based on the Orowan model and written:

$$\tau = \tau_o + C_{25} \frac{Gb}{2\pi} \frac{1}{D_{Af}} \ln \left(\frac{D_{Af}}{b}\right) \tag{2.36}$$

where D_{Af} is the planar surface spacing (free distance between particles)

G is the shear modulus, and C_{25} is constant = 1 for edge dislocations and $1/1-\gamma$ for screw dislocations. Correction for particle and matrix strain hardening was considered in terms of dislocation density and a fairly good correlation was found.

2.9 Creep Behaviour

Ansell and Weertman[125] investigated the creep behaviour of a dispersion strengthened aluminium material. The as-extruded alloy showed an approximately steady state creep which, with constant temperature, depended exponentially on the applied stress, following a creep equation of the type

$$\text{Creep rate} = K' = C_{15} \exp \frac{(C_{16}\sigma)}{k^* T} \qquad (2.37)$$

k^* is Boltzmann's constant, T is the absolute temperature, σ = stress. The temperature dependence of the creep rate was expressed in the form $\exp(-Q/kT)$ where a value of 150 Kcals/mole was found for the activation energy Q. Creep equations were derived for dispersion hardened, coarse grained alloys assuming that the rate controlling process for steady state creep was the climb of dislocations over second phase particles. At intermediate stresses a fourth power stress dependence was found and at high stress an exponential stress dependence. The deviation of the creep rate equations assumed that there was either a three dimensional dislocation network present, or short dislocation segments extended from one plate to a neighbouring plate to act as dislocation sources. The main effect of the fine dispersion was to inactivate the dislocation sources rather than to hinder movement of dislocation.

Ansell and Lenel[126] examined the creep behaviour of a recrystallised S.A.P. type alloy, and under stresses $> 2\mu^* b/\lambda$ (λ = distance between dispersed particles, μ^* = shear modulus), the steady state creep rate K was given by an equation:

$$K' = C_{17} \exp\left(-\frac{Q'}{k^*T}\right) \frac{\sigma^4}{\mu^{*3} k^* T} \qquad (2.38)$$

Q = activation energy of self diffusion.

The rate controlling process for steady state creep was regarded as the climb of dislocation loops rather than single dislocations. It was concluded that in the particular S.A.P. type alloy investigated, the usual three dimensional dislocation network was not present and the activation energy for creep was in good agreement with that of self diffusion in aluminium. Experimental creep behaviour of other dispersion strengthened alloys have shown large deviations from the predictions of this model.

Reynolds et al[127] found agreement with the model by Ansell and the activation energy the same as that for self diffusion of aluminium. Recrystallised dispersion strengthened solid solutions were found to have stress and temperature sensitivities quite unlike those observed in single phase solid solutions having the same composition and grain size. The alloys exhibited essentially a 4.0 power stress exponent in agreement with the model of Ansell and Weertman.

2.10 *Summary of present knowledge*

There has been a considerable amount of literature concerning the structure, mechanical properties, and creep properties of S.A.P. which has led to the idea of finely dispersed aluminium oxide particles within an aluminium matrix. With improving electron microscopy

techniques and understanding of dislocations, the S.A.P. structure was seen in terms of the dispersed phase particles pinning dislocations. Attempts to correlate particle spacing in terms of yield strength have only been partially successful as the results only showed qualitative agreement.

The interaction of dislocations with the dispersed particles is still not fully understood although it is acknowledged that the particles hinder dislocation movement or nucleation.

In more recent work, using the electron microscope, the presence of a matrix substructure as well as the dispersed phase structure, has been shown by Hansen. The room temperature strength of the extruded product is an additive combination of the sub grain structure and the oxide strengthening; at elevated temperatures, oxide strengthening alone is of importance.

The interaction between dispersion strengthening and precipitation hardening has not been investigated to the same extent as the particle interaction problem with the matrix. The little reported work in this field does show an improvement in strength of a product if the two mechanisms are superimposed. However, the effects were not additive as annealing the material for a long period overaged the specimen. Room temperature properties were improved; an equivalent strengthened S.A.P. type alloy did not have as much ductility and thus was not as easily cold worked.

The effect of the extrusion process variables on the extruded product has only been dealt with in a very superficial manner and the results obtained often contradictory. The important variables have

been found to be particle size, temperature, and alloy type, and to a lesser extent, reduction ratio, speed of extrusion, and heat treatment of extruded products. Reduction in area during extrusion is the process variable that has shown the most unpredictable results on the mechanical properties of the extruded products.

CHAPTER 3

Theory

3.1 Introduction

At the moment no exact solution for the estimation of load during extrusion is available and thus methods have been developed to establish values for the load. One of these methods is an over estimate (an upper bound), the other an underestimate (lower bound). Upper bound solutions are particularly useful as they enable an estimate of a particular load, to perform a particular operation. The solution give loads in excess of those predicted by using slip-line fields[61]; but in many cases these are only little in excess. Slip-line field solutions are, generally, themselves upper bounds[130] but their success in many instances, when compared against experimental results, indicate that they are near the truth. However, to obtain these solutions, careful analysis of the slip-line field and lengthy numerical procedures must be carried out.

Both slip-line field and upper bound solutions are based on the plane strain limitation. This is not the case in practise, for with a round billet axially symmetric rather than plane-strain conditions occur, thus precluding the use of slip-line field theory. A solution to the problem is the development of a large number of solutions to plane-strain or sheet extrusion by Hill[61]. The round container is imagined to be replaced by a rectangular container of infinite wid th and the extruded product being an infinitely wide sheet. On the basis of many experiments Dodeja and Johnson[55] have shown that the extrusion pressures estimated in plane-strain correspond closely to those in axial symmetry, for the same reduction in cross-sectional area. The

condition of plane-strain is then approached in practice as two of the stresses in the triaxial state of the axi-symmetric process tend to counteract themselves.

3.2 The Upper Bound Theorem

3.2.1 Assumptions

The main theoretical assumptions made in deriving the solution are:-

(i) the material is rigid perfectly plastic and non strain hardening

(ii) frictional conditions and other boundary conditions remain the same during plastic deformation

(iii) plane-strain conditions exist

3.2.2 'Upper Bound' Expression

This is obtained from consideration of any velocity distribution that satisfies both the velocity boundary conditions and the condition for incompressibility of the material. In other words the main concern is with strain increments and the conditions they have to fulfil in a fully plastic body[131].

The expression is derived by considering a body of volume V and total surface area S. On this body let the surface stresses T_i be specified over part of the surface, S_T, and let the displacement increment, du_i, be specified over the portion of the surface Su. Any other different or assumed field let the displacement increment be denoted by du_i^* such that $du_i^* = du_i$ on Su, i.e. du_i is prescribed over the part of the boundary Su. Both fields are required to fulfil the incompressibility equation, i.e. $\partial u_i^*/\partial x_i = 0$ and $\partial u_i/\partial x_i = 0$. This condition enables a decision to be made on whether the assumed

field is valid or not; if it is valid, it is possible to find the displacement increments at each point in the field.

Considering the body, shown in fig. 3.1, a discontinuity line is indicated with a surface S_D^*. A kinematically admissible displacement increment field may have discontinuities in the tangential component along certain surfaces S_D, but to avoid plastic volume change the normal components must be the same on either side of such a surface.

$d\varepsilon^*_{ij}$ denotes the assumed plastic strain increment for the displacement field du_i^*.

Applying the principle of virtual work to the kinematically admissible displacement increment field and the actual stress field, σ_{ij}, provides the equation:-

$$\int_S T_i du_i dS = \int_V \sigma_{ij} d\varepsilon^*_{ij} \, dV + \sum \int_{SD} q \left| dV^* \right| dS_{D^*} \qquad (3.1)$$

where dv^* denotes the tangential displacement discontinuity increment on the surface S_D^* and q is the shear stress component of σ_{ij} in the direction indicated in fig. 3.1. For a stress field, σ_{ij}, not necessarily statically admissible, derived using the idea of plastic potential from the strain increment field $d\varepsilon^*_{ij}$,

$$\int_V (\sigma_{ij}^* - \sigma_{ij}) \, d\varepsilon^*_{ij} \, dV \geq 0 \qquad (3.2)$$

dV is volume element

σ_{ij}^* denotes a stress field that satisfies the equilibrium equation $\partial\sigma_{ij}^* / \partial_{xi} = 0$

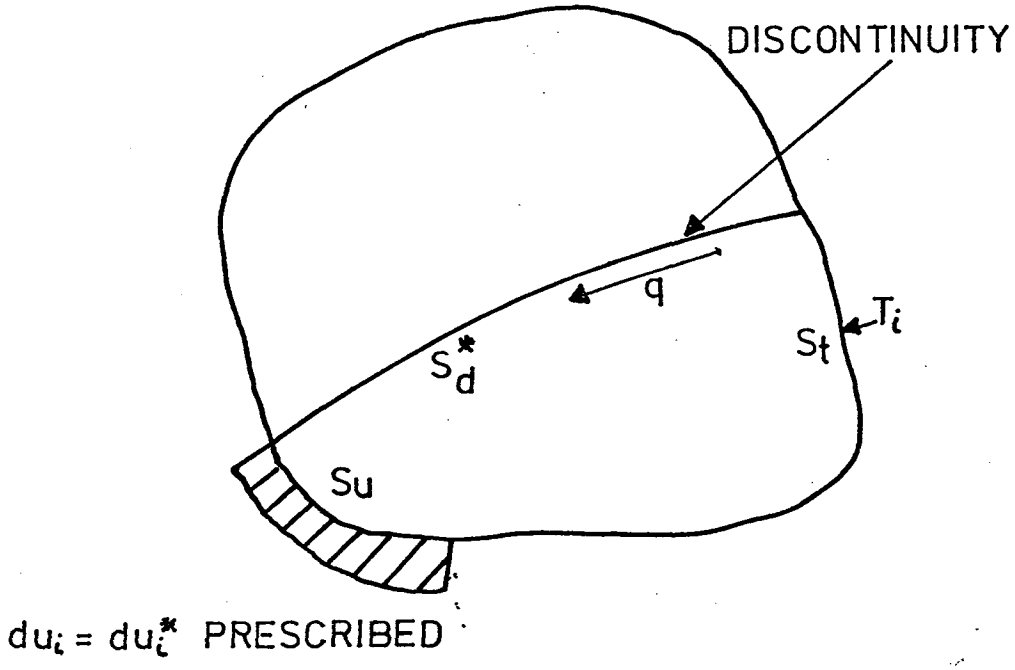

FIG. 3.1 Definition of terms

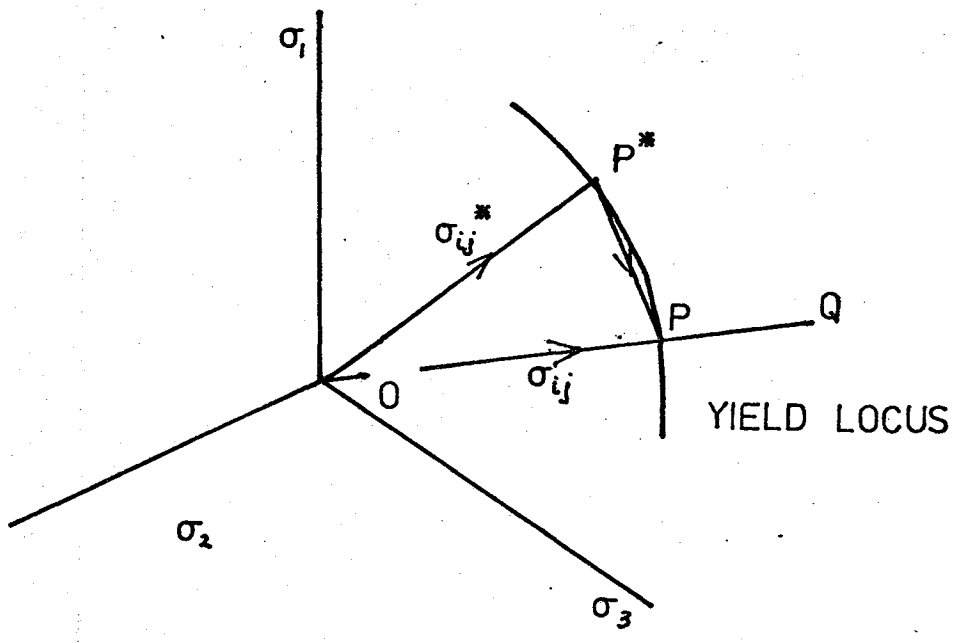

FIG. 3.2

Substituting equation (3.2) into (3.1) given:-

$$\int_S T_i du_i dS \leqslant \int_V \sigma_{ij}^* \; d\varepsilon^*_{ij} \; dV + \sum \int_{SD} k/dV^* / dS^*_D \qquad (3.3)$$

as $k > q$ Now

$$\int_S T_i du_i^* \; dS = \int_{S_u} T_i du_i dS_u + \int_{ST} T_i du_i^* \; dS_T \qquad (3.4)$$

and thus,

$$\int_{Su} T_i du_i \; dSu \leqslant \int_v \sigma_{ij}^* \; d\varepsilon_{ij}^* \; dV + \sum \int_{SD} k/dv^* / dS_D^* - \int_{ST} T_i du_i^* \; dS_T \qquad (3.5)$$

The right hand side of equation (3.5) gives an upper bound for the increment of work of the unknown surface stresses acting on Su.

Considering plane strain conditions in place of

$$\int_v \sigma_{ij}^* \; d\varepsilon^*_{ij} \; dV$$

the expression $\int_v k \; dj^* \; dV$ can be written, where k is the shear yield stress in plane strain of the material and dj^* is the maximum shear strain increment. In the situation where the mode of deformation is comprised of rigid blocks of material separated by lines of tangential displacement discontinuity $dj^* = 0$. Further, in every instance examined, the term

$$\int_{ST} T_i \; du_i^* \; dS_T = 0$$

so that equation (3.5) now becomes;

$$\int_{Su} T_i \, du_i \, dS_u < \sum \int_{SD} k/dV^* \; / \; dS_D^*$$

3.2.3 Upper Bound in Plane Strain

In fig. 3.3(a) a rigid parallelepiped of material of unit height, ABCD, is considered which is also of unit thickness normal to the plane of the paper, moving to the left with unit speed. Under conditions of plane strain deformation is only in planes parallel to the paper. All material to the right of XX is rigid, but, after crossing XX, the parallelogram ABCD is instantaneously altered, forms a new rigid parallelogram, A'B'C'D', so that it moves in a new direction, at an angle α to the original direction, with a new speed.

In fig. 3.3(b) the hodograph or velocity diagram appropriate to the field of fig. 3.3(a) is shown. The original unit speed may be resolved into components v_p and v_a, a velocity perpendicular to XX and parallel to XX. Each particle to the left of XX has the components v_p and v_b for the new velocity v_2. The difference between v_b and v_a represents a 'velocity discontinuity' tangential to XX and this discontinuity manifests itself by changing the shape of ABCD to A'B'C'D'. In reality this process is not instantaneous but the velocity change does occur over a narrow band which in the limit becomes a line.

The work done in changing the shape ABCD to A'B'C'D' can be expressed in terms of a rate of dissipation of internal energy. If τ is the shear stress on opposite sides of the block the work done is equal to $(\tau.BC).CC'$ or, in terms of the rate of dissipation of internal energy, $(\tau.BC).CC'/t$ where t is the time for DC to cross XX. As the

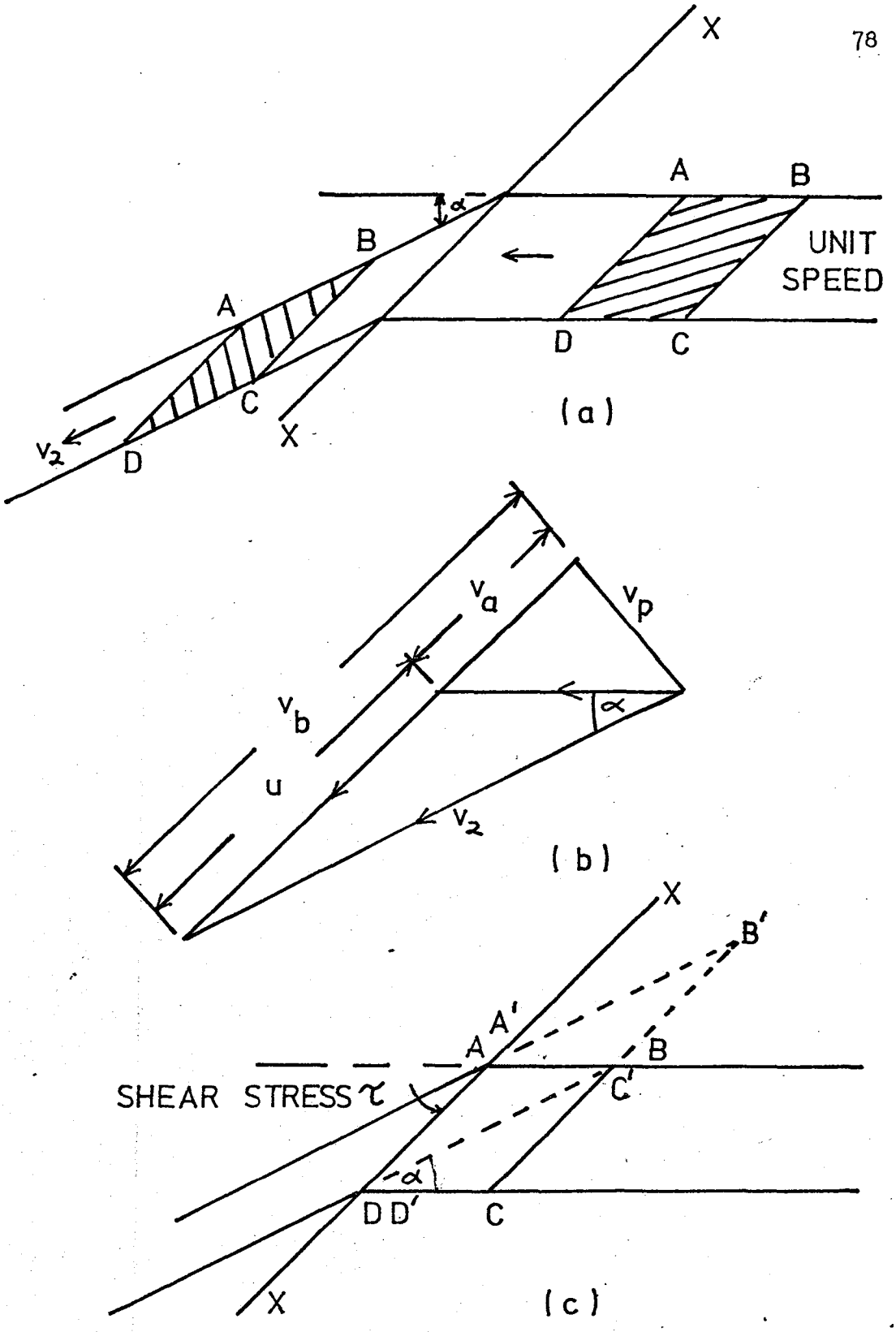

FIG. 3.3 Mode of deformation and hodograph for a plastic rigid material

block is moving with unit speed this can be rewritten as (τ.BC). CC' /DC.

Comparing triangle C'CD in fig. 3.3(c) and the hodograph it can be seen that $\frac{CC'}{DC}$ = u; so that the rate of energy dissipation, dw/dt, can be written as

$$\frac{dw}{dt} = \tau .BC. \frac{CC'}{t} = \tau .B.C. \frac{CC'}{DC}$$

$$= \tau .BC. u \qquad = \tau .AD. u$$

When τ has its greatest possible value, k, the shear yield stress in plane strain,

$$\frac{dw}{dt} = k. AD. u$$

and by having τ = k the material develops its maximum resistance to deformation. If the discontinuity line is curved, then in place of AD is the term dS and thus

$$\frac{dw}{dt} = \int k\ u\ dS \qquad (3.6)$$

the integration being performed along XX. If XX is a straight line equation (3.6) can be written as

$$\frac{dw}{dt} = k. u. s$$

where s is the length of XX and u the same at each point on it.

When considering the extrusion of powdered metal the value of the shear yield stress is not constant but varies according to the relative position of the billet during extrusion. This can be shown by considering an idealized upper-bound solution for plane strain extrusion. Fig. 3.4 shows an upper-bound solution of the type obtained by Johnson[63], where the material is assumed to consist of a number of rigid blocks of uniform quari-static zones, bordered by

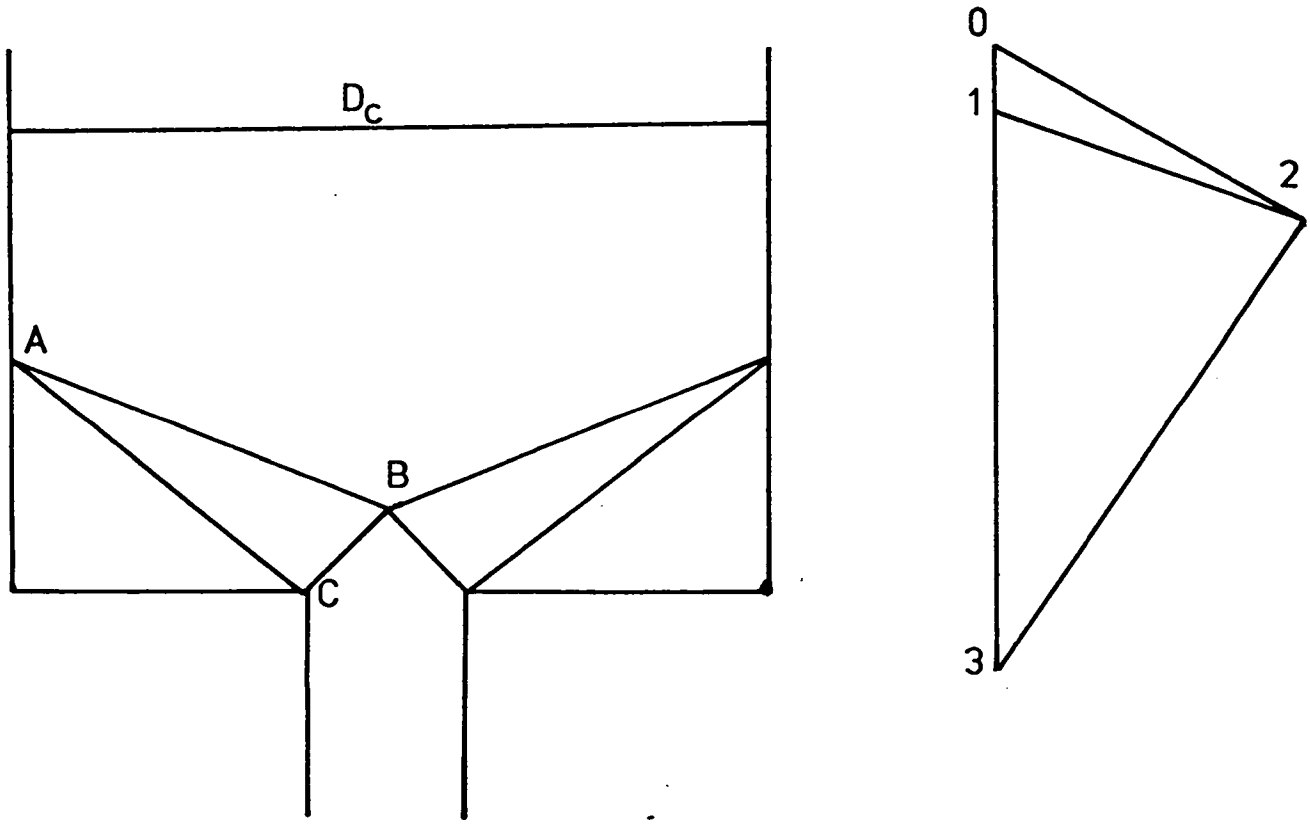

physical plane hodograph

$$p.1.\frac{D_c}{2} = k_i.\overline{12}.AB + k_i.\overline{13}.AC + k_f.\overline{23}.BC$$

FIG. 3.4 Simple upper bound solution for a 30:1 reduction

velocity discontinuities. Thus, referring to fig. 3.4(a), material approaching the velocity discontinuity AB at velocity u_{oa} is forced to travel parallel to the dead metal zone boundary throughout the region ABC. On encountering the discontinuity BC, the material then leaves the extrusion container at a velocity u_{oc}. It is possible to refine the situation further by addition of more discontinuities but for the sake of the argument the discontinuities will be restricted to those shown.

An upper bound solution giving the pressure required for homogeneous deformation and redundant work can be obtained by considering the work done at each discontinuity. Thus:-

$$p.d.u = k.(\text{initial})\ ab\ AB + k(\text{initial})\ ac\ AC + k(\text{final})\ bc\ BC \qquad (3.7)$$

where u is the ram speed.

It is therefore evident that a lower extrusion pressure will be obtained than for a solid billet extruded under the same conditions as the yield stress of the material varies considerably within the quasi-static deformation zone. At the first discontinuity the yield stress k(initial) will be low because of the relatively small contact areas between neighbouring particles. k(initial) will therefore be connected with the powder properties rather than the final material properties. On the other hand, at the discontinuity BC the compact will have acquired the properties of the final product and thus k (final) will be closely related to the yield stress of the extruded product. However, the material does not behave in a discontinuous manner, but rather the opposite, the process actually occurring is one of continuous breaking and welding of particle contacts. The contact area increases so that the shear yield stress also increases

and approaches the value of the final product. When the material reaches BC the deformation is by shear only as in the conventional extrusion process and so k(final) > k(initial). It can be seen that the value of k increases until the material has reached the velocity discontinuity BC and to estimate the pressure of extrusion mean values of k have to be taken for each rigid triangle.

3.2.4 A minimum Upper Bound Solution for Plane Strain.

Johnson and Kudo[64] developed a formula for plane strain extrusion with R, reduction ratio, equal to 2 using a rigid triangle velocity field. By minimizing the formula, they were able to theoretically determine the position of the triangles.

Fig. 3.5(a) represents the rigid triangle field for the procedure to obtain the minimum upper bound for extrusion pressure and fig. 3.5(b) the hodograph.

In fig. 3.5(a)

$$OB = x$$

$$OA = y \,/\, \sin w$$

$$OC = d \,/\, \sin \phi$$

$$AB = \sqrt{\frac{y^2}{\sin^2 w} + x^2 - \frac{2xy \cos w}{\sin w}}$$

$$BC = \sqrt{\frac{d^2}{\sin^2 \phi} + x^2 - \frac{2dx \cos \phi}{\sin \phi}}$$

The relative slip between adjacent rigid triangles are obtained from the hodograph in fig. 3.5(b)

rate of relative slip

$$\overline{13} = \frac{y^3}{dx \sin w}$$

$$\overline{54} = \frac{y^2}{x \sin \phi}$$

$$\overline{23} = \frac{y^2}{dx} \sqrt{\frac{y^2}{\sin^2 w} + x^2 - 2xy \cot w}$$

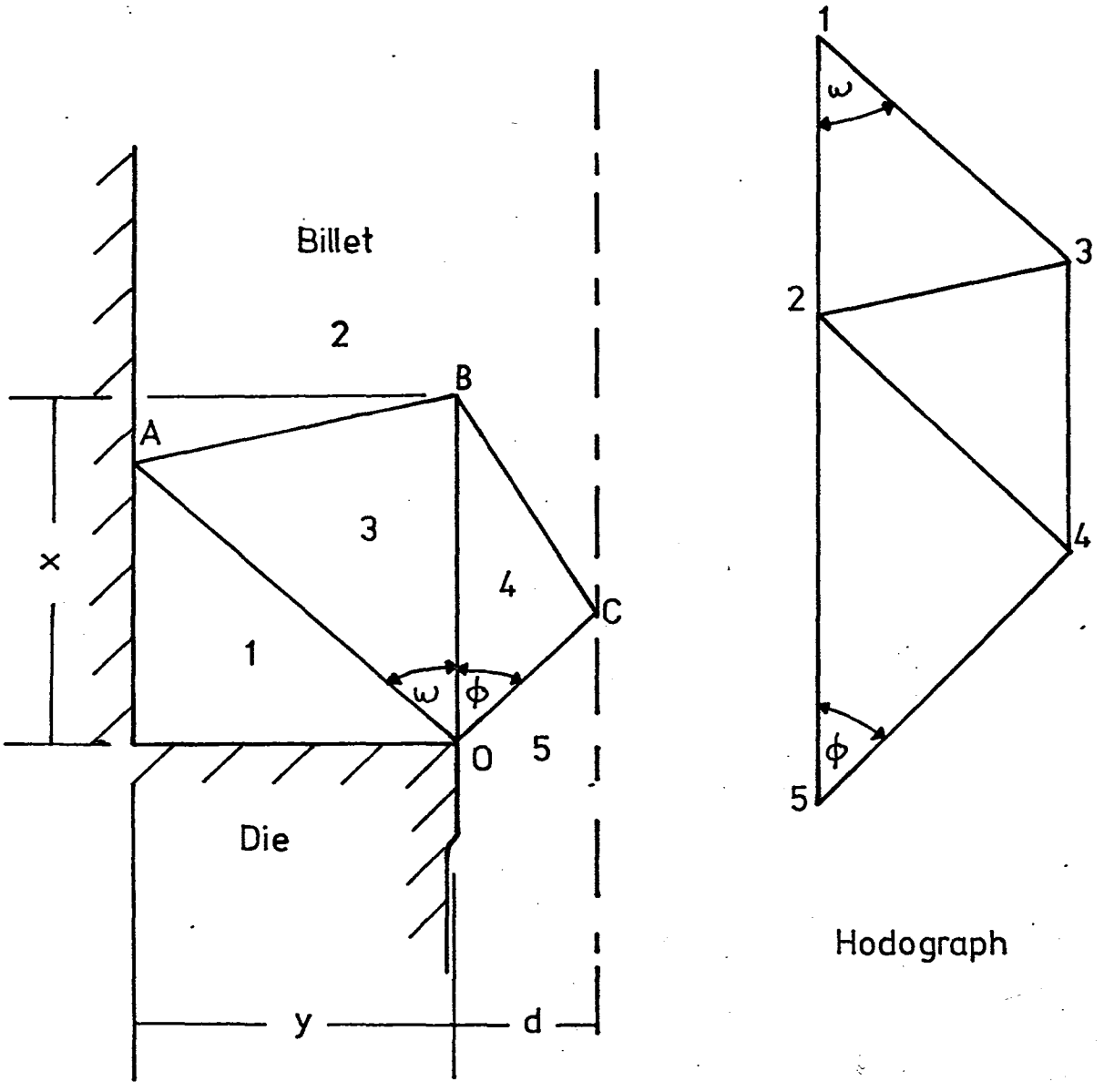

FIG. 3.5 Rigid triangle field and hodograph

$$\overline{24} = \frac{y^2}{dx}\sqrt{\frac{d^2}{\sin^2\phi} + x^2 - 2dx\cot\phi}$$

$$\overline{34} = \frac{y}{d} + 1 - \frac{y^2}{dx}(\cot w + \cot\phi)$$

The rate of energy dissipation in the system per unit thickness in the direction normal to the plane of flow is given by[64];

$$\dot{E} = k\sum l_{ij}\Delta u'_{ij}$$

where l_{ij} and $\Delta u'_{ij}$ represent the length of a straight boundary and the rate of relative slip between triangles 'i' and 'j' respectively. The mean pressure from a smooth container can be calculated from the dissipation thus:-

$$\overline{P}' = \dot{E} / 2(y+d)\ V \qquad (3.8a)$$

and V is the ram speed

Therefore:-

$$\dot{E} = k\ (AB u_{AB} + OB u_{OB} + BC u_{BC} + OC u_{OC} + OA u_{OA}) \qquad (3.9)$$

thus:-

$$\dot{E} = k\ (AB\overline{23} + OB\overline{34} + OC\overline{45} + BC\overline{24} + OA\overline{13}) \qquad (3.10)$$

This can be substituted into equation (3.8) so that the load

$$= K\left[\frac{y^2}{dx}\left(\frac{y^2}{\sin^2 w} + x^2 - 2yx\cot w\right) + \frac{yx}{d} + 1 - \frac{y^2}{d}(\cot w + \cot\phi)\right.$$

$$\left. + \frac{y^2}{dx}\left(\frac{d^2}{\sin^2\phi} + x^2 - 2dx\cot\phi\right) + \frac{y^4}{dx\sin^2 w} + \frac{dy^2}{x\sin^2\phi}\right]\frac{(y+d)}{2}$$

$$= k\left[\frac{yx}{d} + 1 + \frac{2xy^2}{d} + \frac{2y^4}{dx\sin^2 w} - \frac{2y^3}{d}\cot w - y^2\cot w\right.$$

$$\left. - 2y^2\cot\phi - \frac{y^2}{d}\cot\phi + \frac{2d^2y}{x\sin^2\phi}\right]\frac{(y+d)}{2}$$

This expression can be minimised by differentiation with respect to x

$$d\left(\frac{\text{Load}}{dx}\right) = \left[\frac{y}{d} + \frac{2y^2}{d} - \frac{2y^4}{dx^2}\sin^2 w - \frac{2d^2y}{x^2\sin^2\phi}\right]\frac{(y+d)}{2} \qquad (3.11)$$

Therefore at the minimum load

$$x^2 = \frac{2d}{(1+2y)}\left[\frac{y^3}{d\sin^2 w} + \frac{d}{\sin^2\phi}\right]$$

Similarly values for w and ϕ can be obtained

For w

$$\frac{-2\ 2y^4 \cos w}{dx \sin^3 w} + \frac{2y^3}{d \sin^2 w} + \frac{y^2}{\sin^2 w} + \frac{y^2}{\sin^2 w} = 0$$

therefore

$$\cot w = \frac{(2y + d)x}{4y^2} \qquad (3.12)$$

For ϕ

$$\frac{-2\ 2 \cos \phi\ 2\ dy^2}{x \sin^3 \phi} + \frac{2y^2}{\sin^2 \phi} + \frac{y^2}{\sin^2 \phi} = 0$$

therefore $\cot \phi = \frac{3x}{4d}$

It can be seen that w and ϕ are dependent on x and so only an estimate of the minimum value can be obtained.

A process of iteration was used to evaluate x, ϕ and w, so that for a 30:1 reduction ratio. (see appendix)

$$w = 80.5$$

$$\phi = 11.62$$

and the load = (a constant) X 51.75

3.3 Strain Rate

A method of estimating the mean strain rate has been suggested by Feltham[132] who considered the total useful strain occurring in a certain time passing through the deformation zone. The equation developed was:

$$\dot{\bar{\varepsilon}} = \frac{6U}{D} \ln R \qquad (3.14)$$

The time being that equal to:

$$\frac{\text{Volume of die cone}}{\text{Volume of metal extruded per unit time}}$$

This method can be extruded by imagining the deformation to

occur within a conical volume with an angle of 45^{o} to the container and die face. Knowing this volume and the volume of metal extruded per unit time, the time taken to fill this volume can be found. The volume of the die cone above the die

$$= \frac{\pi}{24} (D_1^3 - D_2^3)$$

where D_1 and D_2 are the diameters of the billet and the extruded rod, respecitvely. The volume of metal extruded per unit time is $-\pi/4\ D_1^2U$, so that the time required to fill the cone area above the die will be $(D_1^3 - D_2^3) / 6\ D_1^2U$

However, the total strain, as shown by Dodeja and Johnson, is (a + blnR) not lnR so that the work done per unit volume is Ym (a + blnR) and the mean equivalent strain rate is given by the equation

$$\dot{\bar{\varepsilon}} = (a + b\ln R) \frac{6D_1^2U}{D_1^3 - D_2^3}$$

$$\dot{\bar{\varepsilon}} \approx (a + b\ln R) \frac{6U}{D_1} \qquad (3.15)$$

U is the measure of ram speed.

This equation is very similar to that of Feltham and values of the constants 'a' and 'b' can be inserted, similar to those found by Hirst and Ursell or Johnson.

It can be seen from the literature that the strain rate is the most difficult extrusion parameter to determine.

3.4 Thermal Activation

The determination of the extrusion process as a thermally activated one has been carried out by Wong and Jonas[133] on commercial purity aluminium. The equation used to relate the mean strain rate with the mean effective stress was that proposed by Sellars and Tegart.

$$\dot{\varepsilon} = A \left[\sinh (\alpha\sigma)\right]^{n} \exp \left(\frac{-\Delta H}{RT}\right) \qquad (3.16)$$

where A, α, n, and ΔH are constants

The calculation of activation energy from experimental data was made using the following procedure. Equation (3.14) can be written in a more general form thus:

$$\dot{\varepsilon} = \text{constant} \times \left[f(\sigma)\right]^{n} \times \exp (-\Delta H/RT)$$

In creep testing, a constant stress is often applied over a range of temperatures so that a plot of log $\dot{\varepsilon}$ at constant stress as a function of temperature can be obtained of the form

$$\left(\frac{\partial \log \dot{\varepsilon}}{\partial T^{-1}}\right)_{\sigma} = \frac{-\Delta H}{2.3\,R} \qquad (3.17)$$

where $\dot{\varepsilon}$ and T are measured experimentally.

In hot torsion a constant strain rate is applied and the resulting stress measured experimentally. The calculation of ΔH at constant stress involves extensive extrapolation and interpolation of the experimental stress strain rate temperature data.

An alternative means of calculating ΔH is to split the equation

(3.15) into partial differentials so that

$$-\left(\frac{\partial \log \dot{\varepsilon}}{\partial \log f(\sigma)}\right)_T \times \left(\frac{\partial \log f(\sigma)}{\partial T^{-1}}\right)_{\dot{\varepsilon}} = \left(\frac{\partial \log \dot{\varepsilon}}{\partial T^{-1}}\right)_{\sigma} = \frac{\Delta H}{2.3R'} \qquad (3.18)$$

where each of the terms on the left hand side of the equation is obtained from experimental measurements. Wong and Jonas, using this method and the hyperbolic sine stress function, found the activation energy from the following equation:

$$\Delta H = 2.303R' \left(\frac{\partial \log \dot{\varepsilon}}{\partial \log (\sinh (\alpha\sigma))}\right)_T \times \left(\frac{\partial \log (\sinh [\alpha\sigma])}{T^{-1}}\right)_{\dot{\varepsilon}} \qquad (3.19)$$

Values of the expression $\frac{\partial \log \dot{\varepsilon}}{\partial \log (\sinh [\alpha\sigma])}$ are obtained by plotting strain rate as a function of the hyperbolic sine stress term yielding a straight line. This represents the stress dependence on strain rate for a particular temperature, i.e. a straight line is obtained for different stress, strain rate values at one temperature. The expression $\frac{\partial \log (\sinh [\alpha\sigma])}{\partial T^{-1}}$ shows the dependence on temperature for one particular temperature. Hence, from experimental measurements performed during extrusion, a value for ΔH, the activation energy, can be calculated.

3.5 Limit diagrams

The maximum load before the press is stalled, can be obtained using a modified form of Johnson's equation

i.e. $$\frac{P}{Ym} = (a + b \ln R) \qquad (3.20)$$

The values of 'a' and 'b' are those found empirically using different reduction ratios at the same temperature and strain rate. Knowing the terms 'a', 'b', and R the mean yield stress at a particular temperature and strain rate can be calculated from the extrusion pressure obtained experimentally. With this value of yield stress, the maximum load for a particular temperature can be calculated using the above modified form of Johnson's equation. Similarly the maximum load can be calculated for a billet of length l using Hirst and Ursell's allowance for friction.

$$\frac{P}{Ym} = (a + b\ln R) \exp \frac{4\mu l}{D} \qquad (3.21)$$

The coefficient of friction μ can be calculated using either the method suggested by Hirst or Ursell, or that using values from the load displacement curve. Hirst and Ursell suggested extruding two billets of lengths l_1 and l_2 through the same reduction and measuring the mean pressures, Pl_1 and Pl_2. It was shown that

$$\mu = \frac{D}{4(l_1 - l_2)} \ln \frac{Pl_1}{Pl_2} = \frac{0.575D}{l_1 - l_2} \log_{10} \frac{Pl_1}{Pl_2} \qquad (3.22)$$

This technique can be applied to two loads on the steady state portion of the diagram and the coefficient of friction calculated using the equation above.

3.5.1 Temperature

The loads required in the limit diagrams are those required from a known initial billet temperature rather than a working or mean temperature.

The limit due to incipient melting can be calculated using the equation shown also by Hirst and Ursell. Knowing the specific heat of the metal and assuming adiabatic conditions it is possible to find the maximum extrusion ratio possible. The value of Ym is a mean value between the initial and final temperature and the temperature rise at infinite speed, that from initial temperature to the melting point.

The temperature rise for strain rates experienced during the extrusion process can be estimated using the expression derived by Raybould[68].

$$T = 23.95\ \sigma\ C_H \left[27.85 + 2.3t^{\frac{1}{2}} + 0.8t^{2/3} + 2.61t^{1/3}\right]^{-1} \qquad (3.23)$$

Using this value of temperature rise, the maximum value of reduction ratio can be calculated for the limit due to incipient melting.

3.6 Petch Equations

Investigations on mild steel by Petch[137] showed an empirical relationship between yield strength and grain size of the form:

$$\sigma = \sigma_o + C\, d^{-\frac{1}{2}} \qquad (3.24)$$

The term σ_o represents the friction stress that opposes the motion of mobile dislocations in a grain and C is a parameter that measures the strength of grain boundaries. This expression is for high angle boundaries but has also been applied to low angle boundaries produced by high temperature deformation. The following relationship has been applied.

$$\sigma = \sigma_o' + C'\, ds^{-\frac{1}{2}} \qquad (3.25)$$

d_s is the mean sub grain size and σ_o', and C' are empirical constants. In place of yield strength the experimental (0.2%) proof stress is

applied so that the above equation becomes

$$\sigma(0.2\%) = \sigma_o\ (0.2\%) + C''\ d_s^{-\frac{1}{2}} \qquad (3.26)$$

Again σ_o (0.2%) and C' are empirical constants.

It has been found[86] that the sub grain diameters of an extruded aluminium powder product are approximately proportional to the diameter, dp, of the aluminium powder particles. Therefore equation (3.24) can be written thus:-

$$\sigma = \sigma_o + C''\ dp^{-\frac{1}{2}} \qquad (3.27)$$

Similarly for the proof stress values

$$\sigma\ (0.2\%) = \sigma_o''(0.2\%) + C''\ dp^{-\frac{1}{2}} \qquad (3.28)$$

The values of σ_o'' (0.2%) obtained by extrapolation will be similar to those of the flow stress (0.2%) of coarse grained aluminium obtained under the same conditions. Room temperature and elevated temperature results of proof stress can be plotted against the mean particle diameter and for each temperature in the limit $\sigma(0.2\%)$ is the value expected for a pure aluminium coarse grained specimen.

3.7 Dispersion Strengthening

The strength given by the Orowan relation in a precipitation hardened alloy is determined by the stress required to low out dislocations between the precipitates. This is given by the equation

$$\tau_h = \frac{2jGb}{\lambda} + \tau_a \qquad (3.29)$$

where G is the shear modulus of the matrix, and b is the Burgers Vector of a glide dislocation. τ_a is the yield strength of the matrix without precipitates.

The factor j is determined from the 'line tension' of a dislocation which is given by $T' = j\ Gb^2$. The relevant value of T'

in the Orowan model must be the line tension of a dislocation in a semi-circular loop shape. A good approximation has been suggested by Kelly and Nicholson,

$$T' = \frac{Gb^2}{4\pi} \quad A^* \ln \frac{\lambda}{2b} \tag{3.30}$$

Where A^* is a constant equal to 1 for edge dislocations, and to $1/1-\nu$ for screw dislocations. λ is the distance between obstacles seen by moving dislocations.

The yield strength of dispersion strengthened products has been written:

$$\tau = \tau_o + A^* \frac{Gb}{2} \frac{1}{DAf} \ln\left(\frac{DAf}{b}\right) \tag{3.31}$$

where DAf is the planar surface spacing (free distance between particles).

To calculate the interparticle distance in a plane for plate shaped particles, the following procedure is used.

The planar centre to centre distance (DA) and surface to surface distance (D_{Af}) are calculated on the assumption that the particles intersecting a plane (N_A) are arranged in a square lattice.

For a uniform distribution of plate-shaped particles with the diameter D^*, N_A is equal to the number of particles per unit volume multiplied by the mean value $\bar{D}$ of the plate diameter projected on the normal to the intersecting plane. $\bar{D}$ is given by the equation[180].

$$\bar{D} = \frac{\pi}{4} . D^*$$

thus $$D_A = \sqrt{\frac{D^* . t}{f}}$$

where f is the volume fraction of the oxide, and t is the thickness of the oxide particles.

The plate particles appear in an intersecting plane as needles of a length varying from zero to D*. The mean length of the needles is

$$Da = \frac{\pi}{4}.D^*$$

D_{Af} is taken as D_A minus the mean value of the needle length Da projected on the line connecting the two particles. The projected diameter is $\frac{\pi}{4} D^* \cos \phi$, and the mean value of the projected diameter is:-

$$\bar{D}a = D^*/_2$$

thus:-

$$D_{Af} = \sqrt{\frac{(D^*.t)}{f}} - \frac{D^*}{2}$$

The planar surface spacing can then be calculated knowing the size of the oxide particles and the volume fraction of the oxide content. (See Appendix for calculation of results shown in fig. 5.43).

As a test of this theory the 0.2% proof stress can be plotted against $\ln (D_{Af}/b) / D_{Af}$, good correlation will be obtained if the points lie on a straight line.

CHAPTER 4

Experimental Procedure

4.1 Introduction

From the earlier discussion of the literature published it can be seen that there is lack of extensive work on the extrusion variables of powder extrusions. Reported work was usually based on the findings of ten or fewer experiments so that the current experimental programme was designed to rigorously cover the range of extrusion variables. The variables investigated were:-

(a) Particle size before extrusion

(b) Initial density of compacted billet

(c) Reduction ratio of extrusion

(d) Ram speed

(e) Initial billet temperature

(f) Heat treatment of product

The initial part of the programme was concerned with the aluminium powders manufactured from commercial pure aluminium and the remainder with the three aluminium alloy powders obtained. The extrusions were performed under reproducible conditions on a large scale laboratory press simulating industrial conditions.

The tooling on the extrusion press was the same as that used by Raybould[68], and so no modifications were necessary to carry out the research programme. Several dies, and a new stem, were designed to replace the original ones that had been damaged through general wear. The tool steel used for these tools was a recommended molybdenum chromium vanadium steel, a Kayser Ellison steel, KEA 145.

4.2 The powders

There are many characteristics of powders that can be considered to enable control and comparison of the initial raw material but not all may be critical for a given application. In the present work the individual powder particles were characterised by size, shape, and specific surface area, and the powder mass by size distribution, density, and chemical analysis. However, as will be noted later, some of these characteristics are themselves inter-related.

4.2.1 Powder shapes

The shapes of the individual powder particles within the powder mass were investigated using a scanning electron microscope. Particles were distributed on small aluminium stubs which were then placed into the microscope and the surface then scanned. For the fine particles, a small quantity of the powder to be examined was dispersed in alcohol and the subsequent slurry allowed to dry on the highly polished surface of the stub. When dried the small particles adhered well to the surface by small electrostatic forces. Coarse, larger particles were affixed to the stub by placing a piece of double sided sellotape on the stub surface and pressing gently onto a layer of particles. This technique allowed a small quantity of dispersed and individual particles to be separated out for viewing.

4.2.2 Powder size

The size, or size distribution parameter of a particular powder is very difficult to determine, as there are so many and varied techniques. The simplest and easiest to use is that of sieving. In the work carried out, the size distribution was determined using this technique but difficulty was encountered with the determination of the end-point. This has been specified as (134):

(a) sieve until the rate at which particles pass through the sieve is reduced to a specified weight or percentage weight per minute.

(b) sieve for a specified time

Technique (a) was preferable but (b) was better for standardisation and so for convenience technique (b) was applied, using a sieving time of one hour for a 150 gram - 200 gram sample.

To investigate the process variable of powder particle size, a series of mesh size fractions were separated from the main bulk of the powder by the action of sieving. The sieving was carried out on conventional 8" diameter B.S. standard wire mesh sieves. The different sizes of sieves were stacked so that the coarsest was uppermost decreasing in size to the finest at the bottom, with a receiver at the very bottom. A lid was then placed onto the uppermost sieve and the whole nest of sieves positioned on an 'Endrock' mechanical sieve. The sieving was then carried out by a mechanical vibratory and rotary motion for one hour and the separate fractions stored. The particle size distribution was then measured by weighing the mesh size fractions separated.

To determine the mean particle size of the coarser mesh fractions, a mean value between two adjoining mesh sieve sizes was taken. For example, the powder passing through a 60 mesh sieve but retained by a 100 mesh sieve, was regarded to consist of a mean size in between these two mesh sizes. In reality a wide range of sizes in between the two mesh sizes existed. Particles below the 45 microns working limit of the conventional wire sieves were measured using a microscope and their mean particle size determined by measuring and counting a large number of particles, 50-100 measurements usually taken.

4.2.3 Surface area

The surface area of the fine powders was determined by a B.E.T. analysis [135]. This process involves the adsorption of gases in a Uni-molecular or multi-molecular layer on the surface of a particle at a temperature near the condensation point of the atmosphere. Derivation of the isotherm equation for multi-molecular adsorption is by a method that is a generalisation of Langmiur's treatment of the uni-molecular layer. In the theoretical treatment it is assumed that the same forces produce condensation, are responsible for multi-molecular adsorption.

The analysis was carried out using Krypton as the gas to be adsorbed, and the temperature of adsorption near the boiling point of nitrogen, ($-196^{\circ}C$). The results were then included as data in a computer programme written by Beaven and Eadington[136], which calculated the surface areas involved for the material used.

4.2.4 Chemical Analysis

The analysis of the powders for their natural oxide content was obtained by a standard wet analysis and difference technique. This involved establishing the aluminium content by reducing a suitable volume of $Fe_2(SO_4)_3$ in sulphuric acid solution under a CO_2 atmosphere and determining the al by permanganometric titration of Fe. The samples were checked for impurities and the Al_2O_3 content obtained by difference. Samples for chemical analysis were taken from the powder mass by a coning and quartering technique.

Different mesh fractions of the aluminium powders and the alloys were also analysed for oxide content to study the variation between different particle sizes within the same powder.

The analysis was carried out within the college by the 'analytical services' department.

4.2.5 Compaction

The process of cold compaction was carried out in the die shown in fig. 4.1, made from tempered, oil quenched E.N.24 steel. The ram was designed so that it was the same length as the container to facilitate the ejection of the compacted billet upon attainment of a particular set of conditions. The ram was machined down to a push fit tolerance to ensure that little powder forced its way up between the ram and container during application of load. Before the container was filled with powder, the walls and tool pieces of the die were lubricated using a teflon based dry film lubricant applied in the form of a spray and allowed to dry. This ensured that there was little pick-up of aluminium on the tooling surfaces and that the frictional conditions were fairly uniform during compaction.

Having filled the container with a known quantity of powder, levelled the top of the powder mass, the powder was then compacted using a 'Tangye' 2MN (200 Ton) press to a pressure of 205 MNm^{-2}. This pressure was calculated from the indicated oil pressure shown, acting on a 10" diameter ram, the ram acting on the stage of the press. The ram displacement at a particular pressure could be measured by the means and use of calipers. After the attainment of a particular pressure the compact was then ejected, the tooling cleaned and resprayed if necessary, and the compacting process repeated for the next quantity of powder. Any excess dry film lubricant on the surface of the compacts was removed using emery paper. The density of the billet was then calculated by weighing and accurately measuring the height and diameter.

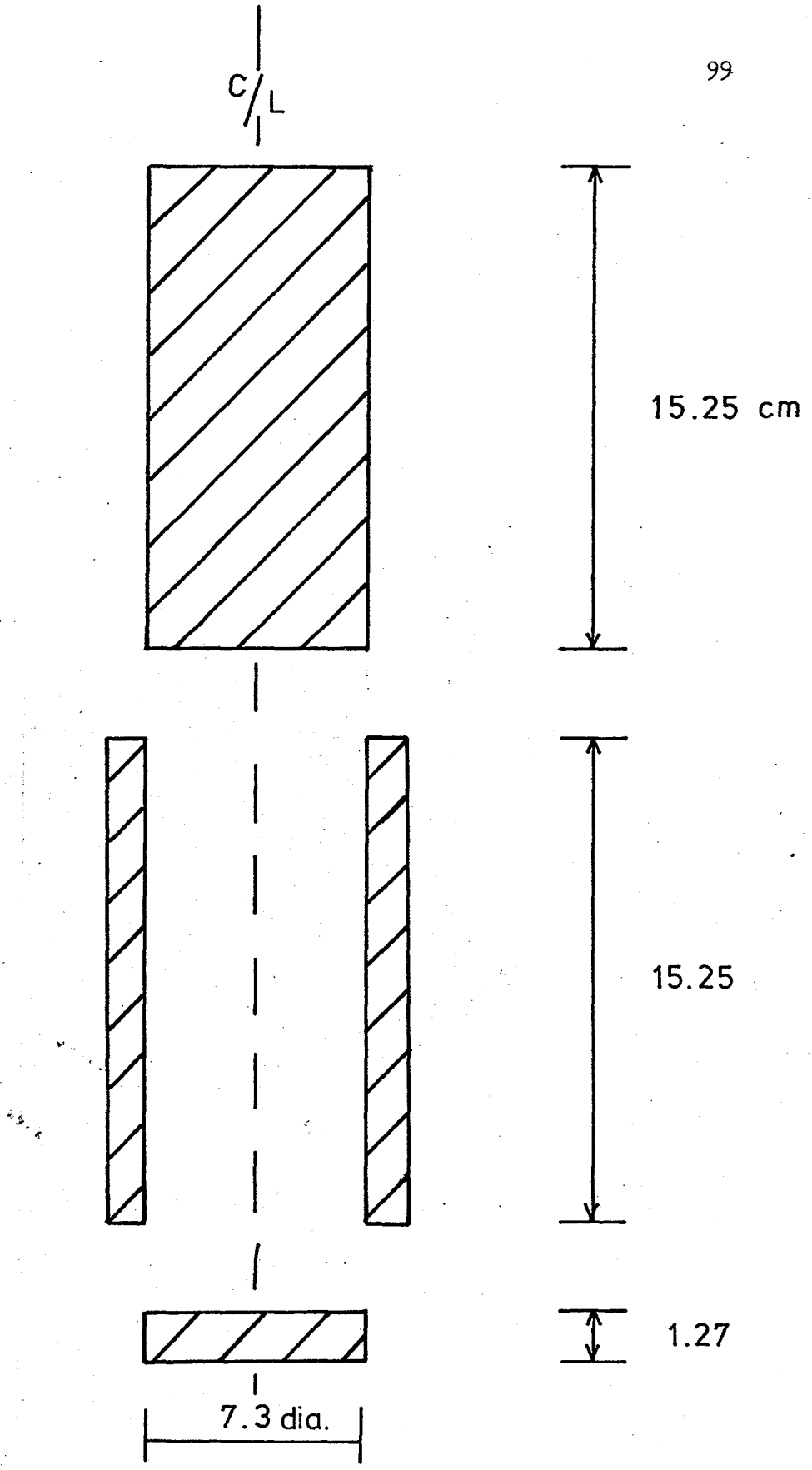

Compaction die mould

Fig 4.1

4.3 Extrusion press

The 5MN (500 Ton) fast action extrusion press was that used in the work by Raybould[68], so that most of the modifications had been carried out before the start of the research programme. The extrusion press was of a vertical design and situated over a run out pit thus enabling direct extrusion with the die fixed into position above the pit by a backing ring. The general layout of the press is shown in plate 4.1, with the controls for operation on the right hand side below the load scale and oil pressure gauges.

The container, fixed onto two hydraulic rams via a cast housing, plate 4.2, was able to take billets up to 75mm in diameter and 158mm in length. The heavy casting surrounding the container, was lifted by the hydraulic rams to permit removal of the extrusion discard and cleaning of the container in situ. Extrusion was carried out with the container resting on the surrounding ring that contained the die holder so that the container bottom mated with the face of the die holder. When the ram was brought down to carry out the extrusion process, the load was applied to the billet through the stem and a pressure pad resting on top of the billet. The ram speed was able to be controlled up to speeds of 13.6mm/sec from 0 by contra flow direct pumping and higher speeds by the accumulator drive. The main hydraulic supply was from two pumps and the flow of oil to the ram controlled either by an adjustable rotor on one of the pumps which worked with or against the second, or by directing part of the flow to the drain tank. The accumulator action enabled speeds up to 250mm/sec ram speed to be attained, and took place when the extrusion load exceeded $3.45 MNm^{-2}$ (500 lbs/sq. in) oil pressure in the ram. The extra ram speed was caused by the action of the oil, stored in nitrogen filled pressure bottles at $20.84 MNm^{-2}$ (3,000 lbs/sq. in) pressure, being released

PLATE 4.1

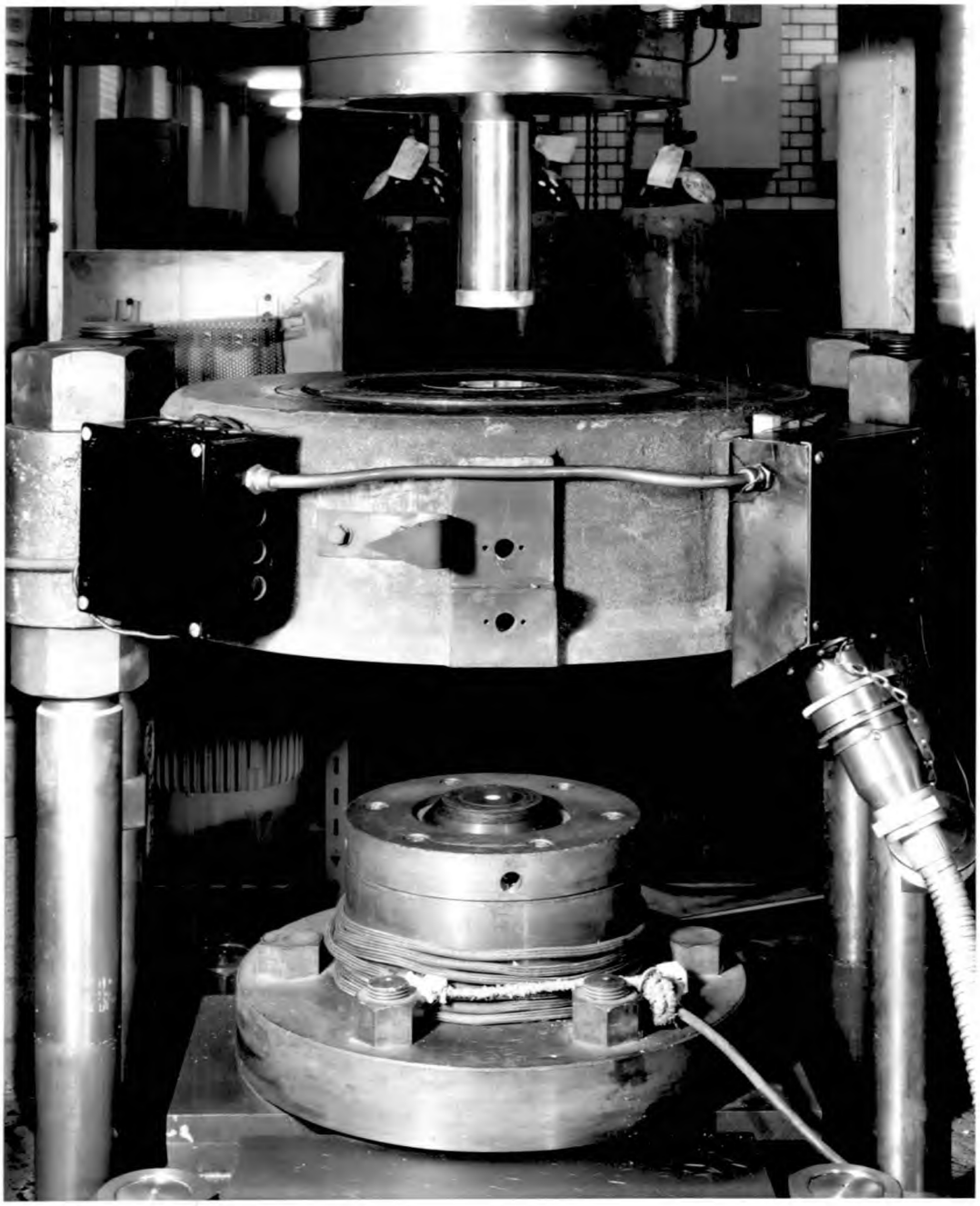

PLATE 4.2

after the attainment of 3.45MNm^{-2} pressure.

4.3.1 The heaters

The billets for extrusion could be heated up to 300°C in situ by the existing heaters installed. The advantage of in situ heating was that there were no appreciable temperature gradients between the billet and container before extrusion. There were eight inconel heating elements placed around the container and held in position inside the container holder casting. These heaters, with a total rating of 12 kilo-watts, had a maximum operational temperature of 650-700°C and to prevent excess of this limit, thermocouples attached to eurotherm controllers, were braised onto each element.

Temperatures in excess of 300°C were obtained by pre-heating the billets for extrusion in an air circulating furmace, capable of attaining temperatures up to 600°C, close to the extrusion press. On attainment of a particular temperature the billet was transferred from the furnace into the container and then extruded after placing the pressure pad onto the hot billet. The initial temperature of the billet before extrusion commenced was determined by the presence of a thermocouple at the rear of the billet. This thermocouple was situated through a small hole in the centre of the pressure pad and its lead threaded back through the stem. The values of the millivolt output from the thermocouple were recorded using the 'data logga' and stored on paper tape. Load cell readings were recorded and stored as well so that the initial temperature at the start of extrusion could be determined. The 'data logga' used was a Dynamco microscan data logging system 59/16274 comprising a digitial voltmeter, low level scanner, scanner drive unit, serializer, and a punch output unit for a Tally punch. This particular piece of equipment did not require repeated

calibration as it measured e.m.f., rather than current, and was able to record up to 10 channels/sec.

4.3.2 Container billet interface

The container had been bored out from 75mm to 87mm in diameter and an inner sleeve made that was placed in this enlarged hole. The liner, with an internal diameter of 75mm, was designed so that it could be removed with a load of 100 tons at room temperature. Backers were also designed by Raybould[68] to hold the liner in position while the remaining skull was removed.

The inner surface of the liner was maintained approximately the same by the use of scraper pads after each extrusion to remove the excess pick up. These pads were designed so that they had a front band, 74.99mm in diameter and 10mm high, and were similar in appearance to the pressure pads. Nevertheless, however efficient the pads were in removing the aluminium pick up, at the start of each extrusion the container liner internal surface was a very thin layer of aluminium. After scraping, it was considered that the frictional conditions were approximately the same for each extrusion.

4.3.3 Lubrication

To discover the most satisfactory form of lubrication, a series of preliminary experiments were performed. The first extrusion performed, using just graphite as a lubricant, resulted in the severe fir tree defect seen in fig. 4.2 due to the excessive die pick up and fiction. To overcome this, without the use of hot pressing, the powder was compacted into a billet inside an aluminium can with the front and rear end plugs made from machined commercial aluminium bar. This did solve the problem of the fir tree defect. However, the preparation of the

Fig. 4.2 Example of the effect of inserting a small aluminium pad on the die face before extrusion. (a) Billet extruded without a pad; (b) Billet extruded with a pad.

cans was tedious and the rear plug was extruded through the rear of the compact into the centre of the rod forming a central cone. This necessitated the rejection of a large quantity of the extruded rod. To overcome this problem it was necessary to leave out the rear plug. This left an open can with a front end comprising a circular pad of aluminium. It was seen from macro-sections that this small piece of material acted as the dead metal zone for the powder billet and also as a sheath for the extruded material passing into the die. Discarding the open can, a compacted billet was extruded using only the circular pad as the potential canning material, with satisfactory results. The reason for this being that, as the powder was extruded through the aluminium it picked up sufficient material to form a can around the extruded section and thus pass through the die smoothly, the aluminium acting as a lubricant. The sheath around the extruded rod was then easily removed by machining if necessary.

This technique of lubrication, using a front circular slab of aluminium was used throughout the series of experiments. The thickness of the slab being 10mm in all cases.

4.4 Extrusion parameters

4.4.1 Billet temperature

The temperature of the extrusion billet when inside the container was measured by means of a thermocouple fitted through the pressure pad to touch the rear of the billet. This ensured a millivolt reading output until the thermocouple broke during extrusion and so gave an indication of the temperature involved during the deformation process. The thermocouple was wired via compensating cable lead to the 'data logga' where the readings were recorded by means of a punch on paper tape. This tape was then read out on a punch machine and the temperature, in

millivolt e.m.f. form, were listed out.

4.4.2 Reduction ratio

The reduction ratios used in the experiments were 5, 10, 20 30, 40, and 50:1. Their different ratios were obtained by the use of interchangeable dies that were easily replaced from the die holder. The die can be seen in plate 4.2, held in place by the holder and retaining ring. To change the die, the retaining ring was removed, the die holder lifted off vertically leaving the die piece and backing ring, and the die removed. A new die, of the particular diameter rod required, was then placed onto the backing ring and the holder and retaining ring replaced.

4.4.3 Ram speed

The ram speed was closely controlled by the adjustment of the pumps to give a wide range of speeds. The speed was measured by a rectilinear potentiometer (model LP/21/85/s, as supplied by Penny and Giles) with a 600m.m. (24") stroke and was fixed between the cross head and the base of the press. The voltage, which varied with ram position, 10 volts over the 600 m.m., was fed into the X-Y recorder and plotted against time thus enabling an average ram speed to be calculated.

4.4.4 Load

The extrusion load was measured by a Mayes load cell placed vertically above the ram stem. The output was indicated on the dial gauge and recorded on the Hewlett-Packard 136A X-Y recorder and on the 'data logga'. The X-Y recorder was set to run at a certain pen speed thus enabling a load/displacement curve to be drawn. Calibration of the load cell was performed using a standard cell supplied by Dennison

placed between ram and the container against the indicated scale and the millivolt output to the 'data logga'.

4.4.5 Extrusion procedure

The container was allowed to attain a uniform temperature, usually by allowing it to heat overnight, before the compacted billet was inserted into the container. The billet was then allowed to reach equilibrium temperature, in situ if temperatures of 300°C or less were required, or by heating for twenty to thirty minutes in the air circulating furnace. When both the billet and container were at the desired temperature, the 'data logga' was switched on, the X-Y recorder started, and the process of extrusion initiated. The extrusion process was then stopped when the load began to increase rapidly in the post steady state, the stem raised, and the container lifted. After sawing, to leave the unextruded part of the billet in the container, the extruded rod was then punched out of the die orifice into the pit below. The remainder of the billet was removed from the container and the container liner cleaned, using the scraper pads. The container was brought down, the die face and container walls sparingly lubricated with graphite, and a small aluminium pad placed in front of the compacted billet before it was placed inside the container. A new pressure pad with a new thermocouple threaded through its centre then added to the top of the billet.

4.5 Properties of the product

The sectioning of an extruded rod using the 30:1 die was as shown in fig. 4.3. The rejection of the first section was suitably adjusted for varying reduction ratios and included the initial part of the aluminium pad extruded and the first part of the compacted billet extruded. Variation of properties in the rod from the regions

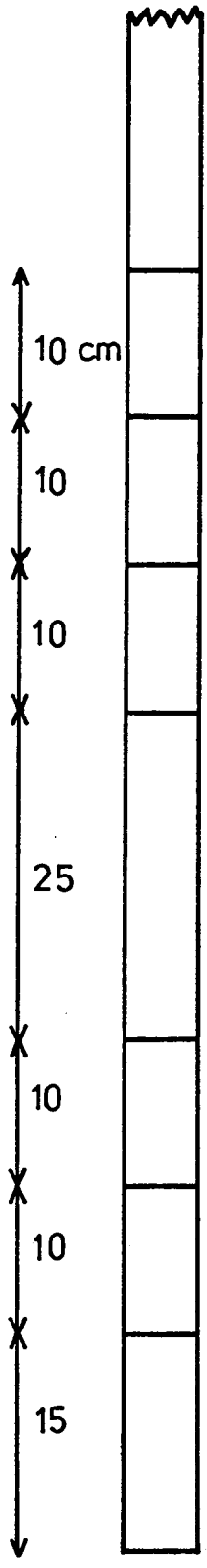

Tensile specimens (400°C)

Tensile specimens (R.T.)

Hardness and microscopy specimens

Spare material

Tensile specimens

Hardness and microscopy specimens

Rejected material

Sectioning of a rod extruded at 30:1

Fig. 4 3

taken and the back end was very small.

Thin sections for electron microscopy specimens were prepared by sectioning the rod length cut, using a water cooled slitting wheel. Both transverse and longitudinal sections to the extrusion direction were prepared using this technique. A length of rod approximately 3cm. long, was placed onto a special block and held in position using a low melting-point temeperature wax. A thin parallel edged specimen was then cut from the rod, 0.5 - 0.1 mm. thick, using the silicon slitting wheel. The whole specimen is subjected to a cooling liquid during this operation to ensure as little temperature rise of the specimen as possible. These parallel edged specimens sectioned were then ready for grinding and polishing during preparation of electron microscopy specimens.

4.5.1 Density

The final density of the extruded materials was checked by the measurement and weighing of small accurately machined specimens. These were prepared from the sections cut from the extruded rod and were machined to approximately 5mm. diameter and 10mm. in length. The dimensions were measured using a micrometer, the volume calculated then checked by immersion in paraffin.

4.5.2 Hardness Tests

Micro and macro hardness tests were carried out using 30 grams on a G.K.N. micro hardness tester, and 2 kilogram on a Vickers macro hardness testing machine respectively. The specimens were prepared by first grinding on waxed silicon carbide paper down to 600 grade then polished with 6μ, 3μ, and 1μ diamond paste, and finally electro polished. The hardness value taken was the mean value of about twelve

indents across the transverse section of the extruded rod.

4.5.3 Tensile tests

The tensile test specimens were machined from the appropriate sections to a standard Hounsfield No.14 size. Four specimens were made for room temperature tests and two for the high temperature tests.

The room temperature tensile tests were carried out on an Instron machine using a cross head speed of 0.01 cm/min. and the initial stress strain curve was recorded on a fast chart speed to ensure an accurate value of the (0.2%) proof stress.

The high temperature tensile tests were performed using a split furnace and were also carried out using a cross head speed of 0.01 cm/min. The split furnace surrounded the tensile specimen and Nimonic rods attached to the Instrom and easily attained temperatures up to 400°C. A thermocouple placed close to the tensile specimen controlled the heating and when the temperature attained the value required ten minutes were allowed for equilibrium conditions before the specimen was pulled. Variation between the two specimens pulled was not appreciable.

4.5.4 Transmission electron microscopy

The transmission electron microscopy was carried out on the College's A.E.I. EM6 microscope. Specimens were prepared by grinding on silicon carbide paper to 0.025mm. This ensured that relatively large areas of a particular specimen could be examined and photographed.

Samples cut from the extruded rods of aluminium powders (A,B,C) were electropolished using an electrolyte of 20% perchloric acid and 80% ethyl alcohol cooled to -30°C and at a potential of 20 volts. A

low temperature was found to be essential to reduce the amount of pitting.

Electropolishing of the alloys (J, K, and L) proved to be quite difficult and the problem was not satisfactorily solved for the powder K, the aluminium magnesium zinc alloy. Several electrolytes including the above, were tried but only one was a success for the alloys (J, L) and only partially successful for alloy K. One of the electrolytes, 40% acetic acid, 30% ortho-phosphoric acid, 20% nitric acid, 10% water, at 20 volts and 0°C was successful for the Al-Mn but not for the other alloys. The other electrolyte used that was the most promising, was a 10% perchloric acid, 10% glycerol, 70% ethyl alcohol, 10% water solution at -10°C and at 15 to 20 volts. Specimens polished with this latter solution, produced good foils with some large thin areas.

To ensure that the window technique was not deforming the specimens several fully annealed specimens were examined. Another test specimen was prepared from a cold worked material to see if many dislocation tangles were unpinned in the polishing as few were seen in the foils examined, prepared from the extruded material. This test proved that polishing did not excessively unpin tangles as was first supposed.

The subgrain size measurements taken were all from transverse specimens photographed as these produced most reproducible results. There was no appreciable difference in size across the transverse section so only one specimen per extrusion was examined.

4.5.5 Partially extruded billets

The flow pattern of the compacted billet during extrusion was observed by polishing and etching a sectioned partially extruded billet.

However, due to the fine nature of the grain size within the billet the flow was not distinctly visible as previously found by Raybould[68]. To overcome this, a billet was prepared that contained copper foil discs within the compact placed approximately 10mm apart. The extrusion was then performed and stopped just after the maximum load was attained. The remaining compact was then removed from the container, cooled, sectioned, then polished. The position of the copper grids seen, formed during the extrusion process indicated the type of flow pattern.

CHAPTER 5

Results

The fully correlated experimental results are tabulated in the appendices and include the mechanical properties determined of the extruded products from tensile tests at room temperature and 400°C. All the straight line graphs were drawn after calculating the gradient using the linear regression technique (see Appendix II)

For convenience the following notation was used,

aluminium powders - A, B, C and D,

aluminium-manganese - J, aluminium-iron - L, and

aluminium-magnesium-zinc - K.

5.1 Powder properties

5.1.1 Powder sieve analysis

The size distribution of the aluminium powders was determined by sieving and the results are presented in tabular form, tables 5.1 to 5.6. The figures shown represent the mean values of 7 or 8 sieving operations.

5.1.2 Powder chemical analysis

The natural oxide content of the powders was determined using the method previously described and the results are included in the size distribution tables. These give an indication of the oxide content for a particular size fraction.

Alloy compositions found by analysis are shown in table 5.7 including some commercial aluminium powders. For the alloys, J, K and L,

TABLE 5.1

Material	Size m	Wt %	Wt % Al_2O_3
A	- 45 22 (mean size)	100	1.9

TABLE 5.2

B	+ 105	9.7	0.55
	- 105 + 75	23.4	0.65
	- 75 + 63	12.6	1.1
	- 63 + 53	21.5	1.3
	- 53 + 45	11	1.8
	- 45	21.8	1.9

TABLE 5.3

C	+ 500	6.38	2.5
	- 500 + 250	15.4	0.6
	- 250 + 150	17.33	0.4
	- 150 + 105	27.24	0.5
	- 105 + 75	13.66	0.5
	- 75 + 63	6.48	0.7
	- 63 + 53	2.26	1
	- 53 + 45	3.22	1.3
	- 45	7.48	1.9

TABLE 5.4

Material	Size m	Wt %
J	+ 250	7.15
	- 250 + 150	35.8
	- 150 + 105	11.07
	- 105 + 75	10.12
	- 75 + 63	14.6
	- 63 + 45	9.15
	- 45	12.3

TABLE 5.5

K	+ 250	9.92
	- 250 + 150	19.1
	- 150 + 105	18.3
	- 105 + 75	16
	- 75 + 63	10.15
	- 63 + 45	14.05
	- 45	12.5

TABLE 5.6

L	+ 250	1.82
	- 250 + 150	4.13
	- 150 + 105	7.85
	- 105 + 75	41.2
	- 75 + 63	15.2
	- 63 + 45	13.8
	- 45	15.35

TABLE 5.7

Chemical Analysis

Material	Al_2O_3 Wt %	Si Wt %	Mg Wt %	Fe Wt %	Cu Wt %	Mu Wt %
Aluminium A	1.9	100 ppm	2 ppm	5 ppm	5 ppm	5 ppm
Aluminium B	1.1	500 ppm	5 ppm	10 ppm	15 ppm	20 ppm
Aluminium C	0.26	500 ppm	5 ppm	15 ppm	20 ppm	20 ppm
Al-Mn J	(9.50)	0.09	50-100 ppm	0.49	0.01	3.59 %
Al-Mg-Z K						
Al-Fe	(10.94)	0.3	100 ppm	2.38	0.13	300-500 ppm
Alcoa 601 AB	0.52	0.27	0.83	0.16	-	-
P/M M P3	0.28	0.03	0.02	0.12	-	-
Alcan 120	0.94	0.03	0.005	0.42	-	-
Aluminium (C)	0.45	0.1	0.1	0.1	-	-

TABLE 5.8

Powder	BET Value m^2/g	Wt % Al_2O_3
Aluminium A	0.333	1.9
Aluminium B	0.168	1.1

TABLE 5.7(a)

Chemical Analysis

Material	Al_2O_3 Wt%	Si Wt%	Mg Wt%	Zn Wt%	Fe Wt%	Mn Wt%	Cu Wt%
Al-Zn-Mg	0.85	Trace	6.69	1.26	0.24	Trace	Trace
	0.74	"	6.98	0.95	0.26	"	"
	0.94	"	6.85	1.67	0.25	"	"
	0.41	"	6.44	1.50	0.24	"	"
	1.31	"	5.58	2.19	0.24	"	"
	-	0.12	6.5	1.6	0.24	-	-
Al-Fe	0.10	0.18	Trace	Trace	2.38	0.55	0.19
	0.26	0.19	"	"	2.56	0.55	0.19
	1.13	0.17	"	"	2.51	0.59	0.12
Al-Mn	0.75	0.21	Trace	Trace	0.49	3.57	0.01
	0.68	0.19	"	"	0.45	3.49	0.01

the major and minor constituents were determined before the oxide content was found, and the initial results are shown in table 5.7. Later results are shown in table 5.7(a).

5.1.3 Powder compaction

Experiments were conducted to determine the variation of density with applied pressure in the production of powder compacts. These were performed by the method described in the experimental chapter and the height of the compact in the die at a particular applied pressure taken as a function of density at that pressure.

The results are presented in the form of a graph, figure 5.1, of lnP against displacement, where P is the applied pressure. This is similar to the work carried out by Bal'shin[36].

A similar graph is also plotted of P/C* against P after the work by Kawakita[39] in deriving a piston compression equation.

$$C^* = \frac{Vo - V}{Vo} = \frac{abP}{1 + 6P}$$ (see nomenclature for definition of symbols)

$$P/C^* = \frac{1}{ab} + \frac{P}{a} \qquad (5.1)$$

P = applied pressure

C* = degree of volume reduction

Vo = initial apparent volume

V = volume of powder at pressure, P

a,b = constants, characteristic of powder

$C^* \propto dl/l_o$

The results plotted in figure 5.1 are replotted using Kawakita's piston compression equation and are shown in figure 5.2. This figure represents the compaction of a coarse mesh fraction of aluminium powder, C., and figure 5.3 shows the compaction behaviour of the dust mesh fraction from the same aluminium powder, with a value of $1/a$, the gradient, equal to 2.

Figures 5.4 and 5.5 represent the compaction of a sample from the aluminium manganese and aluminium iron alloys respectively. The value of $1/a$, the slope of the graph, is again approximately equal to 2.

5.2 Load ram displacement diagrams

In the experimental section, it was noted that the load was recorded on an X-Y recorder so that an autographic type diagram could be produced. These load ram displacements are of the form shown in figures 5.6, 5.7. Figure 5.6 is the autographic diagram obtained during the extrusion of a powder billet, powder B, at an initial temperature of 300°C and using a reduction ratio of 30:1. Figure 5.7 is a diagram obtained during the extrusion of a commercially pure solid aluminium billet under the same conditions as that of the powder.

5.3 Variation in Mechanical Properties through the Quasi-static Deformation Zone

To investigate the mechanical properties of a compacted billet in different regions, specimens were taken from selected areas and tested at room temperature. The regions used are shown in fig. 5.8 and the results of tensile tests performed are shown underneath. The numbered areas were sawn from the partially extruded billet and

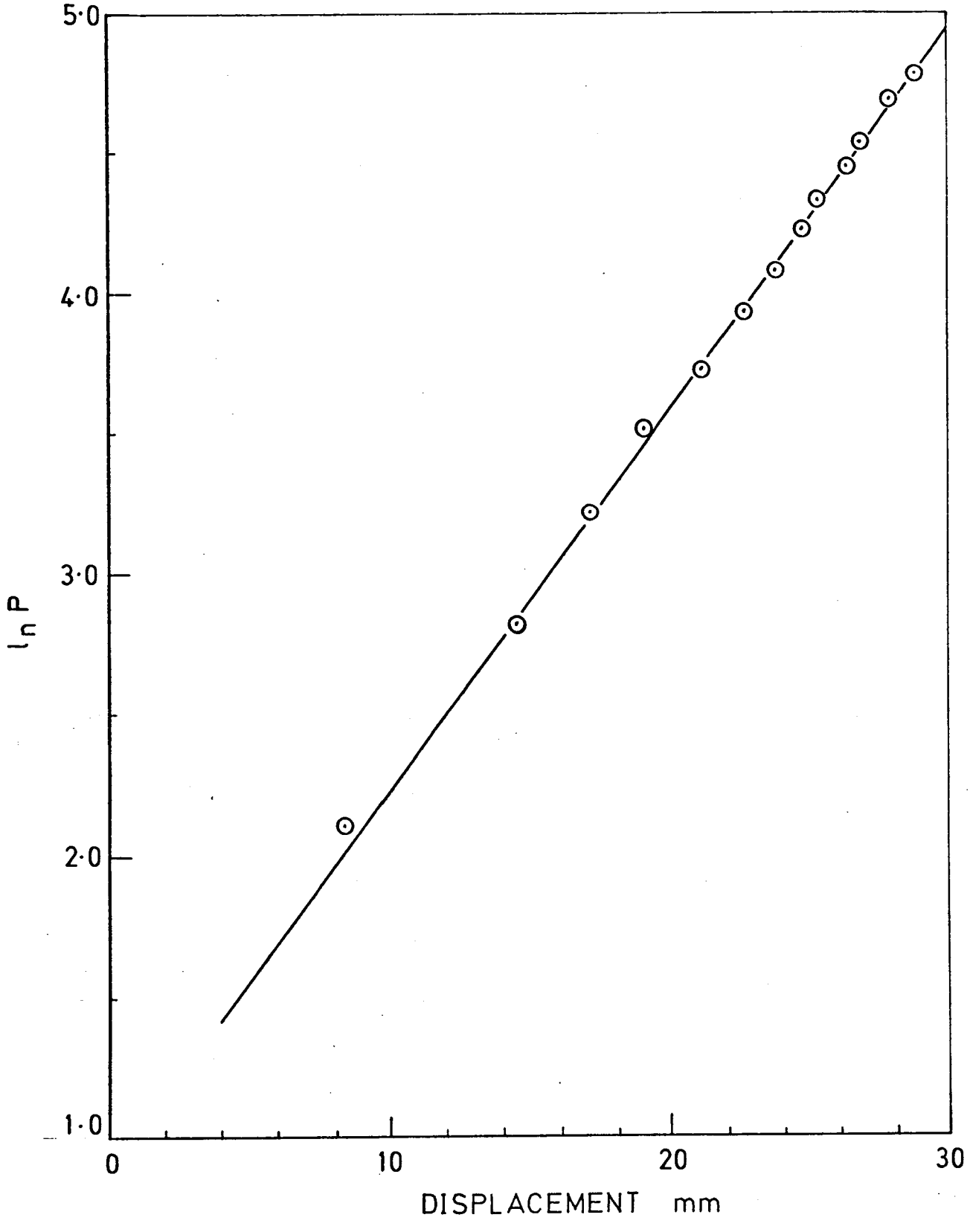

VARIATION OF PRESSURE WITH DISPLACEMENT FOR POWDER B

Fig. 5.1

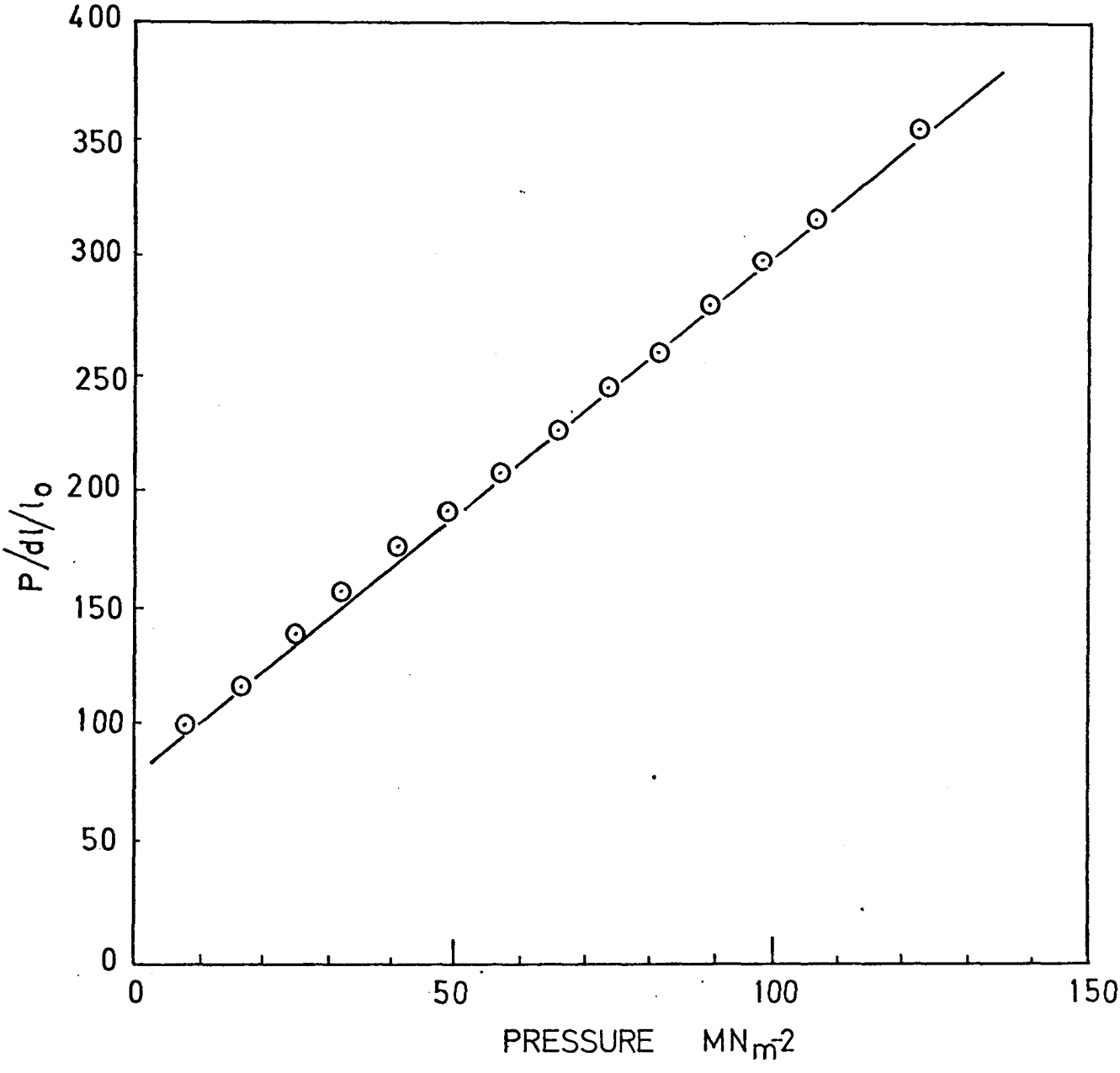

EFFECT OF PRESSURE ON DISPLACEMENT USING KAWAKITA'S EQUATION FOR COARSE MESH FRACTION (22—30 MESH)

Fig 5.2

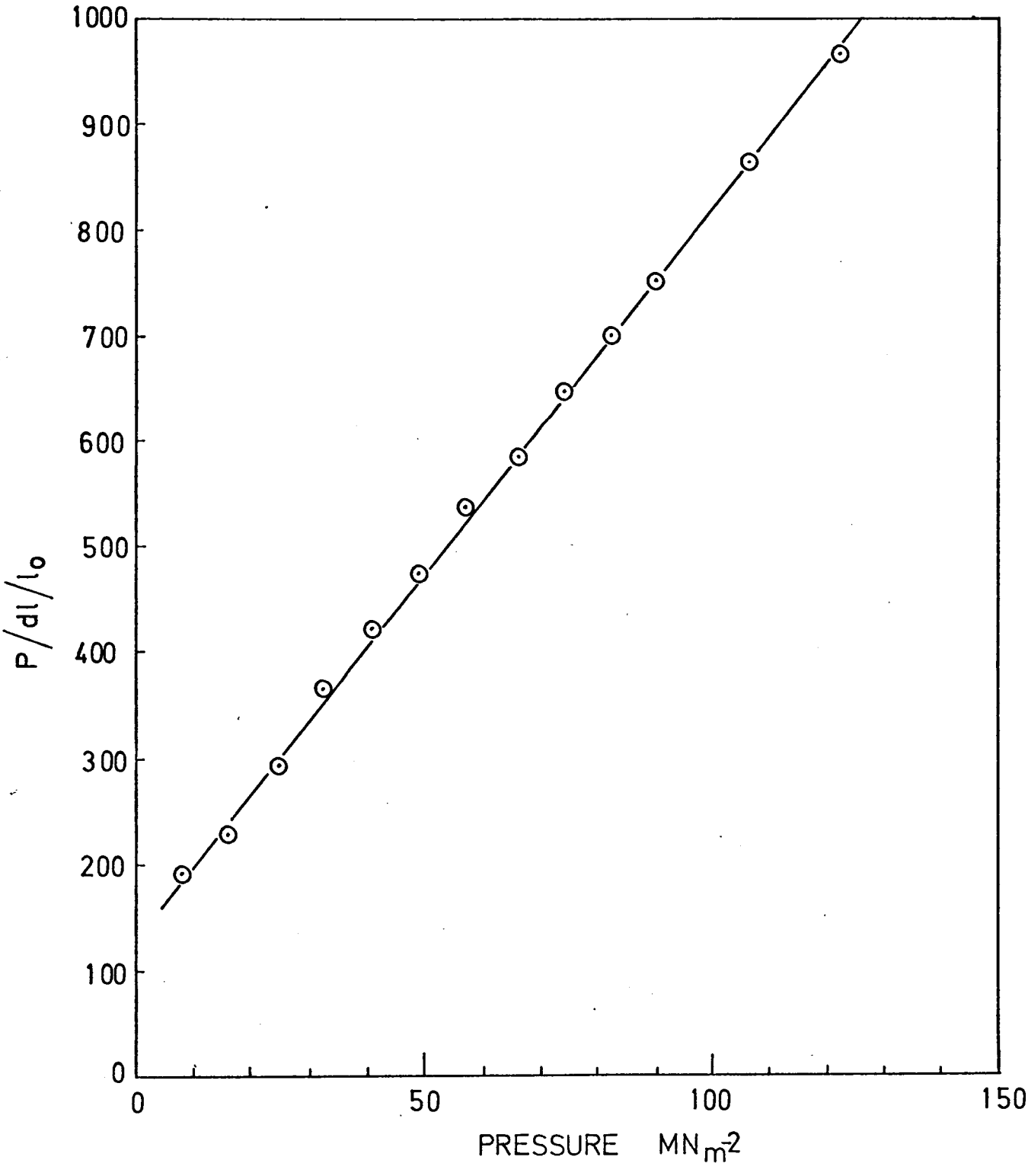

EFFECT OF PRESSURE ON DISPLACEMENT USING KAWAKITA'S EQUATION FOR DUST SIZE

Fig. 5.3

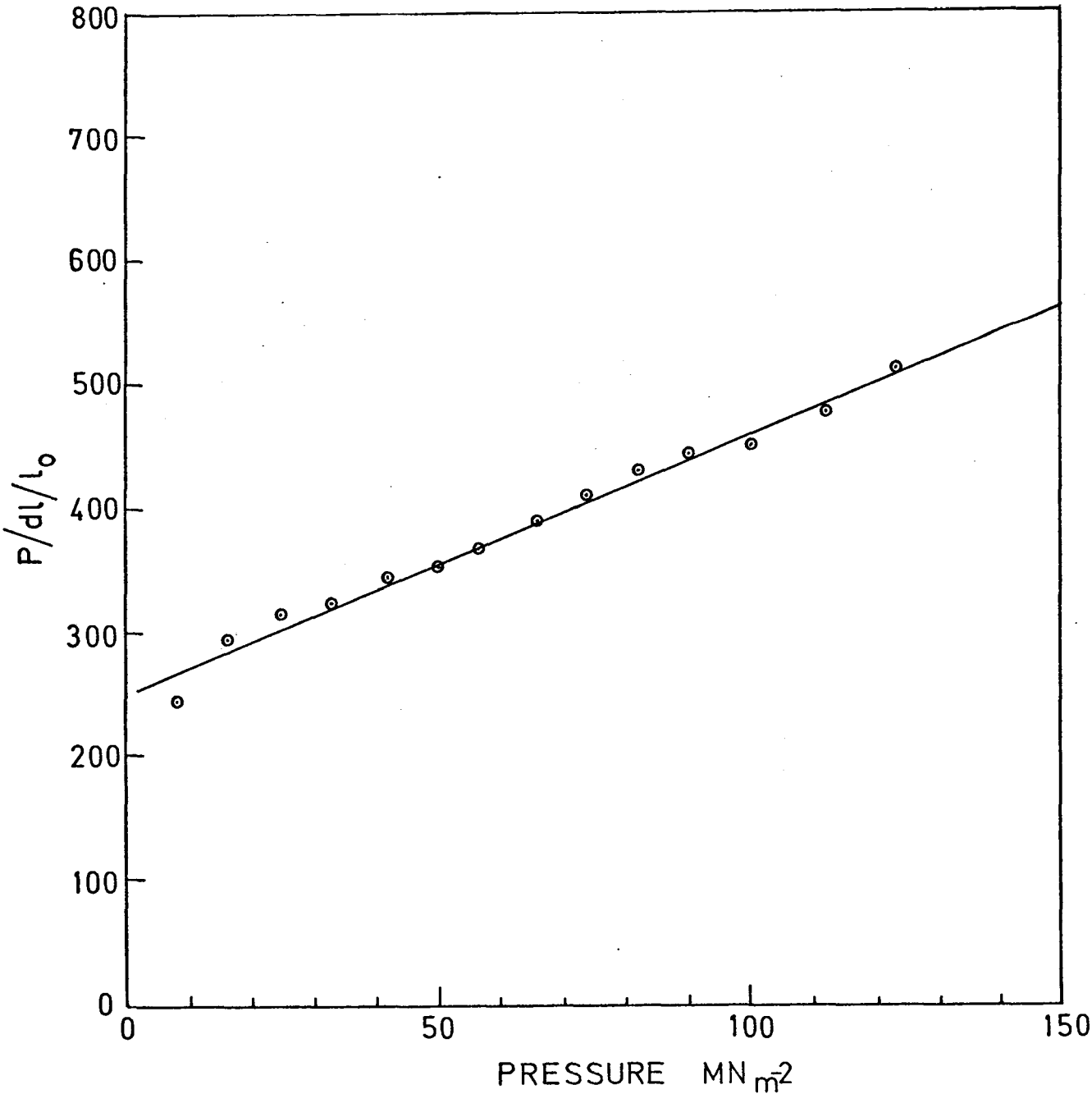

EFFECT OF PRESSURE ON DISPLACEMENT USING KAWAKITA'S EQUATION FOR POWDER J (Al–Mn)

Fig. 5.4

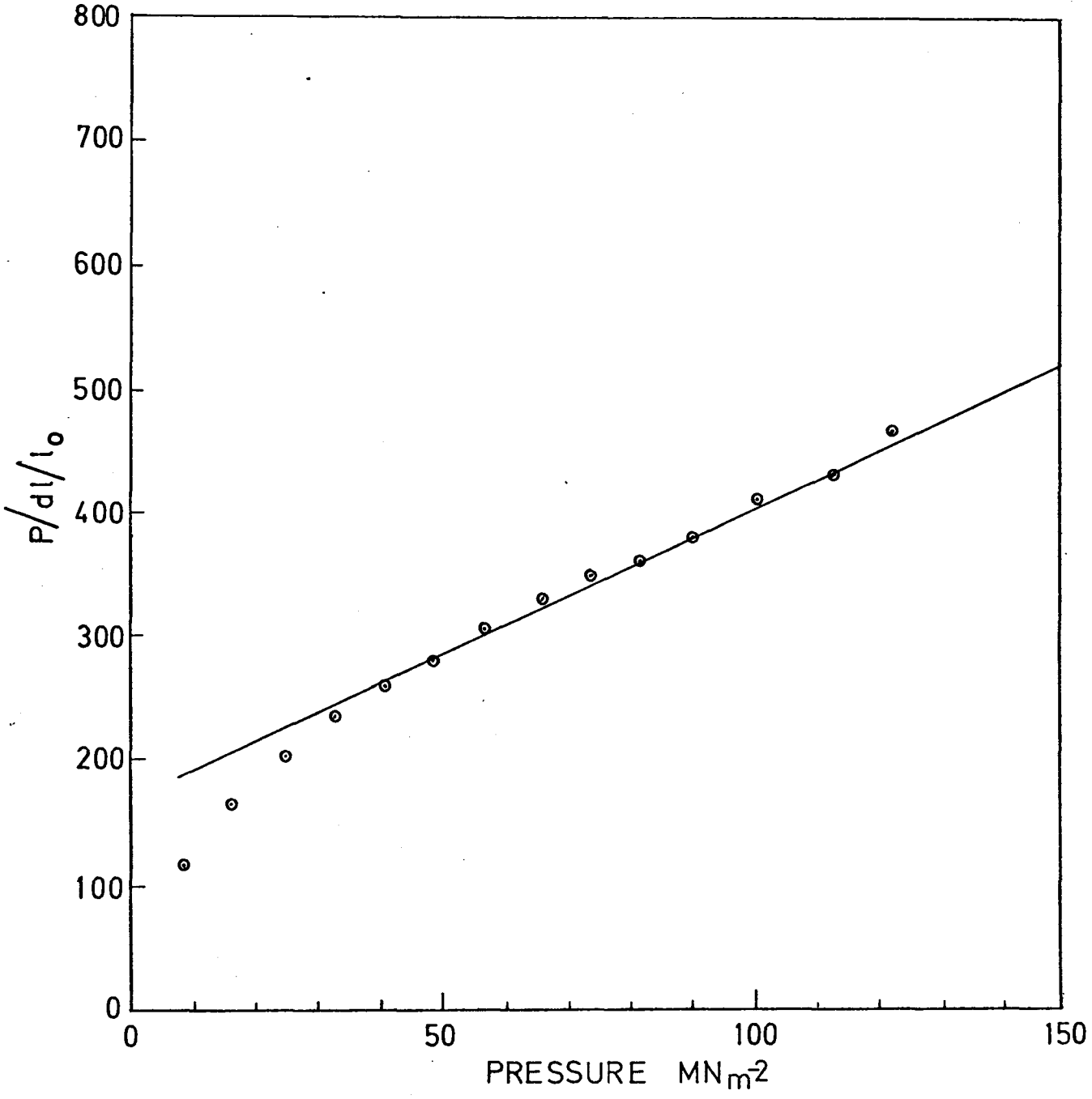

EFFECT OF PRESSURE ON DISPLACEMENT USING KAWAKITA'S EQUATION FOR POWDER L (Al–Fe)

Fig. 5.5

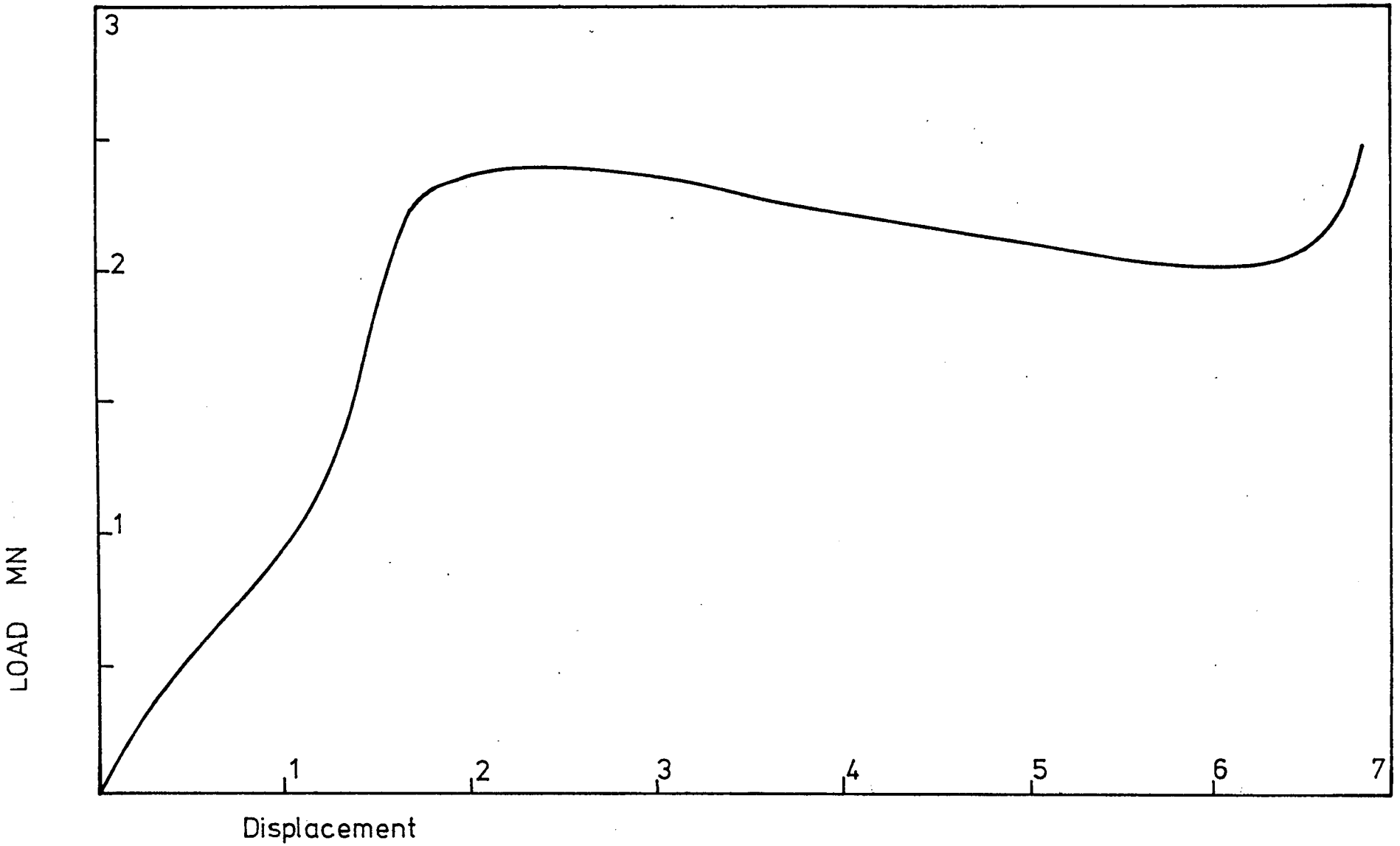

LOAD RAM DISPLACEMENT FOR THE POWDER BILLET (B POWDER)

FIG 5.6

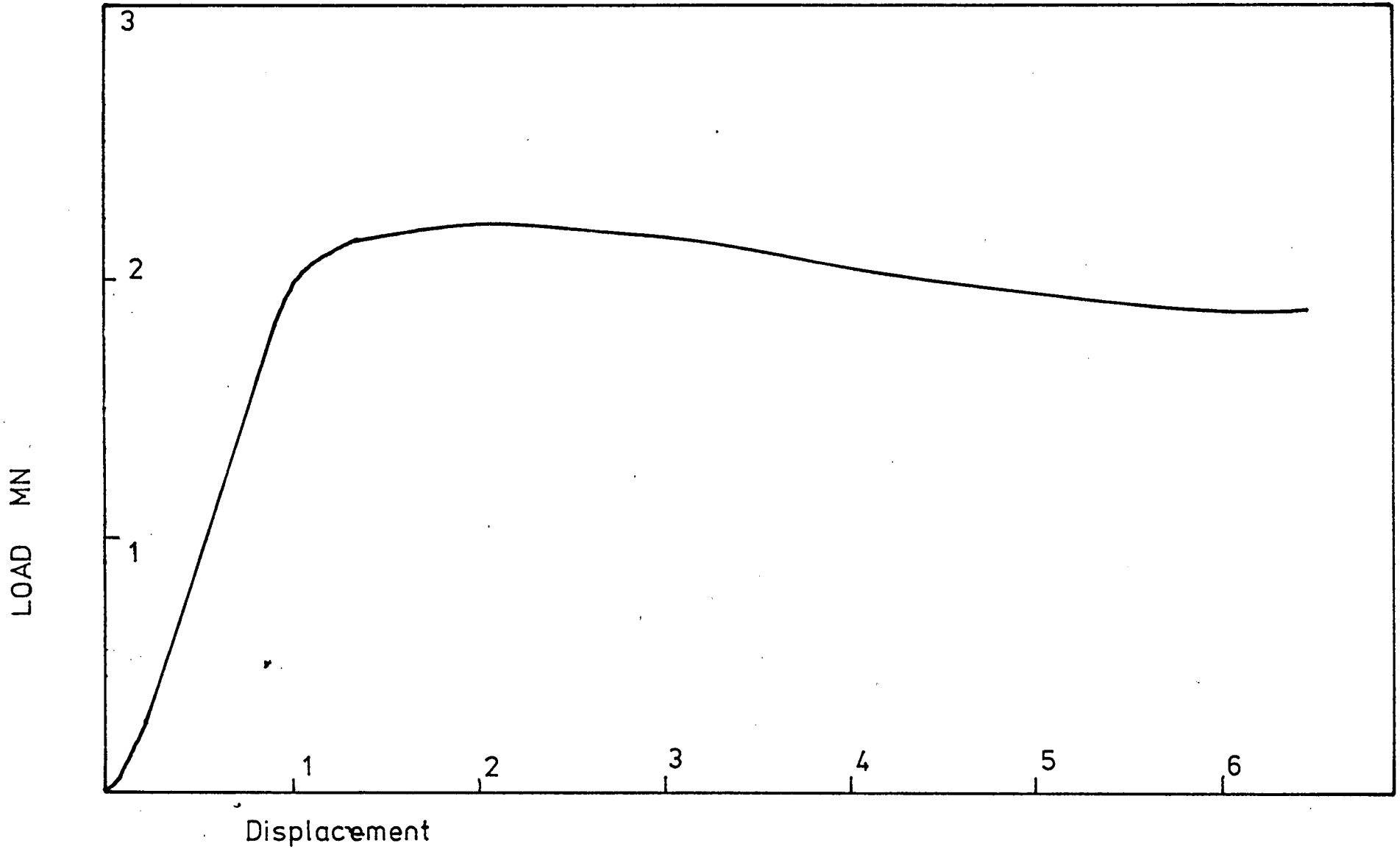

LOAD RAM DISPLACEMENT FOR THE ALUMINIUM BILLET

FIG 5.7

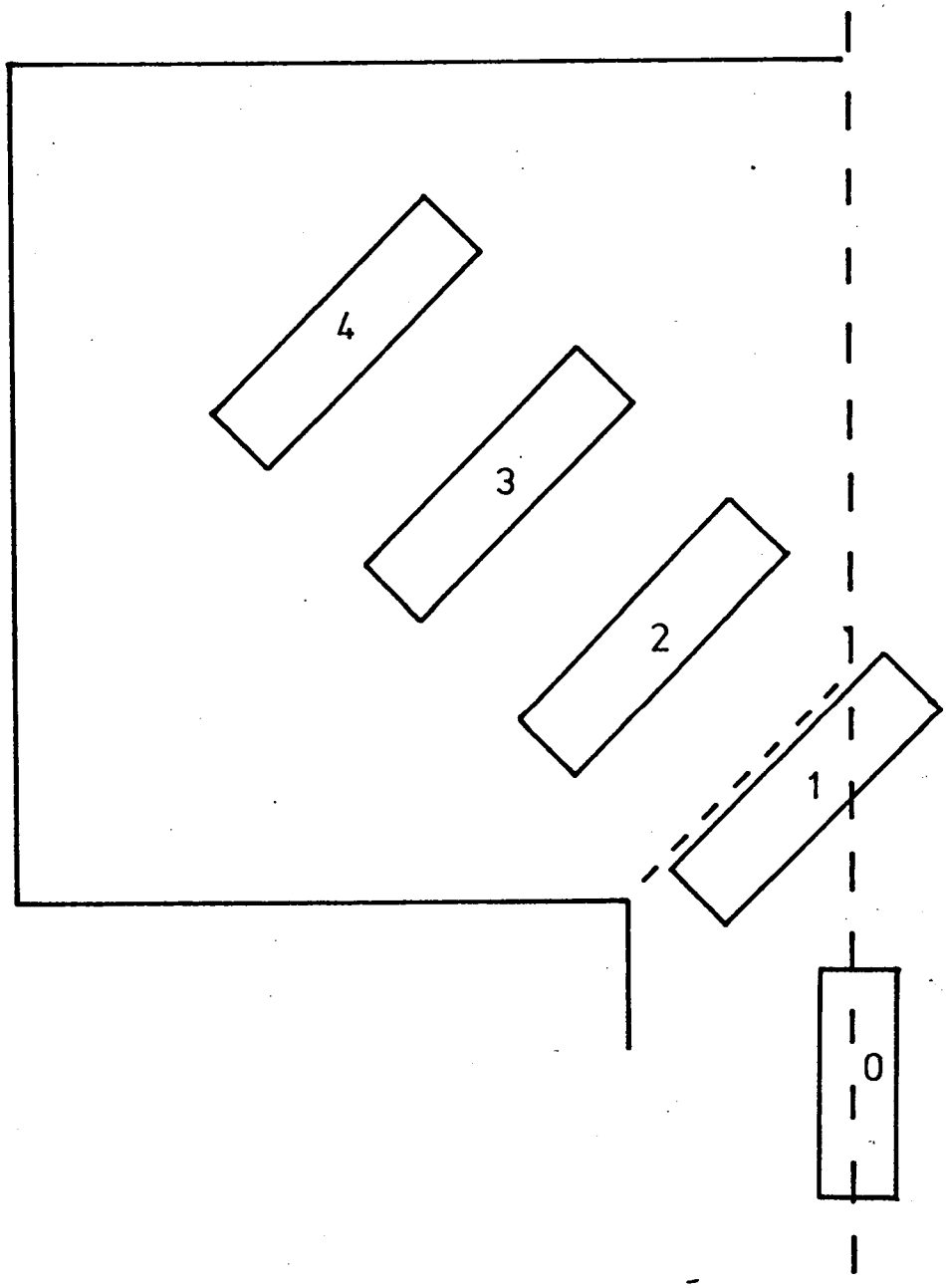

No	0.2% Proof Stress	Tensile stress	% Elong
0	248.8	410.4	16.8
1	215.8	358.9	15.3
2	199	301.6	5.6
3	187	239	3.6
4	180.3	211.4	2.72

Mechanical properties of different regions in the compact, indicated by the numbered regions.

Fig 5.8

machined down to the smallest Hounsfield specimen size, number 12.

5.4 Extrusion parameters

5.4.1 Compaction

The load ram displacement diagrams can be divided into two distinct regions:

(i) the compaction region

(ii) the extrusion region

The loads recorded at the end of the compaction region prior to extrusion, are measured from the diagrams and converted into a pressure term. Fig. 5.9 is a plot of lnP against temperature for the aluminium powder, B, where P is the compaction pressure measured from the diagrams.

The pressure to attain near theoretical density before extrusion commences can be related thus:

$$\ln P = 6.56 - M'T \qquad (5.2)$$

where P is the maximum pressure measured

T is the temperature in ^{o}K

m' is dimensioned constant = $2.25 \times 10^{-3}\ T^{-1}$

The extrusion pressure at the end of steady state extrusion can be related to the redundant deformation and reduction ratio in the normal way, thus:

$$\frac{P}{Ym} = 0.81 + 1.2 \ln R \qquad (5.3)$$

where Ym is the mean yield stress

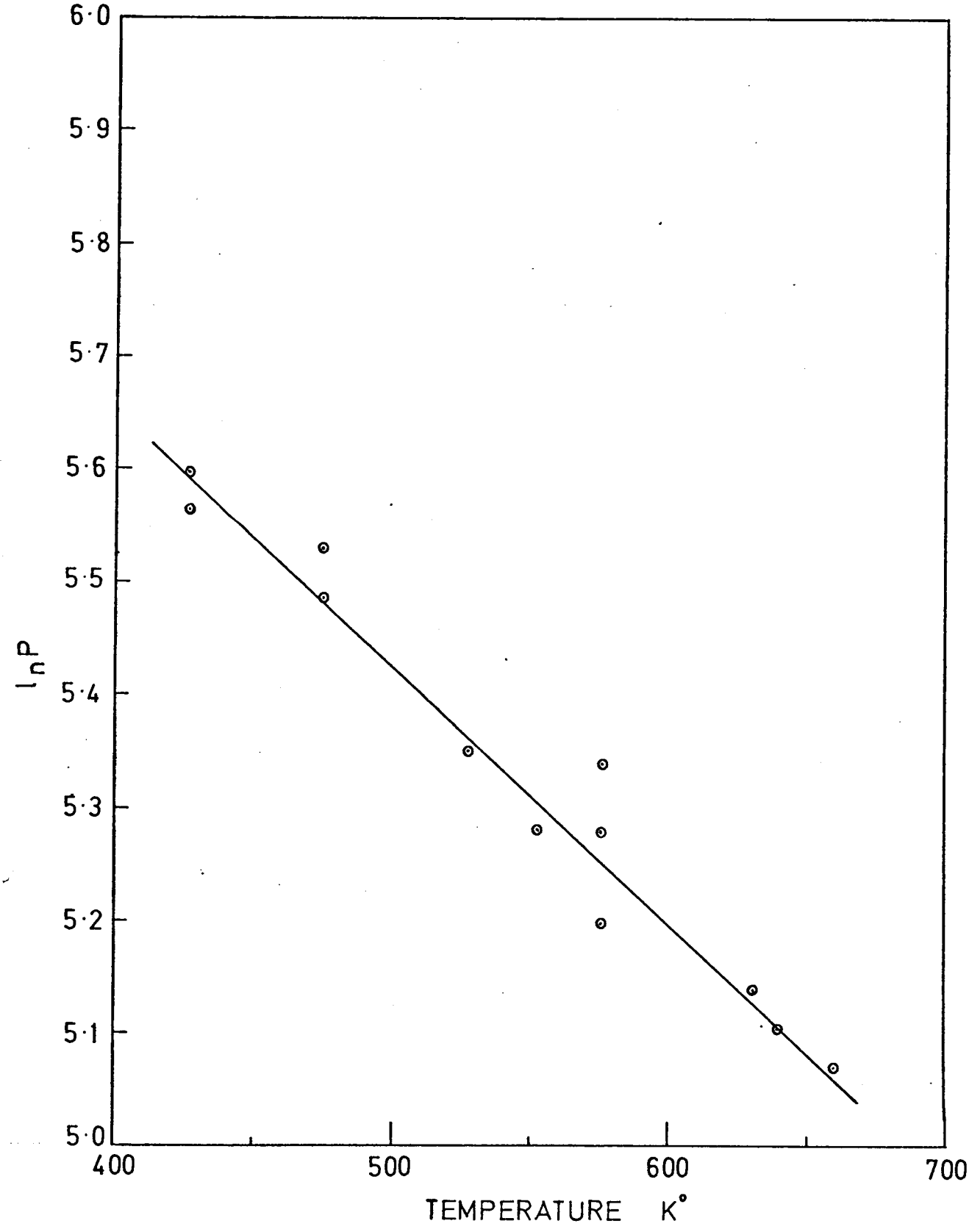

VARIATION OF COMPACTION PRESSURE WITH TEMPERATURE

Fig. 5.9

5.4.2 Extrusion load

The maximum recorded load during extrusion for each experiment is changed into a pressure, MNm^{-2}, and the results are shown in the appendix tables under extrusion pressure.

The loads for the determination of the mean yield stress for the activation energy plots are taken from the autographic diagrams at the end of steady state extrusion prior to the coring point.

5.4.3 Initial billet temperature

The initial billet temperature was measured by means of a thermocouple passed through the back-up pressure pad pressed onto the surface of the rear end of the billet. These temperatures measured thus, yielded the temperatures at the start of extrusion. Figs. 5.10 to 5.13 show the effect of initial billet temperature on the maximum recorded extrusion pressure for the different materials investigated.

5.4.4 Reduction ratio

In order to determine the relationship between reduction ratio and extrusion pressure, extrusions were performed at different ratios under the same conditions to satisfy the well known equation

$$\frac{P}{Ym} = A + B\ln R \qquad (5.4)$$

The results are shown in fig. 5.14 and the pressure values are those indicated at the end of steady state extrusion. This eliminates the frictional effect arising from billet length.

5.4.5 Limit diagrams

Limit diagrams of the type produced by Hirst and Ursell were constructed using experimental results, and the equations shown in

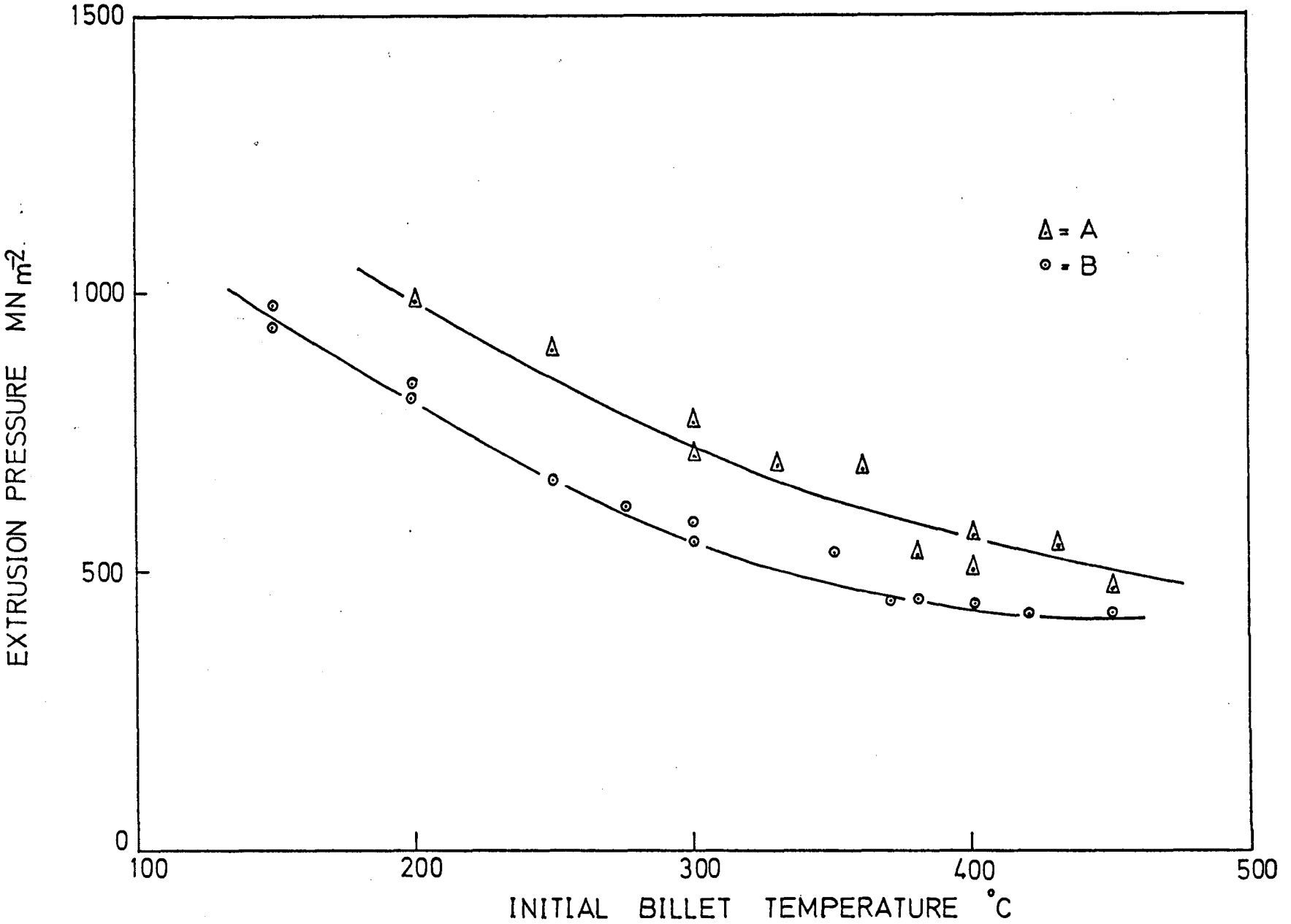

VARIATION OF EXTRUSION PRESSURE WITH TEMPERATURE FOR THE ALUMINIUM POWDERS A AND B

Fig. 5.10

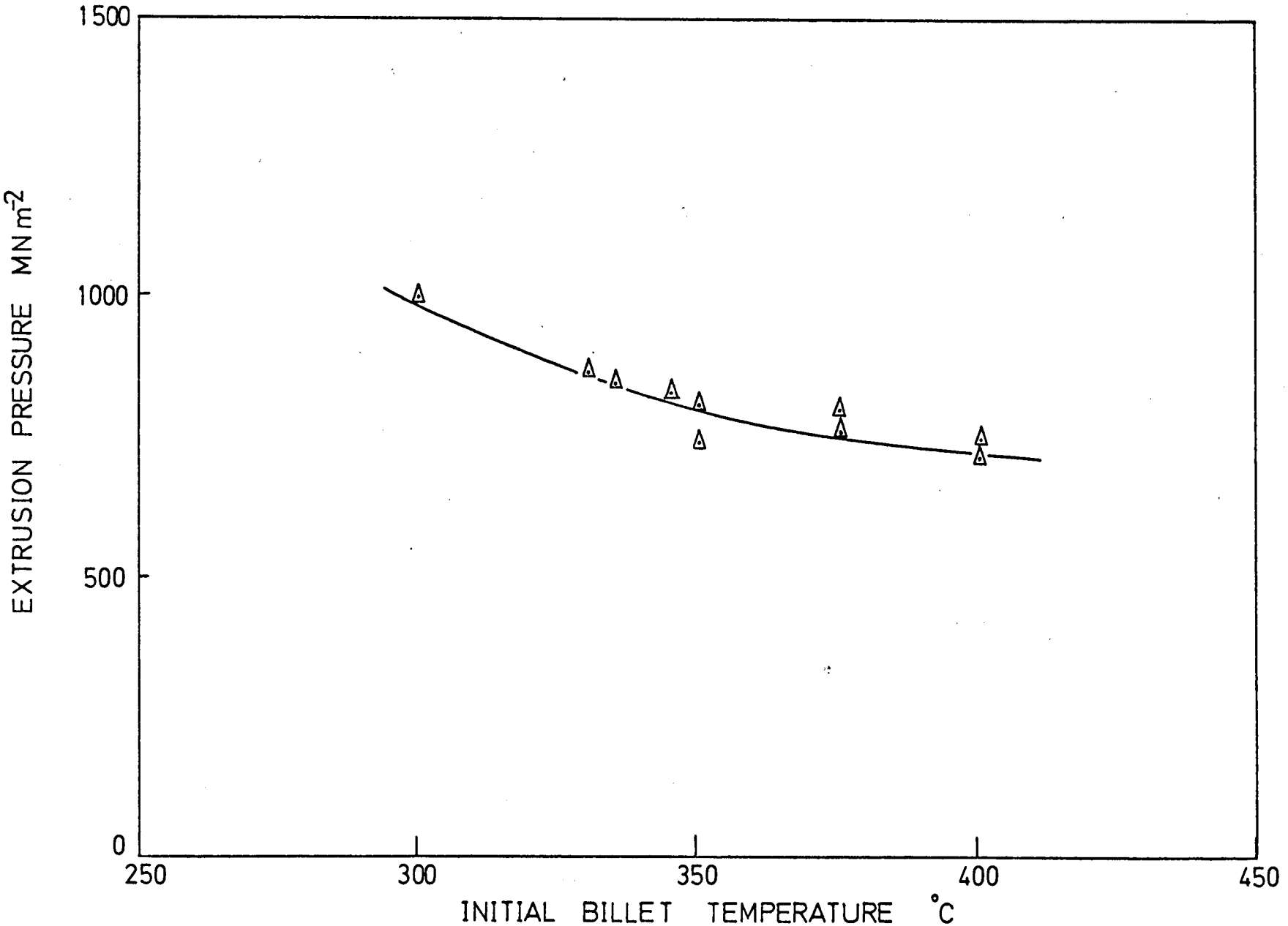

VARIATION OF EXTRUSION PRESSURE WITH TEMPERATURE FOR THE Al – Mn ALLOY

Fig 5.11

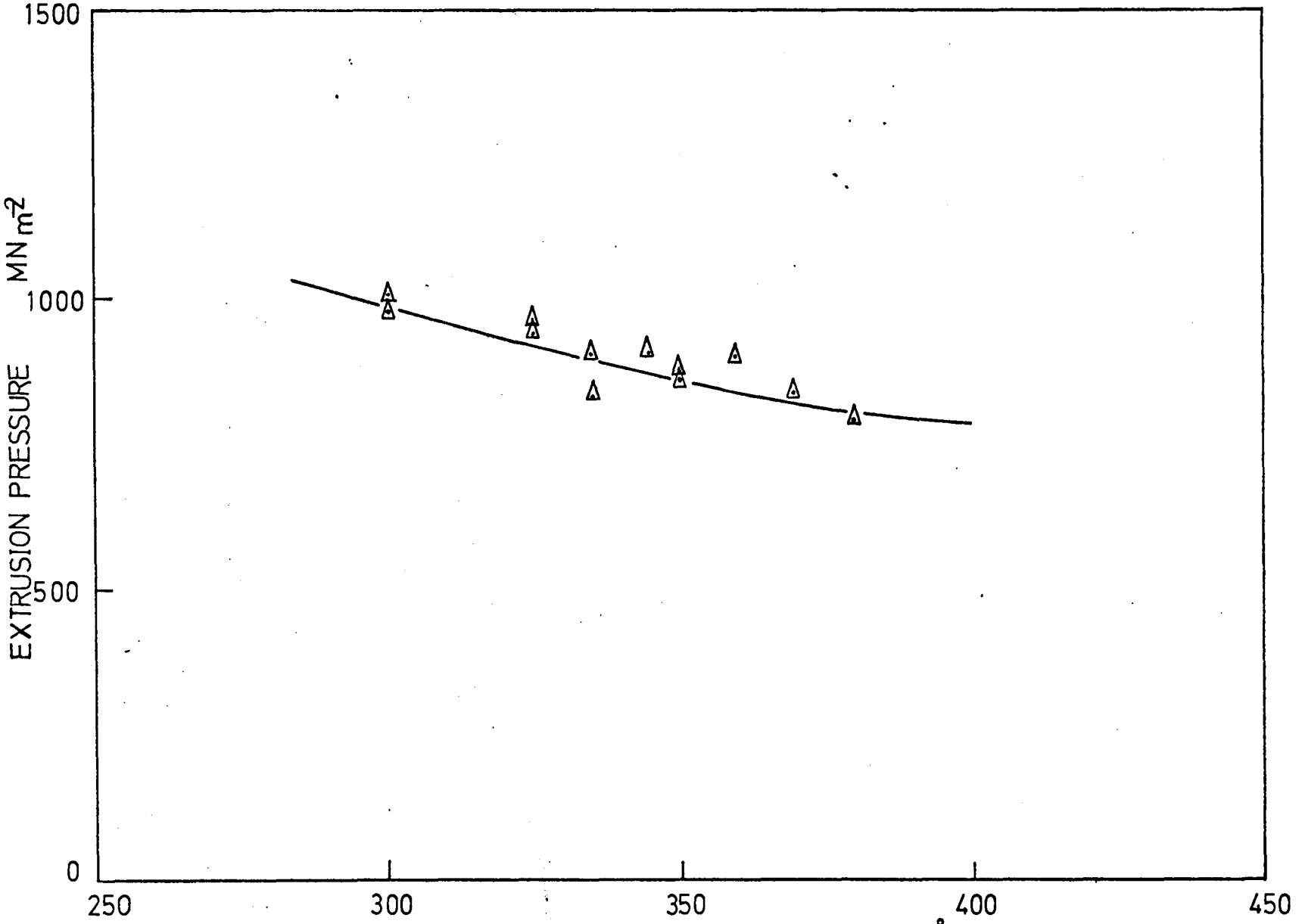

VARIATION OF EXTRUSION PRESSURE WITH TEMPERATURE FOR THE Al—Mg—Zn POWDER

Fig. 5. 12

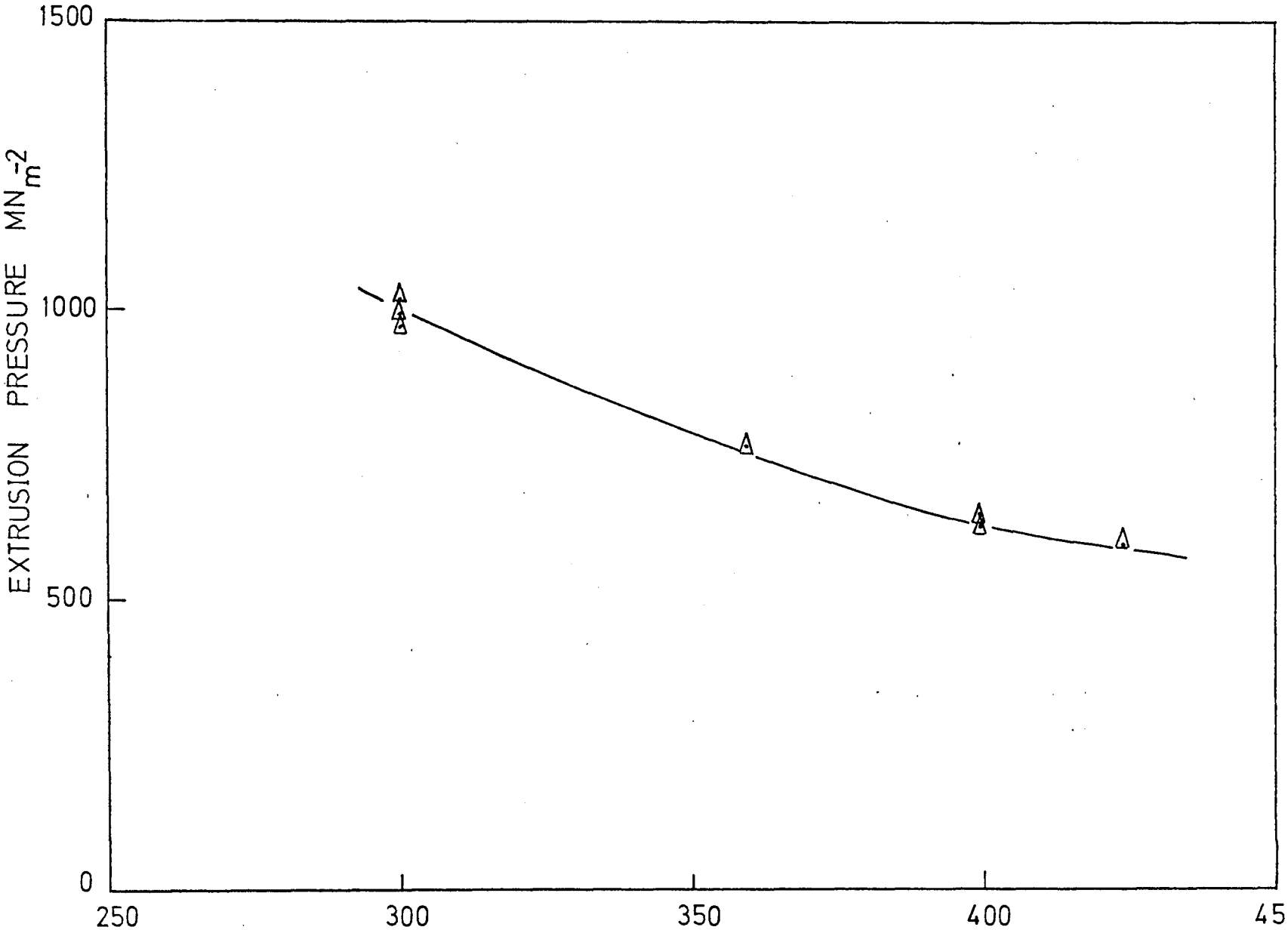

VARIATION OF EXTRUSION PRESSURE WITH TEMPERATURE FOR THE Al–Fe POWDER.

Fig 5.13.

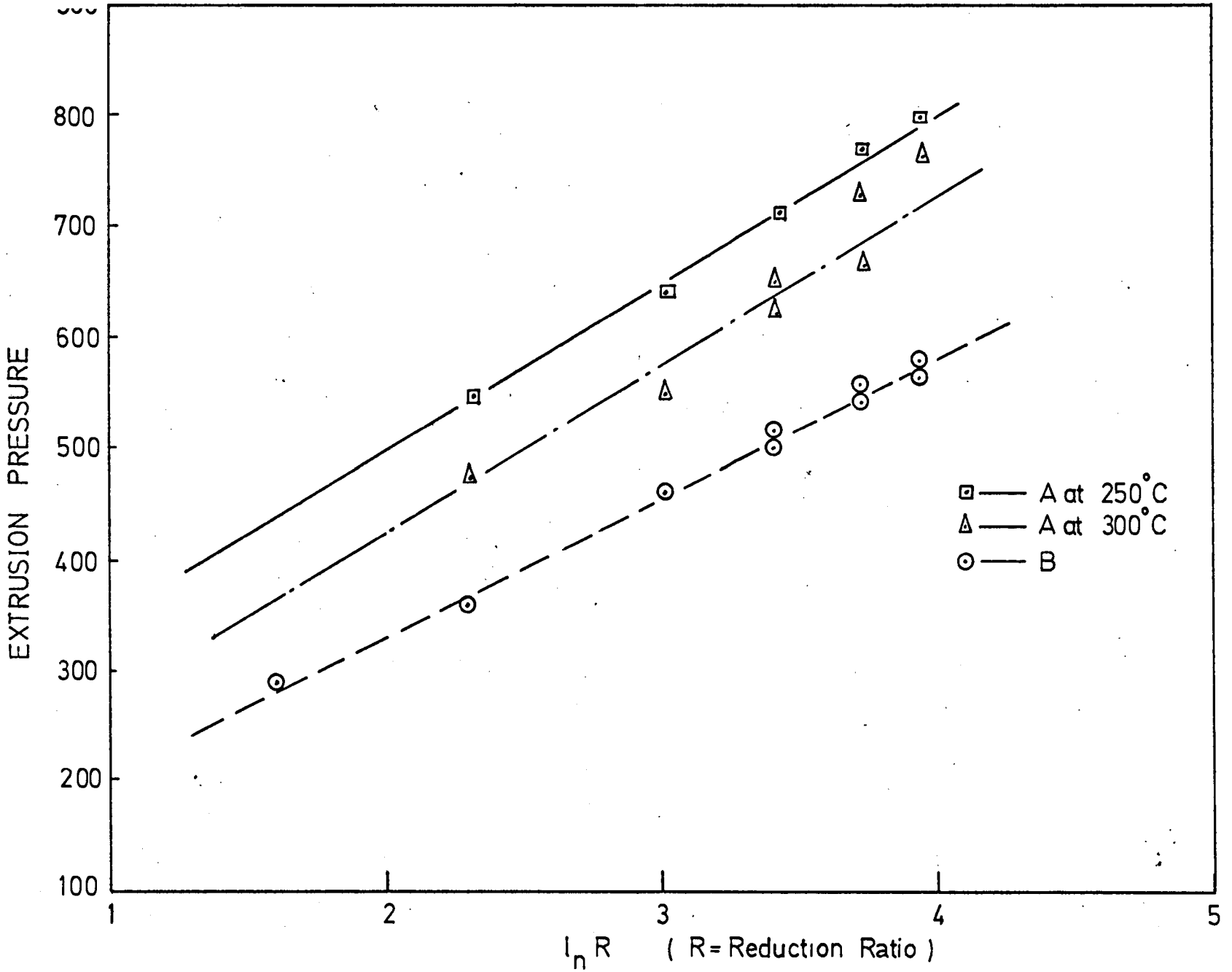

PLOT OF EXTRUSION PRESSURE AGAINST $l_n R$

Fig 5.14

the theory section. The fiction coefficient at a particular temperature was determined using the method previously described, i.e.:

$$\mu = \frac{D}{4(l_1 - l_2)} \ln \frac{P(l_1)}{P(l_2)} \qquad (5.5)$$

Two billets of lengths l_1 and l_2 were extruded through the same die showing mean pressures $P(l_1)$ and $P(l_2)$ respectively. Alternatively two points were taken on the steady state portion of the load curve and the two loads obtained related to billet length hence the friction determination.

The limit due to melting caused under adiabatic conditions is calculated using the equation of the form:

$$\ln R = \frac{4\mu l/D \, C_H (T - To) \rho}{4.43 \gamma_m \{\exp[4\mu l/D_c] - 1\}} - 0.39 \qquad (5.6)$$

This gives the maximum extrusion ratio possible for a given temperature rise T - To at infinite speed, without incipient melting occurring. The limit for a given temperature rise at a finite strain rate, $\dot{\varepsilon} = 11 \, sec^{-1}$, is calculated using the above equation.

The theoretical temperature rise for a particular strain rate is estimated using the method described in the theory by Raybould[68]. Again it must be iterated that this value is a mean overall value and not representative of local temperature rises.

The limit diagrams for the extrusion press used, and the materials considered, are shown in figures 5.15 to 5.18.

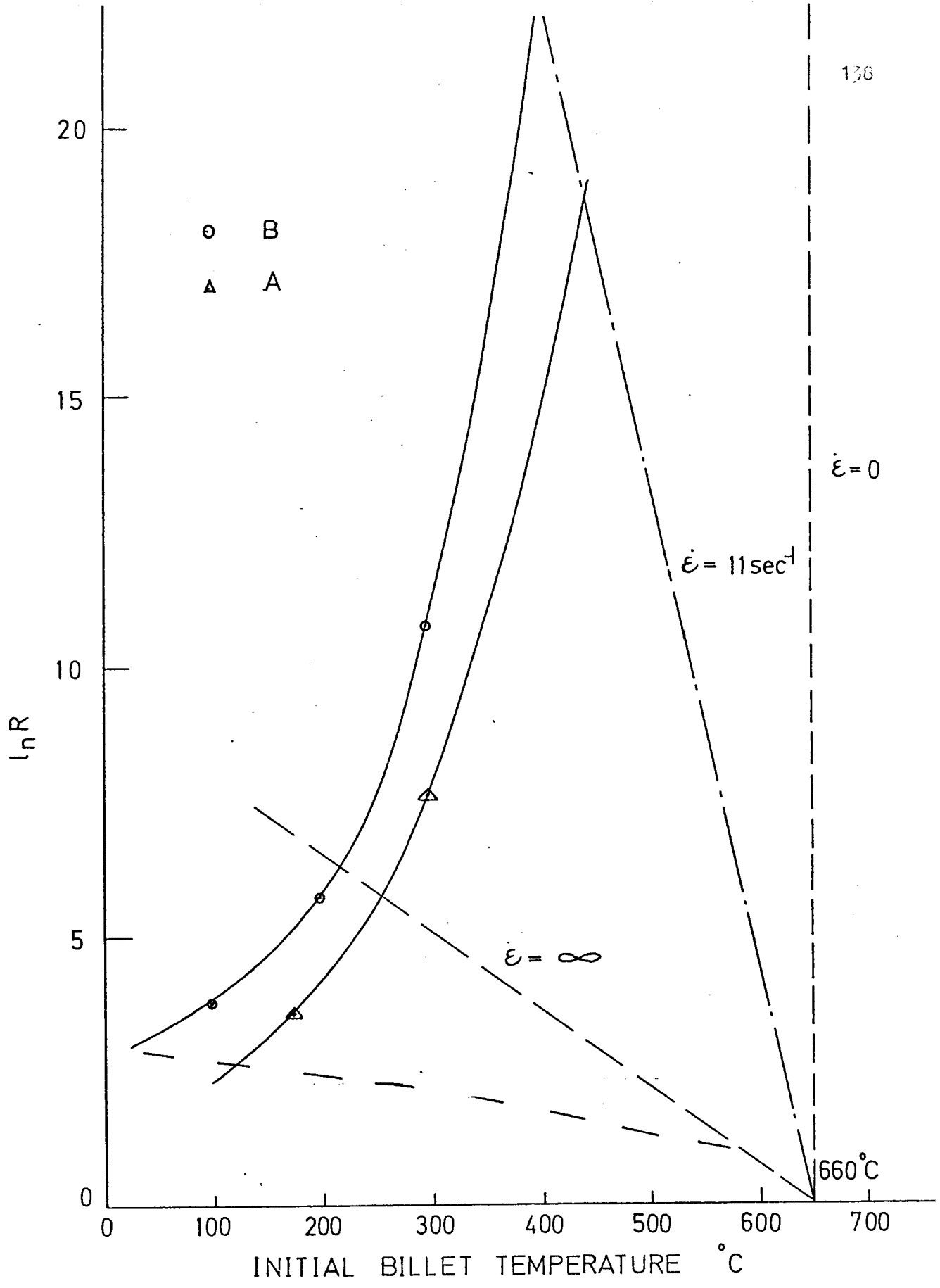

LIMIT CURVE FOR THE EXTRUSION OF Al POWDER

Fig. 5.15

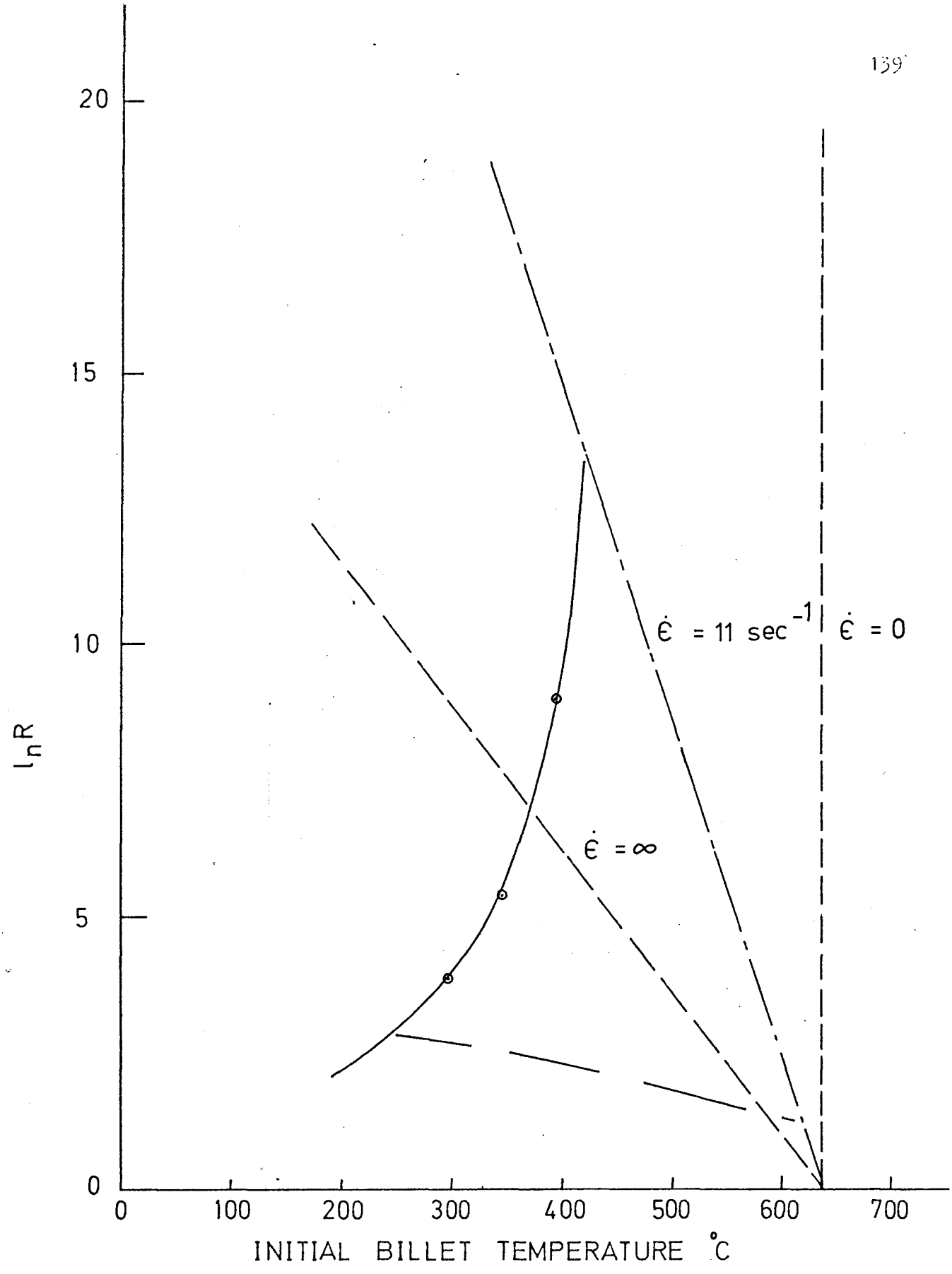

LIMIT CURVE FOR THE EXTRUSION OF THE Al–Mn POWDER

Fig. 5.16

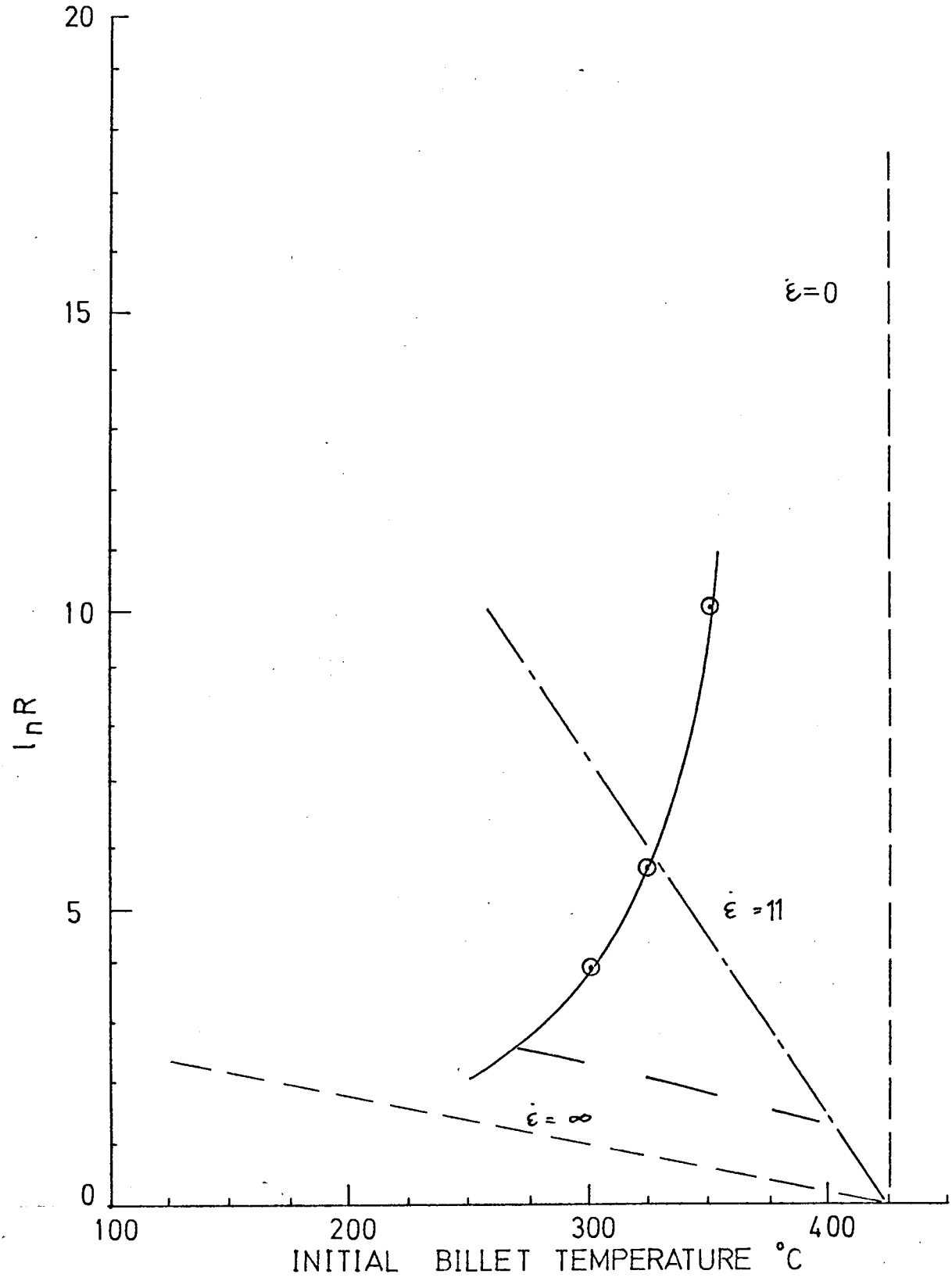

LIMIT DIAGRAM FOR THE EXTRUSION OF THE Al—Mg–Zn ALLOY.

Fig. 5. 17.

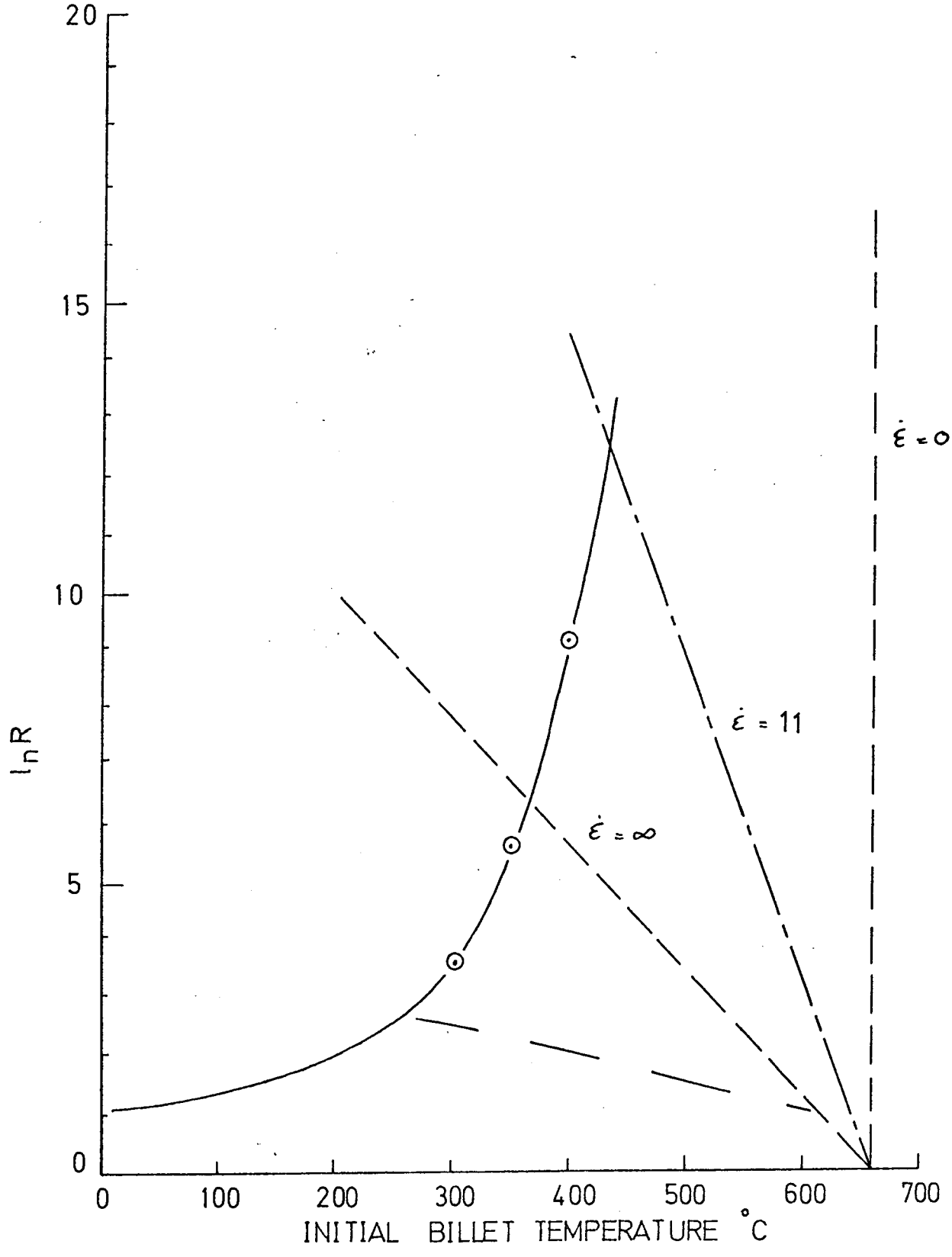

LIMIT DIAGRAM FOR THE EXTRUSION OF THE Al–Fe ALLOY.

Fig. 5.18

5.5 Activation Energy

The activation energy was obtained by using the relationship proposed by Garofalo[83] for creep and applied to hot working by Sellars and Mc. G. Tegart[84].

$$\dot{\varepsilon} = F^* \sinh(\alpha\sigma)^n \exp -\Delta H/R'T \qquad (5.7)$$

The value of α must be determined and this is accomplished by using the stress strain relationship shown to hold for creep.

$\dot{\varepsilon} = A_2 \sigma^n$ for low stress levels

$\dot{\varepsilon} = A_3 \exp(\beta\sigma)$ for high stress levels

These equations approximate to the sinh relationship at low and high stress values.

At high stress values $\dot{\varepsilon} = A_4(\sinh\alpha\sigma)^n = \frac{A_5}{2^n} \exp(n\alpha\sigma)$

and $n\alpha = \beta \qquad \therefore \alpha = \frac{\beta}{n}$

At low stress values $\dot{\varepsilon} = \sigma^n$

so $n = \ln\dot{\varepsilon}/\ln\sigma$

and for $\alpha\sigma = 1.2$ $\beta = \ln\dot{\varepsilon}/\sigma$

if $n = n'$, $\alpha = \beta/n'$

Constant values of n' and α are obtained for the aluminium powders and are shown in table 5.9.

The activation energy is calculated using the techniques suggested by Jonas, i.e.

$$\left[\frac{(\log \sinh(\alpha\sigma)}{1/T}\right]_{\dot{\varepsilon}} \times \left[\frac{\log\dot{\varepsilon}}{\log\sinh(\alpha\sigma)}\right]_T = 2.303\frac{\Delta H}{R'T} \qquad (5.8)$$

The values of log sinh ($\alpha\sigma$) versus $1/T$ for a particular strain rate were plotted using the values of α obtained from the experiments and also the value used by Jonas. The slopes obtained are denoted s*. Stress exponents for strain rate are obtained by plotting log $\dot{\epsilon}$ against log sinh$\alpha\sigma$. Activation energy values for a particular temperature could be calculated using equation (5.8).

In order to compare the values of n and s*, Jonas suggested using a constant value of α, this being 0.0435 m^2MN^{-1}. The activation energies are then recalculated using the same procedure as before. The graphs of log $\dot{\epsilon}$ versus log sinh$\alpha\sigma$ are shown in figures 5.19 - 5.25, and the plots of log sinh$\alpha\sigma$ versus $1/T$ in figures 5.26 - 5.27.

Having obtained the values for ΔH, the activation energy, it was then possible to plot Z, the Zener Holloman parameter, where $Z = \dot{\epsilon} \exp(\Delta H/RT)$, against ln sinh$\alpha\sigma$ figures 5. The resulting straight line relationship for the two aluminium powders and the Al-Mn alloy shows that the same basic recovery mechanism occurs for the alloys. For the Al-Mg-Zn powder the line is steeper showing a different recovery mechanism.

The plots of sinh$\alpha\sigma$ against $1/T$ for the two reduction ratios 30:1 and 5:1 give good agreement showing that the value of $\dot{\bar{\epsilon}}$, the mean strain rate, is consistent.

Table 5.10 includes the results of tensile tests performed at different strain rates. The results are plotted out in fig. 5.24 and the activation energy results shown in table 5.9.

TABLE 5.9

MATERIAL	n'	n	α	β	s	A	ΔH k.cals.
A	21.5	20.5 6.25 4.14	.0047 .0435 .0402	.097	.376 1.32 1.63	20.81 6.42 -	35.6 ±3 37.6 ±3 30.77±3
Tensile tests		4.17	.0435		1.83		34.8 ±3
B	22.3	21.5 6.2 4.14	.0044 .0435 .0381	.092	.394 1.33 1.55	19.9 8.24 8.75	34.65±4 36.5 ±3 30.26±3
Tensile tests		4.42	.0435		1.687	8.52	35.65
B (5:1)	20.7	21.9 6.3 4.14	.0045 .0435 .038	.094	.394 1.35 1.55	20.21 5.1 -	36.9 ±3 37.4 ±3 30.3 ±3
J	29.2	27.4 6.09 4.14	.0043 .0435 .0485	.117	.295 1.39 1.56	23.4 4.14	36.9 ±2.5 37.7 ±2.5 28.5 ±3
Tensile tests		3.85	.0435		1.91	5.85	33.3 ±3
K	12.15	12.06 2.64 4.14 1	.0042 .0435 .0209 .0435	.048 - - -	.645 2.51 1.196 3.85	17.8 9.35 - -	33.4 ±3 30.1 ±3 22.6 ±3 28.1 ±3

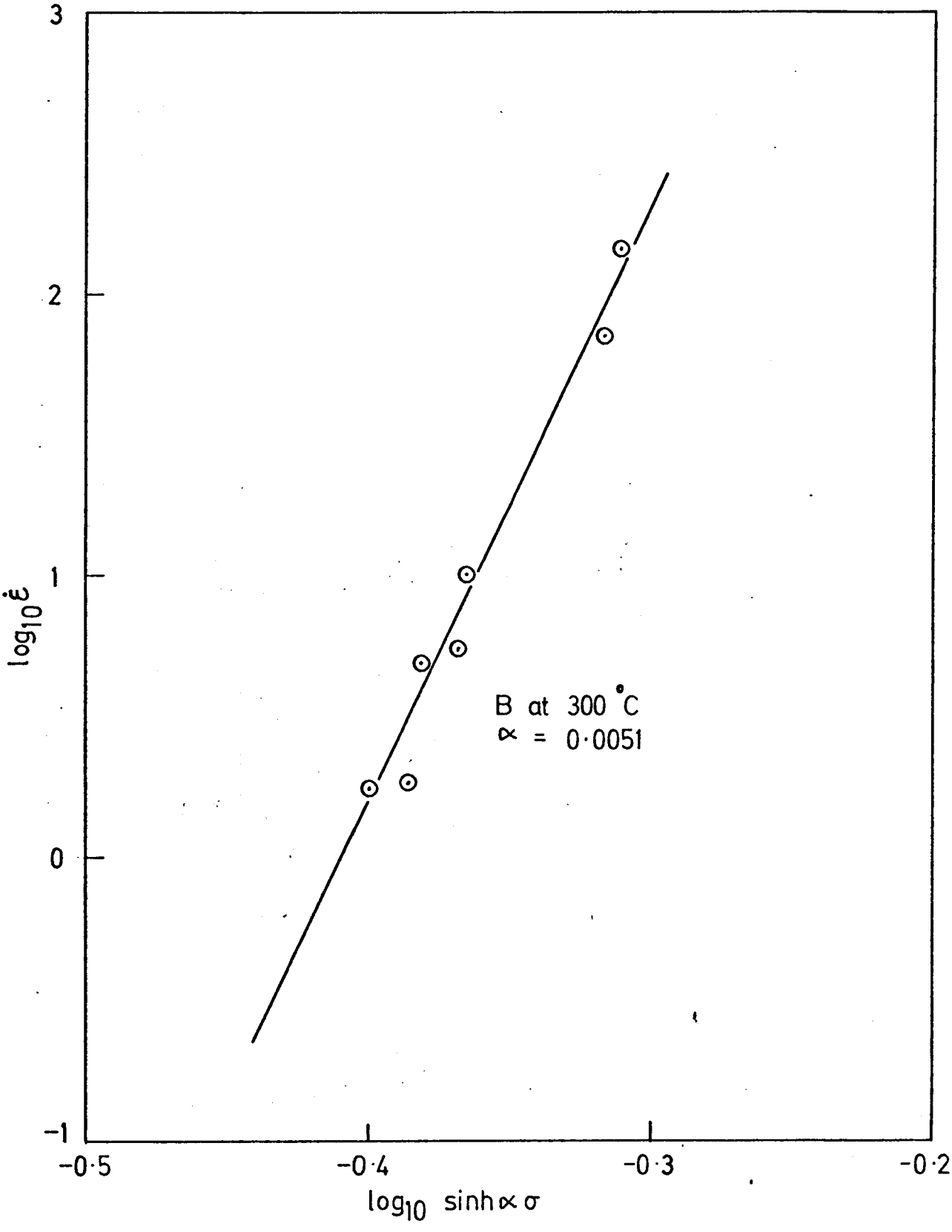

THE STRAIN RATE DEPENDENCE OF THE FLOW STRESS—POWDER B

Fig. 5.19

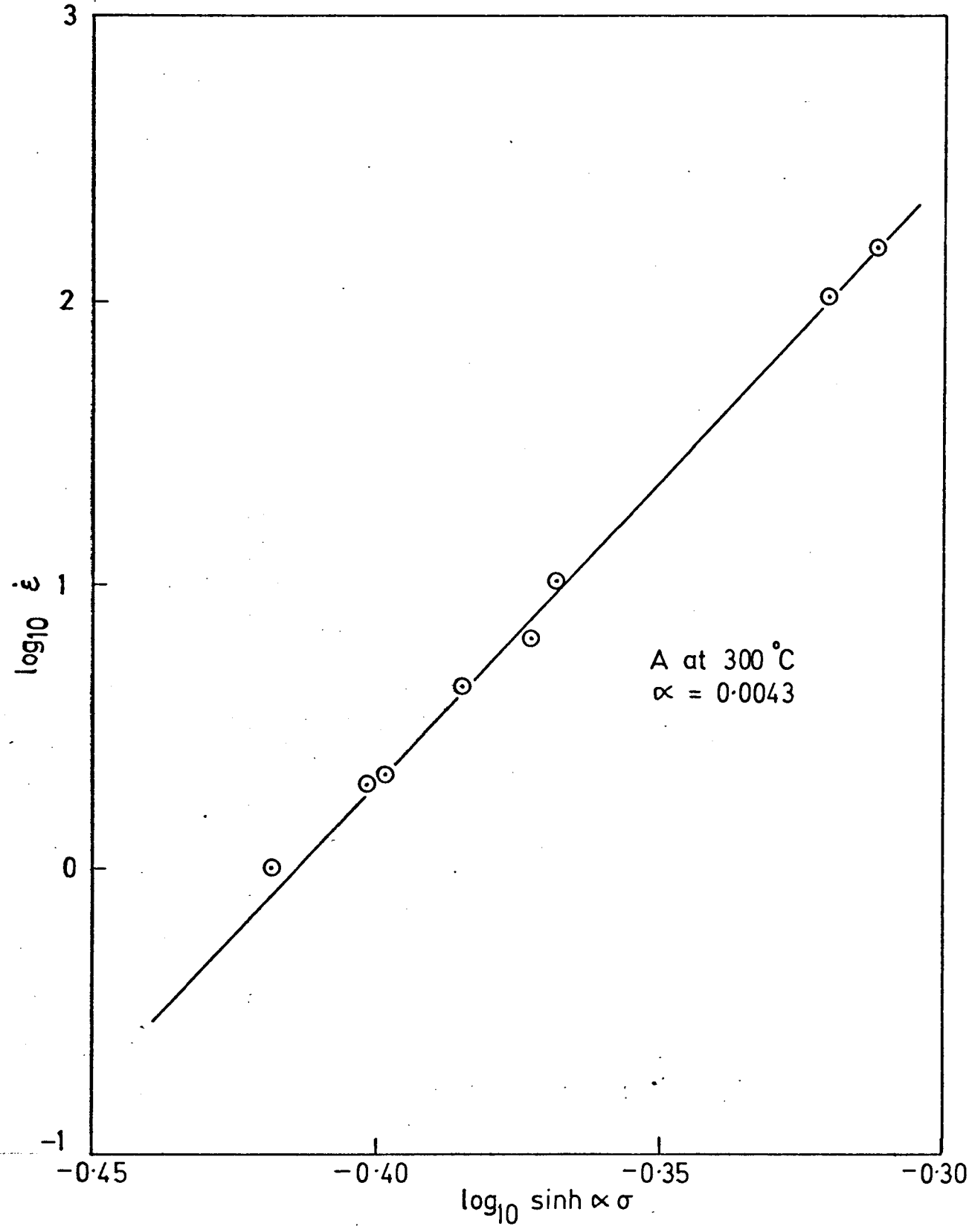

THE STRAIN RATE DEPENDENCE OF THE FLOW STRESS
—— POWDER A

Fig. 5.20

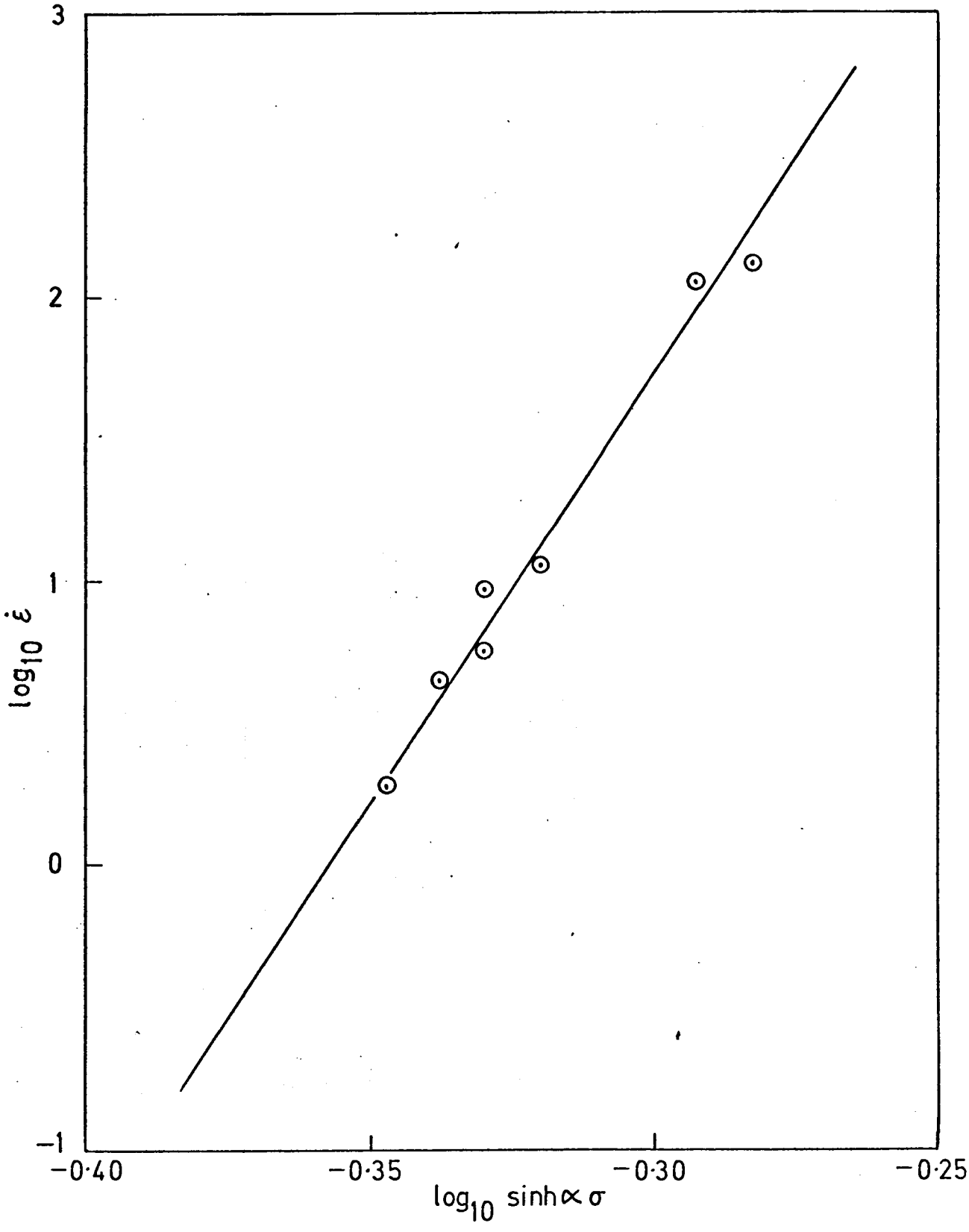

THE STRAIN RATE DEPENDENCE OF THE FLOW STRESS
——POWDER J

Fig. 5.21

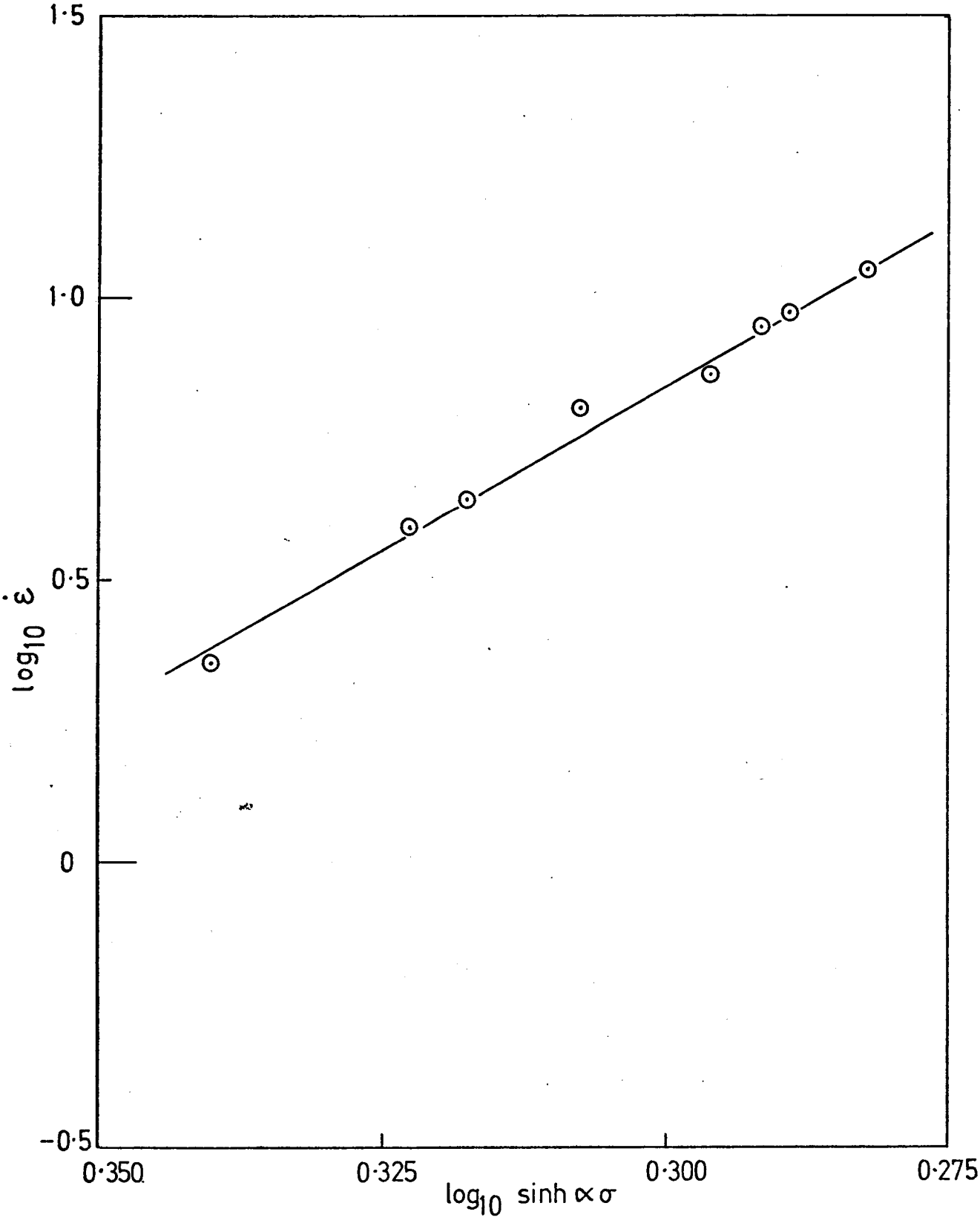

THE STRAIN RATE DEPENDENCE OF THE FLOW STRESS
——POWDER K

Fig. 5.22

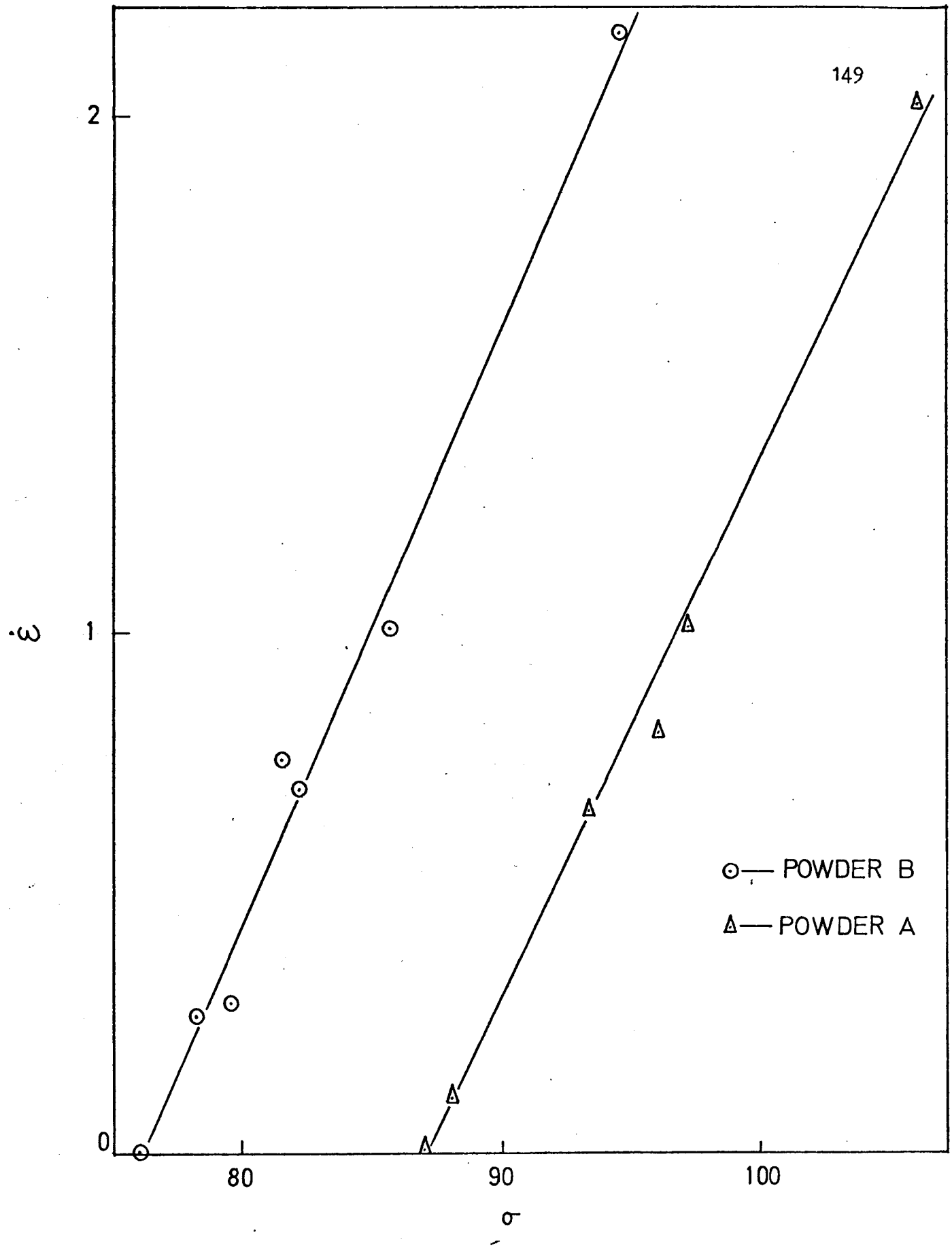

STRAIN RATE DEPENDENCE OF FLOW STRESS

Fig 5.23

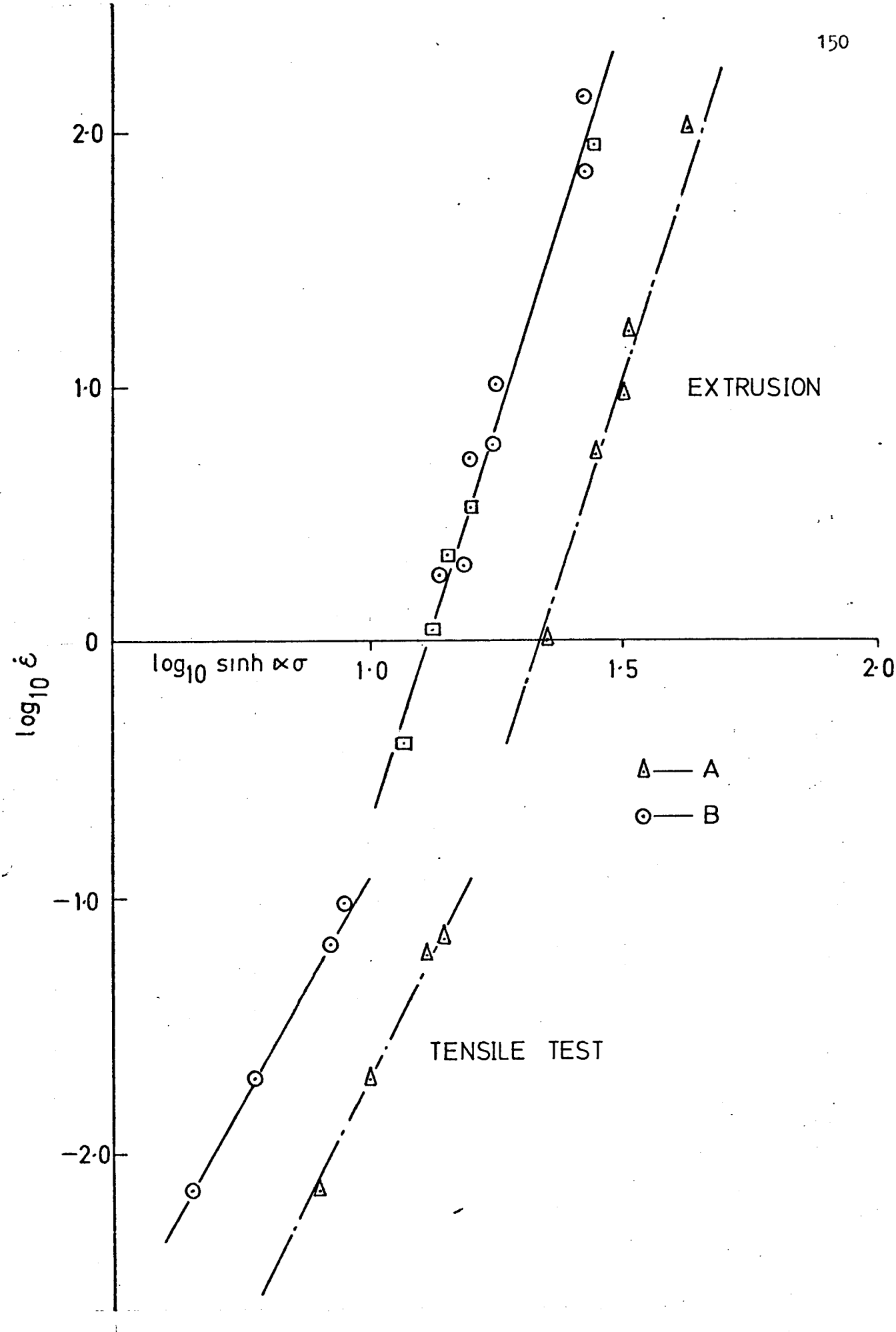

STRAIN RATE DEPENDENCE OF FLOW STRESS

$\alpha = 0{\cdot}0435$

Fig 5.24

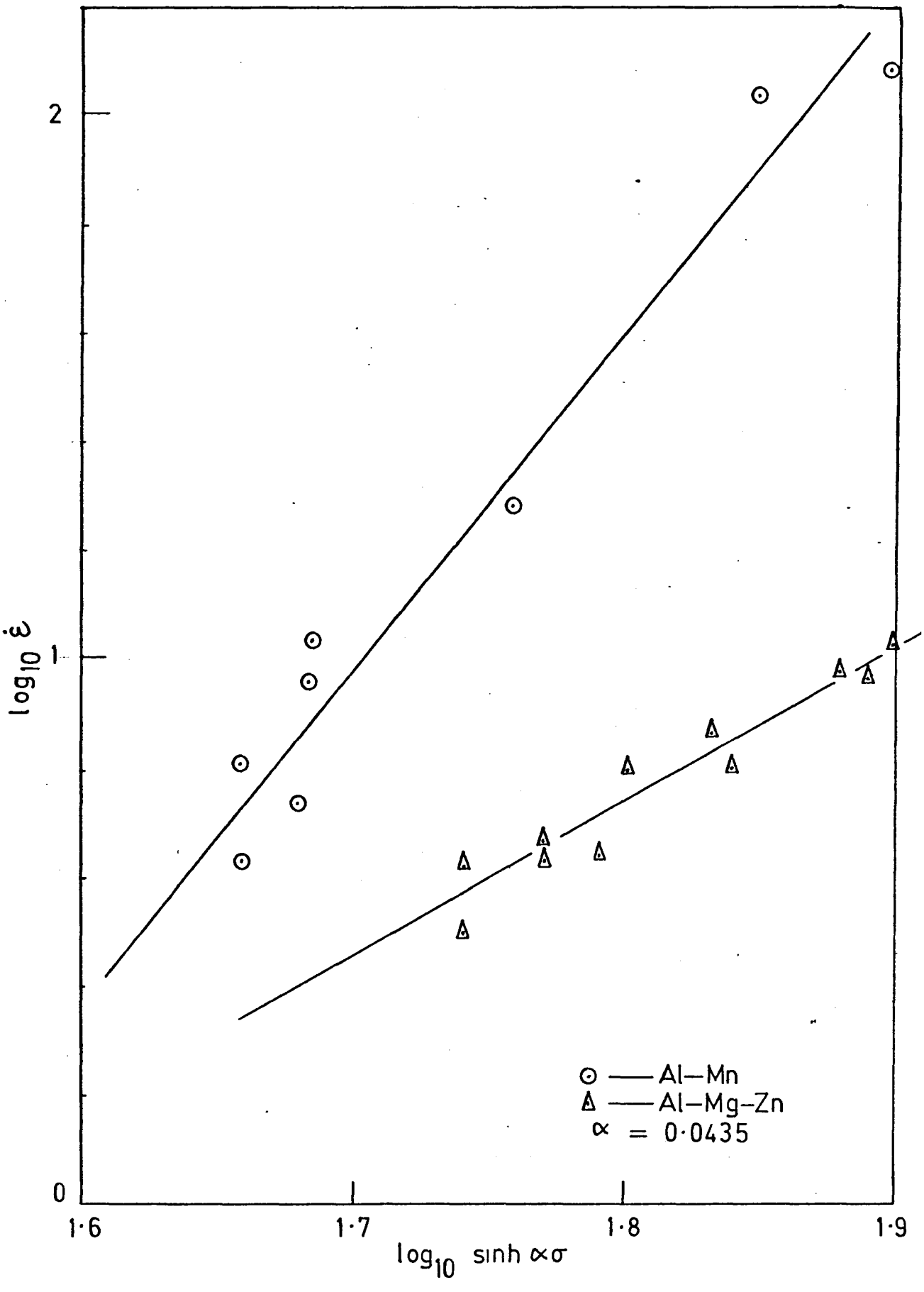

THE STRAIN RATE DEPENDENCE OF FLOW STRESS

Fig. 5.25

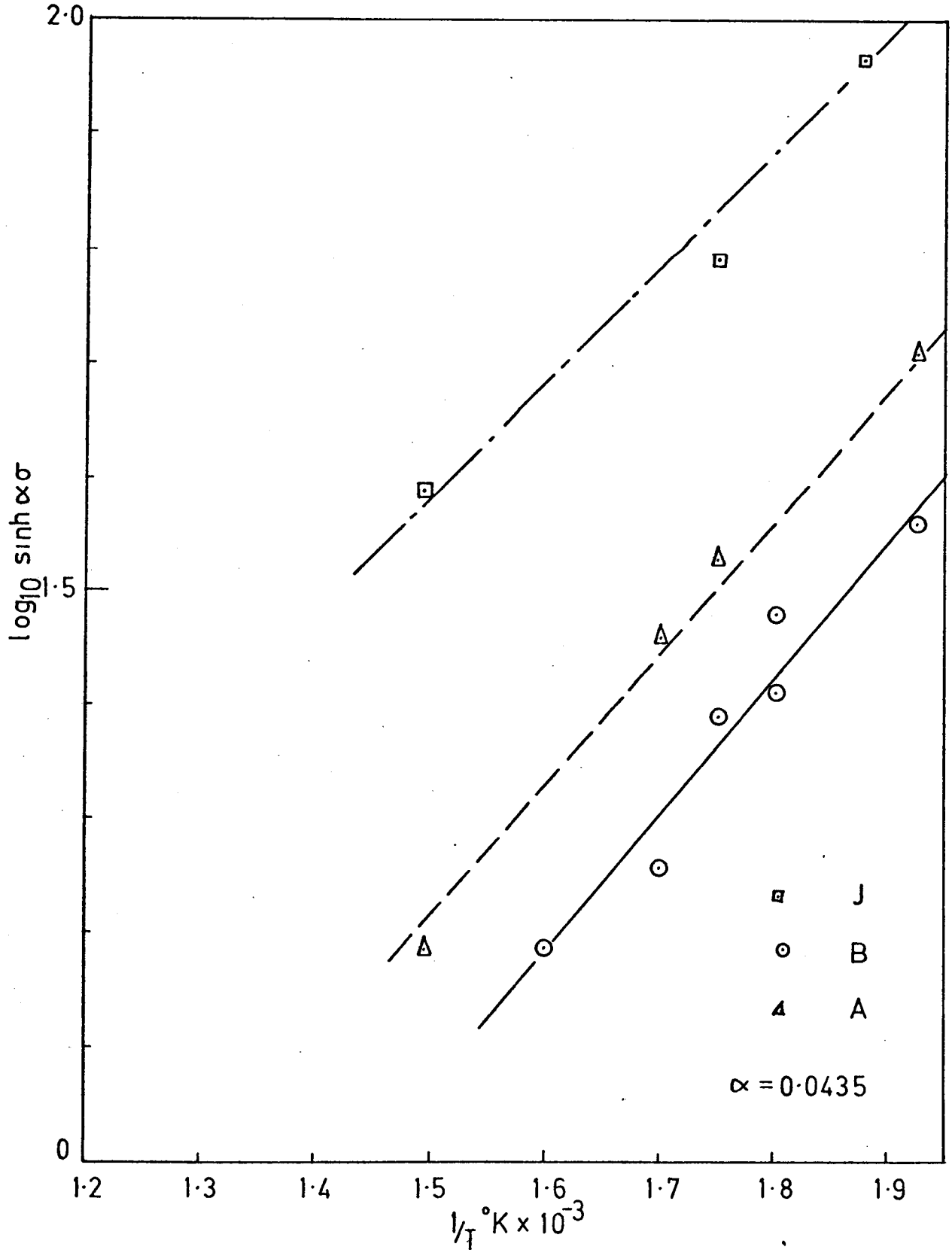

TEMPERATURE DEPENDENCE OF FLOW STRESS

Fig. 5.26

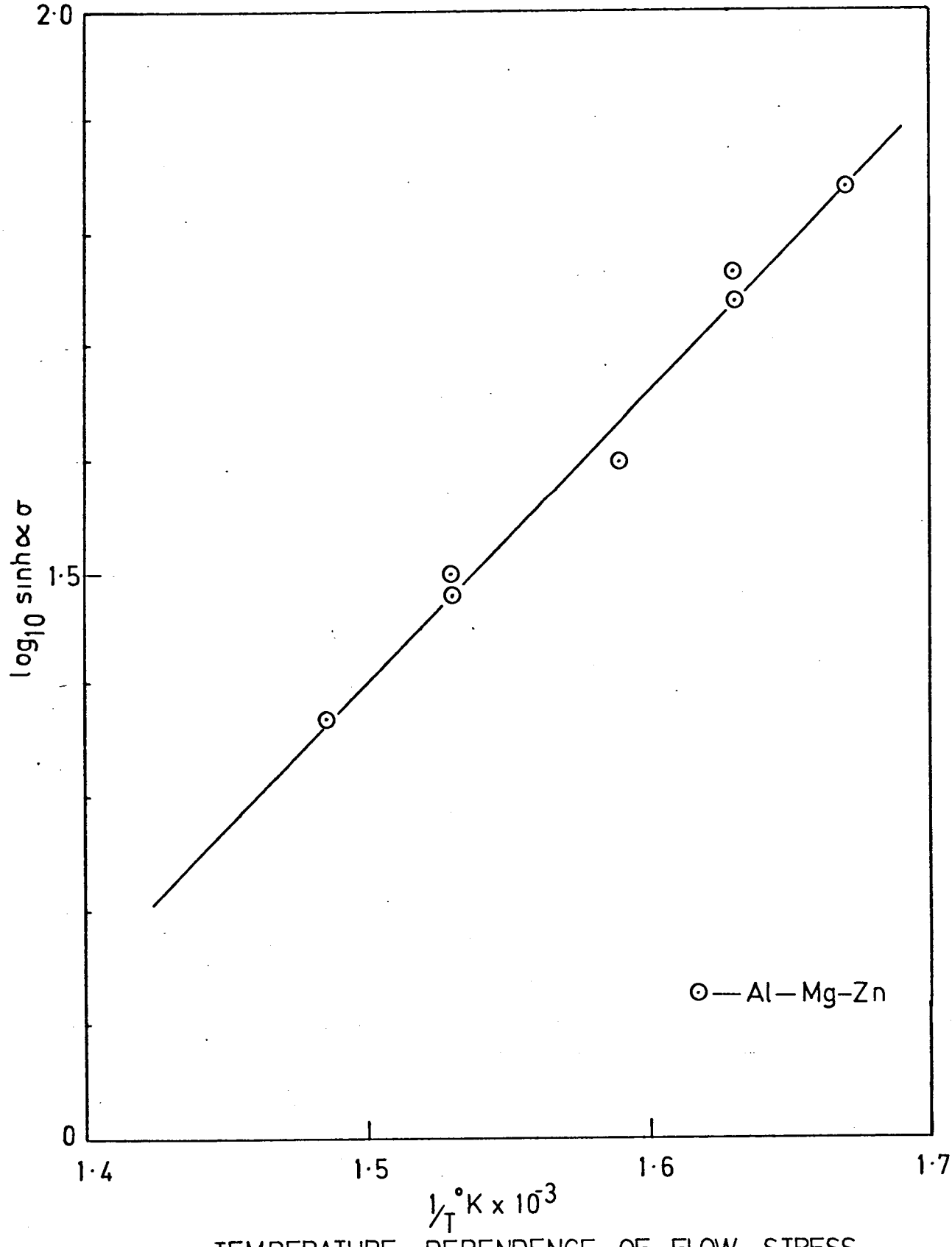

TEMPERATURE DEPENDENCE OF FLOW STRESS

Fig. 5.27

TABLE 5.10

Tensile Tests			
Material	Testing Temp °C	Stress* MNm^{-2}	Strain rate sec^{-1}
A	300	58.5	.007
	300	67.8	.02
	300	69	.063
	300	70	.07
	300	71	.7
B	300	45	.007
	300	56.1	.02
	300	57	.063
	300	58.5	.07
	350	40.1	.007
J	400	69	.007
	400	103	.7
	300	104	.007
K	300	62.1	.007
	200	127	.007

TABLE 5.11

Material	Reduction Ratio	Sub Grain Diameter μm
A	10	0.735
	20	0.746
	30	0.75
	40	0.727
B	10	1.05
	20	1.03
	30	1.05
	40	1.1
	50	1.05

* (0.2%) Proof Stress

5.6 Properties of the extruded product

5.6.1 Initial particle size

The initial particle size has been found previously to be one of the important variable during the production of a solid product. In the literature survey, it was noted that the particle size governed not only tensile properties of the extruded product but also the grain size. Results from the present work on the transmission electron microscope, revealed a dependence of the sub grain size on the initial particle size. Fig. 5.28 is a plot of mean sub grain diameter as a function of particle diameter resulting in a linear dependence.

The tensile properties were obtained at room temperature and 400°C from tensile tests carried out. Proof stress (0.2%) values were used, as being representative of the tensile properties, and are plotted against the reciprocal square root of the mean particle size. This Petch type equation was previously used and discussed[3] to represent the effectiveness of the particle size and is of the form:

$$\sigma = \sigma_o + C_{26}\, dp^{-\frac{1}{2}} \qquad (5.9)$$

where dp = mean particle diameter

σ_o = proof stress of coarse grained aluminium

Tensile values from room temperature and high temperature tests are plotted to form two lines. The dependence on particle size being greater for room temperature properties than elevated temperatures.

This type of Petch plot is also drawn for the alloy powders J, K, and L. The dependence on particle size being very less than for pure aluminium powder, shown in fig. 5.30 and 5.31.

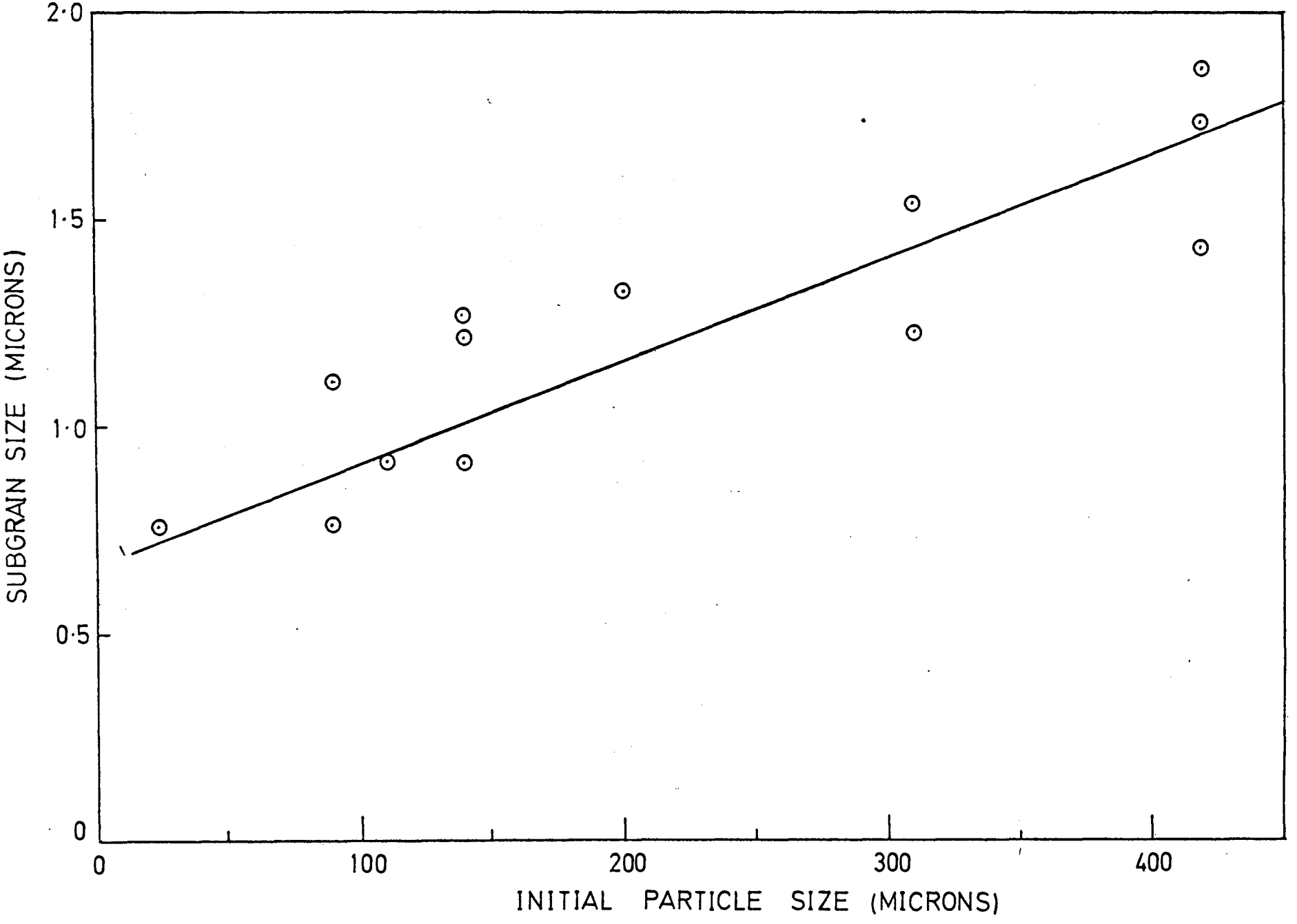

SUBGRAIN SIZE AS A FUNCTION OF INITIAL PARTICLE SIZE — Al POWDER

Fig 5.28

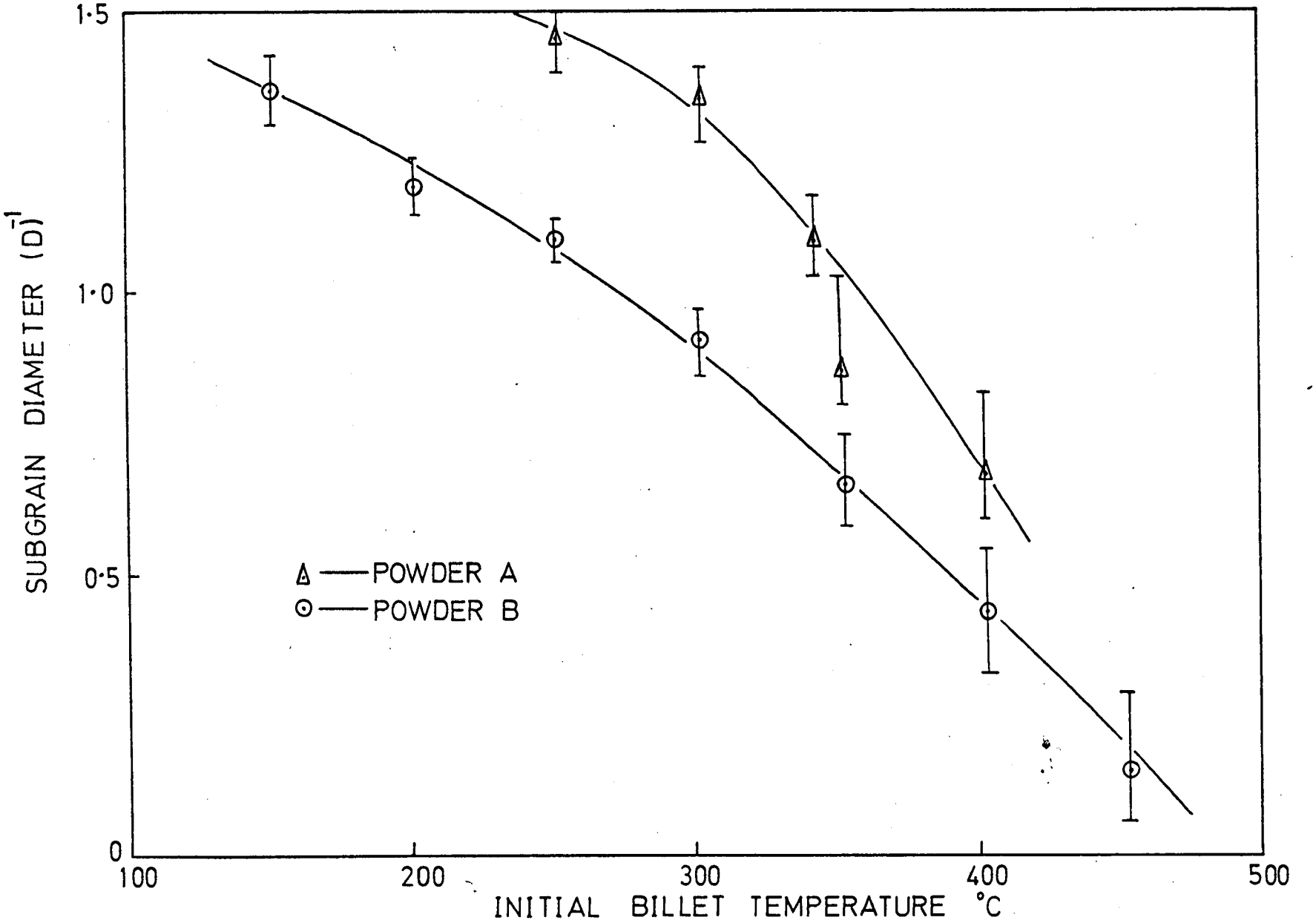

SUBGRAIN DIAMETER AS A FUNCTION OF TEMPERATURE

Fig 5.29

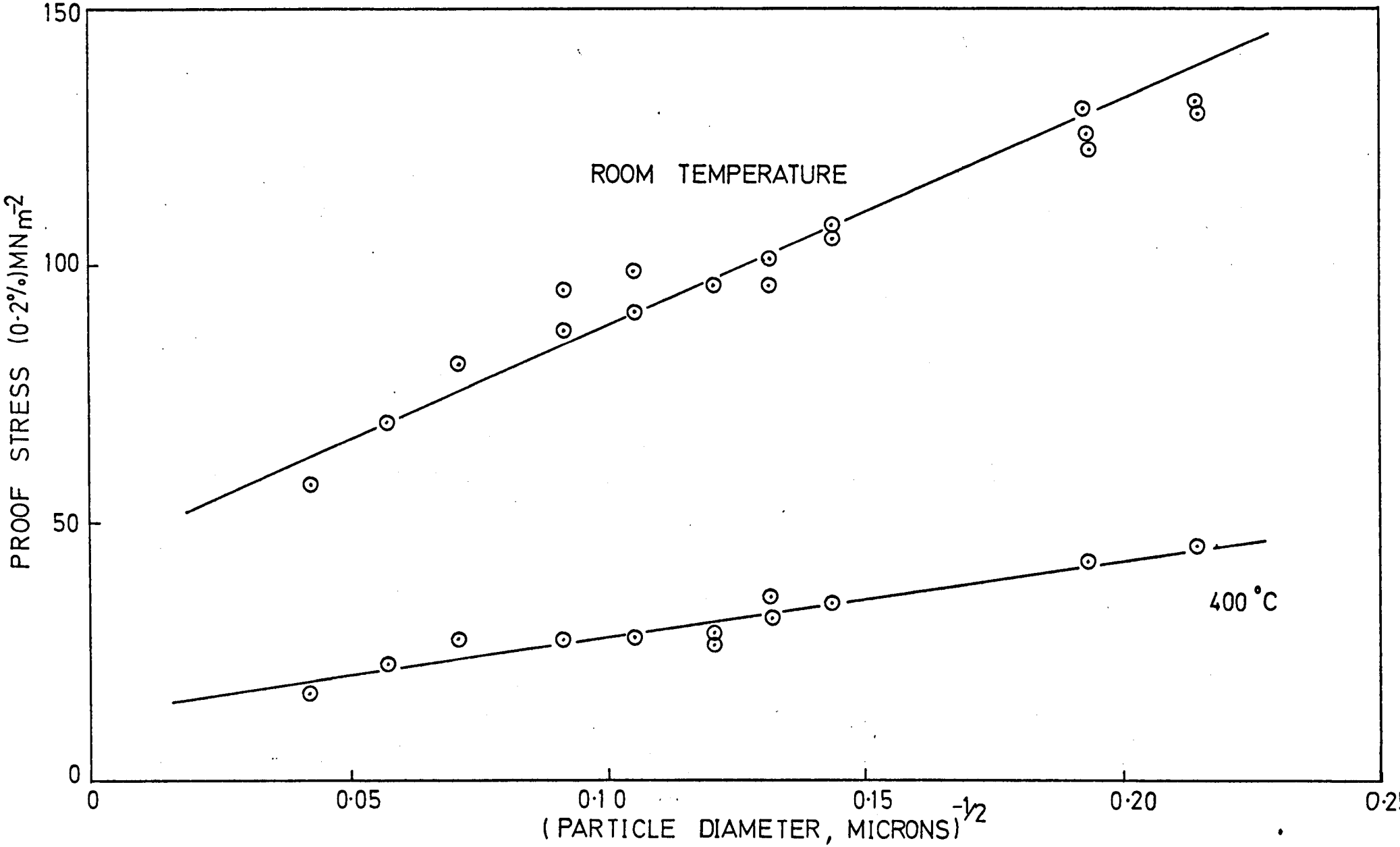

PROOF STRESS (0 2%) AT ROOM TEMPERATURE AND 400 °C AS A FUNCTION OF PARTICLE DIAMETER—(Al)

Fig. 5.30

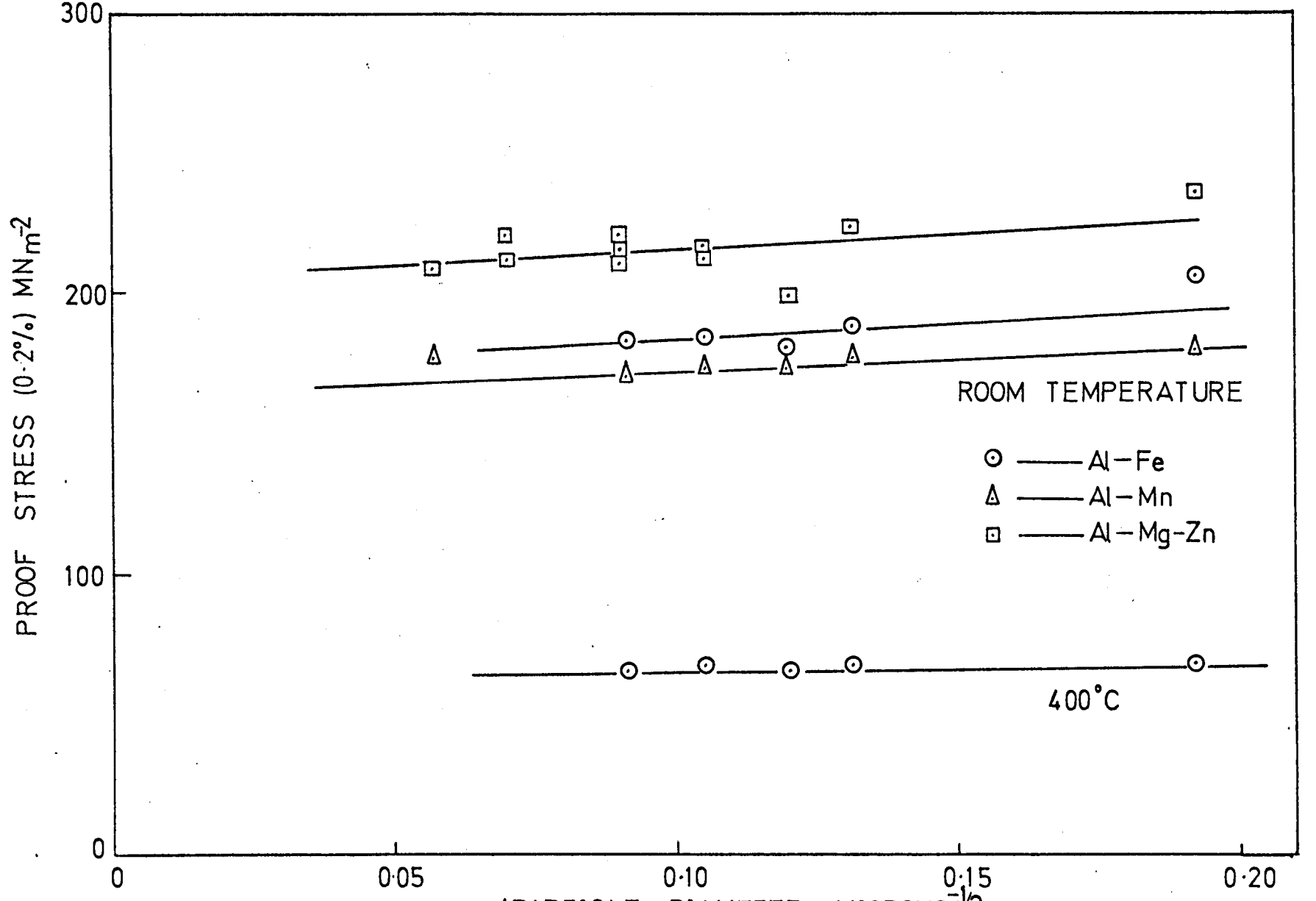

PROOF STRESS (0·2%) AT ROOM TEMPERATURE AND 400°C AS A FUNCTION OF PARTICLE DIAMETER

Fig. 5.31

The results are as follows:

Aluminium B

$$\sigma = 45.14 + 379 \; Dp^{-\frac{1}{2}} \quad \text{(at room temperature)}$$

$$\sigma = 12.77 + 152.4 \; Dp^{-\frac{1}{2}} \quad \text{(at } 400^{\circ}C\text{)}$$

Al-Mn

$$\sigma = 147.6 + 152.5 \; Dp^{-\frac{1}{2}} \quad \text{(at R.T.)}$$

$$\sigma = 52.63 + 65.9 \; Dp^{-\frac{1}{2}} \quad \text{(at } 400^{\circ}C\text{)}$$

Al-Mg-Zn

$$\sigma = 199.4 + 173.8 \; Dp^{-\frac{1}{2}} \quad \text{(at R.T.)}$$

Al-Fe

$$\sigma = 156.6 + 246.9 \; Dp^{-\frac{1}{2}} \quad \text{(at R.T.)}$$

$$\sigma = 64.6 + 24 \; Dp^{-\frac{1}{2}} \quad \text{(at } 400^{\circ}C\text{)}$$

Figures 5.32 and 5.33 are Petch plots relating yield strength, 0.2% proof stress, as a function of sub grain diameter. For the aluminium powder:

$$\sigma = 22.19 + 78.46 \; D_s^{-\frac{1}{2}}$$

Al-Mn

$$\sigma = 32.5 + 121 \; D_s^{-\frac{1}{2}}$$

Al-Mg-Zn

$$\sigma = 37 + 280 \; D_s^{-\frac{1}{2}}$$

Al-Fe

$$\sigma = 36 + 133 \; D_s^{-\frac{1}{2}}$$

5.6.2 Reduction ratio

The effect of reduction ratio on the final product has been found to be very small, i.e. within experimental error. The sub grain size of the product is found to be fairly consistent around a specific

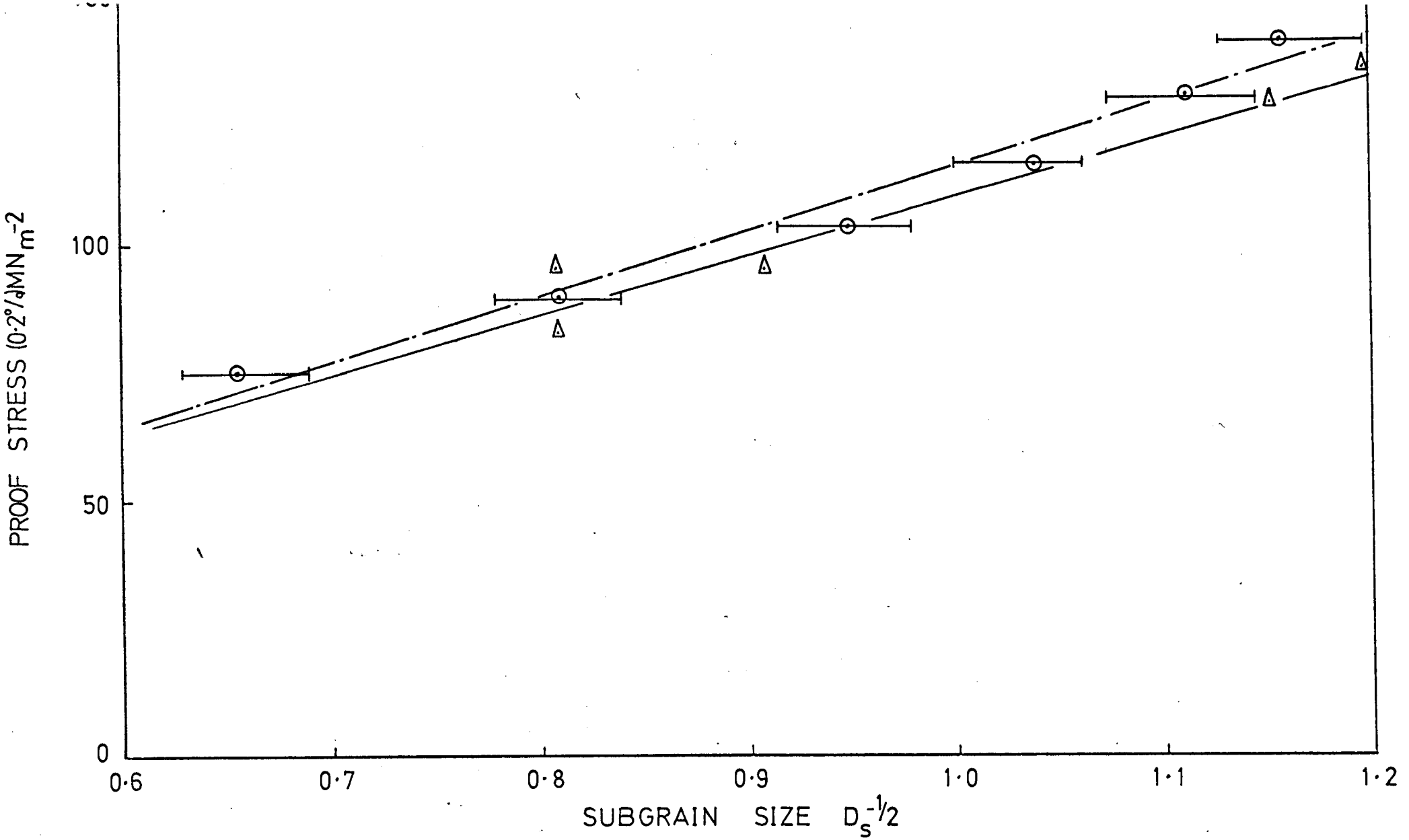

PROOF STRESS AS A FUNCTION OF SUBGRAIN SIZE — (PETCH - TYPE PLOT)

(Al. POWDER)

Fig. 5.32

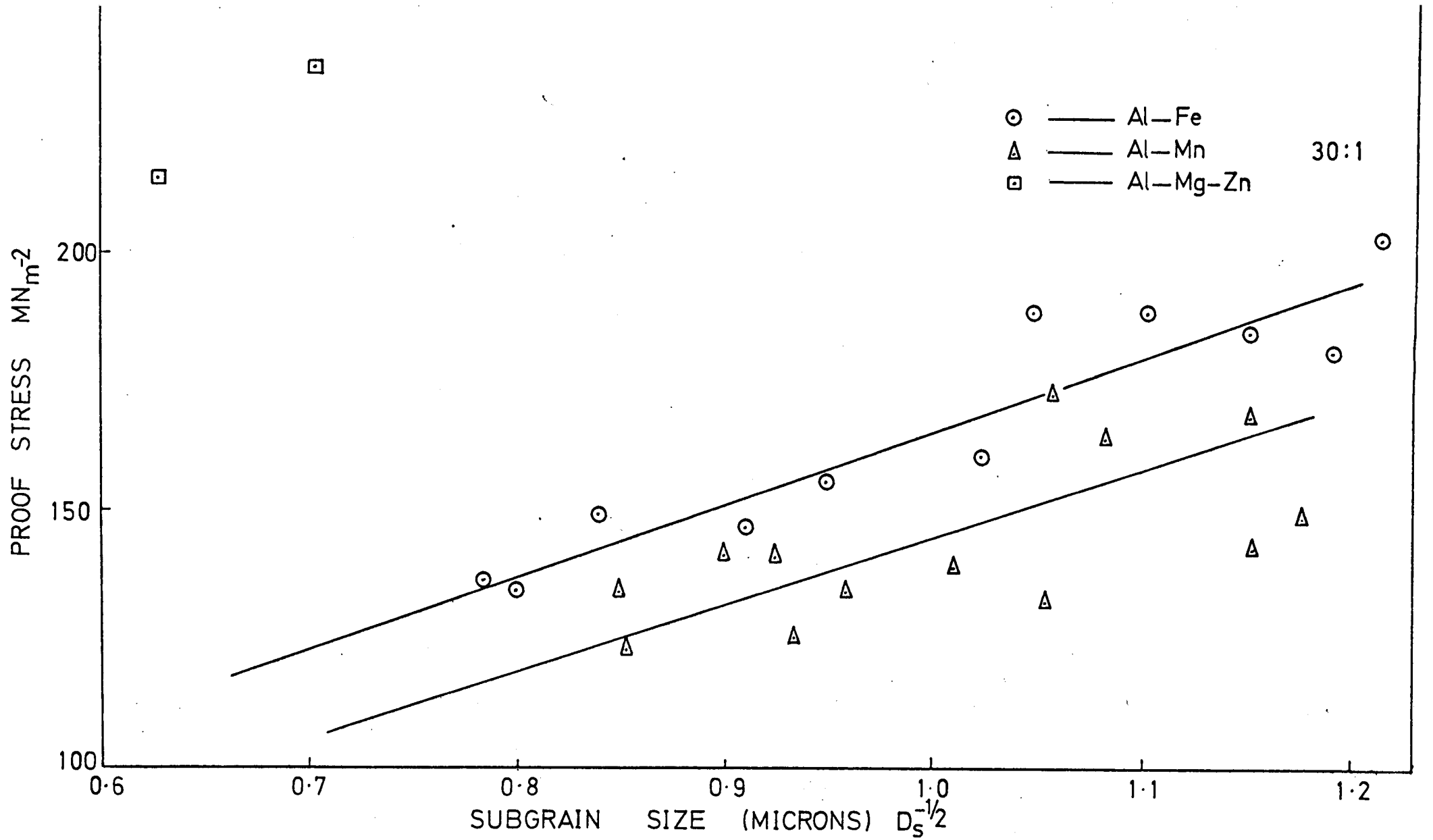

PROOF STRESS AS A FUNCTION OF SUBGRAIN SIZE——(PETCH-TYPE PLOT)

Fig. 5.33

value for a certain powder and the tensile properties are the same. These results are shown in table 5.11

Results of tensile tests of specimens extruded at R = 5:1 show a tendency to fracture unexpectedly at a low stress, indicating a minimum reduction ratio below which extrusion billets were insufficiently worked.

5.6.3 Initial billet temperature

Initial billet temperature is found to be an important parameter for room temperature strength, fig. 5.34, 5.35, whereas at elevated temperatures the initial temperature of extrusion has little effect on the tensile properties. The ductility at elevated temperatures is observed to increase with increasing extrusion temperature.

Fig. 5.29, shows the sub grain diameter as a function of temperature for the aluminium powders A and B.

5.6.4 Ram speed

Increasing the ram speed has little effect on the tensile properties. The extrusion pressure is slightly increased with increasing speed but the difference between the slowest and fastest rates is small. The two extremes being 1 mm/sec and 250 mm/sec respectively.

5.6.5 Heat treatment

Heat treating the extruded product yields a slightly softened recovered material. The degree of heat treating and temperature can be seen in table 5.12. The results show a general decrease in tensile strength with an accompanying increase or improvement in ductility.

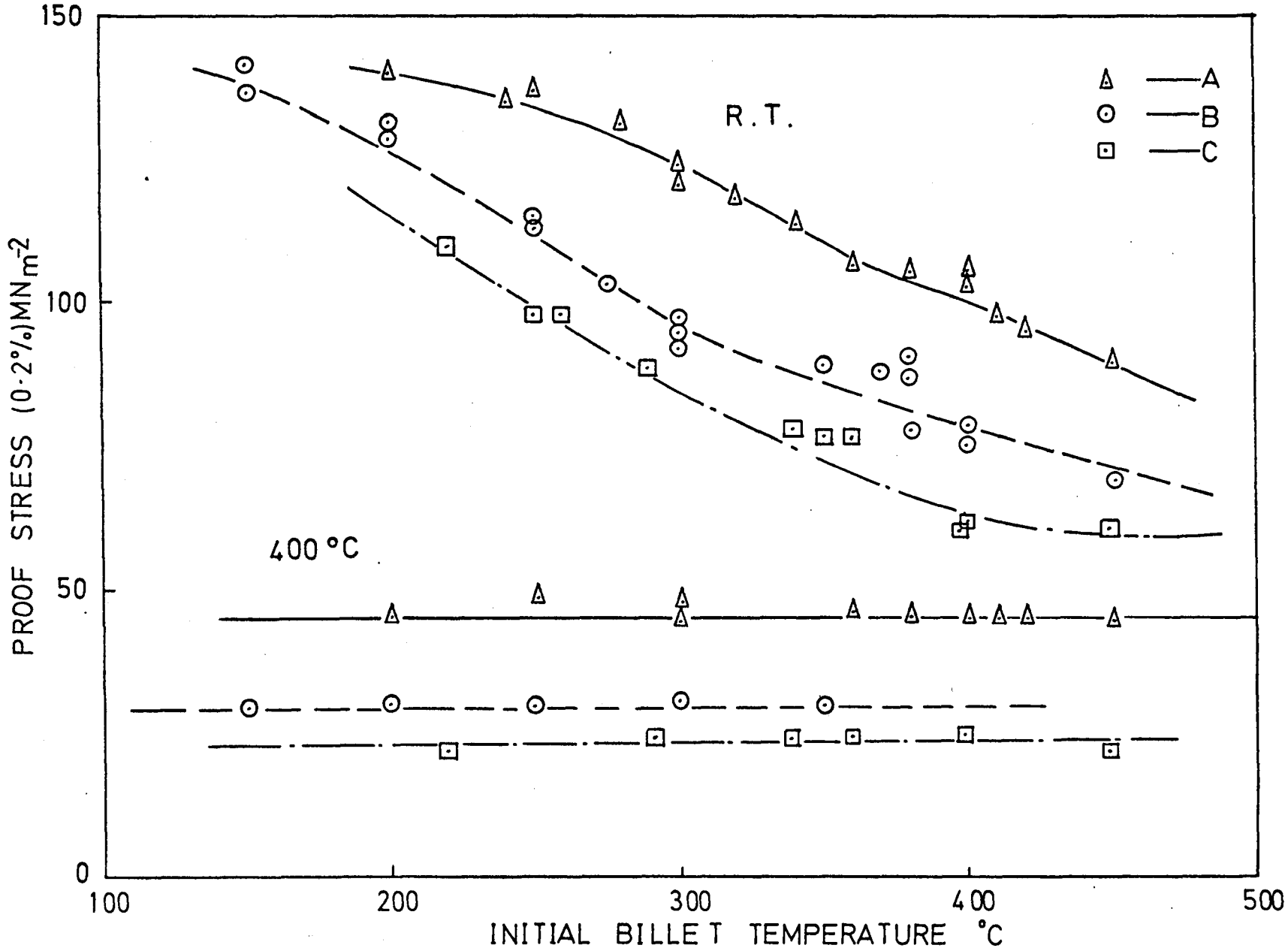

VARIATION OF PROOF STRESS (0·2%) WITH TEMPERATURE — Al. POWDER

Fig. 5.34

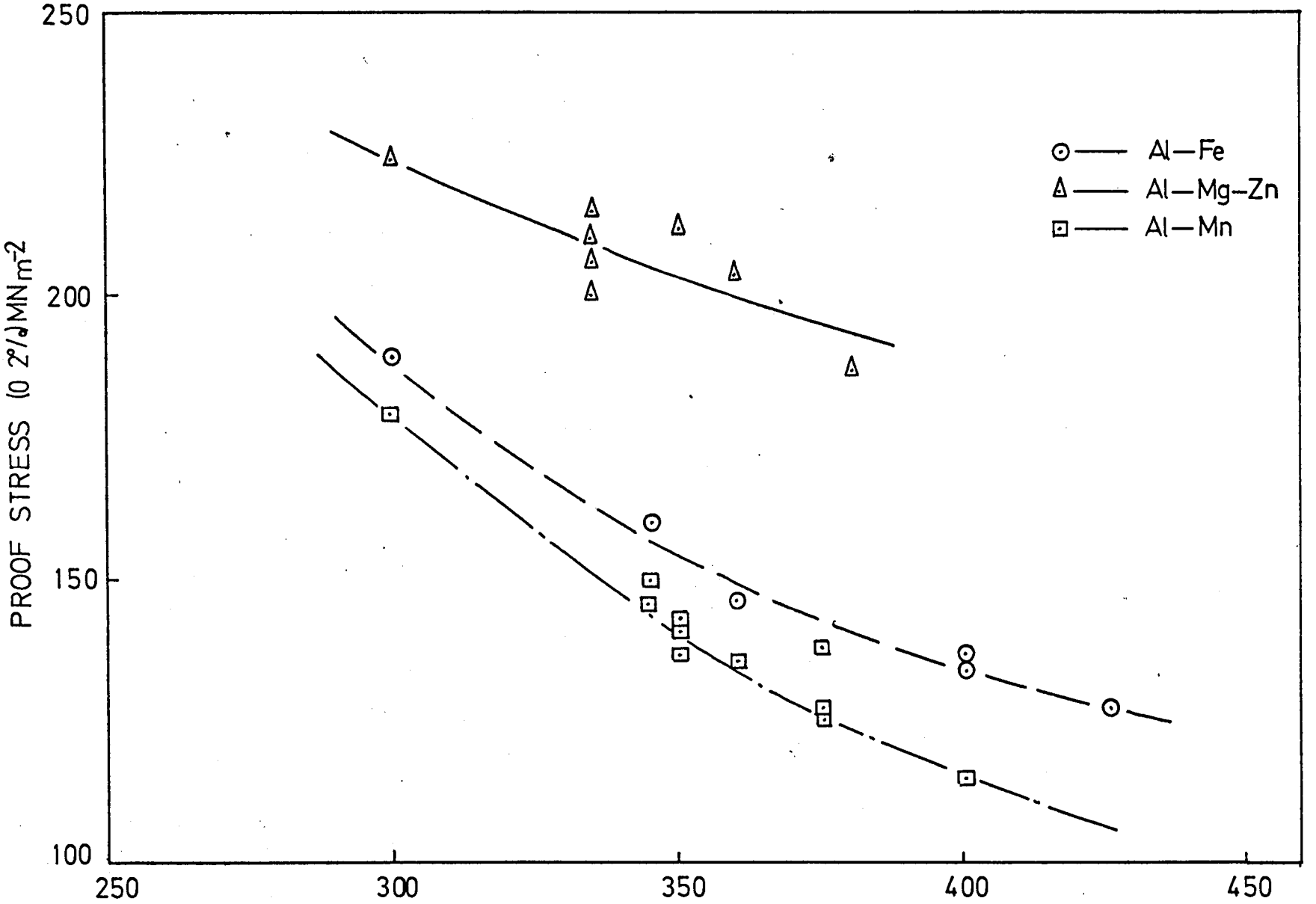

VARIATION OF PROOF STRESS (0·2%) WITH TEMPERATURE

Fig. 5.35

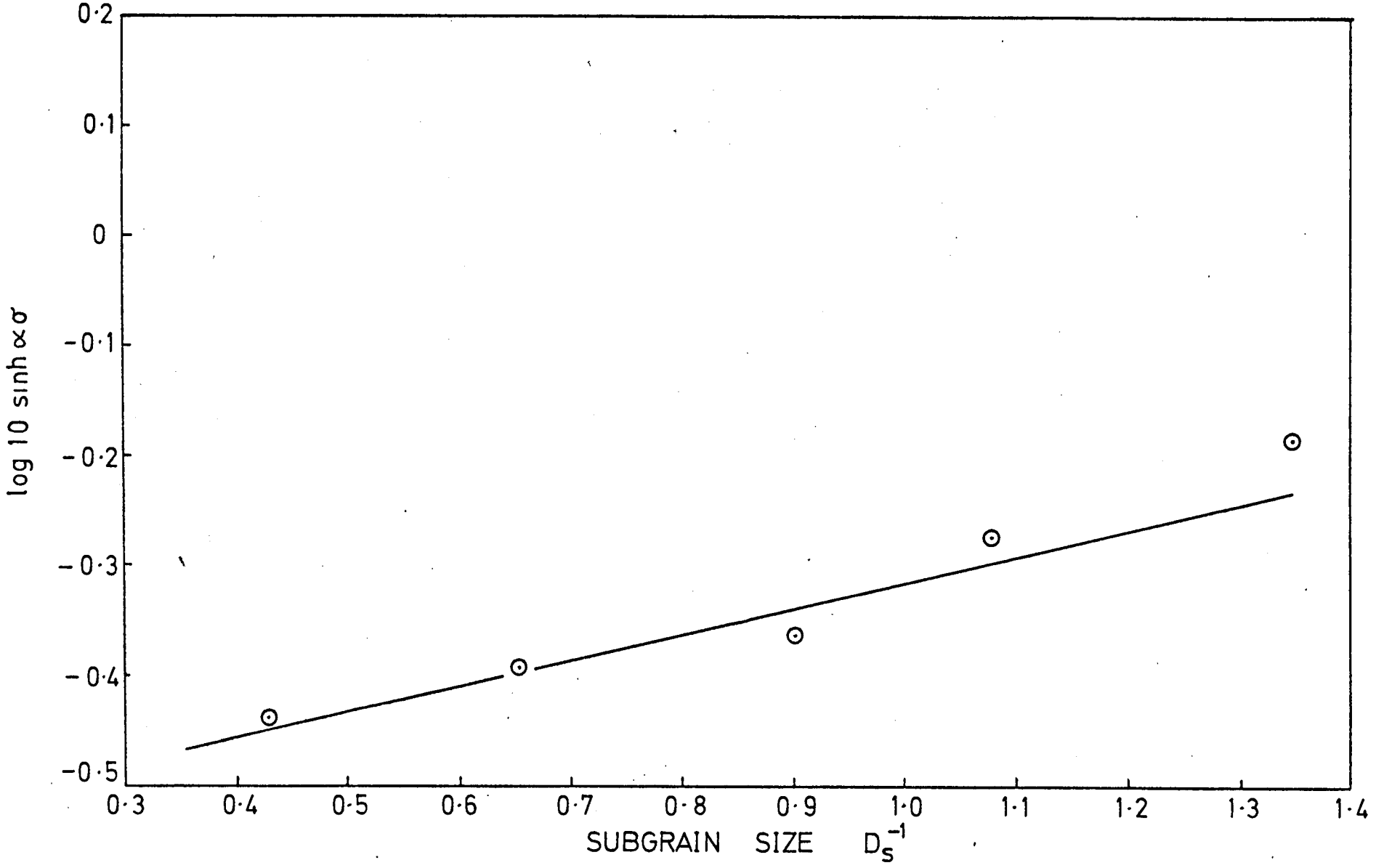

PLOT OF log10 sinh ∝σ AGAINST D_s^{-1} (Al. POWDER B)

Fig 5.36

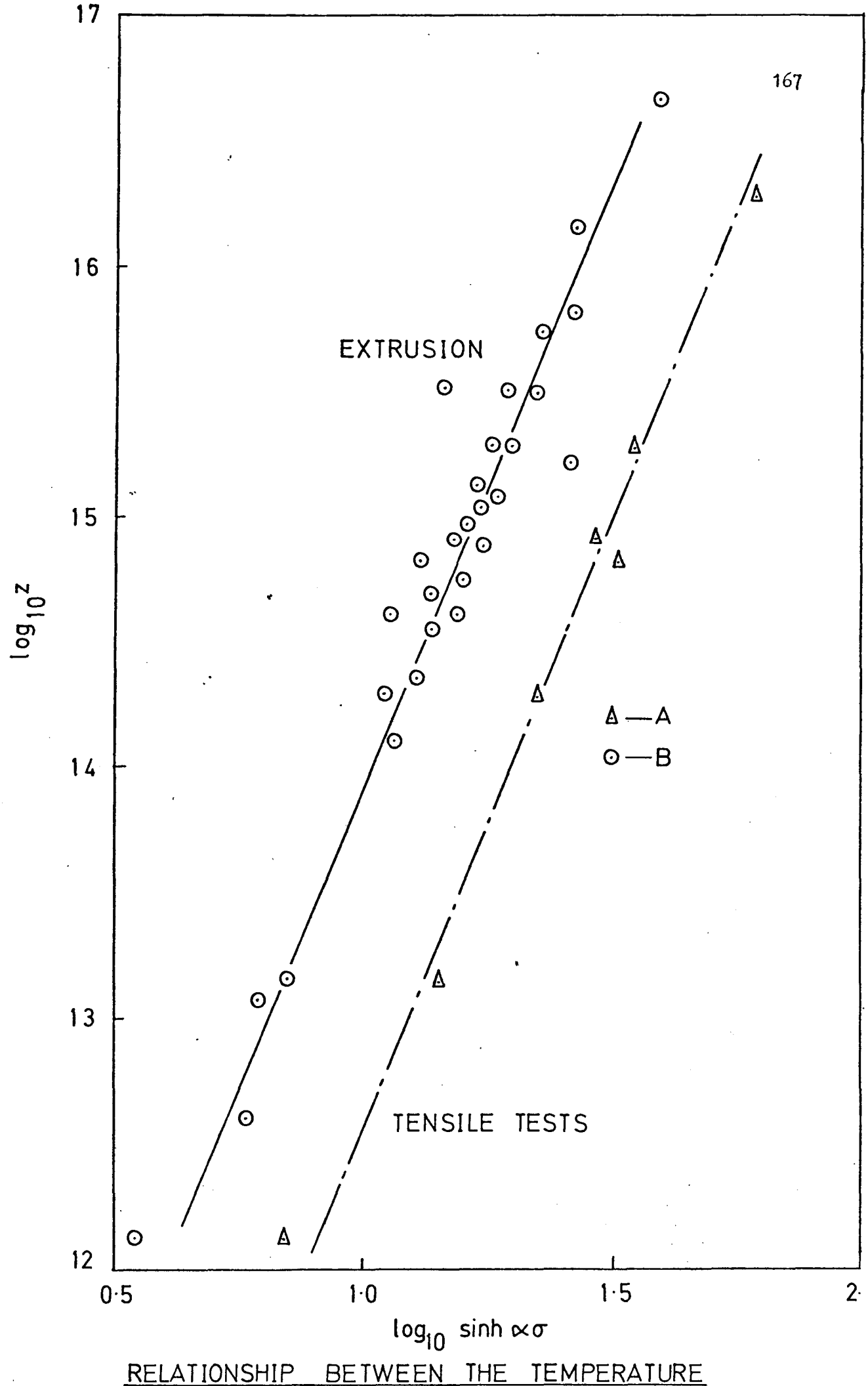

RELATIONSHIP BETWEEN THE TEMPERATURE COMPENSATED STRAIN RATE & THE FLOW STRESS

Fig. 5.37

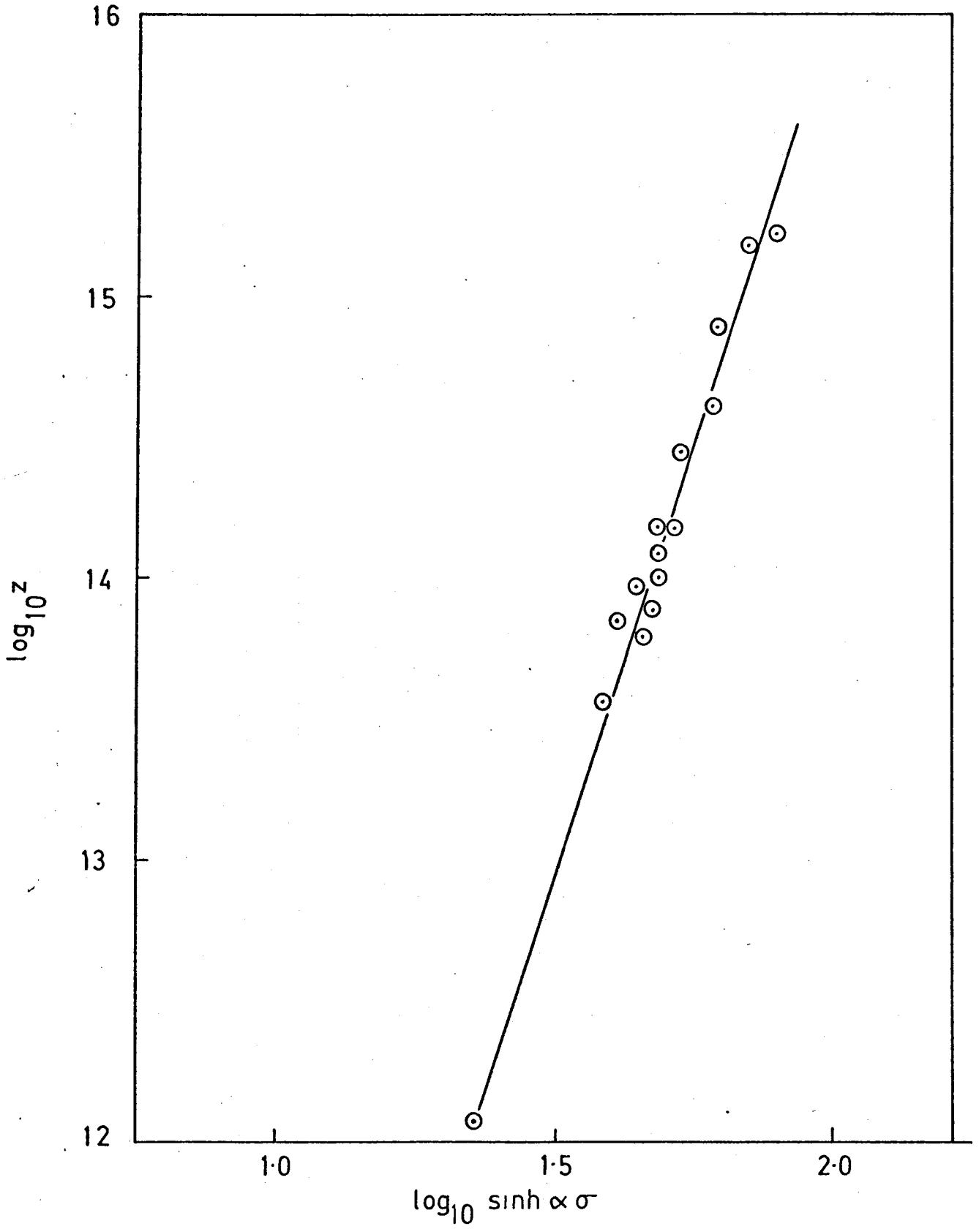

RELATIONSHIP BETWEEN THE TEMPERATURE COMPENSATED STRAIN RATE & THE FLOW STRESS FOR J (Al—Mn)

Fig 5.38

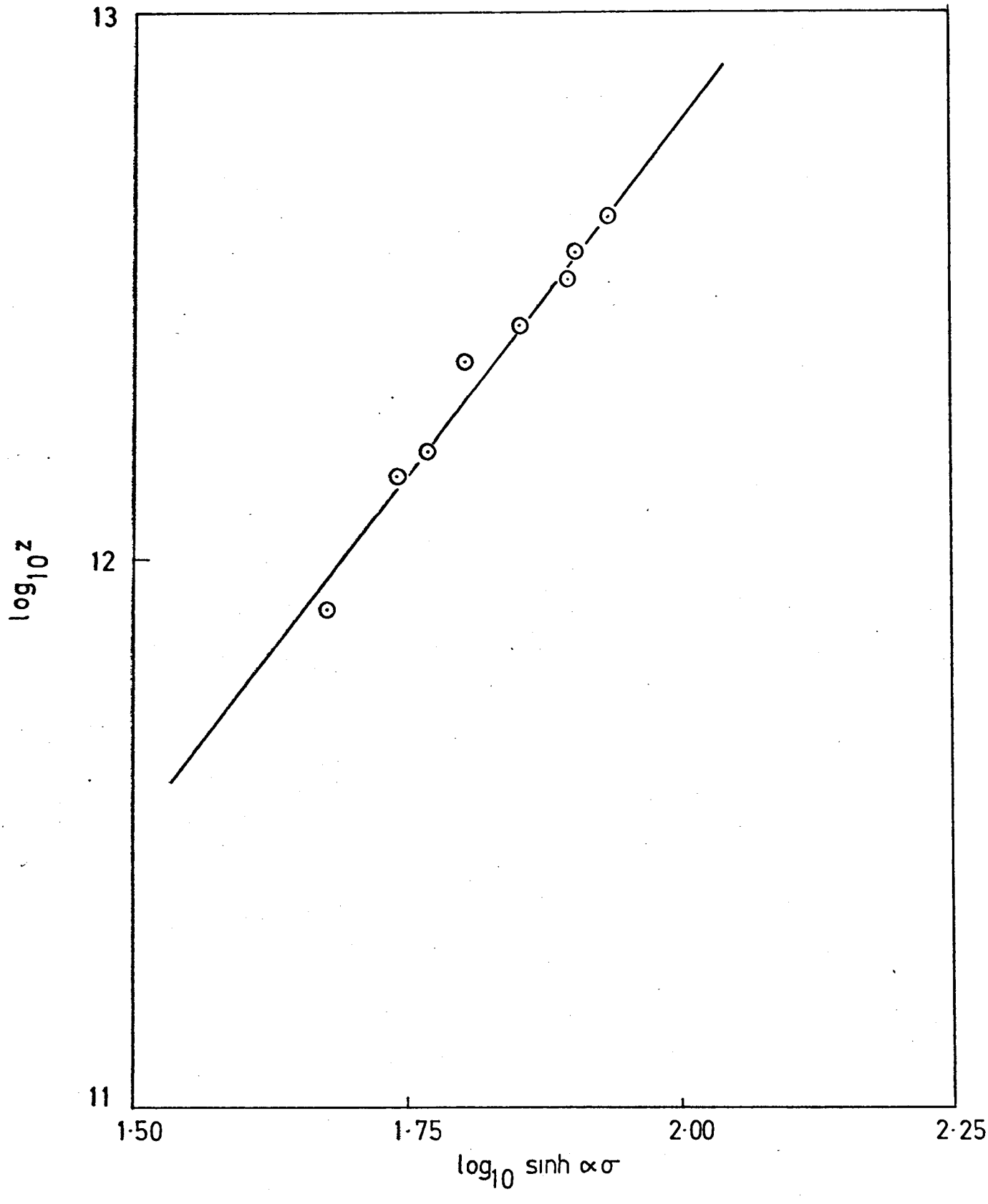

RELATIONSHIP BETWEEN THE TEMPERATURE COMPENSATED STRAIN RATE & THE FLOW STRESS FOR K (Al—Mg—Zn)

Fig. 5.39

TABLE 5.12

Product	Heat Treatment after Extrusion	Proof Stress (0.2%) MNm^{-2}	Tensile Stress MNm^{-2}	Elongation %
C		69.8	104.4	35.4
300°C	2 hrs at 450°C	53.6	80.7	47.8
30:1	2 hrs at 500°C	49.8	79.5	49.1
	2 hrs at 550°C	49.5	80.5	45.03
	2 hrs at 600°C	49.8	82.3	40.3
A		125.3	160.7	24.4
300°C	15 mins at 450°C	120.6	158.5	22.2
30:1	30 mins at 450°C	116.5	156.4	24.7
	45 mins at 450°C	118.4	154	22.2
	60 mins at 450°C	113.5	147	23.6
	90 mins at 450°C	112.1	141.7	21.6
	180 mins at 450°C	111.1	141.4	20.8
B		93.3	129.6	28.5
300°C	15 mins at 450°C	93.3	131.1	29.9
30:1	30 mins at 450°C	89.4	124.7	27.7
	45 mins at 450°C	86.1	124.7	29
	60 mins at 450°C	84.1	122.3	27.4
	90 mins at 450°C	77.4	116.3	28.9
	180 mins at 450°C	75.2	116.9	27.3
B		142.7	154	20.6
150°C	15 mins at 450°C	126.9	148.2	20.3
30:1	30 mins at 450°C	106	133	21
	45 mins at 450°C	98.5	129.9	22.7
	60 mins at 450°C	96.1	131.7	21
	90 mins at 450°C	91.5	122	22.9
	180 mins at 450°C	90	120.4	20.3

5.7 Particle microstructure

The aluminium particles in their 'as received' condition are found to be comprised of a fairly fine uniform grain size. In the large particles there is a tendency towards a columnar type structure near the surface of the particles. The photomicrographs shown in plate 5.7 are of the very coarse mesh fraction of aluminium powder B, with the smaller particles, a very much finer structure is observed.

In some of the large particles of alloy, J, there is evidence of large primary precipitates, plate 5.3.

5.8 Flow pattern

The flow pattern of the billet during extrusion, is observed by etching a macro section of a partially extruded billet. Two billets are shown, plates 5.5, 5.6. One of the aluminium magnesium zinc alloy, and the other of aluminium powder C.

The aluminium billet was prepared with copper foil discs spaced throughout the billet. During extrusion these were deformed with the aluminium powder and helped to show the overall flow of powder during extrusion. The pattern seen, in plates 5.5 and 5.6, is that of type B as shown in the book by Pearson[49]. Further experiments indicated that the pattern does not change with increasing or decreasing reduction ratio and decreasing length of the billet does not affect the flow pattern. The flow patterns seen are not very distinct due to the fine nature of the grain size within the individual particles.

5.9 Micro-structure of the product

The microstructre of the extruded products was extensively

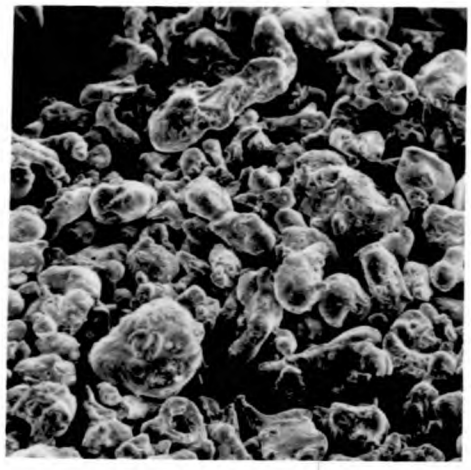

(a)

Powder B (X 230)

(b)

Powder J (Al-Mn) (X 90)

(c)

Powder K (Al-Mg-Zn) (X 90)

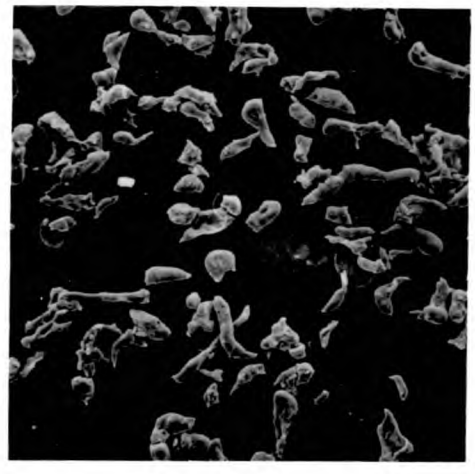

(d)

Powder L (Al-Fe) (X 90)

PLATE 5.1 Scanning electron micrographs of the powders

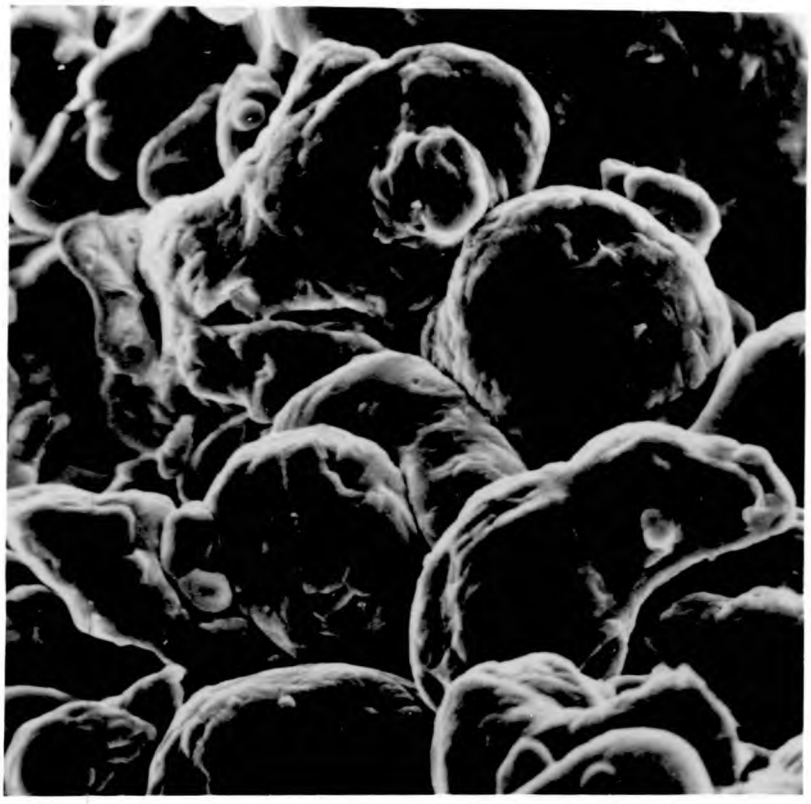

(X 2280)

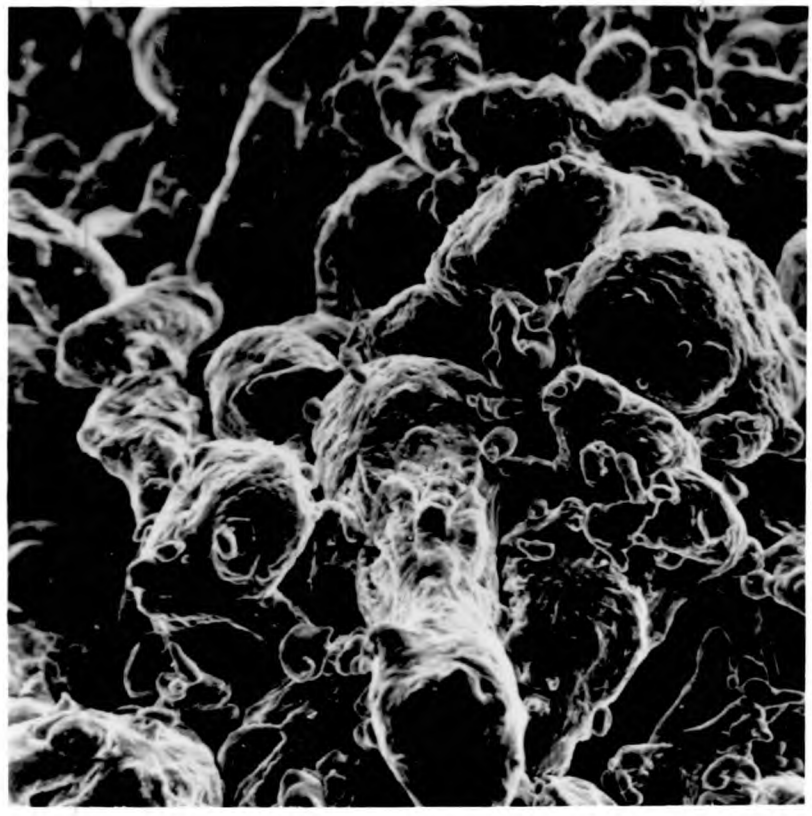

(X 610)

PLATE 5.2 Scanning electron micrographs of compacts of powder B

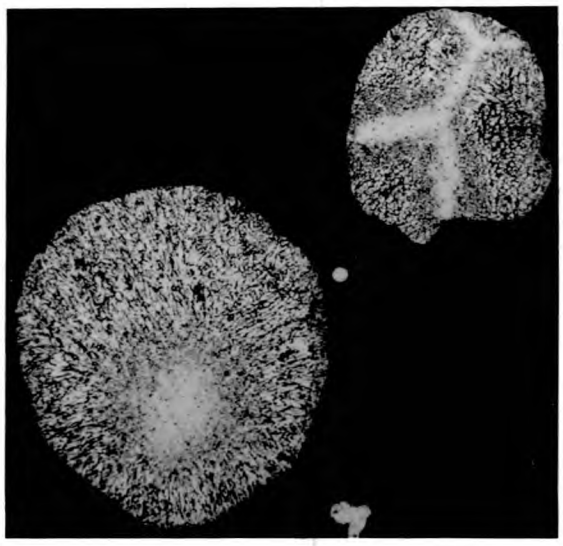

(a)

Powder L (Al-Fe) (X 80)

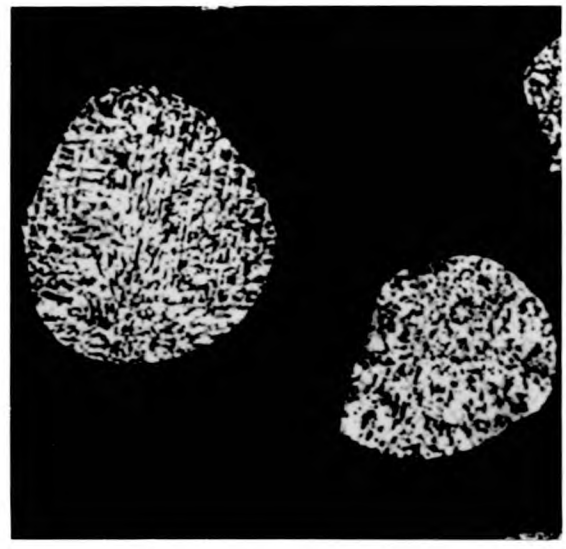

(b)

Powder K (Al-Mg-Zn) (X 80)

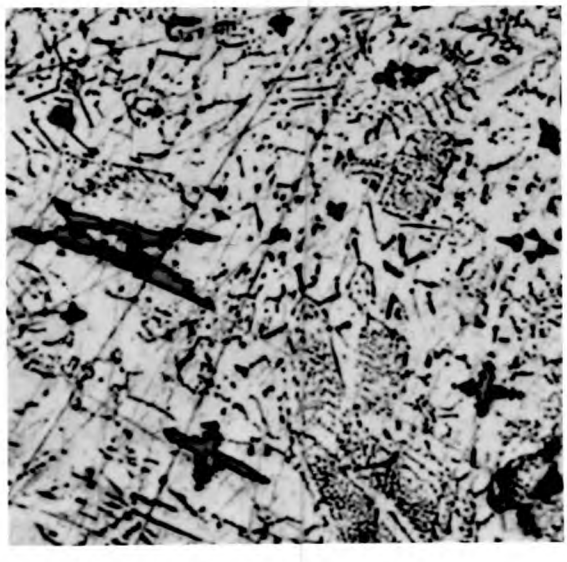

(c)

Powder J (Al-Mn) (X 800)

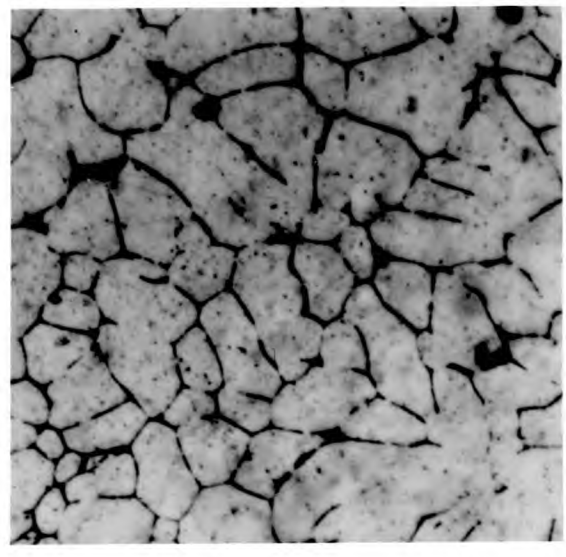

(d)

Powder C (X 400)

PLATE 5. 3 Optical micrographs of the powders in the as-received condition

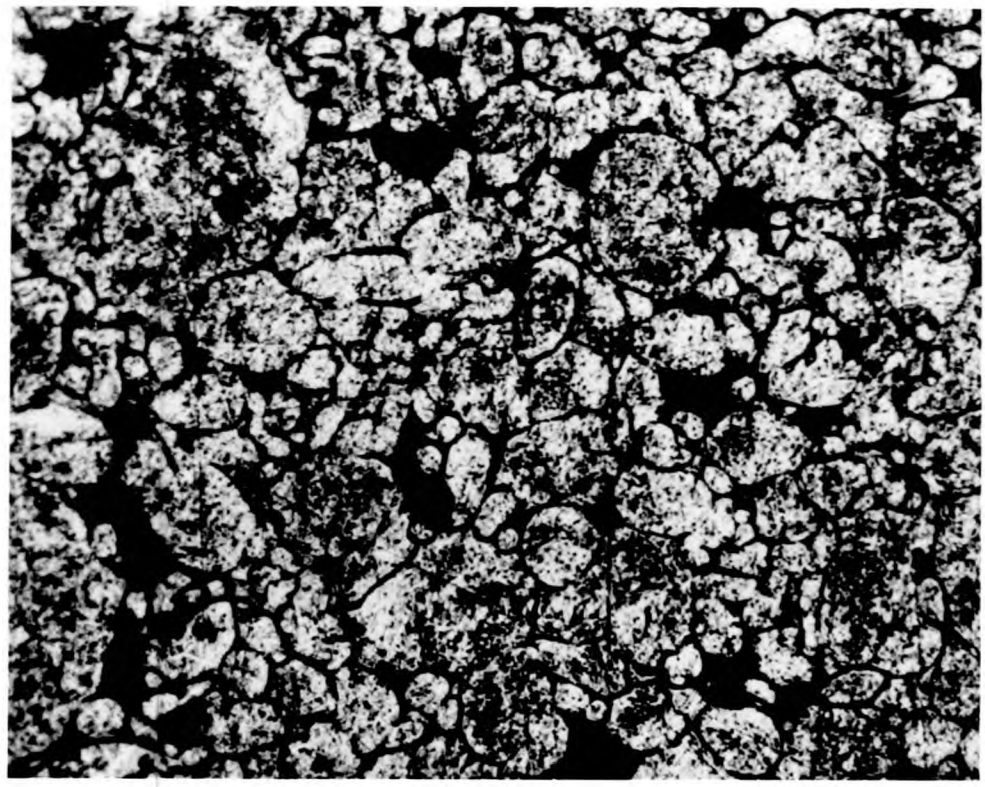

(a) Powder B as compacted (X 540)

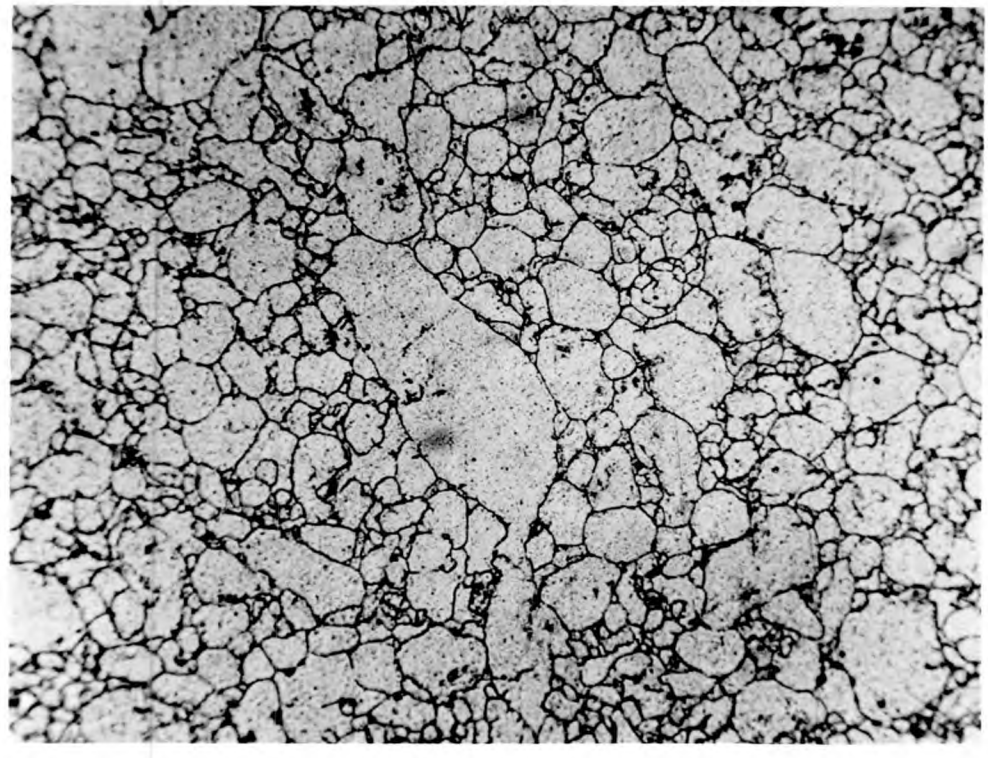

(b) Powder A cold compacted and sintered 24 hrs. at 600°C

PLATE 5. 4 Optical micrographs of two powder compacts

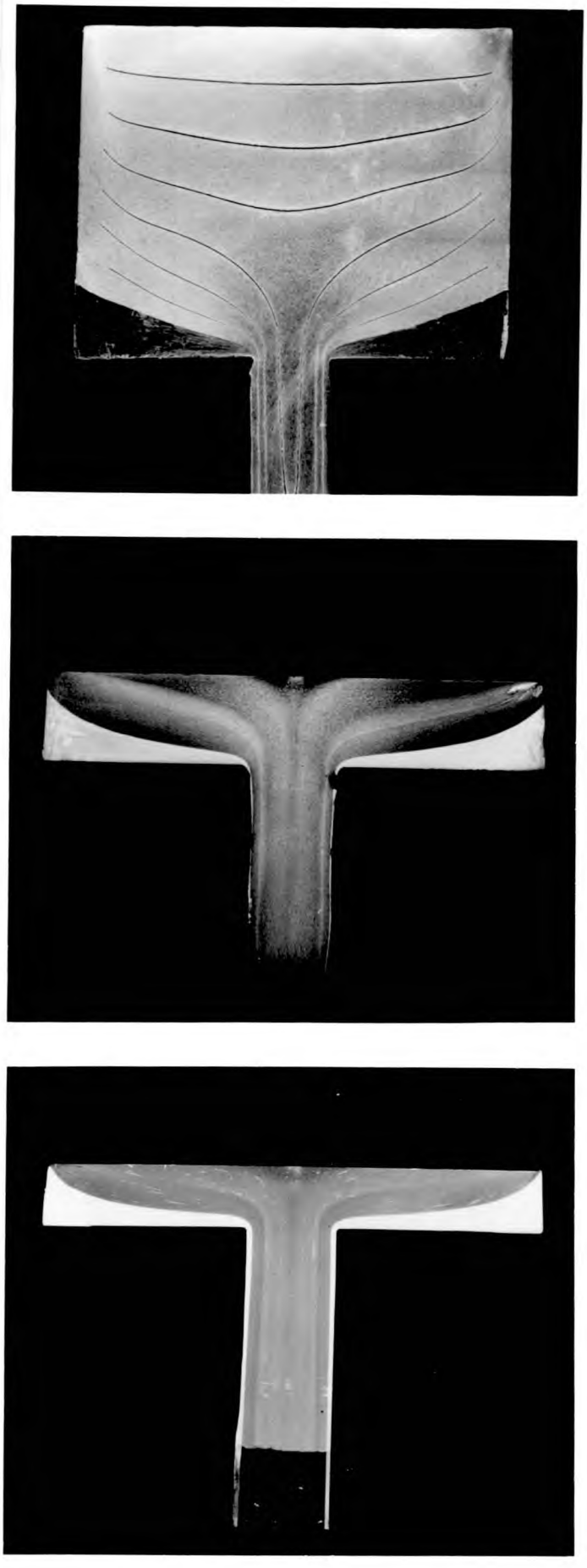

PLATE 5.5 The effect of billet length on the flow pattern

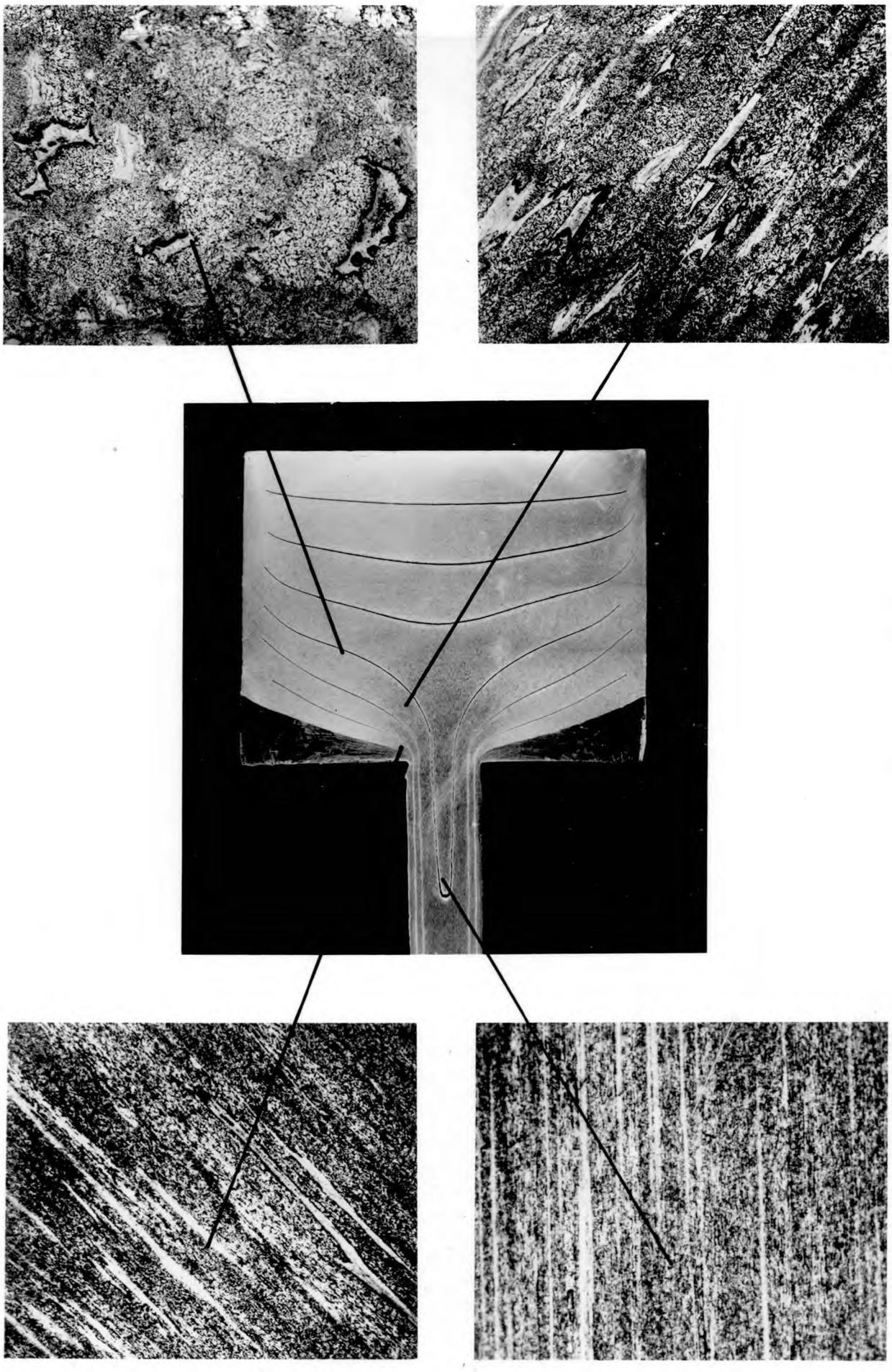

PLATE 5 6 Longitudinal section of a partially extruded billet. Macrophoto, etched. Photomicrographs, etched X 64

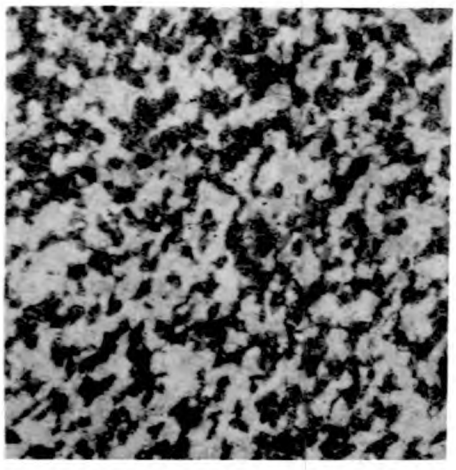

(a)

Powder L (Al-Fe) (X 40)

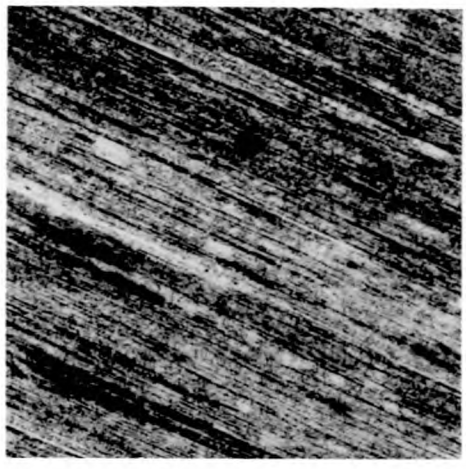

(b)

Powder K (Al-Mg-Zn) (X 40)

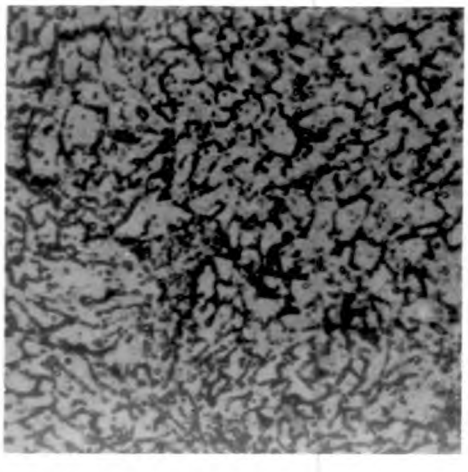

(c)

Powder B (X 450)

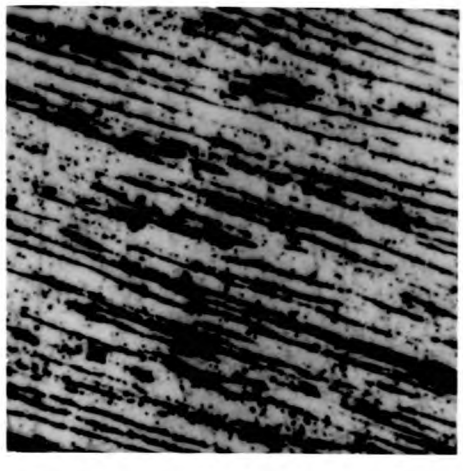

(d)

(X 450)

PLATE 5.7 Optical micrographs of the thermally extruded powders, longitudinal and transverse

investigated using transmission electron microscope. Micrographs taken were studied to determine the effect of the extrusion parameters on grain size and dislocation arrangements. It is found that the material is usually composed of a network of sub grains and the loose dislocations tangled or associated with second or oxide phase precipitates. The sub grains were measured to determine the mean diameter at a particular set of extrusion conditions including the initial particle size.

The electron micrographs, plates 6.1 - 6.11, are included with the discussion, to enable easier reference during reading.

5.10 Mechanical Properties

The tables 5.13, and 5.13(a), show the mechanical properties of commercial alloys produced, and previous experimental products of aluminium powders. Values of the alloys extruded in the present work are included for comparison.

Fig. 5.40 is a plot of Vickers hardness number against initial billet temperature showing a plateau at high initial temperatures. Fig. 5.41, shows the variation of hardness across a transverse section. The value quoted is the mean of these twelve experimental points.

Fig. 5.43 is a graph to test Orowan's dispersion hardening theory as shown in equation (3.31).

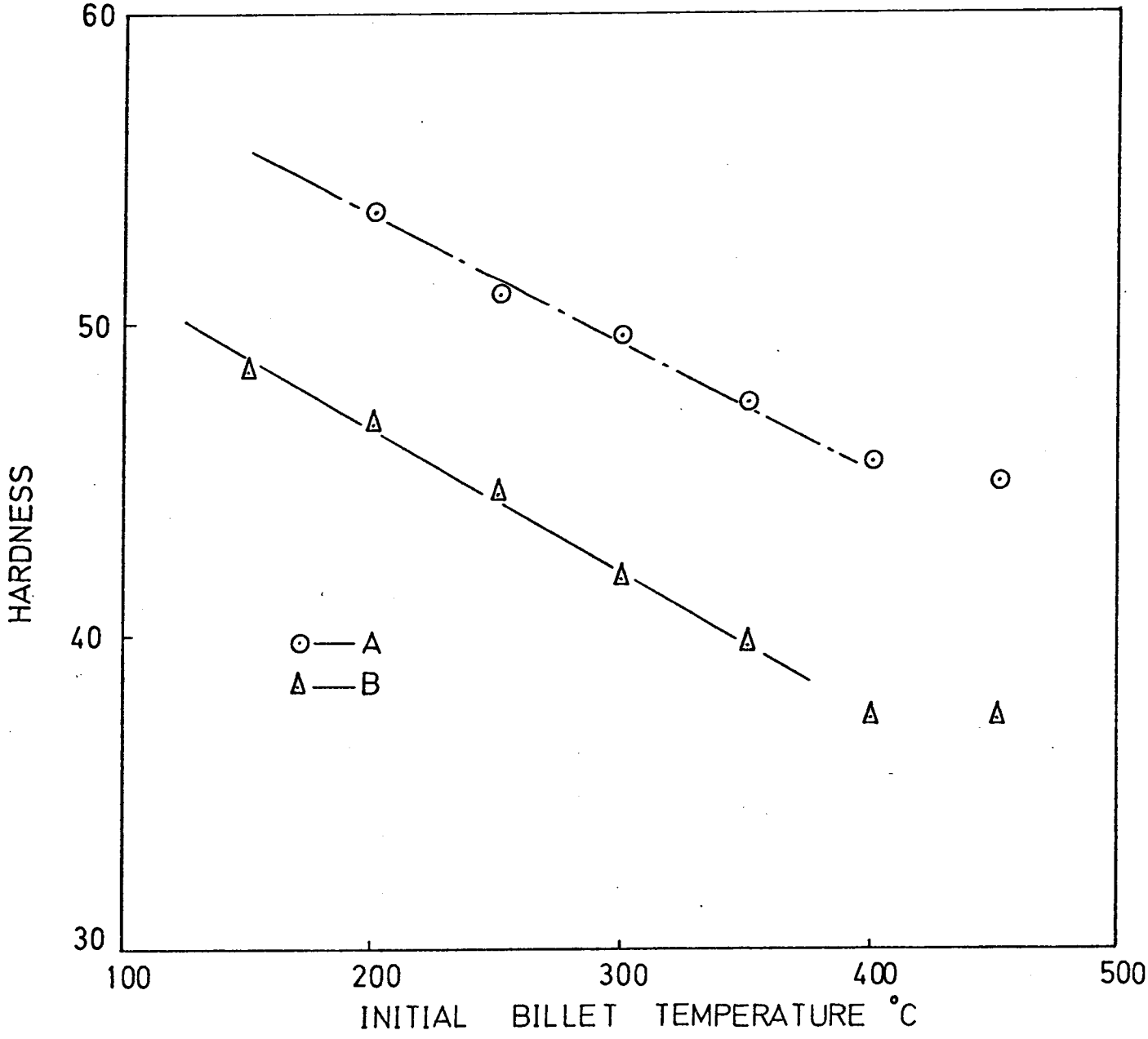

HARDNESS NUMBER AS A FUNCTION OF BILLET TEMPERATURE.

Fig. 5.40

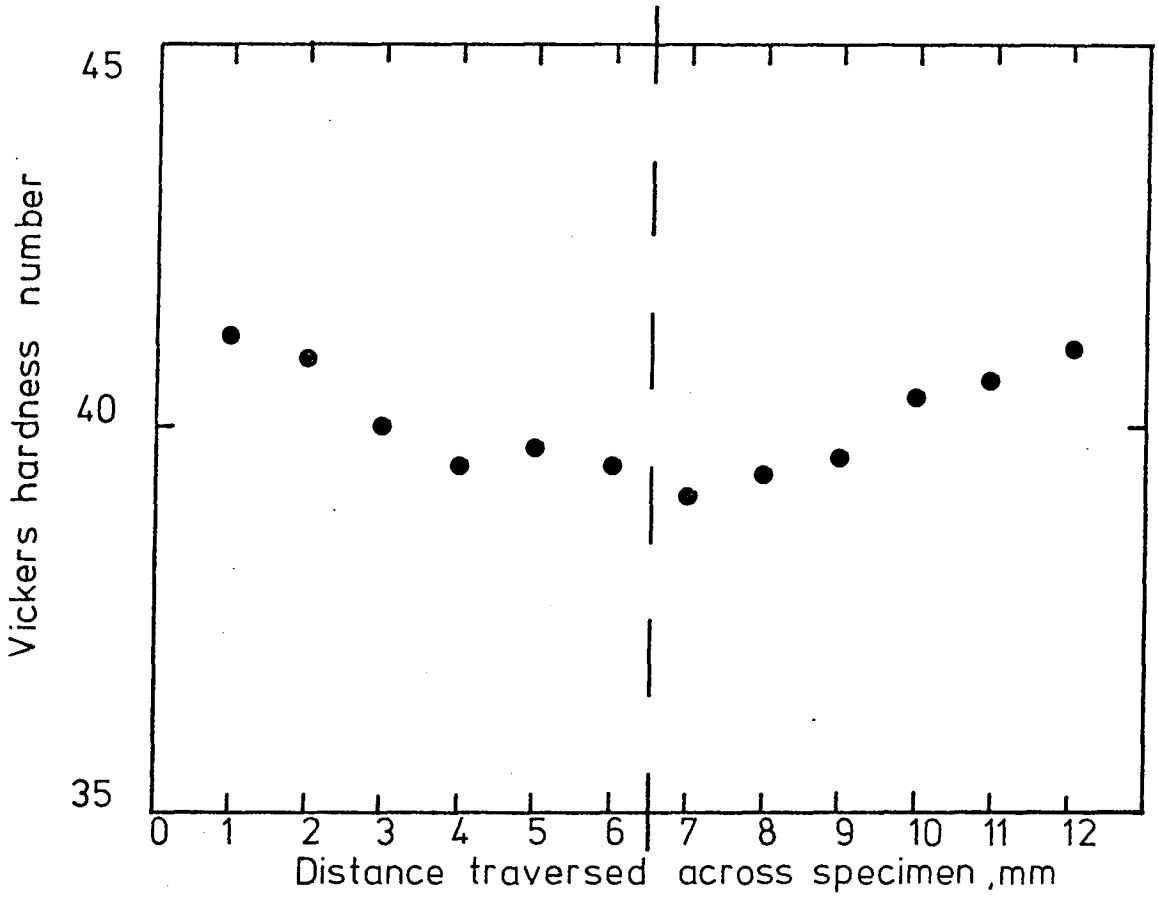

FIG. 5.41 VARIATION OF HARDNESS ACROSS A TRANSVERSE SECTION OF A ROD EXTRUDED AT A RATIO OF 30:1 AND TEMPERATURE OF 300 °C

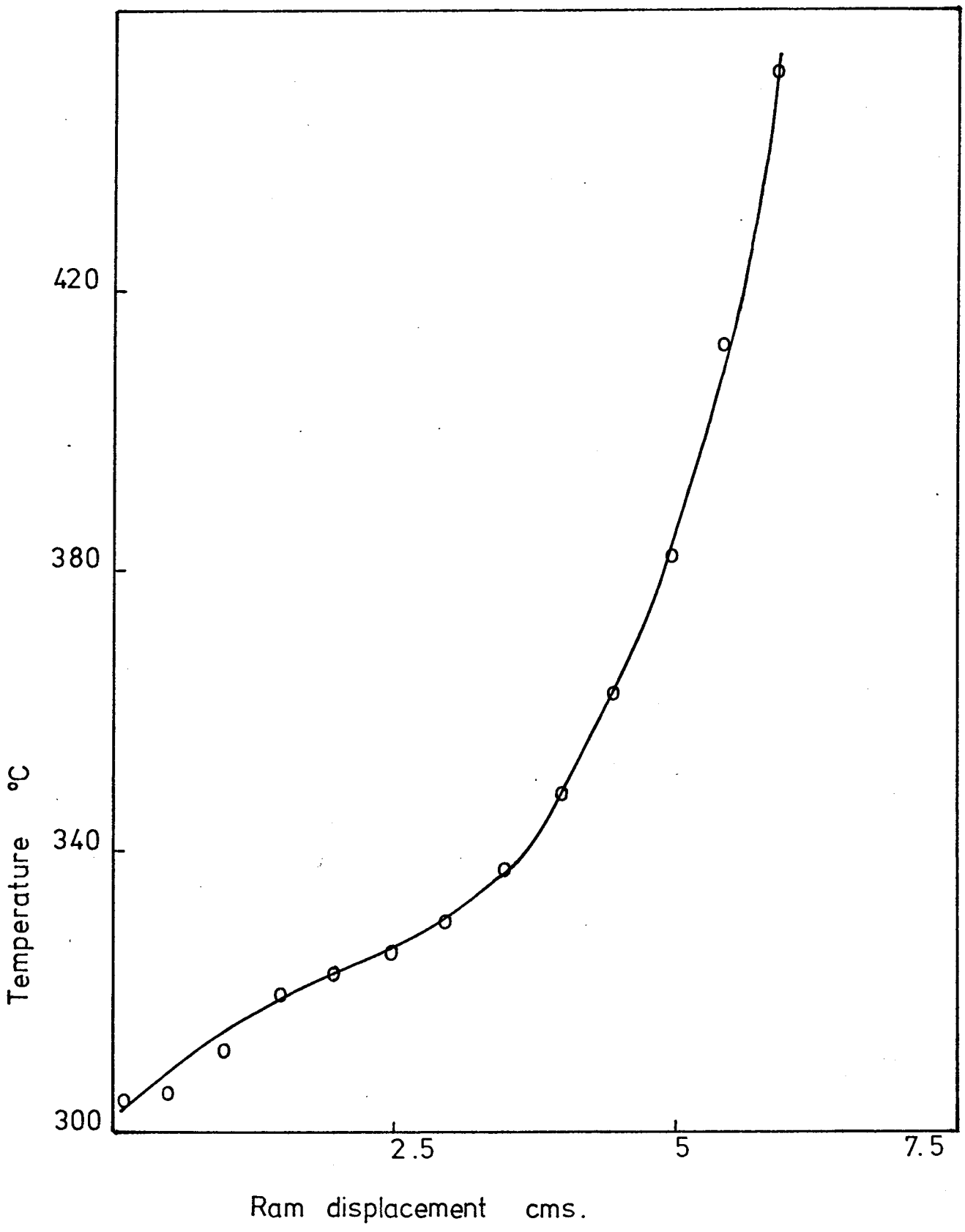

FIG 5 42 Temperature rise during ram displacement

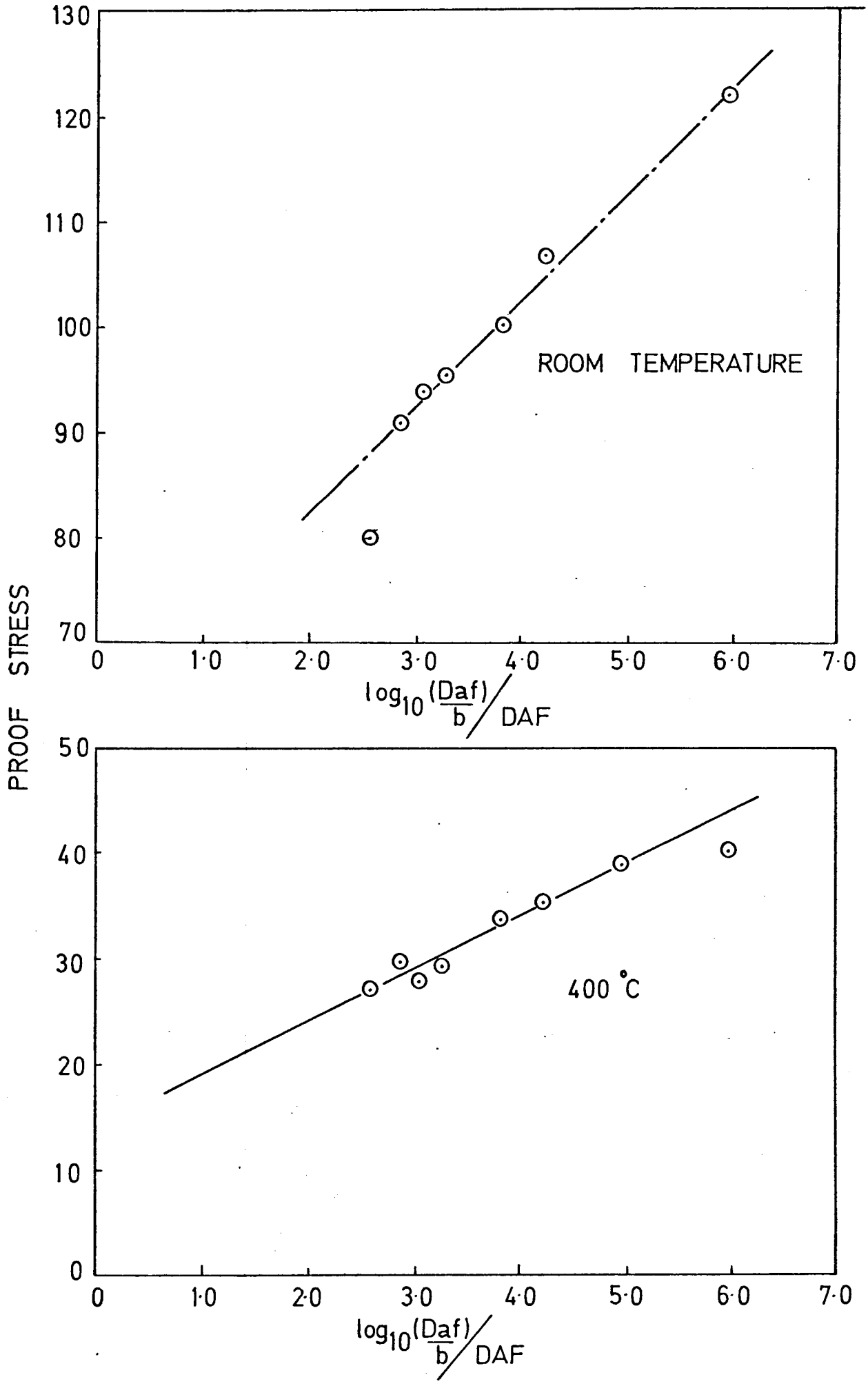

PROOF STRESS AS A FUNCTION OF THE OXIDE PARTICLE SIZE

Fig. 5.43

Table 5.13 Strength values of Commercial Alloys

Material	Comp^{n}	Test Temp	Prf Stress MN m^{-2}	Tensile Stress MN m^{-2}	Elong. %	Ref.
SAP 930	6% Al_2O_3	R.T. 400°C	117.4 68	225 68	22 11	14
SAP 895	11% Al_2O_3	R.T. 400°C	225.5 108.1	363 117	8 3	14
Al	(99.99%)Al 99.8 99.5 99.0	R.T. R.T. R.T. R.T.	- - 38.6	55.6 69.5 77.2 84.9	65 50 45 45	181
Al-Mn	Mn 1.25%	R.T. 371°C	54 14	108 20.1	40 70	
Al-Mg	Mg 2.25% Mn 0.25%	R.T. 371°C	77 20.1	185.3 34	20 130	
Al-Mg-Si	Mg 0.5% Si 0.5%	R.T. 371°C	77 14	154 17	30 105	
Al-Cu-Mg-Si	Cu 1.5 Mg 1.0 Si 1.0	R.T. 400°C	123.6 278 24.7	232 432 * 31	15 15 100	
Al-Zn-Cu-Mg	Cu 1.0 Mg 2.5 Zn 5.7 Mn 0.4	R.T. 400°C	556 31	602 * 45	11 65	

Table 5.13(a)

Material	Comp^{n}	Test Temp	Prf Stress	Tensile Stress	Elong. %	Ref.
Al-Cu-Mg -Si-Mn (duralumin)	Cu 4.4 Mg 1.0 Mn 0.75 Si 0.4	R.T. 400°C	123.6 278 24.7	231.7 432.4 * 30.9	15 15 100	181
Al-Mg-Mn	Mg 4.5	R.T.	125	275	14	
HE 15	Cu 4.0 Si Mg	R.T.	250	390 *	8	
Al-Fe	Fe 8.0	R.T. 400°C	500 -	580 110	5 -	181
Al-Fe	Fe 7.6	R.T. 400°C	- -	320 80	- -	24

* Solution treated and aged.

Table 5.14 Strength values of products made from atomised aluminium powder

Material	Oxide Content %	Test Temp °C	0.2% Prf. Stress MNm^{-2}	Tensile Strength	Elongation	Ref.
M 255	0.5-1	R.T. 316°C	83.4-123.6 52.5	139-170 54.1-61.8	25-31 17-28	14
M 293	1 - 3	R.T.	120.5	188.4	25	14
MD 13	0.2	R.T. 400°C	51.7	108.1 27.8	36-40	94,99
MD 105	1.4	R.T. 400°C	- -	168.3 59.5	33 26	94,99
R3M	1.75	R.T. 400°C	- -	187 64.9	32 28-34	94,99
Atomised	-	R.T. 400°C	137	205 58.7	7.8 7	114
Atomised	-	R.T.	98.8	132.8	23.3	14
1% Ni	-	R.T.	139	199.2	20	14
MD 13	0.2	R.T.	52	107.3	38	86,87
MD 201	0.6	R.T.	87	140.2	26	86,87
MD 105	1.0	R.T. 400°C	145 45	165 53	15.5 9.7	86,87
R 400	1.2	R.T. 400°C	120 47	157 54	20.5 10.1	

Table 5.14(a) Strength values of products made from atomised aluminium powders

Material	Oxide	Test Temp °C	Prf Stress MNm^{-2}	Tensile Stress	Elongation
A	1.9	R.T. 400°C	125.3 45.4	160.7 58.5	24.4 18.6
B	1.1	R.T. 400°C	97 30.8	135.4 36.2	29.9 21.2
C	0.36	R.T. 400°C	85 22.5	122 28.6	35.6 28
D	0.45	R.T. 400°C	74 24	102.2 28	24.3 24
J(Al-Mn)	0.72	R.T. 400°C	140 54	208.3 63.8	26.9 45
K(Al-Mg-Zn)	0.74	R.T. 400°C	217 20	413 25.7	9.9 13.6
L(Al-Fe)	0.51	R.T. 400°C	188 68.1	276 92.3	16.6 24

Table 5.15 Density of the Extruded Products

Material	Density Range g/cm^3
Al - A	2.69 - 2.72
Al - B	2.69 - 2.71
Al - C	2.68 - 2.71
Al - D	2.69 - 2.71
Al-Mn J	2.7 - 2.73
Al-Zn-Mg K	2.66 - 2.69
Al-Fe L	2.69 - 2.73

CHAPTER 6

Discussion

6.1 The Powders

6.1.1 Powder shapes

The atomised aluminium and aluminium alloy particles had been manufactured to produce a variety of rounded shapes. Powders of types C, J, K and L are found to have a tendency to 'tail', an inherent defect of powders produced by the atomization technique using a horizontal air blast on the hot molten stream. In contrast particles of A and B, which had been produced by a vertical hot air blast, generally exhibited good rounded shapes of varying sizes.

Shapes and sizes of particles produced by atomization have been found to depend upon the nature of the impinging gas or water jet on the molten stream and the geometrical configuration of the apparatus[1,2]. To produce spherical particles long cooling times, to allow the surface tension forces to minimize the surface, are necessary. However, to avoid particle coalescence and 'matting' the quenching of the molten particles must be fairly rapid so that they are sufficiently cool and solid on landing.

Powders C, J, K and L are not as spherical in nature as A or B, but, they are the kind that are preferred for commercial applications, as spherical particles do not possess the desired characteristics. Spherical powders provide the lowest degree of mechanical strength because of poor initial point contact between adjacent particles and a low surface to volume ratio. Deviations from sphericity are desirable as this gives better point contacts, larger surface areas, and

sedimentation areas.

In the present work little observable difference was noted between the two types of powders due to the relatively soft nature of the particles and their ease of deformation.

6.1.2 Powder size

The size, or size distribution parameter of a particular powder is very easy to determine as there are so many and varied techniques, but the difficulty arises in setting a standard for comparison. In the present work the technique of sieving was used as it was the simplest and easiest method for the large quantity of material involved. As mentioned in the experimental chapter the end point was taken after sieving a particular quantity for a specified time.

The results of the size distribution obtained, tables 5.1 - 5.6, can still be subject to criticism on the basis of the sampling technique. However, it is considered that a representative sample is obtained from the powder mass after standard coning and quartering the whole drum, using the last quarter separated as the sieving sample. Errors arising from segregation of large particles are overcome as the whole of the material is used in the sampling process. Odd distributions were obtained from the alloy powders as they had been preliminarily sieved by the manufacturers into a size range, and on further sieving the fines were brought out giving a larger tail than expected.

6.1.3 Surface area

The surface area of the fine powders was determined using a B.E.T. analysis and the results are shown in table 5.8. The larger size particles were not able to be analysed due to the size of the sample

needed which would have been in excess of the capacity of the equipment. Nevertheless the results obtained for the powders A and B, give a direct indication of the surface areas involved for the powders and it is seen that the smaller the particle size the greater the surface area. Theoretical calculations can be performed to confirm the experimental results and any departure from the spherical shape will increase the specific area; the sphere is the minimum energy shape hence the smallest area.

The oxide content of a particle can be related to the surface area knowing the thickness of the oxide layer and its density. The smaller the particles, the greater the surface or sedimentation area, the higher is the weight fraction of the oxide. This is confirmed in the results of the natural oxide content analysis and will be discussed in more detail in the following section.

6.1.4 Chemical composition

All the powders were analysed for both major and minor constituents using the technique previously described. It is unfortunate that the analysis of aluminium had to be carried out using a difference and dissolution technique as this led to two main sources of errors. First, the accuracy of the method depended upon the operator, and secondly all the impurities had to be accounted for. Analysis of the alloys, particularly, presented problems as each element was determined separately before the oxide content was determined. After analysis of all the constituents the remaining undissolved remnant was weighed as the oxide content.

The powders B and C were analysed for the natural oxide content for varying particle sizes, and it is noted that the extremely large particles have an oxide content very much greater than the less coarse

particles, or the extremely fine particles. In order to understand the variation of the oxide content with particle size, the size of these particles must be considered in relation to oxidation and cooling. The weight fraction of the oxide can be related to oxide layer thickness and surface area, and the thickness of the natural oxide to the rate of cooling.

From the experimental results it is seen that the oxide content increases slightly with decreasing particle as the sedimentation surface area increases. The high weight of oxide on the large particle fractions is due to the slower rate of quenching during atomization compared to the finer particles. These larger particles are held at an elevated temperature for longer periods than the former and so enhance the diffusion of oxygen through the outside layer to form a slightly thicker coating. Thus, with decreasing particle size, the thinner the natural oxide film becomes, but, the weight fraction increases due to the increase in surface area available. Therefore, it can be seen that the weight fraction of the natural oxide layer is determined by two competing factors, the rate of cooling and the sedimentation surface area.

The high values of oxide content for the alloy powders must be regarded with a degree of scepticism due to the analytical technique. Later results, however, in table 5,7(a), do show a much more reasonable value with the weight percentage of oxide around one weight per cent. This is due to the increased competence and experience of the analyst with the alloy powder. The powder particle size again reveals that the highest levels of oxide are found in the dust samples and the large coarse particles.

Details of the alloy compositions are shown in tables 5.7 - 7(a) in the results section. These show that the aluminium magnesium zinc alloy is much as expected in composition but the dust fraction contains a higher quantity of zinc, over 2wt. pct., and a lower magnesium concentration. However, the significance of this one result is not too important as it is within the sampling error and the variation of percentages of the zinc content of the other particle sizes.

The aluminium manganese alloy is shown to have 3.59 weight per cent of Mn and also a fairly high Fe concentration, about 0.35 pct., with silicon at about 0.18 pct. Therefore, the material is fairly impure and quite a complex alloy will result with Mn, Fe, and Si the main constituents in the aluminium.

Analysis of the aluminium iron alloy shows that the alloy contains 2.38 weight per cent of Fe and not the 5 or 6 pct. quoted by the manufacturers. This is due to the inability of maintaining the temperature of the melt, during atomization, at a high enough temperature to retain the iron in solid solution. Any significant drop in temperature will result in the iron coming out of solution and segregating in solid form within the crucible thus depleting the melt of its iron concentration.

Again the material is shown to be fairly impure with the result that a complex alloy will arise.

6.1.5 Structure

The aluminium particles in their 'as received' condition are found to comprise of a fairly uniform fine grain size. In the larger particles there is a tendency towards a columnar type structure near

the surface of the particles. This structure, similar in nature to a chill cast ingot structure, would be expected in large particles cooled relatively slowly in a blast of air. The aluminium alloy powders reveal the presence of a very fine structure, dendritic in nature, due to the high rate of solidification found in the atomization process. In some of the larger particles of alloy J, the aluminium - manganese alloy, there is evidence of large primary precipitates, plate 5.3. The size of these precipitates in relation to the fine unresolved background indicates that either the particles are cooled very slowly or that the primary phase is precipitated out before the formation of the particles in the air stream. Precipitation before atomization is possible, i.e. having the melt at too low a temperature but not sufficiently low to cause blocking of the crucible orifice, as the temperature of the molten aluminium alloy has to be above 710°C for 4 weight per cent of manganese. It is possible that small precipitates of $MnAl_6$, formed as the liquid temperature falls below about 700°C, will act as nucleii for primary precipitates in the large particles. As these large particles cool relatively slowly the $MnAl_6$ has sufficient time to coarsen and form relatively large primary precipitates within the atomized particles. Electron microscopy reveals no evidence of large precipitates due to the large $MnAl_6$ particles being broken and fractured during the extrusion process.

The two alloys, J and L, Al - 4% Mn and Al - 2.5% Fe, are both alloys that cannot be produced by casting in a useful form, due to the formation of large primary precipitates in a cast structure, at the grain boundaries, thus rendering the material fit only as a master alloy. The process of atomization breaks the molten alloy up into small regions that can be cooled quickly, thus yielding a material with a fine precipitated structure. The cooled material is then a

supersaturated mata-stable alloy containing the normally coarsely precipitated second phase either in solid solution or in fine precipitate form.

6.1.6

The area for study is from a cold pressed compact that has been broken to reveal the nature of packing of the individual particles in the compact. Scanning electron microscope pictures, plate 5.2, reveal that there is little obvious extensive plastic deformation or even localised plastic deformation of individual particles. Previous workers,[31,34] using iron powders, have observed localised deformation during compaction at the contact points between particles. In the present situation this is difficult to prove, added the fact that insufficient pressure was used during compaction to cause extensive particle deformation. It is noticed, however, that the particles have re-arranged themselves during pressing so that the small particles are positioned in the gap between large particles, or those left by 'bridging' in the initial packing arrangement. The larger particles are then in more intimate contact so there is a distinct possibility of plastic deformation at these areas. Thus, any deformation within the compact is localised and restricted to the larger particles.

The distinctive surface markings on the particles are those of a cellular type solidification[176] structure, formed during cooling by segregation of solute impurities in a region of narrow super cooling. This is found in commercially pure aluminium and the segregation of solute forms the basis of cell walls which are regions of high concentration.

6.1.7 Compact structure

The optical micrograph, plate 5.4(a), helps to give an indication of the voids present in the cold compacted state. However, the larger voids seen are due to the small particles, not sufficiently well bonded to their nearest neighbours, being dragged out of the compact during mechanical polishing. The range of particle sizes can be seen, the smaller particles lying between the larger ones. In the same micrograph it is also noted that the larger particles are compacted to form a dense area but still retain their individuality.

In comparison, micrograph, plate 5.4(b), shows a compact of powder A sintered. The density of this material is the same as the compact but due to the sintering process the particles are held together more firmly. The large particle in the centre can be seen to have grown by coalescence with adjoining particles; visible evidence of the sintering process. There are no visibly large pore areas indicating a wide dispersion of fine pores, previously observed by Modi - Onitisch[177].

6.2 Alloy Powders

6.2.1 Commercial alloys

In commercial practice the casting of a high weight percentage Mn or Fe content alloy is restricted to the production of master alloys for increasing a particular element content of an aluminium alloy. Looking at the phase diagrams[142,143]* it can be seen that for both binary alloys, Al-Fe and Al-Mn, there is limited solid solubility of the secondary element in aluminium.

Casting a high weight percentage alloy of these systems presents problems, in segregation of the melt, and coarse precipitates present

* see fig. 6.0.

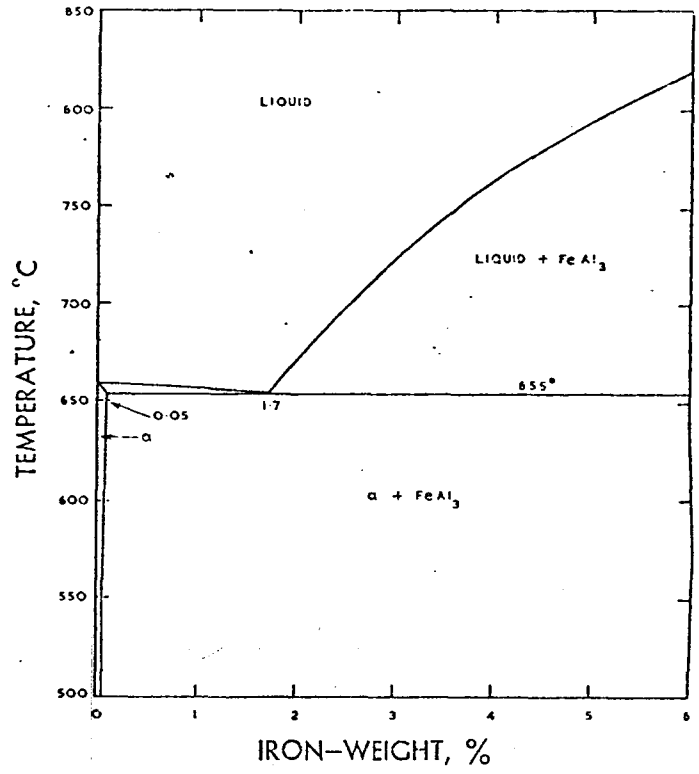

Aluminium-Iron

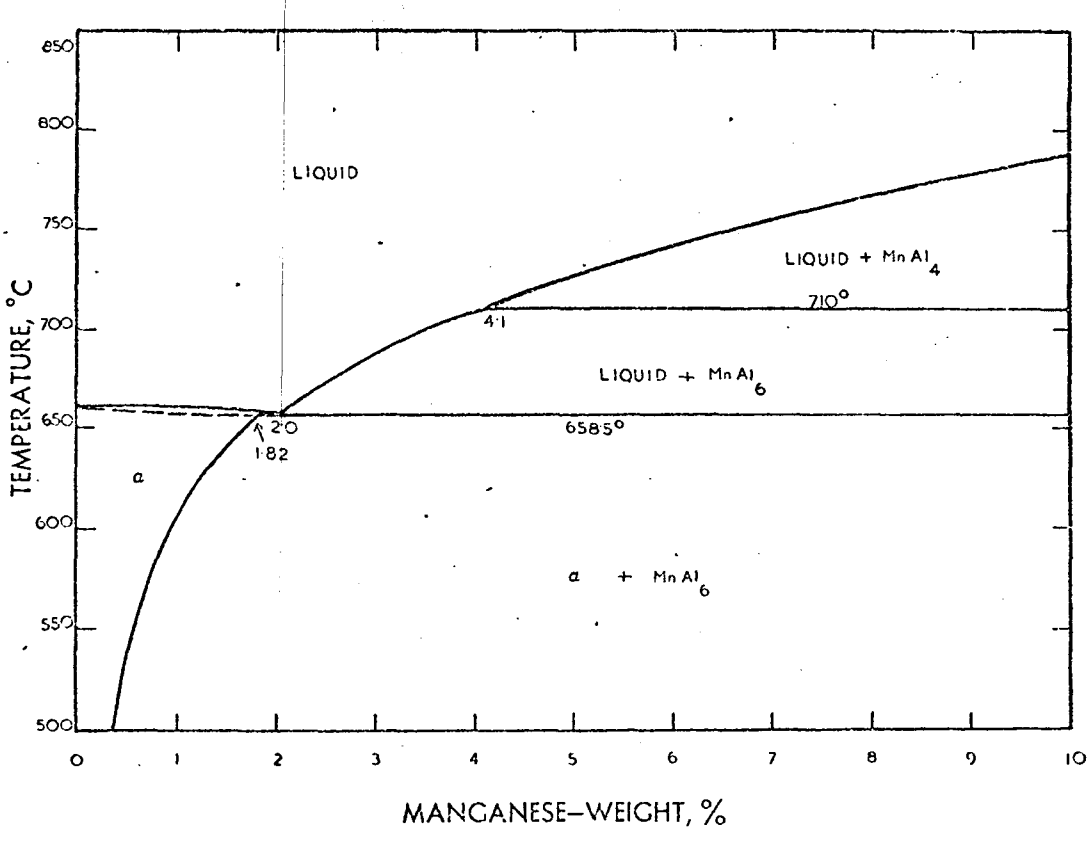

Aluminium-Manganese

FIG 6.0 EQUILIBRIUM PHASE DIAGRAMS

at grain boundaries in the cast structure.

The aluminium manganese alloys used commercially are the Al-1.25% Mn and Al-4% Mn. The Al-1.25% Mn alloy is a general purpose non heat-treatable one, obtainable in many shapes and forms but now generally restricted to wire and beer barrel production. The Al-4% Mn alloy, similar to the French AM4 alloy, is produced only in small quantities and used primarily for gas burners and as an anodising material. This alloy is particularly suitable for use in gas burners as it retains its rigidity up to 650°C and also its polish at these high temperatures.

The Al-1.25% Mn alloy has 0.6% Fe added as a grain refiner; the iron favours precipitation of manganese out of solid solution. A similar addition must be made to the Al-4% Mn alloy but as this alloy is only produced in small quantities, problems of coarse precipitation should not be too severe.

The aluminium iron alloy is not used in its binary form due to the problems previously mentioned for limited solid solubility alloys. Al-Si-Fe, a die casting alloy, is the most widely used aluminium alloy containing iron as an addition. The presence of iron in this alloy decreases the tendency of the alloy to weld and gall in a die.

6.2.2 Aluminium - Manganese

Studying the equilibrium phase diagram[143] of the aluminium system it can be seen that equilibrium cooling yields the phases $MnAl_4$ and $MnAl_6$. Aluminium forms a eutectic with the constituent $MnAl_6$, containing 2% Mn and freezing at 659°C. There is appreciable solid solubility at the aluminium end reaching 1.82% Mn at the eutectic

temperature, but falling to 0.95% at 600°C and 0.35% at 500°C. From 2.0% to 4.1% Mn, $MnAl_6$ is the primary phase and at higher percentages its phase is taken by $MnAl_4$ which reacts peritectically to form $MnAl_6$.

In a rapidly cooled system, not equilibrium cast, the region of solid solubility is extended. The aluminium manganese system is often subject to undercooling and rapid solidification, and it has been found that the eutectic is displaced to 3 or 4%[152]. The presence of iron[153] speeds up the precipitation of $MnAl_6$, usually taken into solid solution in $MnAl_6$, and forms a ternary eutectic with aluminium containing 1.8% Fe and 0.75% Mn freezing at 654°C.

Silicon is the other main impurity in the Al-Mn alloy and this also forms a ternary constituent, designated α(MnSi), which is crystallised in a script form.

6.2.3 Aluminium Iron

The equilibrium diagram shows that a eutectic is formed between the constituents designated $FeAl_3$ and aluminium at 1.7% Fe and 655°C. The solid solubility is very small, at 655°C the aluminium rich solid solution contains 0.052% Fe and with decresing temperature the solid solubility falls to 0.025% Fe at 600°C and 0.006% at 500°C[154]. These values can only be achieved by prolonged annealing and quenching, so that aluminium, even of super purity quality, will normally contain particles of iron bearing constituents.

Solidification of the Al-Fe system has been studied fairly extensively with special interest in splat cooling to produce high iron concentration alloys of high strength. As the rate of solidification are increased changes in constitution and morphology have been observed[117]. Schiel and Masuda[155] found the eutectic composition

shifted by rapid freezing from 1.7% Fe to 6% Fe with an associated change from anomalous to normal (lamellar or rod like) morphology. The solid solubility zone was discovered to be extended by splat cooling from the equilibrium maximum of 0.05% to several per cent[116].

Cooling of the liquid Al-Fe system gives rise to segregation effects as the partition coefficient for iron between solid and liquid aluminium is low and diffusion is required to maintain equilibrium[156]. This gives rise to dendritic solidification with the iron segregated to the dendrite interstices.

6.2.4 Powder advantages

The problems of producing an alloy such as Al-4% Mn or Al-5% Fe are those arising from the high superheat required for casting to obtain a satisfactory melt and the subsequent cooling problems. These being:

(i) a large 'mushy' region exists before solidification

(ii) segregation due to limited solid solubility

(iii) hot tearing in the mould

(iv) porosity

Alloys of the Al-Fe and Al-Mn materials can easily be produced by atomization of the melt. This yields a material in solid form of super saturated solid solution and finely precipitated eutectic phase. Atomizing into fine particulate form ensures that the alloy produced is rapidly quenched without the use of elaborate casting techniques. This method will enable alloys, not normally produced due to coarse precipitation and attendant disadvantages of a large 'mushy' region during casting, to be manufactured. The fine nature of the internal structure of the particles ensures a high strength material which have the added advantage of ductility over the S.A.P. type alloy.

6.3 Compaction

6.3.1 Cold compaction

Compacts of powder A, the finest powder size, had a lower density than compacts of powder B pressed to the same pressure due to the increased friction during pressing of fine powders. The phenomenon of 'bridging' is also prevalent in very fine powder which has to be overcome before a handable green compact can be made. These two factors contribute to localised heating during compaction giving the compact considerable warmth, which can be felt when the compact is ejected from the die.

On ejection from the die, it was sometimes observed that the bottom rim of the compact was easily broken off. This is due to irregular density distribution. This has been studied in some detail by previous workers[29,31] but is of little concern in this present work as the compact is pressed to a higher density in the extrusion container before extrusion commences.

The cold compacted specimens studied on the microscope show that the cold compaction only passes through two stages, as the pressure is insufficient to cause excessive cold working or fragmentation. The two stages concerned are; packing, and elastic and plastic. deformation. Particles in this preliminary pressing easily rearrange themselves and the fine powders the 'bridges' are eliminated. However, the extent of elastic and plastic deformation is not certain.

The results of the cold pressing pressure in terms of compact height are presented in graphical form, figures 5.1 - 5.4. Only a few results are presented, these being representative of the powders, as the other results are very similar numerically.

Figure 5.1, a plot of ln P against height of compact is drawn to show that the results obtained from pressing aluminium powder agree with Bal'shins[36] empirical formula. For the powders investigated, and the small range of pressures used, values of the pressure imposed on a compact affected the relative volume according to the equation of Bal'shin.

Compaction results are also fitted to an equation derived by Kawakita[30], shown in figures 5.2 - 5.5.

$$P/C^* = 1/ab + \frac{P}{a} \qquad (6.1)$$

The constant 'a' is found to be equal to the value of C^*, at infinitely large pressure P, $C^*_\infty = \frac{(V_o - V_\infty)}{V_o} = a$, where V_∞ = net volume of the powder. In the piston compression case, i.e. this situation, the constant 'a' is equal to the initial porosity. Correlation of the constants 'a' and 'b' to the other physical properties has been tried by Kawakita[39], but any clear relationship is doubtful.

It is found that the coarse mesh fraction shows a smaller initial porosity than the other smaller particle sizes. This is due to the heavier individual particles settling and packing better than the small particles which have a tendency to form 'bridges'. The more closely packed particles will then have a smaller porosity, which is shown in figure 5.2, than the dust particles, figure 5.3. The increase of the initial porosity with decreasing particle has also been reported by other workers[30,37-39], the reason being, as explained above, the ability of the coarse mesh particles to counteract 'bridging' and settle more closely by the action of their own weight.

The figures 5.4 and 5.5.for two of the alloy powders show negative deviation from the initial stage of the piston compression equation due to the difficulty in deforming the alloy particles. The first application of pressure is not sufficient to plastically deform the particles, but is sufficient to elastically deform individual particles and cause packing and resettling before the compacts are deformed. Results for the aluminium powders do not show this large deviation as they are relatively soft and easily deformed. A negative deviation will be found at low pressures but the equipment was not sensitive enough to show this. As soon as the packing has taken place and the bulk of the powders in the compact is being deformed the results will follow the linear portion on the graph.

The results were obtained from relatively insensitive instruments but do show that the powders used conformed to the empirical equations derived by previous workers. More detailed analysis of the compaction behaviour could not be carried out without more detailed and redesigned instrumentation for pressure measurements.

6.3.2 Hot compaction

It can be seen from the load/ram displacement diagrams that the first ten millimetres of ram travel represented the compaction of the powder billet to nearly theoretical density. At this point particles were deformed to cause the closest possible contact without losing their separate identities, i.e. separate particles still distinguishable, as seen in plate 5.6 of the partially extruded billet. Considering the stages of cold compaction it can be deduced that at elevated temperatures the second stage, that of plastic deformation, is soon reached and the particles fill the pores left by cold compaction. During hot compaction there is welding together of the particles at

their contact points, mechanical interlocking, penetration of oxide film, particles conforming to contours of other particles, and squeezing of small particles into voids. All these processes take place in the first increase of the applied load prior to extrusion and given the compact relatively good strength but poor ductility. The strength of the compact is then imparted from the welded contact areas, which are relatively small and soon work harden and fracture.

The theories of hot pressing have been derived theoretically and empirically of the form.

$$\frac{dQ}{dt} = -\frac{3}{4}\frac{PQ}{\eta} \qquad (6.2)$$

This equation is difficult to verify from the extrusion results as the point of a particular density cannot easily be determined. If the viscosity is regarded to depend upon self diffusion, as in the Nabarro Herring equation, a value for the average grain radius is needed, but the main difficulty arises from the need to estimate the viscosity. Under the conditions applied, the Nabarro Herring mechanism would not be operative as it is a very slow diffusion process usually found in the later stages of densification after plastic flow.

The operative densification stage during the compaction of the billet, prior to extrusion, is that of plastic flow. The particles are forced into the pores or void areas to give a compact or nearly theoretical density. The time taken to achieve this process is a few seconds so that a Nabarro - Herring type mechanism can be ruled out.

Fig. 5.9, in the results section, shows the variation of compaction pressure with temperature, in the form of ln P against temperature

in ^{o}K. This is an empirical relationship and cannot be easily justified on theoretical grounds.

Verification of the hot pressing equation 6.2 is difficult from the experimental results as the time of hot pressing cannot be accurately assessed from the load/ram displacement diagrams.

6.4 Flow pattern

Plates 5.5 and 5.6, etched macro sections of partially extruded billets, show the variation of the regions associated with the extrusion of a powder billet. The optical micrographs taken illustrate that the powder particles retain their individual identity up to and into the deformation region. The micrograph taken of a small section of this zone reveals that particles are extensively deformed in this region by the mass action of adjoining particles and the resultant movement towards the die orifice. Particles lose their identity as they pass from the deformation region into the die orifice and into the solid product.

6.5 Mode of deformation

Combination of the results of tensile tests of specimens taken from different regions in the partially extruded billet, and the photomicrographs of the same specimens, help to build up a picture of the mode of deformation.

Tensile tests were performed on very small Hounsfield specimens machined from sections cut out of the billet. Unfortunately the size was still relatively large in comparison to the region of deformation, but this size was the smallest machined size feasible. Results from larger sized specimens did not show the trend of

increasing tensile strength as well, as they covered a much larger area.

The photographs in plate 5.6 show that the rear end of the powder billet is composed of closely packed particles with little deformation. The tensile specimen from this region shows that the yield strength and tensile strength are very close; i.e. the material work hardens only a relatively small amount before fracture. In this region the material that is deformed is that which forms the contact area between the particles. During deformation this is soon work hardened and fractured due to its relatively small area in comparison to the rest of the compact.

The next specimen taken, labelled 3 in fig. 5.8, shows a little more ductility and tensile strength than the previous specimen, but not a very large increase, as the contact areas have not been greatly increased. However, a slight increase is expected as there is a small degree of inter particle movement with a resulting contact area increase caused by the general relative downward motion of the particles.

The next specimen, number 2, taken near and in the deformation zone shows a much greater increase in tensile strength as there has been more movement near this region. Optical micrographs reveal that in this area the particles begin to lose their identity and subsequently increase the inter-particle intimate contact. This is reflected in an increase in strength and ductility approaching the final properties of the product. In the deformation region there is a considerable amount of particle motion and thus a degree of welding and rewelding that builds up a large contact area. This continues into the next region, number 1, where the strength and ductility is

improved to almost that of the product.

Considering the upper bound analogue, the strength of specimen 1 should be the same as that of the product, specimen 0. The values differ, because the specimen 1 could not be taken solely from the region 1 as the size of the tensile specimen was not small enough. However, the results do give a direct indication that the strength and ductility increase as the die orifice is approached. The material gradually acquires the properties of the final material by a process of continuous breaking and rewelding of particle contacts becoming more difficult as the material approaches the die. In the region 1 deformation of the material will be by shear as in the conventional extrusion process.

Understanding of the deformation mechanisms during extrusion with the aid of the upper bound analogue will help to explain the lower, than expected, extrusion pressures.

In the theory section the load for steady state extrusion using the minimized upper bound solution based on Johnson and Kudo's equation[64] is as follows, see fig. 6.1,

$$\text{Load} = K\,(AB\overline{23} + OB\overline{34} + BC\overline{24} + OC\overline{45} + OA\overline{13})$$

However, it has been shown experimentally that the shear yield stress is not constant but is dependent upon relative position in the billet. Therefore the equation will become:

$$\text{Load} = K_1 AB\overline{23} + K_2 BC\overline{24} + K_3 DB\overline{34} + K_4 OA\overline{13} + K_5 OC\overline{45}$$

Values of K_1 - K_5 are all different, K_5 K_1 - K_4

Looking at the room temperature results of the tensile tests carried out it can be seen that only K_5 will approach that of the shear

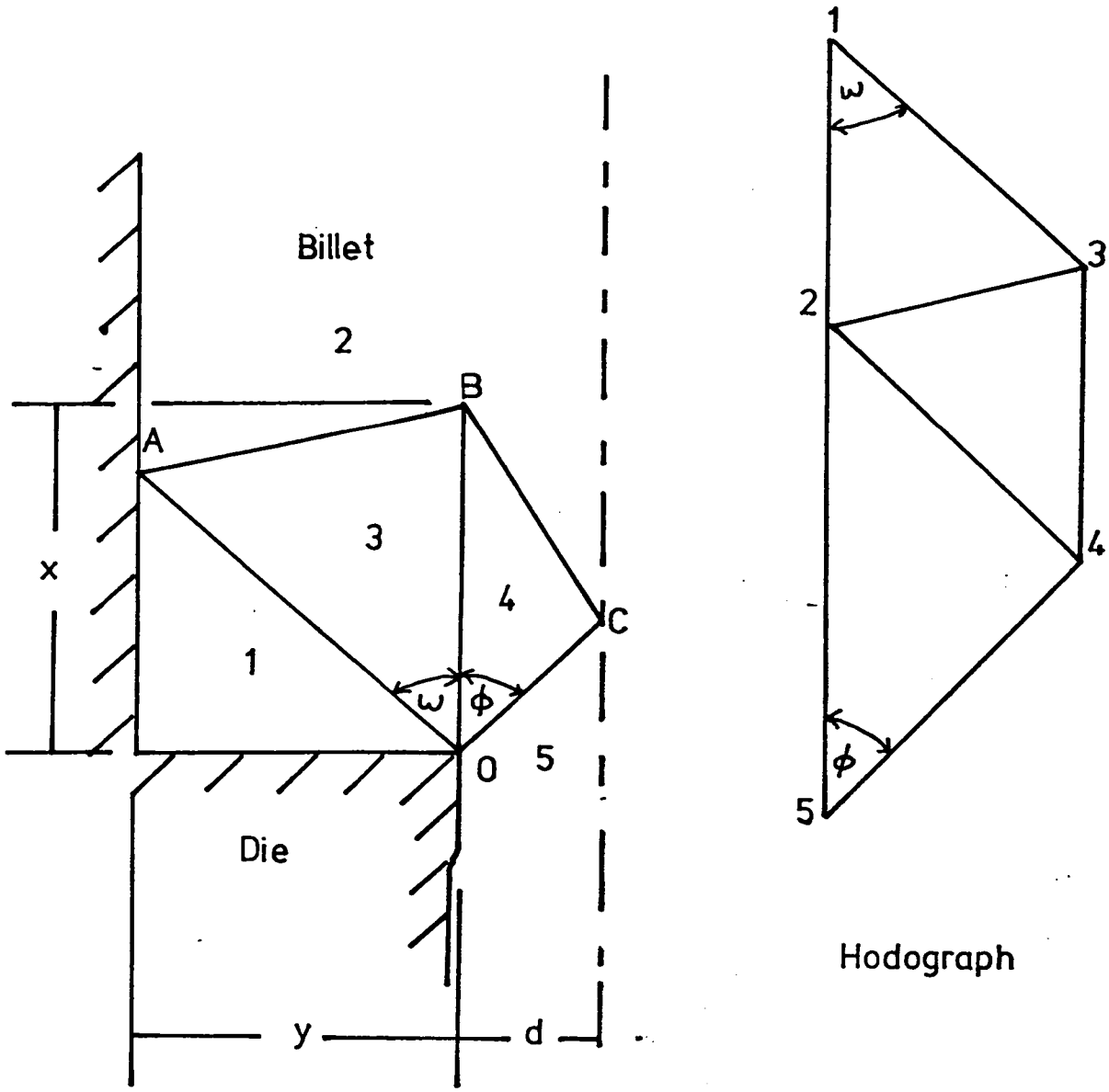

FIG 6 1 Rigid triangle field and hodograph

yield stress of the product. K_1 to K_4 will be much smaller about the same value as the specimen at the rear of the billet.

Considering the proof stress values; assume that they are representative of high temperature properties, then the values of K_1 to K_4 can be expressed as a fraction of K_5 so that:

$$\text{Load} = \frac{n}{5} K_5 \left(AB\overline{23} + BC\overline{24} + OB\overline{34} + DA\overline{13} + OC\overline{45}\right)$$

The sum provides that the average value of K_5 is $0.8K_5$. If the tensile stress values are considered the average value of K_5 will be $0.6K_5$.

A value of mean shear yield stress found for the Al-Mg-Zn alloy is 3t.s.i at 300°C. If this is considered as being 0.8 and 0.6 of the final product value, using the upper bound solution for a 30:1 reduction, the load expected will be 385 Tons and 518 Tons respectively. The load calculated from the equation.

Load = 51.75 X (constant)

It is thus evident that the loads obtained during extrusion are lower than expected by quite a considerable amount as the final product properties are not developed until the material passes the last velocity discontinuity. For the aluminium powders, the load obtained will not be very much greater than that of an extruded solid aluminium billet. This can be seen in figs. 5.7-8. The figures quoted are only an approximation but give an indication of the loads expected if they were calculated using the upper bound solution and one constant value of K, that of the final product.

To show the difference between theoretical and practical extrusion pressures, the pressures obtained are compared to the yield

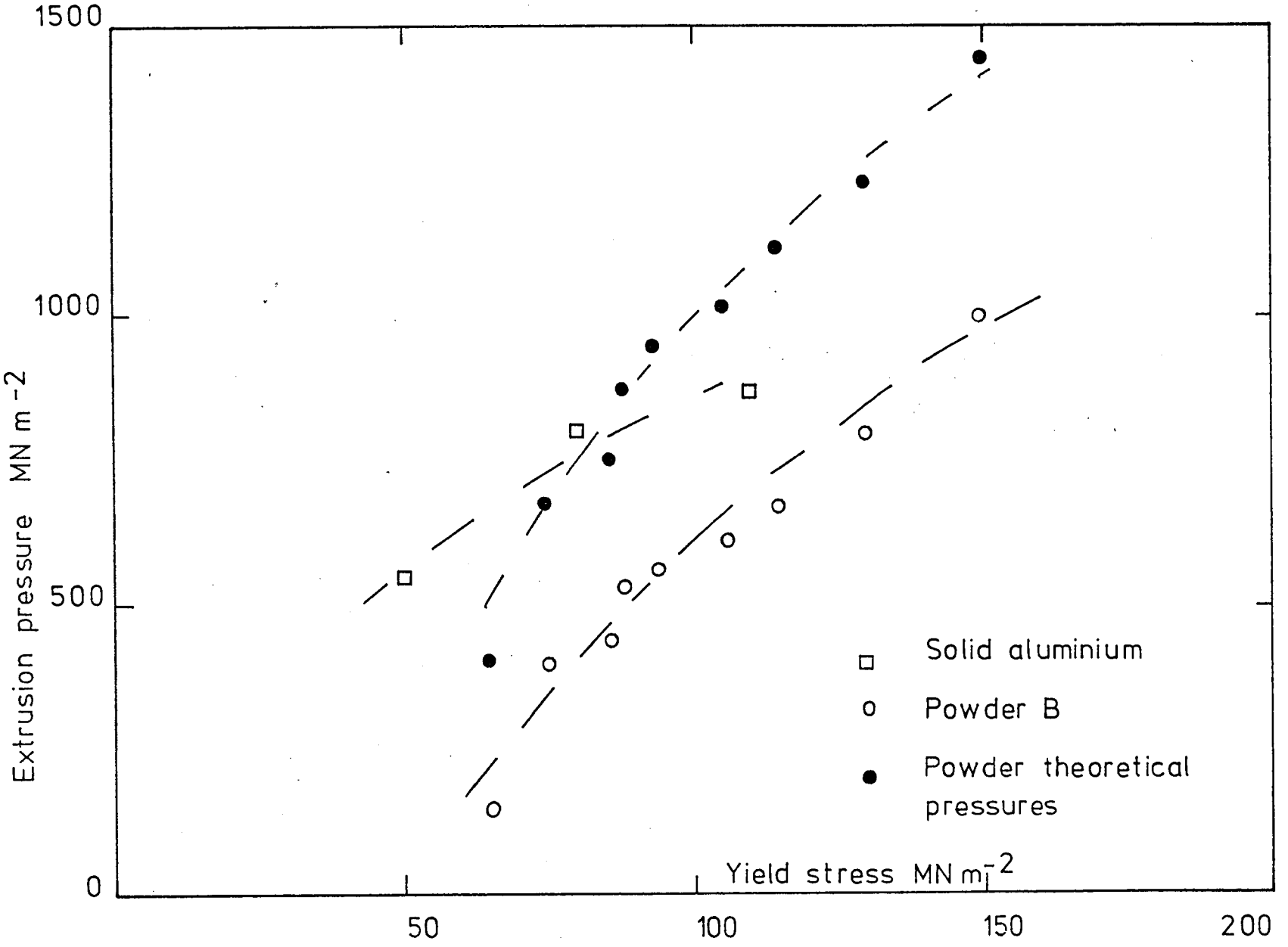

FIG 6.2 PLOT OF PRESSURE VERSUS YIELD STRESS FOR POWDER B

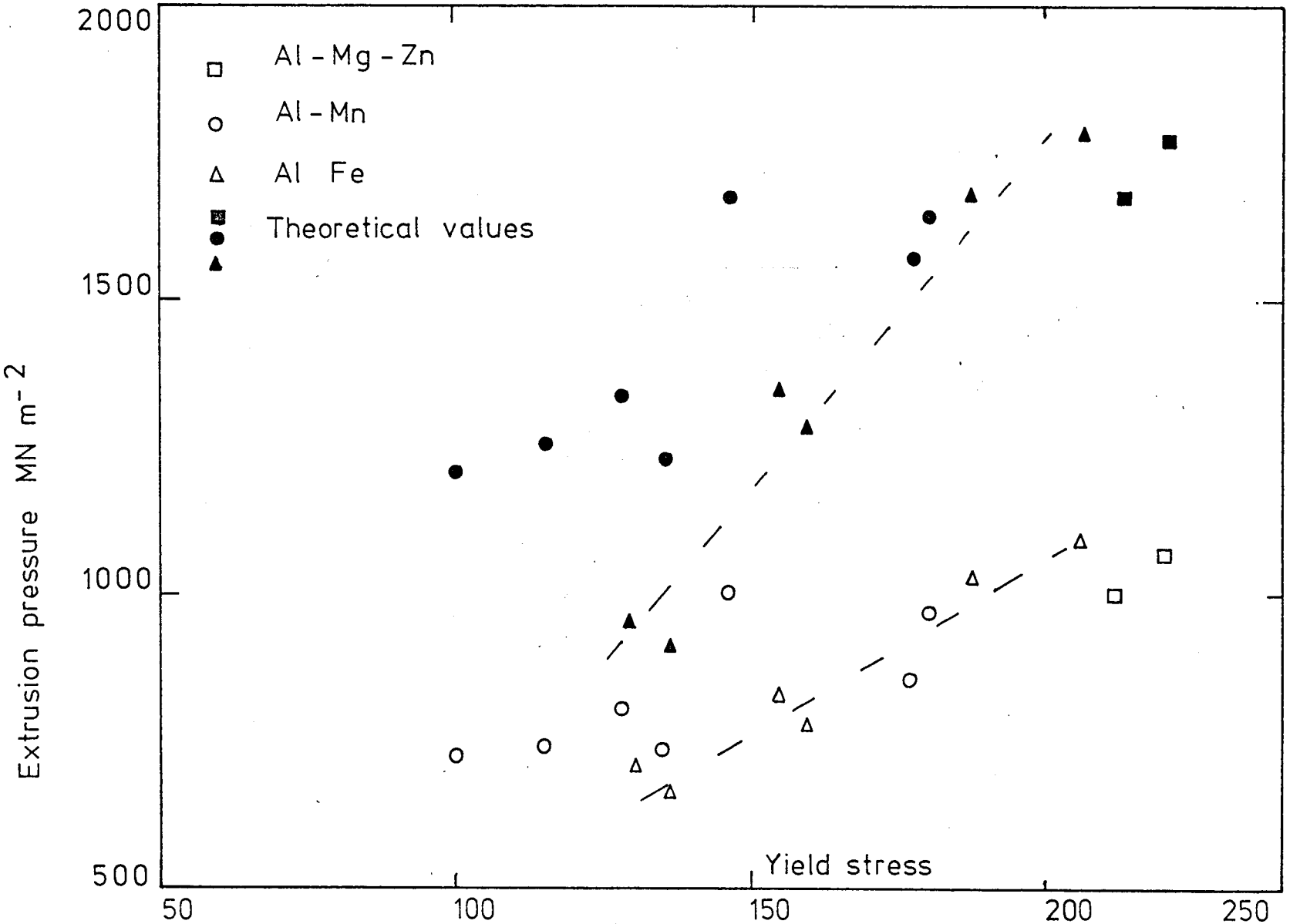

FIG 6.3 PLOT OF PRESSURE VERSUS YIELD STRESS FOR ALLOY POWDERS

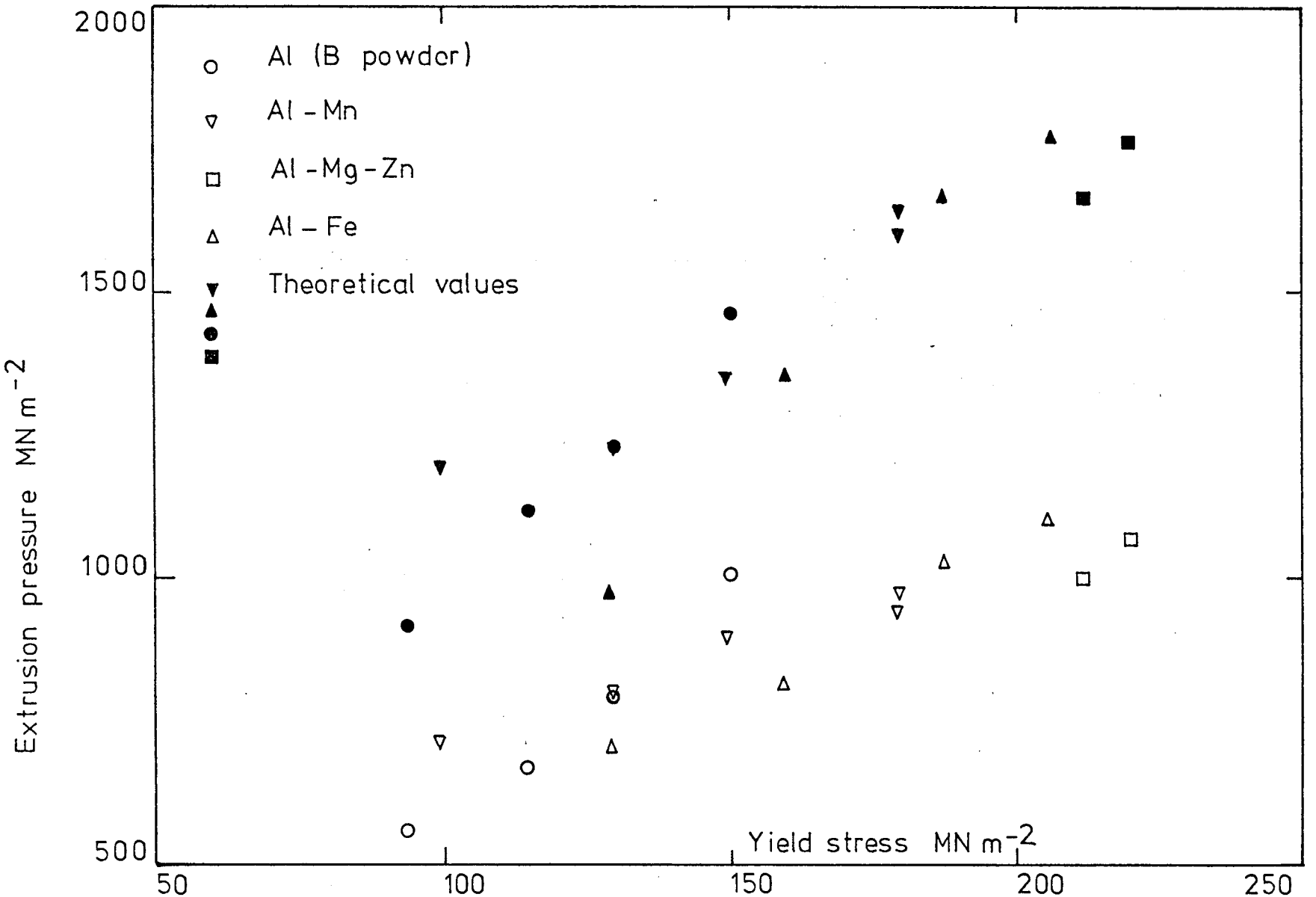

FIG. 6.4 COMPARISON OF THEORETICAL AND EXPERIMENTAL VALUES

strength of the final product. This is shown in fig. 6.2 where the extrusion pressures obtained experimentally are plotted against room temperature yield strength. For the aluminium powder B, compared to commercially pure solid aluminium, it can be seen that a much stronger product is produced, with the same pressure requirements, than the solid billet. Similarly, for the alloy powders over a non-heat treated product of a solid alloy billet.

Using the values of the mean yield stress for the materials found by the upper bound solution, theoretical pressures required can be calculated. These values are shown in fig. 6.3 for the powder billets, aluminium and aluminium alloy powders, in relation to their room temperature properties of the extruded products.

A comparison of the two sets of results is shown in figure 6.4 and it can be seen that much lower pressures are required to extrude powder billets with a high strength extruded product than solid billets with an equivalent strength product.

6.6 Extrusion

The extrusion operation was carried out as described in the experimental section and the problems of lubrication overcome by the method described in the same section.

In the extrusion of powders the problem of 'pick-up' on the die surfaces is generally prevalent and will cause unnecessary die wear and unsatisfactory surface finish of the product. This can be overcome with the aid of lubrication or a new die design.

The use of an aluminium disc at the front of the powder billet

in effect changes the die design, as the aluminium forms the dead metal zone forcing the powder to flow through a cone shaped die into the exit. The use of a conial die for the extrusion of powders has been proposed by Gregory[178] to eliminate the sharp edges on a square shouldered die, that encourage die 'pick-up' and 'galling'.

A conical shaped die, however, would not eliminate die 'pick-up' without the use of a lubricant as the powder particles have a tendency to weld to the die material at any slight cavity or asperity. The presence of a lead-in radius into the die orifice would help the flow of material and effectively produce a flow pattern of material obtained in the experiments.

Thus a die designed to the shape of the flow of the powder into the die orifice would enable satisfactory extrusions to be produced.

6.6.1 Load/ram displacement diagrams

These diagrams, sometimes referred to as autographic curves, have been previously discussed with reference to that of a solid billet extruded under the same conditions[3]. The initial increase in load is that which corresponds to the densification of the powder to about 100 per cent theoretical density. As previously explained, this represents the region where all the particles are in intimate contact but are still distinguishable as separate particles. Initial contact areas in the cold compacted billet have been enlarged by additional plastic deformation and after the attainment of this condition the diagram follows that of solid billet extruded. The deformation of the powder billet has been previously discussed and helps to explain the lower than expected loads obtained.

Diagrams obtained from the alloy powders also show the same trend previously discussed, particularly lower loads than expected.

The series of experiments performed to determine the effect of initial billet compact density on the extrusion process found no effect, within experimental error. This was experienced as the compacted billets were pressed to near theoretical density before they were extruded, as explained at the beginning of this section.

6.6.2 Pre-sintering

The effect of pre-sintering a compacted aluminium billet had little observable effect on the extrusion process or product. It was noticed, however, that sintered aluminium billets were easier to machine due to the increased interparticulate contacts. Upon examination of an extruded section of a sintered billet it was found that there were large areas of oxide formed during the prolonged sintering. These oxide areas were often large and diffuse around the periphery indicating a chemical reaction by diffusion. As well as the oxidations of the fractured surfaces exposed during compaction the aluminium reacts with the water vapour present in the natural oxide layer as Modl - Onitch showed, to form additional oxide thus:

$$2Al + 3H_2O - = . Al_2O_3 + 3H_2$$

6.6.3 Reduction ratio

The extrusion pressure at the post steady state prior to cor·ng is plotted as a function of R, the reduction ratio; figure 5.14 is a plot of extrusion pressure against ln R. The straight line obtained corresponds to the well known equation:

$$\frac{P}{Ym} = A + B \ln R \qquad (6.3)$$

The values of A and B are found to be 0.81 and 1.2 respectively. The value of Ym was obtained for a particular set of conditions by using the upper bound solution for plane strain. Knowing this value of the mean yield stress the constants A and B could be calculated from the slope and intercept shown in figure 5.14. This formula is similar to that developed by Johnson[55,58] for rough container walled sheet extrusion.

The value A, represents the redundant work during deformation and its high value is indicative of high friction conditions existing between particles. It is necessary to overcome this friction between the particles as well as the shear deformation within the particles for the material to flow from the side to the centre.

The experimental formula derived, is limited in its application as it applies only to flow type 'B'[49], and the set of frictional conditions encountered during the experiments. However, it is relatively simple to use, as it is derived from extrusion data, and can give an idea of the ratio required for a given set of conditions.

6.6.4 Billet temperature

The temperature of the billet during extrusion was measured by a thermocouple placed at the rear of the billet. The temperauture rise recorded is not consistent or completely accurate but gives an indication of the order of magnitude of the rise. The temperature rise, shown in fig. 5.42, is typical of the temperature rises experienced at the rear of the billet. This presents the overall temperature and not the localised temperatures at the particle contacts

where pressure welding takes place. There are no figures given in the literature on pressure welding that help to give an accurate assessment of the local temperatures experienced. At regions of high frictional conditions there may be sufficient heat generated to cause a small molten pool to be formed in an alloy with a low melting point eutectic.

In the aluminium alloy powder K, Al-Mg-Zn, the temperature rise indicated in fig. 5.42, for an extrusion at 300°C and 30:1, is sufficient for the material to obtain the temperature of its ternary eutectic point. At this point, 447°C, liquid eutectic will be present and if near the surface will react with the moisture in the oxide coating of particles to evolve hydrogen. This phenomenon will give rise to the formation of pockets of gas, often seen as bubbles on the surface of extrusions of this powder. Even at very low ram speeds they were observed at the rear of the extruded rod. These bubbles are seen as fissures as in the optical micrograph shown in plate 5.7(b).

6.6.5 Limit diagrams

Limit diagrams of the type presented by Hirst and Ursell are drawn and shown in figures 5.15 - 5.18. The coefficient of friction for several temperatures was determined using the technique described by Hirst and Ursell[57]. Two billets of lengths l_1 and l_2 were extruded through the same die and the mean pressures measured so that the coefficient of friction μ is given by:

$$\mu = \frac{0.575}{l_1 - l_2} \log_{10} \frac{Pl_1}{Pl_2}$$

For other temperatures, not investigated by this method, the coefficient

of friction was determined from the load ram diagram by taking the load at two different points, hence two different lengths, thus enabling determination.

The limit diagrams of the various powders used are shown and it can be seen that the Al-Mg-Zn powder has a very limited range. The incipient melting line was drawn using a theoretical temperature rise, calculated using the technique described in the theory section. However, as previously mentioned this will be a mean overall temperature and local temperatures at the points of contact may be in excess of a low melting point eutectic. In the case of alloy K, with the low melting point ternary eutectic, local hot shortness will occur causing formation of bubbles on the final product. The limit diagram for this particular alloy, fig. 5.17, is very limited in its use particularly as the actual temperature rises at the particle interfaces were not measured. The other alloys investigated do not suffer the same fate and thus the limit diagrams drawn will be useful.

A lower threshold line is drawn on the load line to indicate the limit of the lowest possible reduction ratio. In the earlier reported work[3] it was discovered that below a reduction ratio of 5:1 the material did not experience sufficient plastic deformation to produce a soundstrong extruded product. This line will remain fairly steady even with increase in temperature as compacted powders will still require sufficient deformation to bond adjacent particles.

This threshold reduction ratio is then another limit to add to the limit diagram to ensure that a high enough reduction in area is applied to the powder billet to produce a fully strengthened extruded product.

The alloys, A, B, J, and L, theoretically, have quite a broad range of temperature and reductions, but, it must be remembered with the pre-alloyed powders that the higher the extrusion temperature the lower the strength of the extruded rod. The decrease in strength associated with recrystallisation and precipitation from the initially supersaturated solid solution. A limiting cap can be drawn on these diagrams, similar to Raybould[68], to indicate the limit in temperature, at a particular strain rate, below which products can be extruded having sufficient strength or sub grain size.

The limit diagrams drawn are for one particular strain rate and the values of R, the reduction ratio, are plotted against the initial billet temperature. The use of the limit diagrams is dependent on the definition of a stalled press at the maximum load capacity of the press. When a press is stalled, the ram is stopped and is therefore effectively at zero strain rate and no further extrusion takes place. It is known that once the ram speed is rapidly reduced extrusion becomes impossible, so with decreasing strain rate the maximum load will be slightly reduced. Therefore the limit reduction ratio will be that calculated from the maximum load at the slowest strain rate. At the slowest strain rate the temperature rise is small, therefore the deformation temperature will be lower, and the value of R will be slightly lower for an equivalent load at a faster strain rate. Thus, to allow for experimental error a limit diagram should be constructed for the slowest strain rate.

Unfortunately the limit diagrams cannot be compared with any other work of powder extrusions but the load line has the same basic form as previous work by Ashcroft and Lawson[65] and by Raybould[68]. The peak values of R found were similar to those of Raybould[68]. At high

strain rates, i.e. high reduction ratios, the temperature will be near that of the solidus so the yield stress will be reduced and the value of R increased fairly rapidly giving a peaked appearance to the load line and the solidus, incipient melting, line. Hence quite extensive reductions can be performed at a relatively low temperature.

6.6.6 Strain rate

The rate of strain at any particular point in a billet during extrusion is different from another even at the same ram speed, therefore a mean strain rate is estimated to cover the material passing from the container and through the die. The equivalent mean strain rate, $\dot{\bar{\varepsilon}}$, has been found to be approximately

$$\dot{\bar{\varepsilon}} = (0.81 + 1.2 \ln R) \; 6 \, u/_D \qquad (6.4)$$

However, it is extremely difficult to be certain of the most satisfactory method for the determination of the strain rates of other deformation processes. It is thought that the above equation is representative of the strain rate equations and it is considered that the results will be consistent if only one equated is used throughout. It has been noted previously[68] that the magnitude of the strain rate is important so long as there is a consistent determination.

It can also be seen from the literature that the strain rate is the most difficult extrusion parameter to determine and no satisfactory uniform method for determination exists.

6.7 Activation energy

The activation energy for hot deformation of the alloys was

determined for the powders A, B, J and K; all except K were close to the value of self diffusion of aluminium, K was slightly lower.

The activation energy for the extrusion of commercial purity aluminium has been determined by Jonas[133] and found to be 37.3K cals. The value of n, the stress exponent, when related to strain rate in the work by Jonas was found to have a value equal to 4 compared to n = 4.4 for commercial purity aluminium during creep. For the dispersion strengthened products produced from extruded powder the value n = 4.14 has been determined by creep tests[127]. The few tensile test results carried out at an elevated temperature show values of n = 4.17 for powder A and n = 4.4 for the coarser powder B which are are in very good agreement with previous results. The slightly higher stress exponent value for powder B compared with A is due to the coarser dispersion of oxide in the aluminium matrix in the former. Powder A, the extremely fine mesh size powder, produces a fine and fairly uniform dispersion of oxide phase after extrusion. This situation in the extruded product approaches that of the material used by the previous workers, also seen in the experimentally determined value of n. The experimental stress dependence found in the tensile tests agrees with the value in the model proposed by Ansell and Weertman[125]. They proposed a model to describe steady state creep behaviour of a coarse grained dispersion strengthened metal based on the climb of dislocations above the second phase particles. The creep rate was proposed to a function of stress and inter particle spacing where:

$$K' = \frac{2 \alpha \pi \sigma^4 L^2 D}{d \mu^3 k^* T}$$

L = inter particle spacing (see Appendix 1 for nomenclature)

The model also assumes that a three dimensional dislocation network has been found in all the alloys, plate 6.11, and the dispersed particles hinder dislocation motion rather than activate dislocation sources. It was considered that in aluminium oxide products climb was by the interchange between aluminium atoms and vacancies. There was no experimental evidence to confirm this but it is thought that climb would not be the only mechanism operative during deformation. The presence of networks in the dispersed structure has been found, plate 6.11, and growth of these during recovery involve climb of edge dislocations and migration of jogs along the dislocation so that the recovery rate is dependent on the coefficient of diffusion. Therefore the network provides the dislocation sources and the rate controlling mechanism for deformation is the climb of edge dislocations or the motion of jogged screw dislocations.

The values of n, in the present work, for the extrusion process have been determined to be about 6 for the powders A, B, and J. This, therefore, shows that the powder material during the extrusion process is not as strongly dependent on the strain rate as the solid final product. This can be explained by the model proposed for the mode of deformation of the powder billet during extrusion. The material does not fully develop its final properties until it has passed through the die and can be regarded as a series of local particle contacts rather than a fully coherent junction. The particle contact areas increase as the die orifice is approached by a process of pressure welding. Associated with these plastically deformed regions are the porous oxide films of the original particles broken during contact. The particles in intimate contact are welded together where the oxide films are ruptured and further deformation leads to formation and multiplication of dislocations and high local temperatures

due to the high friction conditions are prevalent. The presence of vacancies at or near the amorphous oxide film pressed together, where the particles have not been metallically joined, act as dislocation sinks. These porous regions enable the highly mobile dislocations at the welded junctions to be quickly and easily absorbed. Absorption of the rapidly multiplying dislocations during deformation cause a lower strain rate dependence on stress of the powder compact material than the solid final product.

The value of n for the Al-Mg-Zn alloy is found to be equal to 2.64 during extrusion and 1.8 in the extruded product form revealing or greater dependence of stress on strain rate than the other materials investigated. However, the powder billet form still shows less stress-strain rate dependence than the solid product due to the mechanism previously described.

The low values of n found for both solid and powder form is due to a difference in the structure compared to the other materials used. Material K, upon metallographic examination shows few precipitates of a second phase suggesting that most of the magnesium and zinc are present in the form of solid solution. The other alloy powder investigated for activation energy values, the Al-Mn alloy, shows extensive precipitation after extrusion so that only a relatively small amount of Mn remains in solid solution. The Al-Mg-Zn alloy powders during extrusion are raised in temperature causing the fine precipitates to be re-dissolved into solid solution forming solute clusters in the form of embrionic G.P. zones, found in the Al-Mg-Zn system. These small and numerous clusters act as barriers to dislocation sources and also as a friction effect on moving dislocations by attractive and repulsive barriers. They are known as Cottrell-Lomer

barriers. Dislocations nucleated by the plastic deformation process are either locked or retarded by the action of solute atoms increasing the stress necessary to move them hence increasing the stress dependence on strain rate. In the case of the solid product the material work hardens to such an extent that brittle fracture results with little or no necking in the tensile specimen tested.

It has been proposed by Weertman[78] that a high solute concentrations than found in commercial pure alloys the rate controlling process for dislocation motion is that of viscous dislocation glide rather than dislocation climb. It was proposed that the steady creep rate could be determined by:-

$$K = \frac{\sigma^3 b^2}{\mu \bar{A} \bar{B}} \qquad \bar{B} = \frac{\mu b^2}{2\pi(1-\nu)}$$

where $\bar{A}$, the constant, is dependent upon the viscous drag mechanism. The creep models of Weertman suggest that the stress dependence of steady state creep in single phase solid solution of Al-Mg decreases from a value of 4.5 for pure aluminium to 3 for an Al-Mg alloy due to the change in the rate controlling process for dislocation motion from climb, in pure aluminium, to viscous dislocation glide, in solid solution alloys.

It is seen that the stress exponent of powder K is small, as also is that for the Al-Mg solid solution without the dispersed oxide phase. The change in the exponent for the solid material, in comparison to the other alloys A, B, or J, is explained by a change in the rate controlling mechanism for steady state creep similar to that from dislocation climb to that of viscous drag of solute stress upon dislocations moving in their slip planes in the theory proposed

by Weertman[78]. Values of n, for the products of powder K and extrusion are lower than that estimated by theory due primarily to the finely dispersed solute clusters as G.P. zones as well as solute atoms in the solid solution acting upon the dislocations.

This change in the rate controlling mechanism is shown by comparing figs. 5.37, 5.38 to fig. 5.39. The temperature compensated strain rate dependence on stress is found to be different for the Al-Mg-Zn alloy from the other alloys clearly indicating a different rate controlling mechanism. The dependence of stress on strain rate for this alloy is very much greater.

The values of ΔH, the activation energy, are calculated using the same procedure as that of Jonas[133]. The activation energy of A, B, and J for the extrusion process's close to that of the activation energy for the lattice self diffusion of aluminium. In contrast the activation energy for the alloy K is much lower indicating a change in the rate controlling mechanism. This result agreed with previous observations on the activation energy for self diffusion in Al-Mg[127,136]. In previous work on solid Al-Mg creep tests the values varied from 27 to 38K cals/mole depending on the solute concentration. A similar observation was reported[127] for the activation energy of creep of a dispension strengthened Al-Mg alloy. In more recent work by Raybould[68] the activation energy for extrusion of an Al-Zn-Mg alloy was found to be 37.3K cals in the single phase deformation region and 27.2K cals in the two phase deformation region. This clearly indicates a change in the rate controlling mechanism similar to that reported by Dorn et al[137]. They considered the hot and cold working regions of super pure aluminium and results show the rate controlling mechanism changes with temperature.

The Al-Mg-Zn alloy, due to its fine solute structure, has a lower activation energy and a rate controlling mechanism for dislocations of viscous glide in the slip plane. These are different from the other powders investigated which have an activation energy value close to that of self diffusion of aluminium in aluminium and therefore a different rate controlling dislocation mechanism.

The activation energy results of the aluminium - aluminium oxide materials and the aluminium manganese alloy correspond closely to thoseobtained from creep experiments. This, therefore, suggests that the kinetics of dislocation movement in creep is the same as that during extrusion. The value, ΔH = 36K cals/mole, indicates that in the dispersion strengthened materials investigated the rate controlling process is connected to the aluminium rather than the oxide. If the oxide was directly involved in the process a value of ΔH = 150K cals/mole would be expected, as first thought by Ansell and Weertman[125] but later changed to 37K cals/mole. However, it is thought that the oxide particles play a more indirect role by acting as obstacles to dislocation motion or dislocation nucleation. The area of mis-match between the oxide particle and matrix acting as a sink or source for vacancies. The rate controlling process will still be that of interchange of vacancies and aluminium atoms giving a value of activation energy close to that of self diffusion of aluminium.

The value of ΔH for the Al-Mn alloy indicates that in this alloy the rate controlling process is the same as in the aluminium - aluminium materials.

6.8 Extruded structure

6.8.1 Optical microscopy

The optical micrographs taken show the fibrous cold worked structure with the original particles elongated in the direction of extrusion and forming parallel chains. These chains have a distance of separation dependent upon the extent of reduction during extrusion, i.e. the reduction ratio of extrusion. The transverse section of the material exhibits the formation of irregular loops rather than a continuous network as seen in the optical micrograph plate 5.7(d).

In the work on the Al-Mg-Zn, K, alloy, the dark platelet regions which are prevalent in the extruded bars of this particular material, are fissures, plate 5.7(b). These fissures are large porous regions formed during the extrusion process. Considering the phase diagram[138] of this material it can be seen that the solidus surface for the phase T - aluminium solid solution - and $Mg_2 Al_3$ starts at 447°C. This temperature is about 150°C above the normal initial billet starting temperature and is reached during extrusion by inter particle fiction, even at the slowest strain rates. Fig. 5.42 is a plot of temperature recorded at the rear of the billet against displacement. Although this is not an accurate recording of temperature rise during extrusion it does give an indication of the magnitude involved. Previous work on temperature measurement by Raybould[68] indicates that this temperature measured is lower than the die or dead metal zone temperature so, in fact, the temperature of the material will exceed the eutectic point during steady state extrusion. This will give rise to small quantities of liquid at, or in the particle surfaces. As mentioned previously, the porous oxide film contains a degree of water vapour which the liquid eutectic will readily react with to form hydrogen gas similar to that shown by Modl-Onitch[177]. Bubbles are formed, similar to those seen in

the heat treated specimens, and large concentrations are observed as fissures or blisters in the extruded rod. There is also a large number of small pores throughout the material, which caused considerable problems when electro-polishing specimens for the electron microscope.

6.8.2 Electron Microscopy

Specimens examined using the electron microscope are seen through an oxide film formed almost immediately after preparation. This is sometimes visible as a fine network pattern which is thought to be a surface manifestation of an underlying three dimensional network. A model has been proposed based on the segregation of impurity atoms similar to that of a cellular solidification[176] but could have been based on the dislocation network where the dislocations that intersected the surface acted as activation sites for oxidation.

Electron microscopy of a longitudinal section of an aluminium powder extrusion indicates that the aluminium oxide from the surface of the aluminium particles is often not well dispersed, and there is no evidence of visible porosity. The oxide phase, usually present as discrete particles, is often distributed in large stringer clusters, as in Plate 6.2(a), outlining the original particles. The needle-type shape formed after extrusion, plate 6.2b, shows that the particles are deformed into elongated shapes in the extrusion direction. If one assumes the aluminium particles to be originally spherical in shape, the process of deformation through a small circular orifice will give the particle a needle type shape. The original surface oxide film is still present in a recognisable form around the relatively undeformed tip of the original particle. The porous oxide film present on the remainder of the particle has been fractured and redistributed during working primarily by the process of making and breaking of contact

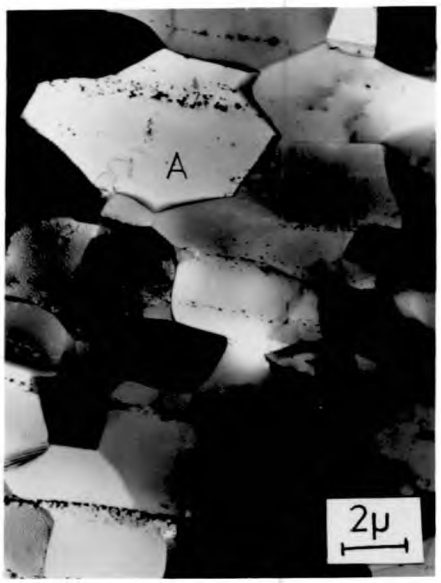

(a)

Powder B, 40:1 , 300°C

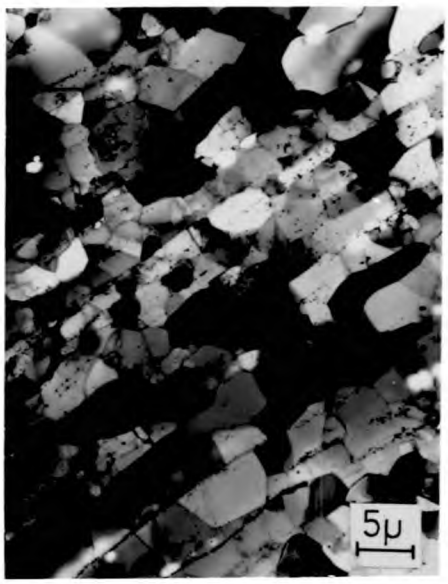

(b)

Powder B 30:1 300°C

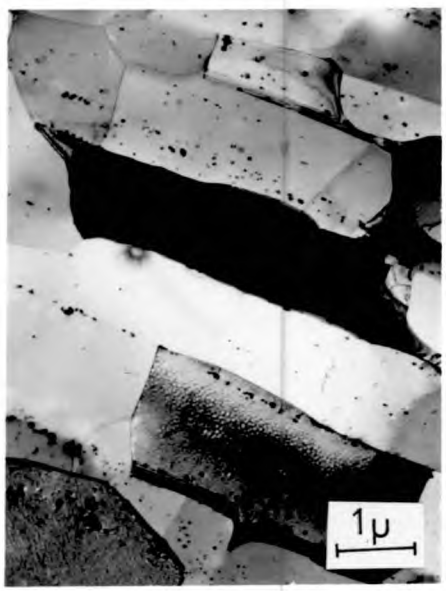

(c)

Powder B 30:1 250°C

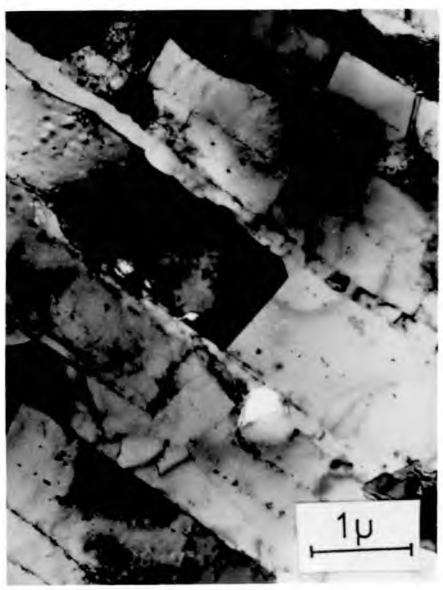

(d)

Powder A 30:1 300°C

PLATE 6.1 Longitudinal sections of extruded aluminium products

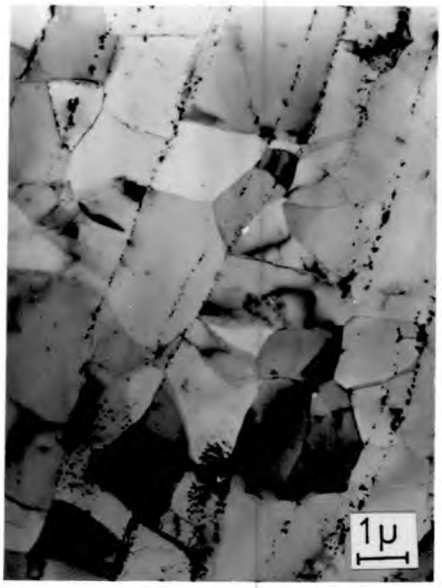

(a)

Powder B 30:1 300°C

(b)

Powder B 30:1 300°C

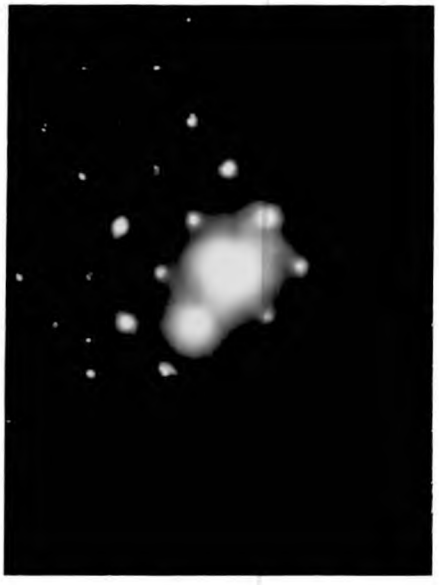

(c)

S.A.D.P.

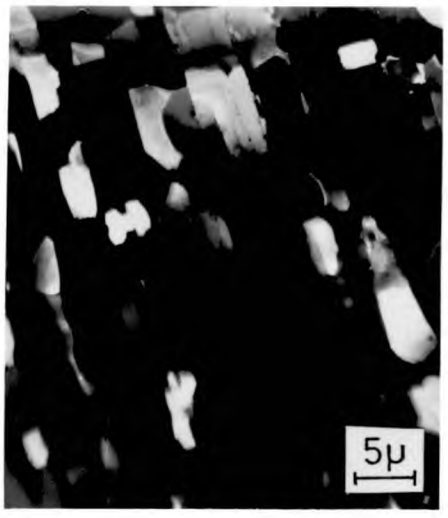

(d)

Dark field image

PLATE 6.2 Longitudinal sections, S A D P, and dark field image

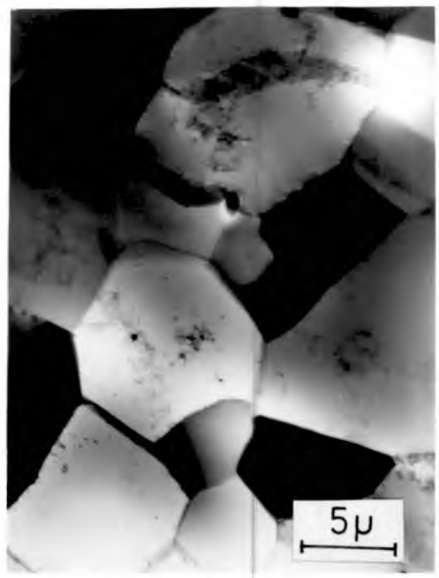

(a)

Solid aluminium (Commercial purity) 30:1 300°C

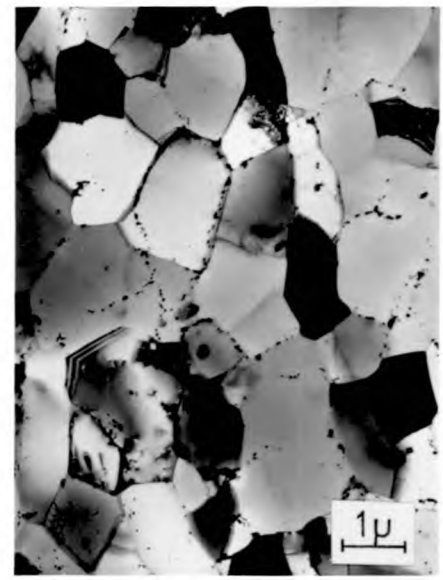

(b)

Powder B 30:1 300°C

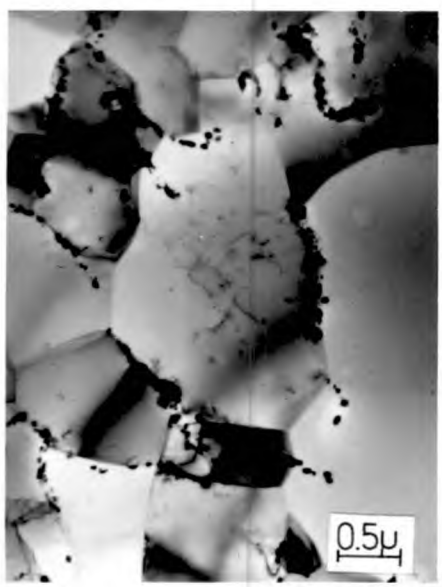

(c)

Powder B 30:1 350°C

(d)

Powder B 30:1 150°C

PLATE 6.3 Transverse sections of extruded aluminium products

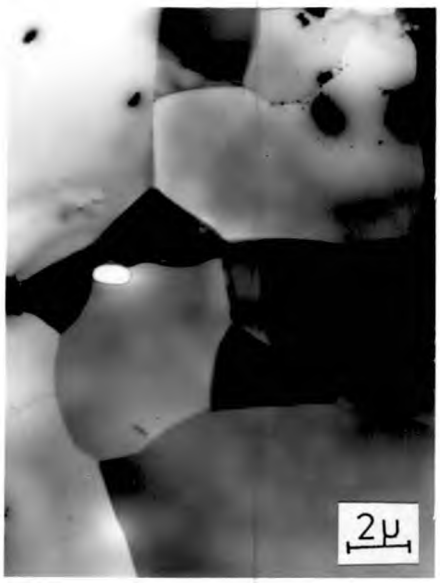

(a)

Powder B 30:1 425°C

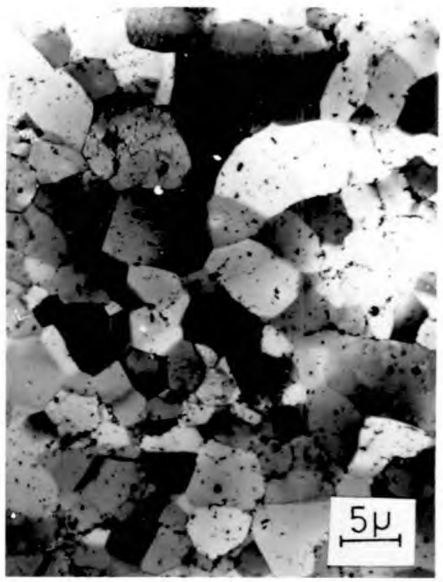

(b)

Coarse mesh fraction

30:1 300°C

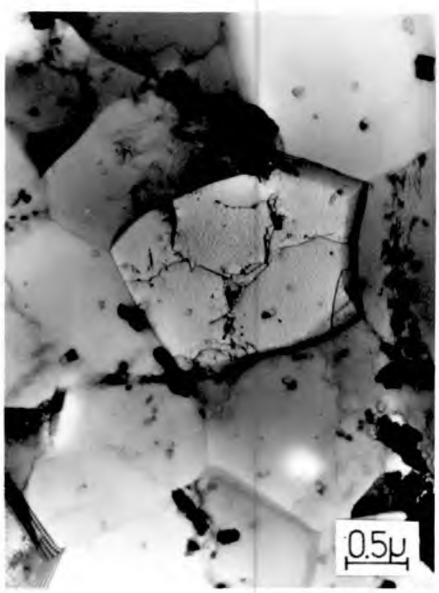

(c)

Powder C blended with Al_2O_3

30:1 300°C

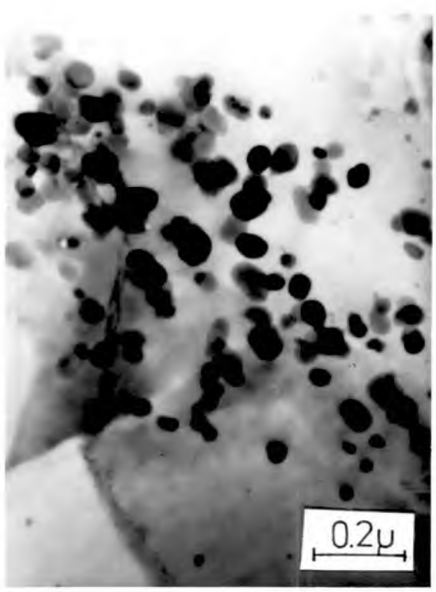

(d)

Oxide particles

PLATE 6.4 Transverse sections of extruded aluminium products

areas between intimate particles. This process, described in the deformation mode, is the method by which the oxide particles are distributed into the aluminium matrix. As the contact area becomes larger between adjacent particles the oxide layer is broken up and distributed inside the welded area and the individual oxide particles dispersed. The shape and size of the oxide particles can be seen in plate 6.4(d) where discs are present of nearly constant size, 100A thick, and 1000-1500A in diameter.

The dispersion of the oxide was found to be governed by the particle size of the powder, and the spacing determined by the volume fraction and extent of reduction. The smaller the initial particle size the better the overall distribution due to the smaller deformation of the finer particles during mechanical working.

The general appearance of the structure is one of an extremely fine grain size, fibrous in nature, with cylindrical grains or sub grains in the extrusions direction, particularly noticeable in fig. 6.1(c). These sub grains are formed during deformation of the billet by rapid rearrangement of dislocations and subsequently elongated as they pass through the extrusion die. They are further sub-divided during recovery of the material. The dislocation density within the subgrains is small as the process of air cooling has effectively annealed the material, by removing most dislocation tangles and forming relatively high angled well defined subgrains.

The final subgrain size is found to be independent of the state of the starting material containing an initial sub structure. It has been previously reported that the sub grain size produced at steady state deformation during extrusion was the same as that produced in the

initially annealed material[68,144]. This observation has been confirmed by the working on the varying initial density; the denser the cold compacted billet the more cold worked it becomes thus giving a more intricate dislocation network. Upon extrusion the variation in mean sub grain size is within experimental error.

In the transverse section of an extruded aluminium powder the aluminium oxide particles are seen in the form of a cellular pattern as reported by Hansen[96], see fig. 6.3(b). However, with the variation of particle size in powder B, a regular network of oxide particles is not feasible and as a result is not observed, only traces are seen.

It is of interest to note that a smaller subgrain size is observed in the product manufactured from the dust powder, plate 6.1(d), when compared to a coarse mesh fraction product, plate 6.1(b). Measurements of the subgrain size found in the transverse section were measured and the results are presented in graphical form, fig. 5.28, which is a plot of mean subgrain size against mean particle size. The mechanical properties of the extruded products show that the smaller the initial particle size the stronger the final product at room temperature and 400°C. It is, however, difficult to assess the relative strength of the subgrain structure on the final strength as no recrystallised structures were investigated. An idea of the contribution to strength can be assessed from fig. 5.29, a plot of subgrain size against initial billet temperature for powder B, containing initially a range of particle sizes. The mechanical properties show an increase in tensile strength at room temperature, but not at 400°C, for decreasing sub grain size. The fine dust powder size products show better strength at 400°C than the coarser fraction products indicating that most of the room temperature strength of the former product arises from the finer

oxide dispersion. Smaller subgrain sizes with decreasing particle size have previously been observed in work on fine particles of internally oxidised copper[145-6] and silver[147-8].

Comparison of the extruded subgrain size of a commercially pure aluminium solid billet and powder billet can be seen in plates 6.3(a, and b). Both billets were extruded using the same ram speed, reduction ratio, and initial billet temperature. In the micrograph, 6.3(a), the solid billet, there is evidence of remaining dislocations present from original sub grain boundaries that have been annealed out during air cooling. The adjacent grains or enlarged subgrain are mostly high angle indicating a stable structure due to the recovery process.

In comparison, micrograph 6.3(b), of the powder billet, shows a smaller subgrain size but again there is evidence of subgrain coalerence. There are very few dislocations observed in the subgrain interiors and few are seen tangled with oxide particles at the boundaries. As mentioned previously, the action of air cooling and dynamic recovery has helped to anneal out the tangled dislocations into a stable sub structure.

A similar sized subgrain structure as the solid billet can be found in a powder billet extruded at 400°C. Assuming the substructure strength of the powder product is the same as the solid material it can be seen that the tensile strength is improved by over 50% by the oxide dispersion, from 80MN m^{-2} to 130MN m^{-2}, with a consequently decreasing ductility.

The subgrain size of the extruded product is observed to be dependent upon temperature as seen in the micrographs 6.3 b,c,d, and

6.4 a,b. The mean size increases with increase in temperature and the higher the temperature the narrower and more well defined the sub boundaries. Micrograph 6.4a, of a specimen taken from a transverse section of a rod produced from a billet with an initial billet temperature of 425°C. This specimen is a recrystallised structure with well defined boundaries, high angled, and the grain interiors have very few dislocations. Billets extruded below this temperature show a subgrain structure with distinctive evidence of subgrain growth, plate 6.4b. There are three adjacent grains that have coalesced by rotation of the subgrains, as proposed by Li[73] and Hu[74]. This particular specimen, produced from a coarse mesh fraction, has been taken from the first ten centimetres that is usually rejected, thus has experienced only slight deformation. The subgrain size is slightly coarser than that of a section further along the rod as few dislocations were created during extrusion.

The longitudinal sections extruded at 300°C also reveal a degree of recrystallisation by subgrain growth, evidence of this can be seen in plate 6.1a, in the grain labelled A.

Subgrain growth mechanism for recrystallisation has been proposed by Li[73] and Hu[74] where the coalescence of adjoining subgrains forms a recrystallized grain. The initial deformed structure contains some relatively high angled sub boundaries and a few subgrains with large orientation deviations with respect to the matrix. Subgrains with the high angle sub boundaries begin to coalesce during the recovery process by eliminating their common boundaries, which have only a slight misorientation, so that the misorientation across them is reduced to zero. This process is possible by the slight rotation of adjoining subgrains until their lattices match. As a result the angular misfit

of the other boundaries around the rotated subgrains becomes greater. The mechanism continues until there is sufficient geometrical adjustment of original boundaries to produce a recrystallised grain at a very early stage of development. In the micrograph in question, plate 6.1(a), it can be seen that subgrain rotation has joined two adjacent subgrains so that the oxide debris is left within the grain and a few pinned dislocations associated with the oxide particles. The original subgrain boundaries are still faintly recognisable and parts of the interface of the recrystallised grain, A, are now high angled boundaries, evidence seen in the sharp contrast of adjoining subgrains. The dislocations present in the grain are aligned in such a way as to indicate that a subgrain boundary existed there before adjacent subgrains were rotated. The mechanism of Li and Hu is thought to be more abundant in aluminium - aluminium oxide alloys due to the rate of co-operation of dislocation climb and grain boundary migration.

Recrystallisation by subgrain growth and rotation has also been observed by Nobili[149-151] and his co workers in their work on recovery and recrystallisation of aluminium powder products. It was found that in these materials the predominate mechanism for recrystallisation was that of subgrain growth and rotation.

Plate 6.1b again shows evidence of the start of recrystallisation by subgrain coalescence. Several regions of this specimen show that the original oxide film has an influence on the final structure to such an extent that it forms a distinct barrier between adjoining sub-grains.

To improve the strength of the powder products, fine aluminia was blended into powder B, but it is found that the added oxide is present

in large clusters, plate 6.4c. The final strength is about the same as when no additions are made, it is thought that to obtain a fine uniform dispersion of oxide, a fine initial aluminium powder particle size is required. This would ensure that during blending the aluminia addition does not agglomerate.

The effect of reduction ratio on the microstructure of aluminium products is found to have little effect on the subgrain size, see table 5.11. However with increasing reduction ratio it is seen that the oxide particles are better distributed, plates 6.1a, 6.2a, due to the greater degree of particle deformation drawing out the original oxide skin into more uniform stringers. This is a general observation noted by previous workers who have studied the effect of reduction ratio.

Temperature of extrusion can be seen to affect the microstructure by varying the size of the subgrains formed in the final product. The lowest initial temperature used was 150°C which yielded a product with the highest tensile strength at room temperature compared to the products extruded at higher temperatures. The tensile strength, in the form of 0.2% proof stress, is found to be a function of the subgrain size in a relationship similar to the Petch equation, which relates grain size to yield stress, and is shown in fig. 5.32. However, results of tensile tests performed at 400°C show that the subgrain boundaries are relatively ineffective at this temperature and the strengths of materials produced at different extrusion temperatures are the same, within experimental error.

The diffraction pattern, plate 6.2c, shows the (iii) orientation associated with the fibrous texture produced by dynamic recovery. Continuous recrystallisation by subgrain growth results in the working

texture being preserved, while the motion of the high angle boundaries produces a cube texture.

Aluminium - Manganese

The reported literature concerning the phase transformations of this alloy presents a rather confusing picture of the precipitation products. It has been reported that a meta stable phase, denoted G[157], is formed during the annealing of a super saturated Al-Mn solid solution. The formula proposed for the G phase was $MnAl_{12}$, and the diffraction pattern fitted to a primitive cubic cell with a = 13.28A°. This structure is the same as the ternary G phase in the Al-Cr-Mn system. In more recent work[158-9] on quenched alloys of aluminium manganese the Mn was found to be distributed in small clusters causing considerable lattice distortion and formation of a meta stable phase. This phase was again denoted G and was formed during the annealing of a supersaturated Al-Mn solid solution. The G phase was found as irregularly shaped particles and prisms with a b.c.c. structure, a = 7.48A°.

The G phase has also been found[153] to be a b.c.c. structure with a = 12.65A° by indexing a.S.A.D.P. This lattice fits the b.c.c. structure of α - $Al_{12}Mn_3Si$ of the ternary Al-Mn-Si system. This work also found that the G particle had a matrix particle interface parallel to {110} type precipitate crystal lattice planes.

From this rather confusing picture it emerges that the meta stable phase G formed from the supersaturated solid solution is definitely of the form of a cubic structure with a lattice parameter between the value a = 4.04A° of the aluminium lattice and a = 6.498A° of the equilibrium orthorhombic $MnAl_6$ structure. The $MnAl_6$,

orthorhombic structure, has 28 atoms/unit cell with the following latture dimensions,

$$a = 6.498, \quad b = 7.552, \quad c = 8.87A^{\circ}$$

The electron microscope pictures of the Al-4% Mn alloy, plate 6.8 a - d, show the presence of large primary precipitates at subgrain or grain boundaries formed before the eutectic. The large precipitates, especially seen in plate 6.8a, are the nucleii for the subgrains formed during the extrusion process and the small precipitates seen are those from the eutectic phase and precipitation from solid solution. During extrusion the supersaturated solid solution is relieved of the excess manganese by a precipitation mechanism similar to that of an age hardening system. The manganese of the supersaturated solid solution is present in small clusters that cause considerable lattice distortions and the process of plastic deformation will cause the formation of a more stable phase by the action of thermal energy and lattice strains. The small precipitates from the solid solution can be seen, in Plate 6.8(c) and (d), in conjunction with the large primary and equilibrium precipitates. The longitudinal micrographs, plate 6.9(a) and (b), show that any large precipitates are broken up and then stretched out into the extrusion direction. Extremely large precipitates, seen in the optical microscopy of the individual powders, are not detected, so have been broken during extrusion.

Oxide particles as seen in the products of powder A and B are not detected as the precipitated phase of the Mn from the solid solution is also very fine. There is no evidence of any interaction between the precipitated phase and the oxide dispersion. The yield strength values found experimentally show an increase, both at room temperature and

(a)

Powder L 30:1 400°C

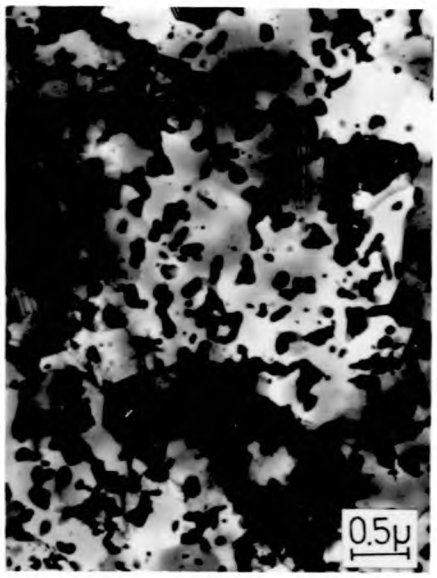

(b)

50:1 380°C

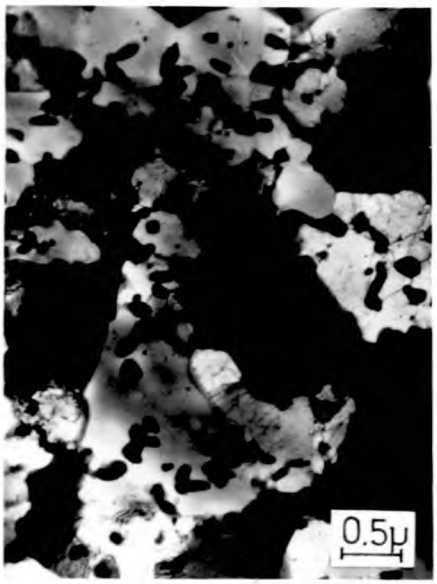

(c)

20:1 300°C

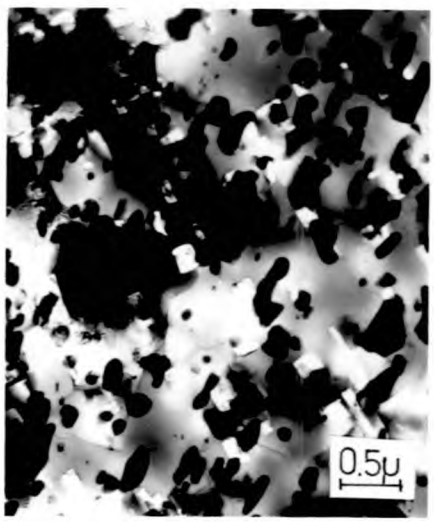

(d)

30:1 400°C

PLATE 6.5 Transverse sections of Aluminium Iron products

(a)

(b)

Powder L 20:1 300°C

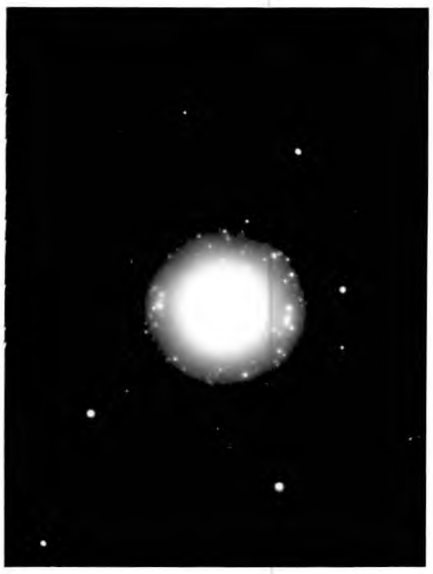

(c)

S.A.D.P of large precipitate

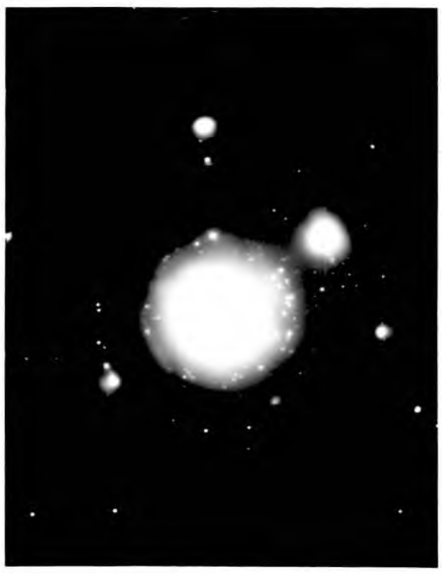

(d)

S.A.D.P

PLATE 6.6 Longitudinal section and S.A.D.P.s of extruded aluminium-iron powder

(a)

Powder L 30 : 1 400°C

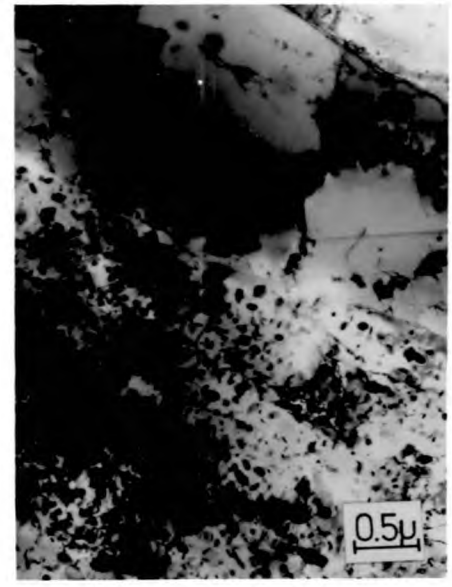

(b)

30 : 1 300°C

(c)

Powder L 30 : 1 300°C

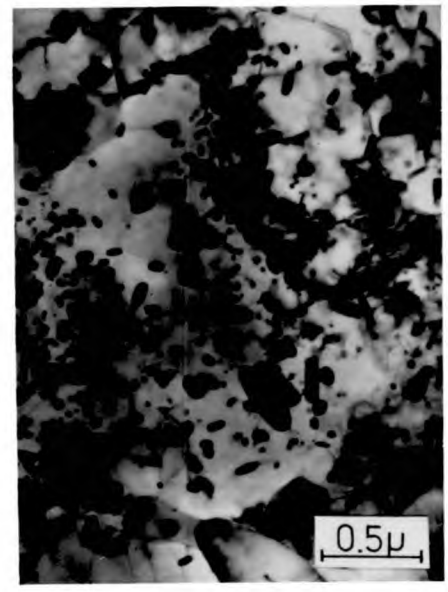

(d)

Powder J 30 : 1 345°C

PLATE 6.7 Precipitates in extruded products of aluminium iron and aluminium manganese powders

(a) (b)

Powder J 30 : 1 345°C

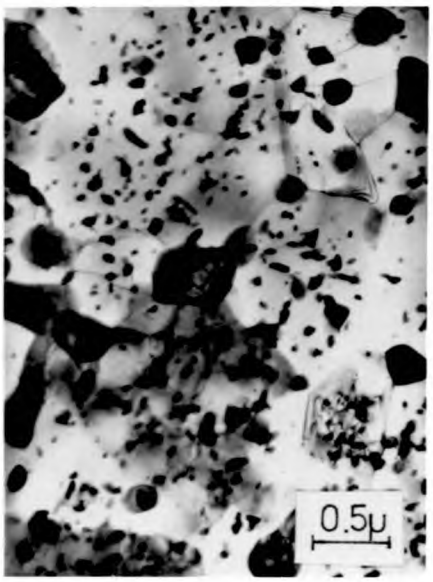

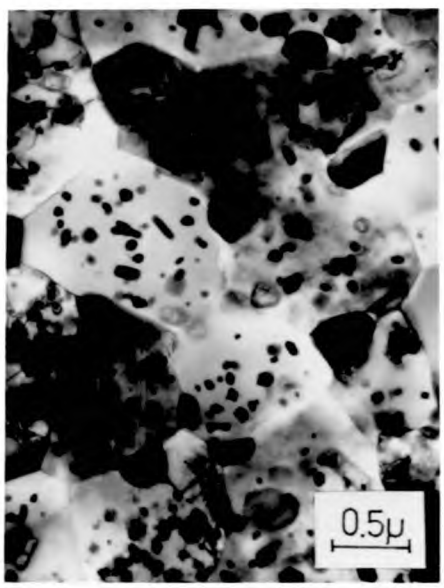

(c) (d)

30 : 1 360°C 50 : 1 405°C

PLATE 6.8 Transverse sections of Aluminium Manganese extruded products

(a)

Powder J 30 : 1 340°C

(b)

30 : 1 350°C

(c)

30 : 1 350°C

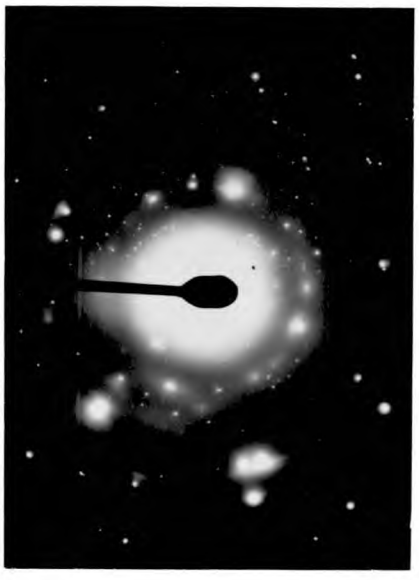

(d)

S.A.D.P. of large precipitate

PLATE 6.9 Longitudinal sections and S.A.D.P. of extruded aluminium-manganese products

400°C, over the aluminium powders due to the fine dispersion of Mn precipitates as well as the oxide dispersion. High temperature values are greater than the aluminium powders as the Mn precipitates had insufficient time to coalesce. The room temperature properties depend upon the temperature of extrusion, the higher the temperature the lower the yield strength due to the extent of coalescence of the Mn precipitates.

Plate 6.9(c) provides evidence of dislocation interaction with the primary precipitates, these dislocations being formed during the deformation process are caught in their motion by these obstacles.

Structure of the large primary precipitates of $MnAl_6$ were identified as such by the S.A.D.P. as shown in plate 6.9(d).

Aluminium - magnesium-zinc

The aluminium magnesium zinc alloy is part of the well documented aluminium zinc magnesium alloy system. Looking at the phase diagram[138] the equilibrium precipitates expected would be Mg_2Al_3 and the T phase. The impurities iron and silicon, will be precipitated in the form of Mg_2Si for the silicon, $FeAl_3$ and a ternary of Al, Fe, and Mg for the iron, and also α (FeSi).

The Mg_2Al_3 phase, more correctly Mg_5Al_8, is cubic with a = 28.2A° and with 1166 atoms in a unit cell. The ternary T phase, usually designated $Mg_3Zn_3Al_2$, has a wide range of composition and its structure is cubic with 162 atoms in a unit cell[179]. The lattice parameter varies from a = 14.3 to 14.71A° as the zinc content increases.

The aluminium - magnesium - zinc alloys have been extensively

developed due to their high mechanical properties and the ability of the medium - strength alloys to age harden. Problems with these alloys have arisen because of their susceptibility to stress - corrosion and the bulk of previous research has been directed to the elimination or a complete understanding of the problem.

Plates 6.10(a), (b) show the large rounded precipitates in the large recrystallised grains. There are a few dislocations pinned to these few precipitates which are not redissolved during the extrusion process. The fine precipitates seen in the powder particle micrographs, plate 5.7(b), are dissolved into solid solution by the overall and local rise in temperature. The Mg and Zn is then in solid solution and not precipitated out. These will be present in the aluminium lattice in a cluster formation similar to embryonic G.P. zones and Cottrell - Lomer barriers. These are not resolved in the photographs as they are extremely fine and not resolvable at this particular magnification. The clusters from the main barriers to dislocation motion and hence the highest yield strength experienced of the alloys with the product fracturing before noticeable necking occurred. The yield strength measured at 400°C is very low due to the low melting point ternary eutectic, at 447°C, and thus at this testing temperature the material is near its useful limit.

Holes are seen around the grains in the electron microscopy specimens and are present due to initial porosity by the mechanism previously described, or to dissolution of precipitates at grain boundaries.

Aluminium Iron

The aluminium iron system produces supersaturated solid solution

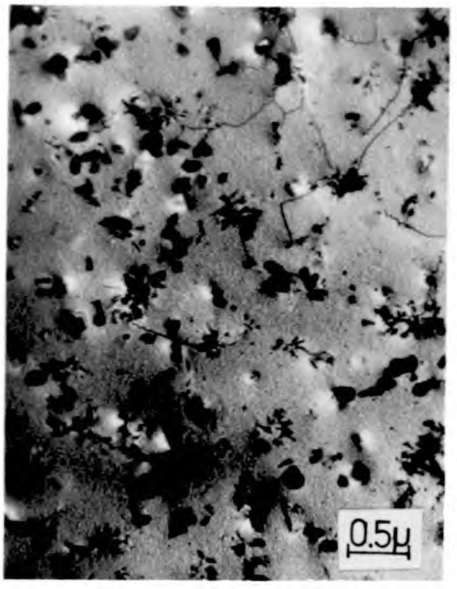

(a)

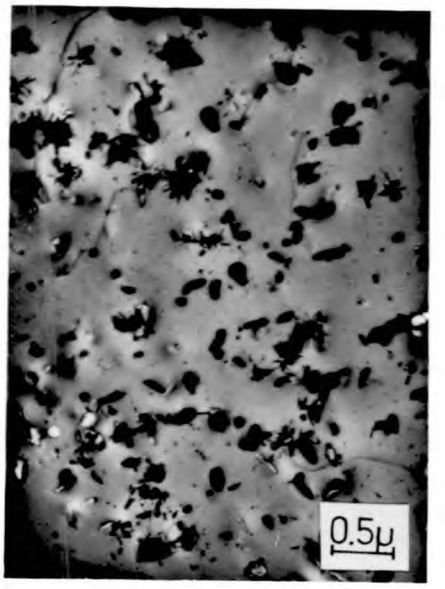

(b)

Powder K (Al-Mg-Zn) 30 : 1 300°C

(c)

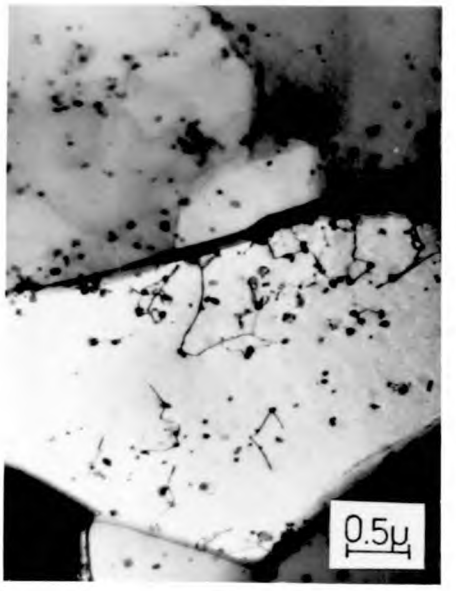

(d)

Powder B Dislocation inter-action with oxide particles

PLATE 6.10 Transverse of Aluminium Magnesium Zinc extruded products and dislocation inter-action in powder B

and even with extreme cooling will only retain 0.17wt% Fe in solution. Precipitation of $FeAl_3$ from solid solution has been observed to occur as semi - coherent flat meedles in the <100> direction and {100} habit[160-162]. The needles had their length parallel to the cube direction of the matrix in the form:

(010)	needle	//	(100)	α-Al
[100]	needle	//	[010]	α-Al
(010)	needle	//	(100)	α-Al
[100]	needle	//	[001]	α-Al

The monoclinic system has a one two fold rotation, or rotation inverse axis and the $FeAl_3$ phase has a monoclinic type structure with about 100 atoms in a unit cell, a complex structure of the form,

$$a = 15.49, \quad b = 8.08, \quad c = 12.48, \quad = 107^{\circ}43' \pm 1$$

The lattice parameter b is very nearly twice that of the aluminium lattice distance, $a = b = c = 4.04A^{\circ}$, hence the coherent nature of the precipitates.

In previous work on the Al-Fe system, by earlier research workers, a new Al-Fe constituent, $FeAl_6$, was identified and its parameter compared to that of $MnAl_6$[164]. $FeAl_6$ was thought to have an orthorhombic structure with about 28 atoms per unit cell similar to $MnAl_6$; i.e.

	a	b	c
$MnAl_6$	6.498	7.552	8.87
$FeAl_6$	6.492	7.437	8.78

This was considered to be more favourably precipitated as it had a smaller unit cell than $FeAl_3$, therefore more easily nucleated.

In more recent work[165] the phase $FeAl_6$ was thought to be precipitated in favour to $FeAl_3$ when the rate of precipitation was accelerated by cold working.

However, in contrast, a θ' structure has been proposed[166] as a meta stable phase before the precipitation of the equilibrium precipitate. This phase was found to have a tetragonal structure similar to that of the θ' structure in the Al-Cu system with $a=b=8.08A^{\circ}$, and formed during the transformation of the supersaturated solid solution to stable equilibrium. The transformation of the supersaturated solid solution, a_o, to stable equilibrium ($a_o \longrightarrow a + \theta$) was proposed by the formation of three meta stable phases, probably analogous to the G.P. zones in aluminium - copper, with the θ' phase the most stable.

The microstructure of the Al-Fe alloy, on extrusion, is that of broken dendrite regions and precipitation from the solid solution of the supersaturated alloy. The oxide phase is not easily detectable in the microstructure of this alloy due to the large number of precipitates present and the difficulty in separating each phase and precipitate. It is also observed that the dispersion of the primary $FeAl_3$ in the Al-Fe alloy is aligned in the direction of matrix.

The coarse dendrites of $FeAl_3$ formed during the cellular solidification[177] are broken up during extrusion and are seen as large dark precipitates of primary $FeAl_3$ in plate 6.5 a,b and broken to a lesser extent in plate 6.7(c).

Due to the segregation during cooling the Al-Fe system is extremely inhomogeneous and plate 6.7(b) illustrates two distinctly

different regions, one of aluminium adjacent to one full of precipitates. Plate 6.5(a) has a large oxide band in the matrix, not broken as effectively as the aluminium particle oxide film due to the extremely fine and brittle precipitation layer adjacent to the oxide film. Plate 6.5(c) illustrates the fine grain size observed in certain areas. These grains are well defined, with high angled boundaries and the primary precipitates of $FeAl_3$ distributed along the periphery to give the structure a recrystallised appearance. This particular specimen was taken from a billet extruded at 300°C but is more prevalent in higher temperature extrusions. The higher temperature worked billets produce a structure with the Fe, initially in supersaturated solid solution, precipitated out in the form of coherent or non coherent precipitate. The higher the working temperature the lower the product strength due to coarser precipitation and development of an overaged structure.

Plate 6.5(d) shows the presence of two different precipitates, one in phase, the other out of phase, known as precipitation contrast[167]. This is a form of orientation contrast that arises when a foil is oriented so that a certain set of lattice planes in the precipitate is diffracting strongly whereas the matrix is diffracting weakly, or vice versa. The precipitates seen are either partially coherent or non coherent to form the contrast.

This phenomenon was most noticeable in electron microscopy specimens of this aluminium-Iron alloy that had been preheated prior to extrusion to obtain a satisfactory initial billet temperature. As previously noted, the specimens of this alloy were extremely inhomogeneous and this precipitation occurred in regions of high iron content adjacent to iron depleted regions. The micrograph presented was taken from a billet

extruded at 375°C which involved pre-heating at 450°C for 30 mins. in the air circulating furnace. This preheating will have caused the supersaturated solid solution to precipitate out the excess iron in solid solution giving rise to a meta stable precipitate. The well defined rectangular precipitates observed were those of the meta stable condition coherent with the matrix of the θ′ variety

S.A.D.P. were taken for the large and small precipitates but only the large precipitates yielded sufficient number of spots to be definitely analysed. These spots confirmed the presence of the equilibrium phase $FeAl_3$ as the large precipitate. S.A.D.P. shown in Plates 6.6(d), 6.9(d).

An interesting feature can be noted in plate 6.7(a) where the presence of Moire fringes is observed. The phenomenon of Moire fringes[167], a well known effect in optics, are produced when two crystals with different lattice parameters or orientation produce a contrast effect. Moire patterns in the microstructure show the presence of coherent or semi-coherent precipitation in the solid solution. This confirms the present idea of an age hardening system with the precipitation of coherent precipitates rather than the formation of the orthorhombic precipitate $FeAl_6$. The equilibrium precipitate $FeAl_3$, although of the monoclinic crystal structure, has been found to be coherent with the matrix as one of the sides has a length, 8.08A°, twice that of the aluminium spacing, 4.04A°. It is, therefore, feasible that a coherent meta stable precipitate similar to the Al-Cu system is formed prior to $FeAl_3$ from the solid solution. Two sides of the precipitate will be coherent with the aluminium lattice having a lattice spacing of 8.08A°. This meta stable phase will then be more energetically favourably formed than the orthorhombic structure due

to its coherent nature. The precipitates formed are also of uniform thickness, not platelets or discs, as there is a strong fringe contrast over the whole section.

Plates 6.6(a),(b) are of the same area and show the alignment of the particles into the direction of extrusion. The larger particles are present on the grain boundaries and the needle shaped precipitates, of $FeAl_3$, are seen to lie in preferred orientations due to the semi coherent nature of the phase with the matrix in the cube direction. They are precipitated after extrusion as they are positioned across the direction of extrusion and are formed during the air cooling. A combination of mechanical working causing lattice distortion and annealing, in the form of air cooling, is sufficient to relieve the supersaturated solid solution.

In certain areas of the specimens examined on the microscope there is a considerable amount of precipitation with dislocation interaction and looping around the particles. The dislocations become locked either during deformation or after, during air cooling, depending on the presence of the precipitates.

6.8.3 Dislocation networks

The possibility of a three dimensional network as proposed by McLean[80,81] was investigated. When polishing a specimen to the thickness required for the electron microscope unpinning of the dislocations in the three dimensional network is likely and those dislocations freed escape to the surface of the specimen.

Dislocation networks are sometimes seen in the aluminium - aluminium oxide system, plate 6.11(a), (b), but more often observed

(a)

Powder B 20:1 300°C

(b)

Powder B 50:1 300°C

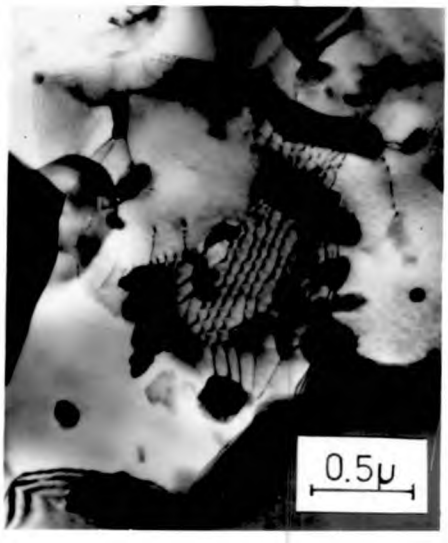

(c)

Powder L 30:1 400°C

(d)

Powder J 30:1 380°C

PLATE 6.11 Dislocation networks

in the alloy systems plate 6.11(c), (d). There is therefore a strong possibility that these could have extended across the subgrain during deformation and the microstructures in plate 6.11 are the remnants of the unpinned dislocation network.

McLean[81] also proposed the possibility of a dislocation network associated with particles where these would retard the dislocation network growth as they retard grain growth and introduce a friction stress during hot working. The process of plastic deformation serves to refine the 3-D network and recovery consists of growth of the meshes of the dislocation networks. The impeding effect of the particles on the network explains the recovery of the dislocation network in the presence of second phase particles. This also helps to explain the presence of distinct boundaries when one would expect broad diffuse sub grain boundaries. The dislocation network is observed in among the precipitates revealed by Moire fringes in plate 6.7(a) showing the distinct possibility of pinning by the second phase particles.

It would, therefore, seem that the possibility of a three dimensional network cannot be dismissed and its presence serves as a useful basis for the dislocation sources within the material.

6.8.4 Recovery and Recrystallisation

When a metal is plastically deformed the work of deformation is stored in the lattice distortions and this stored energy can be released by isothermal annealing, providing the driving force for the two competing processes, recovery and recrystallisation. The recovery process constitutes all those annealing phenomena which occur before the appearance of a new strain free recrystallised grain. Recrystallisation is the nucleation and growth of new strain free grains and the gradual

consumption of the cold worked matrix by the movement of large angle grain boundaries.

Hot worked structures are unstable and tend to recrystallise if held at temperature after deformation.

Observation of the sub structure of the aluminium alloys, similar to sub grain structures of pure aluminium, contributed fairly unambiguous evidence for dynamic recovery. A detailed analysis of recovery phenomena has been carried out by Nobili et al[149-151] who showed that there was no fundamental difference between S.A.P. and pure aluminium except that recovery could occur over a wide range of temperatures due to the increase in the recrystallisation temperature. In the present work, it is found that there is evidence of recrystallisation in a generally recovered structure by the process of sub grain coalescence in rods extruded at an initial temperature of 300°C fig. 6.1(a). The sub grain structure also contained some relatively high angle sub boundaries and a few subgrain with large orientation deviations with respect to the matrix. Annealing by formation growth of subgrains is the main recovery mechanism of the extrusions manufactured from powders, and the movement of dislocations through climb by a self diffusion process.

Recrystallisation has been sub divided into two types[168]

(i) continuous recrystallisation (in situ recrystallisation)

(ii) discontinuous recrystallisation

Discontinuous recrystallisation is that of high angle boundary mobility acting as a reaction front by sweeping out the dislocations ahead of their direction of motion. Dynamic recrystallisation, referred to by Jonas[76], can be included in this sub division as it requires extensive

migration of grain boundaries to form a recrystallised grain; if the grain boundaries are restricted, as in the case of powder extrusion, dynamic recovery takes place.

Continuous recrystallisation is by subgrain growth which leads to the preservation of the rolling texture. The formation of high angle boundaries, that form the basis for recrystallised grains, is by the process of subgrain growth and coalescence as put forward by Li[73] and Hu[74] and discussed already. For the aluminium powders, A and B, this mechanism is the prevalent one for recrystallisation and grain growth and seen in the micrographs, plate 6.1(a), 6.4(b).

The competition between recovery and recrystallisation has been found to increase with concentration of dispersed phases[149-151]. The activation energy for grain boundary migration in the presence of a dispersed phase is greater than that for lattice self diffusion thus increasing the activation energy for the process. If the formation of recrystallisation nucleii is associated with localised recovery process the retardation of recrystallisation in aluminium - aluminium oxide is attributed to the inhibition of boundary migration. The oxide phase present has been found[149] to accelerate or retard primary recrystallisation but secondary recrystallisation is completely inhibited by the presence of oxide phase. In the present work it is seen that recrystallisation is retarded by the presence of the oxide phase and nucleii are formed by a localised recovery process.

The effect of dispersed second phase particles on recrystallisation is less clear where the inter particle spacing is the controlling factor. There is acceleration at wide spacings and retardation at close spacings.[149-151]. It has been found on work with the Al-Fe system[169]

that decreasing the grain size of two phase alloys caused acceleration of recrystallisation but the magnitude decreased as the $FeAl_3$ content increased. Plate 6.5(c) shows the presence of a recrystallised grain where the large primary $FeAl_3$ particle has acted as a site for the formation of a nucleii, and increasing the number of these precipitates will increase the number of nucleii. The large precipitates present prior to deformation will accelerate recrystallisation by acting as a sink for line and point defects. Plate 6.7(a) shows a region of the Al-Fe alloy that is saturated with Al-Fe particles and as a result no recrystallisation or sub grain growth is visible. This suggests, also, that the extent of recrystallisation is dependent on the presence of particles before working as particles present subsequent to working will lessen the recrystallisation rate.

The effect of solute atoms on recrystallisation is most apparent at very small concentrations and dependent on the nature of the atoms[170]. It is generally agreed that increasing the solute content of any solid solution alloy raises the recrystallisation temperature and decreases the rate of recrystallisation by reducing the mobility of high angle boundaries surrounding an expanding grain. For the Al-Fe alloy it has been found[171,172] that as the iron content increases the recrystallisation of solid solution alloys is retarded whereas that of the two phase alloys is accelerated. This implies the need for increased driving fone to initiate recrystallisation and decreasing the overall rate of recrystallisation as the solute increases.

Thus it can be seen that the alloy systems will have a structure dependent on the state of the solute present. In regions where primary precipitates exist a region of recrystallised grains can be expected compared to solid solution regions where recrystallisation

would be retarded.

The presence of recrystallised grains associated with large particles present before the extrusion can be seen in plates 6.8 for the Al-Mn alloy and 6.5 for the Al-Fe alloy. Solid solution regions are present in plate 6.7(a) and 6.9(a) for the Al-Fe and Al-Mn alloys respectively.

The Al-Fe alloy, in particular, tends to be rather inhomogeneous due to the difficulty of getting the Fe into the liquid aluminium before casting. Regions of high Fe concentration arise which are those that are not recrystallised and low Fe concentration areas are those that do show recrystallisation. Therefore the presence of recrystallised grains in the Al-Fe is dependent on the initial distribution of Fe.

6.8.5 Dispersion Hardening

The previous models of dispersion hardening offer no completely satisfactory explanation of high strength at elevated temperatures. The dislocation particle inter-action model is not really tenable at high temperatures where cross slip and climb occur readily.

It has been proposed by Clegg and Lund[173], in work on dispersion strengthened nickel alloys, that the dislocation sub structure is not removed at elevated temperatures. The stability of the sub structure arises from the pinning effect of particles in this work. Hultgren[174] suggested that the arrangement of dislocations in the sub structure is only important in that it reduces the dislocation density and the strength of the dislocation walls is determined by the segregation of impurities and misorientation within the sub structure.

The stability of the dislocation sub structure has also been observed in work on creep of aluminium - aluminium oxide material[175] and the main deformation mechanism that of grain boundary sliding. Grain boundary sliding in creep of metals at high temperatures being controlled by lattice self diffusion hence the activation energy for thermal activation is that of aluminium.

In the dispersion hardened aluminium product the aluminia particles act as obstacles to sliding of the grain boundaries and deformation is localised in the vicinity of the particles. This model of grain boundary sliding also requires that the interface between particle and matrix acts as a sink for dislocations and the dispersed place shows no solubility in the matrix.

In the present work there is no evidence to suggest that deformation is localised but there is evidence of a dislocation sub structure especially in the alloy powder products, plate 6.11. The dislocation networks seen, however, are not associated with oxide particles directly so it is thought that the oxide particles inhibit the motion of dislocations through the matrix.

The results of previous research, by other workers in the dispersion hardened field, have been fitted to theories of Orowan[120], Fisher, Hart, and Pry[123] and their own empirical formulae relating mean free path between particles and yield strength. However, there is still lack of agreement as to the precise nature of the dislocation/particle interaction that occurs on straining, from experimental results.

A few experimental results of the present work have been fitted

to the theory of Orowan[120] using the line tension, T', equation proposed by Kelly and Nicholson[122]. These are shown in figure 5.43 and show quite good agreement, alas this is in qualitive agreement rather the quantitative. This is due to the difficulty of finding an even distribution of particles within the matrix.

Problems also arise when relating the yield strength to the oxide particle distribution as the yield strength is obtained by testing a fairly large specimen and the oxide distribution measured from a very small selected electron microscopy specimen area. Due to the relatively large scale of operation in producing the specimens, qualitative agreement to the theory of dispersion hardening is good.

The micrographs shown in plate 6.11 and 6.10(c), (d) reveal the presence of dislocation networks and free dislocations looped around precipitate and oxide particles thus endorsing the theory of a dislocation sub structure in a dispersion hardened material. The process of deformation will then be a refining process of the dislocation network, i.e. the mesh size of the network decreases with increasing deformation, as proposed by McLean[81]. The materials investigated had been allowed to air cool and so, to a certain extent, the structure was that of a recovered structure with many of the dislocation tangles annealed out. However, the micrographs do reveal some dislocations interacting with particles thus indicating that these do influence the structure within the matrix. The full extent of dislocation/particle interaction could not be established without the use of precise techniques outside the scope of the present work.

6.8.6 Heat treatment

A small number of experiments were performed to determine the

effect of heat treatment on the extruded products. The results of tensile tests are shown in tables 5.12. The subgrain size is slightly increased and correspondingly the tensile strength is slightly reduced. The effect of heat treatment at an elevated temperature is a general softening stress relieving operation. In some of the high temperatures, treatments of specimens extruded at low temperatures or specimens from the dust powder blistering was observed on the products after heat treatment. This had previously been observed by Ansell who vacuum pre-sintered the powder to overcome this problem, which was thought to have occurred from the combined water in the oxide reacting with the aluminium. It is considered that the combined water in the oxide reacted with metallic aluminium to form hydrogen which eventually caused blistering.

6.9 Mechanical Properties

The results of the mechanical properties of the extruded products of tensile performed at room temperature and 400°C, are presented in more detail in the appendices. Properties of commercial alloys and results of previous workers are shown in tables 5.13 and 5.14 respectively.

Aluminium and its alloys have a wide range of uses and applications because of their low density, high strength, durability, and ease of fabrication, i.e. hot extrusion. Starting with commercial aluminium, with a yield strength of 50 MNm^{-2}, this can be strengthened considerably, by suitable alloy addition, by the action of precipitation hardening. The most common heat treatable alloy used, is that known as 'duralumin' which can attain a yield strength in excess of 400 NMm^{-2} after heat treatment. Unfortunately raising the service temperature over-ages the material with attendant softening, thus losing the gained increase

of strength at elevated temperatures.

It can be seen that the alloys J, K, and L, prepared from pre-alloyed atomized powders, compare favourably with the commercial alloys. The elevated temperature properties are an improvement but unsufficient soaking at the testing temperature was carried out to enable a true companion to be made.

However, it can be seen that the precipitation hardened alloys prepared by atomization, give increased strength over the aluminium powders products and commercial alloys without the use of an additional heat treatment stage. This is an added advantage to the powder alloys, for, by eliminating the heat treatment stage, the cost of producing a high strength alloy is decreased.

Comparison of the high strength alloy powder products to commercial S.A.P. shows that the atomized powders have the advantage of greater ductility over the S.A.P. alloys. This ductility enables the alloy materials to be more easily plastically deformed and manufactured into suitable shapes. Unfortunately the strength at elevated temperatures is not retained due to the coalescence of the precipitates whereas oxide particles remain the same, giving S.A.P. superior elevated temperature strength.

The most important parameter in the extrusion of aluminium powders A, B, and C is that of particle size. It has been previously noted[87] that the oxide boundaries were similar to that of a network structure resembling a grain boundary structure of a polycrystalline metal; the Petch relation gives the yield stress as a function of grain size

$$\sigma = \sigma_o + k' dg^{-1/2}$$

$$\sigma = \sigma_o + C_{26} dg^{-1/2} \qquad (6.3)$$

where σ is the yield stress, σ_o is a type of 'friction stress' due to the lattice, and dg the grain size. This equation is applied to the particles where the grain size in the Petch equation, is replaced by the particle size. The plot of proof stress (0.2%) against the immerse of the square root of particle diameter yields a linear relationship similar to that of a Petch-type equation. On extrapolation the values obtained are greater than those for coarse grained aluminium due to the variation of subgrain size with particle size as seen in fig. 5.30. The coarser the powder the coarser the subgrain size, so eventually the coarse grained aluminium billet extruded will have a subgrain structure similar to that seen in plate 6.3(a). The values, on extrapolation, of fig. 5.30 yield the values obtained for commercial pure aluminium tested on the machine under the same conditions.

Similar plots are also drawn for powders J, K, and L, fig. 5.31 but little difference is observed in the proof stress values with decreasing nature of the precipitates within the particles. Results of tests performed at 400°C show very little variation with particle size indicating a stable structure at that temperature, fig. 5.31.

Petch-type plots are also shown for the powders B, J, K, and L using proof stress values and subgrain sizes measured, figs. 5.32 and 5.53. A linear relationship is shown to exist between proof stress and the inverse square root of the subgrain size similar to that of the Hall-Petch relationship for low angle boundaries at room temperature used by Raybould[68].

$$\sigma = \sigma_o + C_{27} D_s^{-1/2} \qquad (6.4)$$

where D_s is the mean subgrain diameter

It is also shown that

$$\log_{10} (\sinh \alpha\sigma) = C_{28} D_s^{-1} \quad \text{in fig. 5.36}$$

where the stress, σ, is that measured as the mean during extrusion.

The effect of temperature of extrusion billet is shown in fig. 5.3 - 5.35 where the proof stress (0.2%) obtained from tensile tests are plotted against initial billet temperature. These plots indicate that a decrease in the billet temperature, increase the strength. This strength increase is accompanied by a similar decrease in ductility and decrease in subgrain size. The results obtained from tests at 400°C show that the structures of differing extrusion temperatures are the same at this temperature, i.e. the subgrain boundaries ineffective at this temperature. The alloys Al-Fe and Al-Mn decrease in strength quite rapidly as the temperature of extrusion is increased due to the coarsening of the second phase particles. Al-Mg-Zn is the strongest alloy due to its nature of producing uniform solute clusters. During extrusion a phase transformation temperature is either attained or exceeded causing the solute atoms to be re-dissolved if in precipitate form and not precipitated out when cooled. The tensile test stress strain curves showed small serrations similar to the Portevin - Le Chatelier effect and also sharp peaks where the material broke at the fissures in the specimens. In the Al-Mg-Zn materials the specimens fractured at the maximum point on the curve showing little or no necking and brittle fracture. This is due to the solute atoms hindering mobile dislocations either by locking or forming atmospheres around them, the material is then very easily work hardened and very dependent on strain rate.

6.9.1 Reduction ratio

The effect of reduction ratio during extrusion on the mechanical properties of the extruded rod is extremely small. The proof stress values show a small decrease with increasing reduction ratio as also did the elongation value. A slightly more uniform distribution of the oxide phase in high reduction ratios was also observed. Table 5.11 shows the approximately constant subgrain size for different reduction ratios of specimens extruded at the same temperature.

6.9.2 Ram speed

The results of tensile properties of the extruded product show that the ram speed has little effect on the final properties. This is in contrast to commercial aluminium where the effect of strain is to alter the size of the subgrains formed during the extrusion process. The reason for the lack of strain rate dependence of the extrusion process on the final properties, is that the presence of oxide particles within the matrix hinder dislocation motion and cause formation of subgrain. Also the ram speed does not greatly increase the extrusion load, in contrast to solid billet extrusion, due to the mechanism previously described of the material acquiring its final properties as it passes through the die. Combination of this and the former mechanism ensure that subgrains of nearly constant are produced at different ram speeds.

One interesting feature of the tensile properties is that the percentage elongation is slightly reduced on specimens extruded at a very high strain rate, probably due to an excess of dislocation tangles.

CHAPTER 7

Conclusions

An investigation has been made into the effects of extrusion on the structure and strength of the aluminium powder alloy products. The results obtained have shown that:-

1. The extrusion pressure required to extrude a powder billet, with a product strength the same as a conventional alloy, is much less.
2. The stress dependence on strain rate for the powders during extrusion is less than for solid materials.
3. Cold compaction results agree with previously derived empirical equations.
4. Achievement of 100% theoretical density during extrusion is governed by the relationship.

$$\ln P = 6.62 - 2.25 \times 10^{-3} T \quad (T \text{ is } {}^{o}K)$$

5. There is a transition ratio below which coherent material is not obtained, this being about 5:1.
6. An empirical pressure reduction ratio equation exists of the form

$$\frac{P}{Ym} = 0.81 + 1.2 \ln R$$

7. During extrusion there are high local indeterminate temperature rises at particle interfaces giving rise to consequent dynamic recovery.
8. The deformation during extrusion of metal powders occurs in a zone that may be divided into two merging regions, one representing the 'powder properties' and the other

'final, product, properties'. The existence of this 'powder properties' region is shown to account for the low pressures observed during extrusion.

9. The activation energy values calculated using the sink relationship, show that the rate controlling processes for dislocation motion during hot deformation are the same as for commercial aluminium alloys. The Al-Zn-Mg alloy has a rate controlling mechanism similar to that of a solid solution conventional alloy.

10. Alloys Al-Mn, Al-Fe, not easily cast, can be produced by atomisation and extruded into a useable form.

11. Materials produced have a proof stress, as a function of sub grain size similar to a Petch equation.

12. Materials extruded have a proof stress, at room temperature, at least twice that of a conventionally produced material and at 400°C, seven times or greater depending upon alloy.

13. A relationship exists between original particle size and product proof stress, given by

$$\sigma = \sigma_o + C D_p^{-1/2}$$

14. The oxide content distribution improves with increasing reduction ratio.

15. Precipitation hardening mechanism is in qualitative agreement with Orowan's theory.

16. Extrusion of atomised aluminium alloy powder is a feasible industrial process for alloys that present difficulties when conventionally produced and subsequently worked. Atomisation of alloys with poor casting properties compares economically favourably with normal casting.

REFERENCES

1. R. L. Sands & C. R. Shakespere, 'Powder Metallurgy' George Newnes Ltd. 1966
2. C. G. Goetzel, 'Treatise on Powder Metallurgy' Interscience 1949
3. T. Sheppard & P. J. Chare, Powder Metallurgy 1972 15 17
4. P. Loewenstein, Powder Metallurgy Ed. W. Leszynski p. 563
5. J. Williams, Powder Metallurgy 1958 1/2 94
6. W. D. Jones, Metal Ind. 1940 57 2 27
7. British Patent 231, 192 C. H. Fischer 1924
8. U.S. 2,148,040 P. Schwarzkopf 1939
9. R. Irmann, Tech Rund 1949 41 (36) 19
10. A. Von Zeerleder, J.I.M. 1948/49 75 1143
11. R. Irmann, Aluminium 1951 27 24
12. R. Irmann, Metallurgia 1952 46 125
13. R. Irmann, Metall 1952 6 608
14. E. A. Bloch, Met. Rev. 1961 6 193
15. D. H. Roberts et al, Powder Metallurgy 1962 10 132
16. F. V. Lenel, Powder Metallurgy 1962 10 119
17. B. J. Eastwood, D. A. Robins, Powder Metallurgy 1964 7 99
18. B. J. Eastwood, D. A. Robins, Powder Metallurgy 1966 9 175
19. D. J. Brown, Symposium on Powder Metallurgy I.S.I. 1954 248
20. H. G. Cole, J.I.M. 1957-58 86 29
21. L. L. J. Chin, N. J. Grant, Powder Metallurgy 1967 10 344
22. R. S. Busk, T. E. Leontis, Trans. A.I.M.E. 1950 188 297
23. J. P. Lyle, Metal Progress 1952 62 12 109
24. R. J. Towner, Metal Progress 1958 73 5 70
25. N. F. MacDonald & A. Ransley, ref. 19 p. 242
26. C. R. Shakespere & D. A. Oliver, Powder Metallurgy 1964 7 203
27. N. Hansen, Riso Report No. 223 1971

28. N. Hansen, H. Lilholt, M. Jensen, Riso Report No 48 (1961), Suppl 1 (1964), Suppl 2 (1965), Suppl 3 (1967).

29. W. D. Jones, 'Fundamental Principles of Powder Metallurgy' Arnold London 1960

30. K. Kawakita & K. Ludde, Powder Tech 1970/71 4 61

31. R. P. Seeling, 'The Physics of Powder Metallurgy' Ed. W. E. Kingstan p. 344

32. R. P. Seeling, Trans A.I.M.E. 1946 166 492

33. C. Orr, 'Particulate Technology' MacMillan New York 1966

34. P. E. Evans & G. C. Smith, Powder Met 1959 2 26

35. L. F. Athy, Bull. Am. Assoc. Petrol Geologists 1930 14 (1) 1

36. L. V. Bal'shin V. Metalloprom 1931 18 124

37. R. W. Heckel, Trans A.I.M.E. 1961 221 671

38. R. W. Heckel, Trans A.I.M.E. 1961 1001

39. K. Kawakita, J. of Japan Soc. Powder Met. 1963 10 236

40. L. Ramqvist, Powder Met. 1966 9 (17) 1

41. F. Thummler & W. Thomma, Met. Rev. 1967 69

42. P. Murray, E. P. Rodgers, A. E. Williams, Trans. Brit. Ceramic Soc. 1954 53 474

43. R. Shuttleworth & J. K. Mackenzie Proc. Phys. Soc. 1949 B 62 833

44. M. S. Kovalchenko & G. V. Samsonov, Sov. Powder Met 1961 (2) 3

45. G. E. Mangsen, W. A. Lambertson, B. Best, J. Amer. Ceramic Soc. 1960 43 55

46. T. Vasilos, J. Amer. Ceramic Soc. 1960 43 517

47. J. D. McClelland, E. H. Zehms, J. Amer. Ceramic Soc 1963 46 77

48. R. I. Garber & L. M. Polyakov, Physics Metals, Metallography 1961 11 81

49. C. E. Pearson & R. N. Parkins, The Extrusion of Metals J. Wiley

50. J. F. Bishop, Met. Rev. 1957 2 361

51. R. Chadwick, Met. Rev. 1959 4 189

52. E. K. Haffner & R. M Elken, Met. Rev. 1957 2 263

53. J. M. Alexander, J.I.M. 1962 91 193

54. J. M. Alexander & K. Brewer, 'Manufacturing Properties of Materials' Van Nostrand

55. L. C. Dodeja & W. Johnson, J. Mech Phy Solids 1957 5 267

56. R. J. Wilcox & P. W. Whitton, J.I.M. 1959 89 289

57. S. Hirst & D. H. Ursell, Proc. Conf. Tech of Eng. Manufact. Inst. of Mech. Eng. 1958

58. W. Johnson, J. Mech Phys Solids 1955 3 218

59. W. Johnson, J.I.M. 1955 84 165

60. W. Johnson, J.I.M. 1956 85 403

61. R. Hill, 'The Mathematical theory of Plasticity' Clarendon Press Oxford 1950

62. H. Kudo, Int. J. Mech. Sci. 1960 157 229 366

63. W. Johnson, Proc. Inst. Mech. Engs. 1959 173 No. 1 61

64. W. Johnson & H. Kudo, 'The Mechanics of Extrusion' Manchester University Press

65. K. Ashcroft & J. Lawson, J.I.M. 1960 89 369

66. B. J. Meadows & M. J. Cutler, J.I.M. 1969 97 321

67. A. R. E. Singer & D. Coakham, J.I.M. 1960 89 177

68. D. Raybould, Ph.D. Thesis London 1971

69. H. K. Hardy, Metallurgia 1944 30 240

70. W. A. Wong, H. J. McQueen, J. J. Jonas, J.I.M. 1967 95 129

71. P. R. Swann, 'Electron Microscopy and Strength of Crystals' 1963 Interscience

72. W. J. Mc G. Tegart, J.I.M. 1961 90 17

73. J. C. Li, Acta Met 1963 11 563

74. H. Ju, Trans. A.I.M.E. 1962 224 131

75. H. P. Stuwe, I.S.I. Special Report No. 108 1968 p. 1

76. J. J. Jonas, C. M. Sellars, W. J. Mc. G. Tegart, Met. Rev. 1969 12 130

77. J. J. Jonas, W. A. Wong, & H. J. McQueen, ref 75 p. 24

78. J. Weertman, J.A.P. 1955 26 1213

79. J. Weertman, J.A.P. 1957 28 362

80. D. Mclean, Rep. Prog. Phys. 1966 29 1

81. D. Mclean, Met. Rev. 1964 7 481

82. C. Zener & J. H. Holloman, Trans A.S.M. 1944 33 163

83. F. Garofalo, Trans. A.I.M.E. 1963 351

84. C. Sellars & W. J. Mc. G. Tegart, Mem Sci Rev. Met. 1963 63 731

85. Brit. P. 734, 778 R. Chadwick 1955

86. N. Hansen, Powder Metallurgy 1967 10 (20) 94

87. N. Hansen, Powder Metallurgy 1969 12 23

88. J. H. Schwartzwelder, I.J.P.M. 1967 3 53

89. R. Biais et al, Powder Met. 1967 10 116

90. T. M. Nilsson, I.J.P.M. 1969 5 43
J. Nucl. Matrls. 1968 220 28

91. EUR 4074 1969

92. J. A. Dromsky & F. V. Lenel, Trans A.I.M.E. 1964 230 1289

93. E. J. Westerman & F. V. Lenel, Trans A.I.M.E. 1960 218 1010

94. F. V. Lenel et al, Trans A.I.M.E. 1957 209 124

95. N. Hansen, Trans A.I.M.E. 1969 245 1310

96. N. Hansen, Trans A.I.M.E. 1969 245 2061

97. E. Gregory, N. J. Grant, Trans A.I.M.E. 1954 200 247

98. J. Herenguel & J. Boghen, Rev Met. 1954 51 265

99. F. V. Lenel et al, Trans A.I.M.E. 1957 209 117

100. C. D. Wiseman et al, A.S.M. Trans Quart 1963 56 717

101. J. H. Dudas & W. A. Dean, I.J.P.M. 1969 5 (2) 21

102. C. F. Dixon & H. M. Skelly, I.J.P.M. 1965 1 (4) 28

103. P. Ramakrishnan & B. K. Agrawal, I.J.P.M. 1969 5 (2) 79

104. T. Wantanabe & K. Yamada, I.J.P.M. 1968 4 (3) 37

105. H. H. Stout, Trans A.I.M.E. 1941 143 326

106. J. Tynowski, Trans A.I.M.E. 1941 143 335

107. N. Hansen, Trans A.I.M.E. 1964 230 263

108. N. J. Grant, Trans A.I.M.E. 1957 209 349

109. R. S. Goodrich & G. S. Ansell, Trans A.I.M.E. 1964 230 1372

110. N. Hansen, Acta Met. 1970 18 137

111. N. Hansen, Trans A.I.M.E. 1968 242 954

112. G. S. Ansell, Trans A.I.M.E. 1959 215 294

113. C. L. Meyers & O. D. Sherby, J.I.M. 1961/62 90 380

114. C. L. Meyers et al, J. Aus. Met 1963 8 171

115. C. L. Meyers & K. Stulpe, Metallography 1969 2 (1) 41

116. H. Jones, Mat. Sci. Eng 1969/70 5 1

117. M. H. Burden & H. Jones, Metallography 1970 3 307

118. G. Thursfield et al, Conf. on metastable metallic alloys Brela, Yugoslavia Sept. 1970

119. M. Gensamer et al, Trans A.S.M. 1942 30 938

120. E. Orowan, 'Symposium on Internal Stresses in Metals and Alloys' p. 451 (discussion) 1948 London (Ints. Metals)

121. G. S. Ansell & F. V. Lenel, Acta Met 1960 8 612

122. A. Kelly & R. B. Nicholson, Prog. Mat. Sci. 1963 10 149

123. J. C. Fisher, E. W. Hart, R. H. Pry, Acta Met 1953 1 336

124. M. F. Ashby, Phil Mag 1966 14 1157
Z. Metallk 1964 55 5

125. G. S. Ansell & J. Weertman, Trans A.I.M.E. 1959 215 838

126. G. S. Ansell & F. V. Lenel, Trans A.I.M.E. 1961 221 452

127. G. H. Reynolds et al, Met Trans 1971 2 3027

128. N. Hansen, Acta Met 1969 17 637

129. M. F. Ashby, Acta Met 1966 14 679

130. W. Prager, Proc. Inst. Mech. Engrs. London 1955 169 p. 41

131. W. Johnson, P. B. Mellor, 'Plasticity for Mechanical Engineers' Van Nostrand

132. P. Feltham, Metal Treatment 1956 23 44a

133. W. A. Wong, J. J. Jonas, Trans A.I.M.E. 1968 242 2271

134. B. S. 1796, 1952

135. S. Brunaver, P. Emmett, & E. Teller, J. Amer. Chem. Soc. 1938 60 309

136. C. H. J. Beaven, P. Eadington, Chem. and Ind. 1966 1484

137. J. E. Dorn et al, Acta Met 1957 5 219

138. H. W. L. Phillips, Inst. Metals Monograph No. 25

139. B. Cuff & J. Grant, J.I.M. 1958-59 87 248

140. C. R. Barrett & W. D. Nix, Acta Met 1965 13 1247

141. S. K. Mitra, D. McLean, Metal Sci. J. 1967 1 192

142. H. W. L. Phillips, A.E.D. No. 13 1955

143. H. W. L. Phillips, A.E.D. No. 17 1955

144. G. A. Redfern, C. M. Sellars,
'Deformation under hot working Conditions'
Special Report No. 108 p. 29 1968
London (I.S.I.)

145. F. J. Humphreys, J. Martin, Acta Met 1966 14 775

146. M. H. Lewis, J. W. Martin, Acta Met 1963 11 1207

147. J. L. Brimall et al, Acta Met 1966 14 459

148. M. J. Klein & R. A. Huggins, Acta Met 1962 10 55

149. A. Desalvo, D. Nobili, J. Mat. Sci. 1968 3 1

150. D. Nobili et al, J. Mat. Sci. 1968 3 382

151. D. Nobili, R. De Maria, J. Nucl. Mat 1965 17 5

152. E. Nes et al, Z. Metallk 1972 63 248

153. D. Goel, Proc. Seventh Int. Conf. Electron Microscopy
1970 Vol 2 537

154. J. K. Edgar, Trans A.I.M.E. 1949 180 225

155. E. Scheil, Y. Masuda, Aluminium 1955 31 51

156. D. E. J. Talbot, M. Bishop, J.I.M. 1967 95 119

157. K. Little et al, J.I.M. 1946 73 83

158. A. Fontaine et al, Compt. Rend 1970 271 (3) 237

159. G. Bassi, H. Bichsel, Z. Metallk 1970 61 493

160. W. D. Donnelly, M. L. Rudeo, Trans A.I.M.E. 1964 230 1481

161. I. Miki, H. Warliment, Z. Metallk 1968 59 254

162. J. Grewen, H. V. Heimendahl, Z. Metallk 1968 59 205

163. P. J. Black, Acta Cryst 1955 8 43 175

164. E. H. Hollingsworth et al, Trans A.I.M.E. 1962 224 188

165. C. A. Stickels, R. H. Bush, Met Trans. 1971 2 2031

166. E. Blank, Z. Metallk 1972 63 324

167. P. B. Hirsch et al, 'Electron Microscopy of thin crystals' Butterworths 1965

168. H. Ashlborn, G. Hornbogen, J. of Mat. Sci. 1969 4 944

169. P. R. Mould, P. Cotterill, J. of Mat. Sci. 1967 2 241

170. J. G. Byrne, 'Recovery, Recrystallisation, and Grain growth' MacMillan & Co. London

171. N. Ryum, J.I.M. 1966 94 191

172. R. E. Green et al, Trans A.I.M.E. 1959 215 610

173. M. A. Clegg, J. A. Lund, Met Trans 1971 2 2495

174. C. Hultgren, Trans A.I.M.E. 1964 230 898

175. K. Milicka, J. Cadek, P. Rys, Acta Met 1970 18 733

176. B. Chalmers, 'Principles of Solidification' J. Wiley & Sons Ltd.

177. E. M. Modl-Onitisch, Powder Met. 1959 4 120

178. E. Gregory, Metal Progress 1959 75 113

179. L. F. Mondolfo, Met. Rev 1971 5 95

180. R. L. Fullman, J. Metals 1953 5 447

181. C. J. Smithells, 'Metals Ref. Book' Butterworths London 1967

182. J. E. Freund, 'Mathematical Statistics' Prentice-Hall 1962

APPENDIX I

Nomenclature

A	Load constant, redundant deformation
A_2, A_3, A_4	Frequency purity factors
$\bar{A}$	constant, viscous drag mechanism (Weertman's Equation)
a	constant same as α' (Weertman's Equation)
a'	constant (Kawakita's Equation)
a_o	lattice parameter
α	apparent activation volume
α'	constant, = 1 for edge dislocations, = 1/1-γ for screw dislocations
B	Load constant, useful work term
$\bar{B}$	Constant (Weertman's Equation)
β	same as α
b	Burgers vector
$C_1 - C_{27}$	constants
C^*	Volume reduction (Kawakita's Equation)
C_H	Specific Heat
D	density
$\tilde{D}$	chemical diffusivity
D_{AF}	planar surface spacing
D_c	diameter of container
Dp	particle diameter
Ds	sub grain diameter
Dv	diffusion coefficient
d	grain diameter
da	particle diameter in slip plane
de	extruded grain size

dr	recrystallised grain size
ΔH_o	activation enthalpy
ΔQ	activation energy
ε	tensile strain
$\dot{\varepsilon}$	strain rate
F	constant
F*	constant
f	volume fraction of second phase
G	shear modulus
H_v	Vickers Hardness number
K	shear yield stress
K'	creep rate
k*	Boltzmann's constant
l	length of extrusion billet
L	inter particle spacing (Weertman)
L'	modulus of pressing (Bal'shin)
λ	mean planar spacing
λ'	average spacing between jogs
M	dislocation source density
μ^*	shear modulus
μ	coefficient of friction
n, n'	stress/strain rate exponents
n*	porosity
N	Number of dislocation loops
P	pressure
Q	porosity
Q'	activation energy for self diffusion
R	Reduction ratio
R'	Gas constant
r	radius of second phase particles

ρ	density
ρ_s , ρ_d	dislocation density
s*	temperature dependence on flow stress
σ	yield stress
$\bar{\sigma}'$	mean yield stress
σ_o	yield stress (friction stress)
$(0.2\%)\sigma$	proof stress
T	Temperature
T_m	solidus limit
T'	Line Tension
t	time
tm	mesh size of oxide particles
τ	shear stress
θ^*	averaging term for screw and edge dislocations
v_o	atomic volume
v	activation volume
r'	number of dislocation loops
X	penetration distance of deformation
x'	number of atoms per unit cell
Ym	mean yield stress
Z	Zener Holloman parameter, temperature compensated strain rate
ϕ_f	Strucutre factor
η	viscosity
ϕ	die angle
w	deformation cone angle

APPENDIX II

Linear Regression and Correlation Coefficient[182].

A standard programme was used that calculates the equation of the straight line of best fit of a net of data points. The best fit is determined by minimising the sum of the squares of the deviation of the data points from the line.

The programme calculates m and b for the equation

$$y = mx + b$$

The programme also calculates a correlation coefficient r, an indication of goodness of fit

$-1 \leqslant r \leqslant 1$ where the sign corresponds to slope m

if r = o, this no correlation, and if $r = \pm 1$ there is perfect correlation or a perfect fit.

The defining equations are

$$m = \frac{\sum_{i=1} (X_i - \bar{X})(Y_i - \bar{Y})}{(X_i - \bar{X})^2}$$

$$b = \bar{Y} - m\bar{X}$$

where $\bar{Y} = \frac{\sum_{i=1}^{n} Y_i}{n}$ and $\bar{X} = \frac{\sum_{i=1}^{n} X_i}{n}$

$$r = \frac{\sum_{i=1}^{n} (X_i - \bar{X})(Y_i - \bar{Y})}{\sqrt{\sum_{i=1}^{n} (X_i - \bar{X})^2 \sum_{i=1}^{n} (Y_i - \bar{Y})^2}}$$

APPENDIX III

Proof of the relationship

$$(\sinh\alpha\sigma)^n = \frac{1}{2}\exp n\alpha\sigma$$

when $\alpha\sigma > 1.2$

By definition

$$\sinh(\alpha\sigma) = \frac{(e^{\alpha\sigma} - e^{-\alpha\sigma})}{2}$$

Considering $e^{\alpha\sigma} - e^{-\alpha\sigma}$ and letting $\alpha\sigma$ tend to infinity gives e^{∞} as $e^{-\infty}$ tends to zero. (For $\sigma = 1.2$, $e^{-1.2} = 0.3$ and $e^{1.2} = 3.3$, so that the difference in the two relationships is less than 10%)

Therefore, at large values of

$$e^{\alpha\sigma} - e^{-\alpha\sigma} = e^{\alpha\sigma}$$

Therefore

$$\sinh(\alpha\sigma) = \frac{1}{2}e^{\alpha\sigma}$$

Considering the n^{th} term

$$\left[\sinh(\alpha\sigma)\right]^n = \left[\frac{1}{2}e^{\alpha\sigma}\right]^n$$

$$= \frac{1}{2^n}(e^{\alpha\sigma} \times e^{\alpha\sigma} \ldots)$$

Thus

$$\left[\sinh(\alpha\sigma)\right]^n = \frac{1}{2^n}e^{n\alpha\sigma}$$

APPENDIX IV

Material	Temp	D_s	D_s^{-1}	$D_s^{-\frac{1}{2}}$
Al-Mg-Zn	300	2	.5	.707
	300	2.5	.4	.632
Al-Fe	300	.75	1.33	1.15
	300	.7	1.43	1.195
	300	.82	1.22	1.104
	300	.673	1.49	1.22
	300	.9	1.11	1.05
	300	.9	1.11	1.05
	360	1.21	.826	.91
	360	.925	1.081	1.04
	380	1.43	.7	.836
	400	1.52	.66	.811
	400	1.56	.64	.801
	400	1.62	.62	.786
Al-Mn	300	.75	1.33	1.15
	305	.975	1.026	1.013
	330	.85	1.18	1.085
	345	.975	1.03	1.01
	345	1.21	.83	.91
	345	.89	1.12	1.06
	345	.75	1.33	1.15
	345	.885	1.13	1.06
	345	.93	1.075	1.04
	345	1.01	.99	1
	345	.8	1.25	1.12
	350	1.09	.92	.96
	350	1.38	.73	.85

Material	Temp	D_s	D_s^{-1}	$D_s^{-\frac{1}{2}}$
	350	.97	1.03	1.02
	360	1.23	.813	.9
	370	1.35	.74	.86
	375	1.14	.88	.94
	380	1.18	.85	.92
	400	1.2	.83	.91
Aluminium A	300	.7	1.43	1.195
	300	.735	1.36	1.166
	250	.7	1.43	1.195
	400	1.5	.667	.816
B	300	1.1	.91	.953
	300	1	1	1
	300	1.2	.832	.912
	300	1.05	.952	.976
	300	1.1	.91	.953
	150	.75	1.33	1.15
	200	.8	1.25	1.12
	350	1.23	.813	.9
	400	1.5	.667	.816
	500	6	.167	.408
(430)	300	1.73	.58	.76
(310)	300	1.35	.741	.861
(200)	300	1.3	.78	.88
(120)	300	1.13	.89	.95
(75)	300	.95	1.05	1.03
(25)	300	.75	1.33	1.15
(25)	300	.7	1.43	1.195
		1.19	.84	.92
	150	.74	1.35	1.16

Material	Temp	D_s	D_s^{-1}	$D_s^{-\frac{1}{2}}$
	250	.93	1.08	1.04
	300	1.1	.903	.95
	350	1.53	.655	.81
	400	2.33	.43	.655

APPENDIX V

Material	$1/T^{\circ}K \times 10^{-3}$	$\log_{10} \dot{\varepsilon}$	σ	$\log_{10} \sinh \alpha\sigma$
A	1.745	0	87.1	1.341
		.63	93	1.456
		.8	96.2	1.51
		1	97	1.53
		2	99.3	1.578
B		.258	78.3	1.134
		.279	79.3	1.178
		.682	81.4	1.197
		.752	82	1.236
		1.003	85.6	1.248
		1.85	91.4	1.416
		2.145	91.8	1.42
		.22	75.6	1.063
		.08	77.7	1.13
		.44	78.6	1.154
		.5	81.5	1.203
		1	87	1.261
		1.92	90.1	1.34
J	1.61	.641	103.7	1.66
		.749	105	1.68
		.978	105	1.683
		1.045	105.3	1.683
		2.05	114	1.853
		2.11	116	1.9
Al-Mg-Zn	1.67	.5	106.5	1.74
		.63	106.5	1.74
		.67	108	1.77

Material	$1/T^{\circ}K \times 10^{-3}$	$\log_{10} \dot{\varepsilon}$	σ	$\log_{10} \sinh \alpha\sigma$
		.64	108	1.77
		.63	109.5	1.79
		.8	110.7	1.8
		.87	116	1.852
		.97	116.4	1.852
		.98	117.5	1.88
		1.03	118.1	1.89
B	2.36	.752	139.9	2.34
	2.11		119	1.95
	1.905		100	1.59
	1.745		82	1.24
	1.61		77.2	1.16
	1.486		69.1	.857
			62.6	.72
Al-Mn	1.38	1.05	88.2	1.389
	1.486		100	1.58
	1.61		110	1.77
	1.75		118.7	1.94
Al-Mg-Zn	1.486	.64	88.8	1.39
	1.53		99.7	1.58
	1.63		109.2	1.76
	1.67		114	1.854

APPENDIX VI

Material	Prf Stress	$D^{-\frac{1}{2}}$	Material	Prf Stress	$D^{-\frac{1}{2}}$
	57.5	1.16	Al-Mn	176	1.01
	57.5	1.12		174	.91
	57.5	1.09		173	1.06
	69	1.05		142	1.15
	80	1.08		132	1.06
	91	1.05		139	1.01
	91	.98		141	.90
	94	1.025		170	1.04
	112.5	1		134	.96
	130	.93		178	1
	141	.93		127.5	.94
	141	.91		162	.86
				175	1.02
Al-Fe	184	1.15		164	1.09
	180	1.2		175	.91
	188	1.1		168	1.15
	202	1.22		145	1.12
	188	1.05			
	188	1.05	B	142.7	1.16
	134.4	.801		115.3	1.04
	136	.786		97	.95
	166	.909		88.6	.81
	149	.84		76.2	.66
	155	.81		100	.98
				112.5	1.01
Al-Mg-Zn	214	.632		94	1.01
	235	.707		91	.92

Material	Prf Stress	$D^{-\frac{1}{2}}$	Material	Prf Stress	$D^{-\frac{1}{2}}$ D
	224	.67		141	1.15
	232	.7		89.3	.84
A	137	1.2	A	103	.91
	127	1.15		89.6	.815

APPENDIX VII

P/C*	P/C*	P/C*	P/C*	P
90.51	240.5	116.8	200.6	8.2
107.75	298.6	164.9	235.2	16.4
125.7	309.1	200.2	292.3	24.6
143.65	320.6	233.6	359	32.8
161.7	343.7	260	406	41
174.1	346.3	280.4	454.7	49.2
188.6	384.8	306.7	507.9	57.4
205.6	405.8	350.5	556.9	65.6
221.3	424.4	359.5	613.9	73.8
235.7	503.5	467.4	655.9	82.0
254			707.8	90.2
271.5			806.1	106.6
288.5			897.5	123
320.3	577.1	549.8		164
DUST	Al-Mn	Al-Fe	coarse	

Cold Compaction

Coarse	slope = 6.18	$^1/_{ab}$ = 148.6
Dust	slope = 1.98	$^1/_{ab}$ = 76.4
Al-Mn	slope = 2.05	$^1/_{ab}$ = 249.4
Al-Fe	slope = 2.16	$^1/_{ab}$ = 136.9

APPENDIX VIII

Particle dimensions 250A°, 500A°

$$b = 2.8 \times 10^{-7} \text{ mm}$$

D_{Af}	(0.2%) (R.T.)	(0.2%) (400°C)
9.63×10^{-4}cm	80.1 MNm^{-2}	27 MNm^{-2}
8.61×10^{-4}cm	91.2 MNm^{-2}	29.7 MNm^{-2}
7.86×10^{-4}cm	94 MNm^{-2}	27.5 MNm^{-2}
7.28×10^{-4}cm	95.8 MNm^{-2}	27.5 MNm^{-2}
6.09×10^{-4}cm	100.6 MNm^{-2}	33.5 MNm^{-2}
5.34×10^{-4}cm	106.9 MNm^{-2}	35.2 MNm^{-2}
4.41×10^{-4}cm	129.5 MNm^{-2}	45.4 MNm^{-2}

Pressure - Temperature

Pressure	ln P	T°K
260 MNm^{-2}	5.561	423
268 MNm^{-2}	5.511	423
240 MNm^{-2}	5.48	473
250 MNm^{-2}	5.52	473
220 MNm^{-2}	5.394	523
200 MNm^{-2}	5.3	573
210 MNm^{-2}	5.347	573
185 MNm^{-2}	5.22	573
185 MNm^{-2}	5.22	623
175 MNm^{-2}	5.165	653
170 MNm^{-2}	5.136	693
165 MNm^{-2}	5.106	723

Powder	Particle Size	Extrusion Ratio	Ram Speed mm sec^{-1}	Initial Billet Temperature °C	Extrusion Pressure MNm^{-2}	Hv	Mechanical Properties					
							Room Temperature			400°C		
							0.2% Proof Stress MNm^{-2}	Tensile Stress MNm^{-2}	Elongation %	0.2% Proof Stress MNm^{-2}	Tensile Stress MNm^{-2}	Elongation %
A		40	7.62	300	721.8	49.6	120.5	156.8	23.1	45.7	57.3	14.3
		30	8.38	250	887.9	51.0	136.7	164.6	20.7	48.9	59.5	9.1
		30	7.77	200	978.7	53.7	139.4	178.3	20.8	45.4	56.4	8.3
		10	7.77	300	553.6	50.2	120.4	157.2	22.7			
		30	7.77	300	697.5	50.9	120.6	158.5	22.2	45.4	58.7	16.6
		20	7.77	300	695.3	50.7	128.3	160.2	21.8	54.3	67.2	10
		30	7.6	360	531	43.9	76.1	133	29			
		20	11.1	250	789.9	53.1	134.2	168.9	19.9	48.6	58.9	14.8
		10	10.36	250	679.5	55.7	134.2	169.3	17.4			
		50	3.25	300	762	53.2	122.7	164.9	22.4	45.4	57.4	10.5
		50	3.25	250	910	54.4	142.7	174.9	21	47.5	58.3	9.7
		40	2.03	300	834	54.4	136.3	174.1	22.4	47.1	56.9	10.1
		30	13.4	300	759	50	120.9	165	25.4	47.6	54.4	14
		30	8.76	360	683.9	47.5	106.4	161	30	45.7	53.8	21
		30	9	380	616.3	45	105.6	160.4	31.2	45.4	52.3	22.4
		30	9	420	530.2	45	95.5	154.3	31.1	45.7	52.2	23.2
		30	9.15	450	490.5	44.7	89.6	154.2	31.4	44.3	52.7	14.1

		30	7.77	370	692.7	48				43	46.2	23
		30	7.77	410	541.3	47.6	97.5	160.1	32	40.3	45.6	22.8
		30	7.77	400	532.4	46.5	103.8	158.3	31	45.6	53.5	22.7
		30	5.26	400	558.9	47.5	105	158.9	32	40.4	44.2	23.2
		30	8.27	400	534.6	39.9	77.8	143	31.6	40.3	51.2	22.1
		30	33.5	355	500	41.7	83	150	28.3			
		30	53	350	522.9	42.1	89	139	29.2	58.4	64.5	22.4
		30	9.7	350	479.5	41.2	79.5	130	17.6	40.4	50.7	32.1
		30	110	320	655.3	44.8	85	152.3	26.5	41.9	57.1	27.6
		30	96.3	300	664.1	50.7	140	173	22	57.1	106.2	35.2
B		30	73.2	300	655.3	40.7	98.5	133.8	28	39.7	51.2	22.2
A		30	.85	300	636.1	39.0						
A		30	.61	300	631	39.0						
B		30	.73	300	622.2	40.5						
A		30	3.91	200	964	52.8	138.8	169.8	20.9			
		30	5.92	240	921	52.2	134.6	168.4	20.6			
		30	5.92	280	813	48.7	131.2	164.7	20.2			
		30	7.48	300	728	46.4	122.7	167.8	22.2			
		30	5.92	310	635	46.2	124.6	163.2	22.9			
		30	7.62	320	588	46.5	124.4	160.2	24.8			
		30	3.91	340	578.5	46.0	113.3	143.3	24.7			
		10	5.26	285	541.6	45.5	136.4	158.2	23.4			
		20	4.24	380	443	39.8	98.6	126.5	34.5			
		30	5.92	300	713	48.7	115	175.8	30.2			

B		30	5.36	150	971.9	48.4	137.3	168.7	16.9	29	38.4	17.1
		30	6.71	150	931.1	48.5	142.7	154	20.6	29.5	37.4	12.8
		30	5.16	203	827.7	45.7	131.1	166.7	22.7			
		30	7.62	200	801.6	46.8	128.6	144.8	17.8	29.4	38.4	15.5
		30	5.26	250	659.2	45.6	113.3	158.2	26.3	30.5	37.5	19.2
		30	7.9	250	659.8	45.6	117.3	139.9	23.4	29.8	42.7	20
		30	5.26	277	611.5	40.9	103.1	139.7	28.1	30.2	35.9	23.2
		30	3.91	295	580	42	95.1	131.1	27.8			
		30	6.48	297	596.2	40.6	97	135.4	29.9	30.8	36.2	21.2
		30	7.77	300	564.6	41.7	93.3	129.6	28.4	29.8	39.9	20.7
		30	5.36	350	528.5	37.7	88.6	131.9	35.3	31.7	37.8	26
		30	4.24	370	443	37.8	88.6	126.5	34.5			
		30	7.77	380	441.3	37.4	90	130	30	25.9	31.1	21
		30	7.81	380	440.2	37.5	87.5	134.7	30.6	25.7	30.2	22
		30	7.77	400	438	37.5	78.1	135.1	34.8	25.3	30.6	25.6
		30	7.77	400	423.6	37.7	75.3	132.1	34.2	25.2	30.9	27.5
		30	7.81	450	419	37.2	69	132	35.2	25.5	29.6	34
		30	1.24	285	543.4	40.1	95.6	135.3	29.8	28.1	35.4	17.5
		30	2.54	305	552.8	41.3	98.5	135	27.9	25.6	29.1	22
		30	3.91	295	580	42	95.1	131.1	27.8			
		30	5.26	277	611.5	40.9	103.1	139.7	28.1	30.2	35.9	23.2
		30	6.48	297	596.2	40.6	97	135.4	29.9	30.8	36.2	21.2
		30	7.77	300	564.6	41.7	93.3	129.6	28.4	29.8	39.9	20.7
		30	13.57	289	614.1	41.5	103.3	132.3	25.9	30.5	35.6	19.7

		30	13.57	306	563.7	41.6	98.6	132.4	28.3	32.9	39.4	22.3
		30	13.57	279	681.4	41.6	98.6	134.8	27.3	30.2	35.6	23.6
		30	2.48	290	669.6	41.5	103.2	134.8	25.3	30.2	37.4	19.8
		40	2.49	297	543.8	40.9	87.5	129	28.7			
		40	5.44	285	567	40.1	87.3	133.4	28.6	26.8	34	19.3
		40	7.87	300	648.8	42.6	103.8	136.4	28.8	27.2	34.1	20.2
		40	11	293	749.1	40.7	104.4	142.2	27.4	26.2	34	18.3
B		5	6.8	300	407.4	38.8	105.9	115.1	4			
		10	7.77	304	527	42.3	102.3	128.5	21.9	29.8	36	18.4
		20	5.16	271	565.7	40.7	89.5	143.9	30.8	31.1	33.3	21.4
		20	7.93	305	584.6	41.8	101.7	126.7	24	28.6	35.3	17.4
		30	6.48	297	596.2	40.6	97	135.4	29.9	30.8	36.2	21.2
		30	7.77	302	564.6	41.7	93.3	129.6	28.4	29.8	39.9	20.7
		40	5.44	285	627	40.8	87.3	133.4	28.6	28.8	34	19.3
		40	7.87	300	648.8	42.6	103.8	136.4	28.8	29.2	34.1	20.2
		50	5.45	300	688	40.7	100.4	138.5	27.5			
		50	5.45	300	662	42.4	98.6	139.2	30.2	30.6	35.6	18.8
	430	30	5.36	300	443	29.5	56.9	88.2	39.7	16.5	23.2	37.8
	310	30	5.28	300	460.6	32.6	68.8	104.4	35.4	22.2	28.8	36.4
	200	30	5.44	300	504.2	36.1	80.1	119.4	30.4	27.0	33.6	31.6
	120	30	5.22	301	497.8	38.5	86.3	124.4	29.3	29.7	37.8	32.2
	120	30	8.72	288	594	38.5	95.5	136.7	28.1			
	90	30	6.15	280	561.3	40.2	98	136.9	27.9			
	90	30	5.36	301	519.8	39.3	90	136	28.8	27.5	30.8	22.6

	69	30	5.54	290	578.8	40.9	95.8	137.6	28.8	27.3	29.7	23.7
	69	30	5.83	310	522.2	41.1	95	134.2	27.1	26.2	31.6	19.6
	58	30	5.26	280	563.5	41.6	95.8	144.1	29.0	35.4	39.3	22.6
	58	30	5.26	280	681.4	41.4	100.6	147	26.7	31.1	36.1	17.1
	49	30	5.26	270	605	43.2	104.8	152.5	26.5			
	49	30	5.26	300	648.2	43.4	106.9	157.7	26.1	33.8	37.8	18.8
	25	30	8.76	287	698.9	44.6	129.5	168.4	26.1			
	25	30	5.36	300	664	44.3	129.1	169	26.5	42.1	45.2	13.9
	22	30	7.77	300	697.5	46.5	125.3	166	24.4			
	22	30	7.48	300	728	46.4	122.7	167.8	22.2	45.4	57.4	14.3
		30	8.7	350	503	31.0	53.7	102.3	35.1			
C		30	7.54	400	428	33.2	59.9	117	34.6	24.3	27.6	31.4
		30	7.65	400	353	33.9	61.9	122	37.3	22.3	26.6	27.6
		30	8.92	360	430.2	34.1	76.6	121	37.8	24.9	30.4	30.1
		30	8.67	350	467.7	34.9	76.3	122.1	34.3	24.3	29.6	30
		30	10.62	450	386.1	33.4	62.2	188.7	37.7	21.5	26.5	32.4
		30	7.91	340	447.9	34.6	77.8	122.4	34.3	21.7	28.7	28.8
		40	7.77	300	675.1	37.6	96	118.4	26.9	27.3	35.9	26.1
		30	7.8	300	604.5	38.7	94.5	123.7	30.5	27.4	36	32.4
		20	7.77	300	556	38.2	95.3	122.4	33.1	29.8	40.7	30.4
		40	7.89	250	827.4		118.5	132.3	23.5			
		40	10.4	300	600	38.1	92.8	121	31.9	27.4	37.9	33.6
		50	3.25	300	611	39.5	102.5	131.9	28.4	31.9	42.2	25.6
		5	0.6	300	375	38.8	89.1	121	29.9			

	5	4.23	300	390.5	39.1	89.4	122.5	18.2			
	5	9.83	300	395	39						
	5	24.4	300	417	38.8	84.5	118.3	27.5			
	5	6.63	300	397.1	38.5						
	5	6.63	300	639.8	38.7						
	30	11.75	290	496.4	35	79.3	123.4	34.4	22.5	28.6	28
	30	11.87	260	628.8	38.1	100	131.5	32.6			
	30	12.1	250	622.2	37.9	98.4	130.8	29.4			
	30	11.7	220	699.4	39.4	109.6	134.5	28.8			
	30	10.67	300	511	34.1	78.8	122.2	34.2	22.3	28.5	24.1
5wt%As	30	18.2	300	589	30.71	70.6	89.3	13	23.2	26.3	24.2
10wt%As	30	13.7	300	574	32.8	68.4	79.6	8.58	16.2	20.07	15.6
5wt%As	30	18.8	300	624	27.28	60.9	86.3	20.6	13	16.6	30
10wt%As	30	19.0	300	547	28.4						
5wt%SiO_2	30	12.42	300	755	29.2	58.4	105.4	30.9	22.9	25.6	41-300°C
Commercial	30	5.86	300	504.8	28.7	61.7	84.3	46.4	6.4	9.9	112
Commercial	30	10.36	300	523.3	28.6	50.9	78.9	51.1	5.79	10.1	116
5wt%Al_2O_3	30	10.67	300	616.2	33.2	78.3	108.2	29.7			
10wt%Al_2O_3	30	5.16	300	727	32.5	75.6	94.6	15.7	11.9	19.4	24.4
Commercial	30	7.39	300	551.1	26.3	53.4	78.3	49	6.38	9.57	100
Commercial	30	6.48	300	511.5	26.6	46.01	80.1	52.2	5.97	10.7	105
14.6cm	30	6.63	200	101.7							
7.35cm	30	6.63	200	787.6							

	200	30	6.1	345	848	66.9	176	233.6	23			
	200	30	6.1	336	906.8	71.2	177.2	232.2	25.4	61.4	70.6	30.4
J	200	30	8.22	346	820.7	66.3	142.3	210.5	27.8	56.8	67.5	31
	120	30	7	338	880.3	68.9	173.3	227.8	30.4	63	72.2	31.2
	120	30	8.24	336	865	66.4	140	208.3	26.9	60.3	70	31.4
	120	30	8.21	345	841	67.2	143.2	211.3	25.5	57.1	68.2	31
	120	30	7.3	343	881.8	63.5	132	193	20	52.2	63.8	31
	90	30	7.05	343	915.6	71.8	173.6	224.8	27	56.5	67.3	29.6
	90	30	8.24	355	861	68.1	141	202	24	54	63.8	45
	69	30	7.08	343	928.8	70	173.3	224.8	27.2	56.5	67.3	29.6
	59	30	6.12	345	970.8	72.0	174.7	235.2	24.7	63.8	74.3	28.1
	27	30	6.1	345	860.5	70.7	179	228.7	22.6	66.5	73.8	19.3
	27	30	8.24	325	880.3	75.8	179	232.4	22.6	66	73.8	22.1
		5	5.45	300	730.3	76.2	227	289	19.2			
		10	5.48	300	882.5	74.5	227	285	19.6			
		10	0.1	270	948.7	81	250.3	335.2	10.3			
		20	10.5	300	911	72.1	187.7	254.9	21.6			
		20	14.1	300	110.0	73.2	146.1	211.4	23.6			
		30	6.1	300	997.2	74.1	188.6	242.8	22.4	66.8	74.4	30.4
		30	11.8	330	862.7	66.8	168	182.8	23.6	61.4	73.2	29.1
		40	5.18	335	1021.5	74.8	163.2	230	23.8	64.4	71.3	28
		40	9.14	330	1028.1	71.4	164	228	26.3	72.2	82.7	24.5
		50	10.4	410	816.3	67.4	162	216	27.2	50.7	67.8	26.8

		50	14.9	430	772.2	65.7	153.2	205.8	28	61.4	73.2	42
		30	5.8	345	852.6	64.1	149	232	24.6			
		30	7.01	345	830.3	62.1	135.3	198.4	30.8	43.6	57.7	33.3
		30	4.93	345	826.6	72.6	144.8	227.6	28	61.4	70.7	22.7
		30	13.7	350	804.6	67.4	135	209.6	28.8	58.3	70.8	23.9
		30	158.5	350	823.7	63.7	133.7	200.6	27	44.2	60.2	28.1
		30	12.8	350	839	68.2	136.6	193.4	28.2	63.8	70.2	22.8
		30	12.8	350	900	66.8	141.5	208.3	24.2	55.3	67.5	30.1
		30	8.5	375	816.3	61.5	124.4	192.5	31.8	32.6	44.5	26
		30	11.9	375	762.7	56.8	148	182.8	23.6	38.1	47.9	25
		30	5.48	375	796.5	61	125.9	185	28.8	42.4	53.2	28
		30	12.8	375	807.5	61.5	127.5	187.2	27.4	43.1	57.2	41.6
		30	6.09	375	796.5	59.5	126	184.1	30.4	36.8	49.2	36.8
		30	11.9	400	741.3	60	115	192.8	31.4	46.1	56.4	26.2
		30	12.8	400	710.4	61.4	113.5	190	30.8	61.3	73.7	33.4
K	200	30	4.9	300	955	73.3	207	332	14.7			
	200	30	4.87	300	100.8	89	212	344	-	18.7	21.6	
	200	30	4.27	300	883	83.8	219	304	16.3	24.6	28.5	
	200	30	9.75	300	106.7	89	214	310	12.3	18.7	22.6	21
	200	30	95.1	300	108.1		EXTRUDE DISINTEGRATED					
	120	30	10.7	300	977	77.3	210	308	15.8	27.6	35.6	10.9
	120	30	5.48	300	102.2	85	220	329	10			
	120	30	4.87	300	992	87.4	216	334	10	11.7	14.6	20.9

	90	30	4.85	300	995	85.2	212	345		12.9	15.1	12.8
	90	30	4.87	300	945.8	86.2	212	360	15.6	28.5	32.9	6
	90	30	5.48	300	959.7	94	217	406	14.8	11.9	14.4	31.1
	69	30	10.7	300	103.9	77.9	197	301	9.3	63.3	82.5	13
	59	30	4.88	300	984	94.6	224	387	-	13.8	19.2	16
	27	30	10.7	300	102.1	87	225	388	11.1			
	27	30	4.87	300	992.8	96.8	223	418	11.8			
		5	2.82	300	690.6	95	251.9	407.3	12.4			
		10	0.88	300	728.1	97	248.8	410.4	16.8			
		10	9.14	300	743.6	96	234.8	398.6	19.6			
		20	0.61	300	904.6	109	252	437	10.2	38.7	54.1	40
		20	4.85	300	894.3	98.2	247.8	402.2	12.4			
		30	2.7	300	984	94.7	223	404	14.1	19.7	23.9	12
		30	.305	300	944	105	303	435	22.2	25.2	32.5	9.2
		30	5.5	300	990.6	94.9	214	413	-	19.9	25.7	13.6
		30	0.67	300	944.3	95.8	273	434	21.2	10.8	17.5	17.4
		30	0.49	325	973	108	304	439	22.8	11.6	19.3	30
		40	5.48	330	977.4	96.6	216	410	13.1	25.8	29.8	-
		40	9.14	370	944.3	109	199	328	13.7	22.3	32.3	19
		40	6.4	320	959.7	95	217	403	14.3	23.1	27.6	12
		50	8.5	375	921.1	95						
		30	3.66	335	934	98.8	228	412	13.4	21.1	27.1	-
		30	7.01	335	904.6	95.6	205	408	14.8	23	31.3	21.4

		30	6.1	335	940	94.3	214	415	14.4	22.3	30.2	-
		30	5.79	335	864	95.2	199	382.5	14	22.7	27.6	13.5
		30	6.1	335	925	96.3	209	399	13.5	22.1	28.4	11.8
		30	5.48	345	911.2	95	214	419	13.8	19.5	24.6	12.4
		30	5.48	350	875.9	97	211	413	14.3	22.6	28.2	12.6
		30	9.15	350	891.3	95	213	418	13.7	14.3	17.5	14.4
		30	7.92	360	904.6	98.2	213	409	15.3	16.9	20.9	10.6
		30	11.7	380	787.6	95.6	186	354.5	15.6	20	23.4	15.2
L	120	30	9.75	300	1041	81.4	183	263	19.2	66.5	91.9	20
	90	30	6.9	300	1056	78.6	184	250	19.3	67.8	92.3	23
	69	30	6.9	300	1068	86.8	180	276	19.3	66.9	91	14.3
	53	30	9.2	300	931	82.7	188	281	19.3	67.9	91.7	16.4
	27	30	8.55	300	1092	84.0	206	288	14	69.2	92.3	15
		30	9.15	300	1019	81.1	188	276	16.6	68.1	92.3	24
		20	9.76	300	973	81.5	187.5	270.5	17.1	69.2	84.5	17
		30	9.45	300	998	81.5	188	276	17.1	67.9	91	20
		30	6.9	400	635	66.9	134.4	223	26.5	61.4	72.2	27
		30	5.5	400	655	66.7	136	229	23.1	61.5	73.7	26
		30	8.3	425	594	66.6	126.6	200	23.6	49.2	59.6	31.8
		30	1.1	360	777	70.7	146.1	222.3	23.2	61.4	73.7	22.3
		40	5.48	345	772	77.8	159.3	262.7	21.4	69.8	87	21.6
		50	10.4	380	816	74.2	155.4	244.7	24.4	58.3	85.6	28
B	0.68	30	5.48	297	566.8	40.4	95.5	139.1	26.9	29.6	36.6	22.4
	0.77	30	6.45	300	582.3	40.4	96.8	135.9	27.6	29.8	34	21.6

	0.82	30	6.45	299	597.8	40.8	96.7	136.5	29.7			
	0.87	30	6.48	297	596.2	40.6	97	135.4	29.9	30.8	36.2	21.2
	0.93	30	6.09	301	591.6	40.4	96.4	134.5	30.5			
	0.94	30	6.09	299	569.1	40.6	97	135.7	27.3	29.9	35.7	21.3

```
      PROGRAM UPPERB  (INPUT,OUTPUT,TAPE5=INPUT,TAPE6=OUTPUT)
C     PLANE STRAIN UPPER BOUND SOLUTION FOR EXTRUSION
C     PROGRAM CALCULATES VALUES OF X,OMEGA AND PHI BY ITERATION,AND ALSO
C     CALCULATES THE LOAD REQUIRED
C       B = HALF EXTRUSION WIDTH
C        D = HALF INITIAL WIDTH
C       OM = ANGLE OMEGA
C       PHI = ANGLE PHI
C       X = DEPTH OF PENETRATION
C      E.R  = EXTRUSION RATIO
C
       B=0.0
       EOM= 0.0
       EPHI =0.0
       C1=0.0
       C2=0.0
       C3=0.
       C4=0.0
       A1=0.0
       A2=0.0
       A=0.0
       D=0.0
       OM =0.0
       PHI=0.0
       ALOAD =0.0
       X=0.0
       N =0
       J =0
       ER =0.0
       DIF2 =0.0
       DIF1 =0.0
       R2OM =0.0
       R1PHI =0.0
       R2PHI =0.0
       R1OM =0.0
     1 READ (5,100) B,D,OM,PHI,J
   100 FORMAT (4(F10.4) I1)
       IF(J.EQ.9) GO TO 10
       WRITE(6,99) B,D,OM,PHI
    99 FORMAT(1H1,5X,2HB=,F10.4,5X,2HD=,F10.4,5X,3HOM=,F10.4,5X,4HPHI=,F
      60.4//)
       A = D-B
C   CONVERT OMEGA AND PHI TO RADIANS
       R1OM = OM/57.29578
       R1PHI = PHI/57.29578
C   CALCULATE X
     8 A1 = A**2/(1.0+((A/B)*(SIN(R1OM))**2))
       B1 = B*A/(1.0+((A/B)*(SIN(R1PHI))**2))
C   WRITE OUT A1 AND B1
       WRITE(6,105) A1,B1
   105 FORMAT(5X,3HA1=,F10.4,5X,3HB1=,F10.4)
       X = SQRT(A1+B1)
       N=N+1
C   CALCULATE AND WRITE OUT NEW ANGLES
       EOM =(4.0*A*A)/((D+A)*X)
       EPHI =(4.0*B)/(3.0*X)
       R2OM = ATAN(EOM)
       R2PHI = ATAN(EPHI)
       WRITE(6,101) R2OM,R2PHI,EOM,EPHI
```

```
  101 FORMAT(5X,6HOMEGA=,F10.4,5X,4HPHI=,F10.4,5X,4HEOM=,F10.4,5X,5HEPHI
     6=,F10.4)
      DIF1= SQRT((57.29578*(R1OM-R2OM))**2)
      DIF2= SQRT((57.29578*(R1PHI-R2PHI))**2)
C  WRITE OUT DIF1,DIF2 AND X FOR CHECK ON ITERATION
      WRITE(6,102) DIF1,DIF2,X
  102 FORMAT(5X,5HDIF1=,F10.4,5X,5HDIF2=,F10.4,5X,2HX=,F10.4)
      IF(DIF1.LT.0.5.AND.DIF2.LT.0.1) GO TO 9
      IF(N.EQ.20) GOTO 9
      R1OM = R2OM
      R1PHI = R2PHI
      GO TO 8
C  CALCULATE LOAD/K USING VALUES OF X,OMEGA,AND PHI
    9 C1 = (2.0*A**2)/(X*(SIN(R2OM))**2)
      C2 = (2.0*A*B)/(X*(SIN(R2PHI))**2)
      C3 = (3.0*A)/TAN(R2OM)
      C4 = (3.0*A)/TAN(R2PHI)
      WRITE(6,106)C1,C2,C3,C4
  106 FORMAT(5X,3HC1=,F10.4,5X,3HC2=,F10.4,5X,3HC3=,F10.4,5X,3HC4=,F10.4
     6///)
      ALOAD = (2.0*X)+((2.0*A*X)/B)+C1+C2-C3-C4
C  CONVERT ANGLES TO DEGREES
      OM = R2OM*57.29578
      PHI = R2PHI*57.29578
C  WRITE OUT RESULTS FOR EACH EXTRUSION RATIO
      ER = D/B
      WRITE (6,103)A,B,D ,ER,X,OM,PHI,ALOAD
  103 FORMAT(1H0,25X,87H**********************************************
     1**********************************/26X,1H*,85X,1H*/26X,1H*,4X
     2,2HA=,F10.4,5X,2HB=,F10.4,5X,2HD=,F10.4,5X,16HEXTRUSION RATIO=,F10
     3.4,4X,1H*/26X,1H*,85X,1H*/26X,1H*,85X,1H*/26X,1H*,4X,2HX=,F10.4,5X
     4,3HOM=,F10.4,4X,4HPHI=,F10.4,13X,7HALOAD=K,F10.4,3X,1H*/26X,1H*,85
     5X,1H*/26X,87H**********************************************
     6**********************************)
      GO TO 1
C  IF IT WORKS YOU SHOULD ARRIVE HERE IF NOT GIVE UP
   10 STOP
      END
```

THE EXTRUSION OF ATOMIZED ALUMINIUM POWDERS*

T. Sheppard† and P. J. M. Chare†

More than a hundred experiments have been performed to investigate the extrusion mechanism involved and the effect of process variables on the structure, substructure, and mechanical properties of the extrude when processing atomized aluminium powder of varying mesh size. It is demonstrated that extrusion pressure is largely independent of the final properties and that the ductility of the extrude may be controlled by the process variables. A mechanism that agrees with experimental observations is suggested to explain the extrusion mechanics. Transmission and scanning electron microscopy results also support the theses presented.

THE production of metal parts from aluminium powders has been hindered in the past to a considerable extent by the high cost of SAP powders. The advances made in atomization of metal powders has overcome this main obstacle, though it is clear that because the Al_2O_3 content of these powders is somewhat lower than that of the original SAP the tensile properties of the final product are correspondingly less.

A convenient process which ensures that powder compacts form a homogeneous solid product is extrusion, which can combine high- or low-temperature working with large reductions in area. Thus, sintering can, in general, be eliminated from the production sequence. The resultant material consists of an aluminium matrix, dispersion-strengthened by very fine Al_2O_3 particles. Most of the work published so far has been concerned with the extrusion of SAP-type powders and usually the influence of process variables has been ignored.

In recent work by Hansen,[1,2] atomized powder was blended with a fine oxide powder to yield a dispersion-strengthened material possessing high tensile properties. The process variables were, however, only superficially investigated and the experiments appear to have been limited in number. The majority were conducted at 500°C (773 K) using an extrusion ratio of 15:1, but no details were reported of the extrusion process and the control achievable during the process. It should be noted that container surface conditions and temperature as well as die

* Manuscript received 29 December 1971.
† Metallurgy Department, Imperial College of Science and Technology, London.

lubrication can have important effects on both the surface quality and the mechanical properties of the extrude. In addition, the preparation technique has usually involved hot pressing before extrusion, which of course has important connotations when considering the economics of production.

This paper reports the results of well over a hundred experiments, conducted under completely reproducible conditions.

Experimental

Material

Two different batches of atomized aluminium powder were used, one a −300 mesh powder and the other having a mesh size as shown in Table I.

TABLE I

Size, μm	Wt.-%	Wt.-% Al_2O_3
+105	9·7	0·55
−105+75	23·4	0·65
− 75+63	12·6	1·1
− 63+53	21·5	1·3
− 53+45	11	1·8
−45	21·8	1·9

The surface area of each powder was determined by a BET[3] analysis and the natural oxide content was obtained by a standard wet analysis and difference technique. This involved establishing the Al content by reducing a suitable volume of $Fe_2(SO_4)_3$ in sulphuric acid solution under a CO_2 atmosphere and determining the Al by permanganometric titration of Fe. The samples were checked for Cu, Mg, Mn, and Si impurities and the Al_2O_3 content obtained by difference. The results are shown in Table II for powders A–B.

TABLE II

Powder	BET Valve, m^2/g	Wt.-% Al_2O_3
Aluminium A, −53 μm	0·333	1·9
Aluminium B	0·168	1·1

To investigate the effect of particle size, powder B was sieved into various mesh fractions (the same as those listed in Table I) and these used as the raw powder for the extrusion process. The mesh fractions

shown in Table I were then converted to a mean mesh size. This careful characterization of powders ensured that the starting material was completely uniform and reproducible—a factor overlooked by many previous workers.

Preparation for Extrusion

The only preparation required was to compact the powder mass to 85% theoretical density before extrusion.

Extrusion

Extrusion was performed on a 5 MN (500 tonf) extrusion press having a nominal 76 mm (3 in) container. The innermost sleeve of the compound container was removable so that a close check could be kept on surface condition and the sleeve replaced if necessary. The dies used were square edged and reduction ratios of 5, 10, 20, 30, 40, and 50 were investigated. Billets for extrusion up to 300°C (573 K) initial temperature could be heated *in situ* by 12 kW heaters situated on the periphery of the container. Temperatures in excess of this were achieved by air-heating the billets in a furnace situated adjacent to the press and transferring them to the heated container. The extrusion speed, which governs the prevailing strain rate, was controlled at low speeds by contraflow direct pumping and at high speeds by accumulator drive.

Thus, the initial temperature could be controlled closely and the important variables (reduction ratio, initial billet temperature, and strain rate) studied comprehensively.

The hydraulic press is equipped with a strain-gauge load-cell and May indicator, also Penny and Giles speed and displacement transducers, which are connected to both digital and X–Y recorders. Load displacement and speed records were therefore obtained for each experiment.

Lubrication

Initial experiments indicated that die pick-up was leading to a very pronounced fir-tree surface defect. This is illustrated in Fig. 1, which also shows the remedial effect achieved by inserting a small aluminium pad on the die face before extrusion.

Preparation of Specimens for Mechanical Testing and Microscopy

There occurs a progressive change in the structure and mechanical properties along the extruded length; therefore, to ensure a degree of uniformity during testings, the specimens were taken from the same

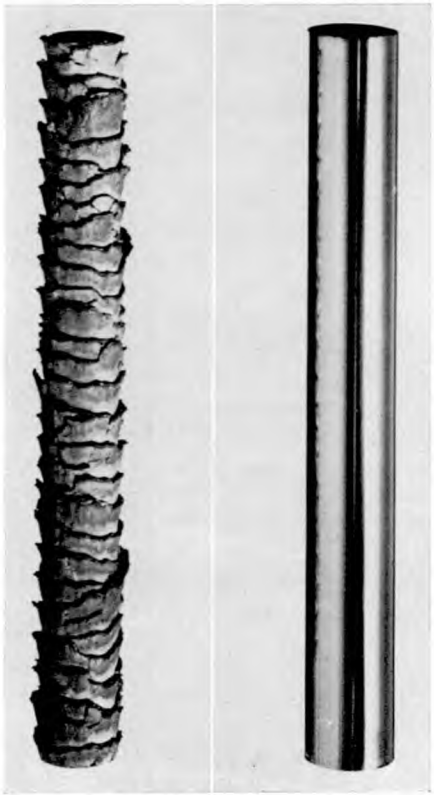

(*a*) (*b*)

FIG. 1. Example of the effect of inserting a small aluminium pad on the die face before extrusion. (*a*) Billet extruded without a pad; (*b*) billet extruded with a pad.

position in each rod. This applied to specimens selected for hardness, electron microscopy, and tensile testing, which were cut from adjacent regions of the product.

For electron microscopy, longitudinal and transverse thin sheets were cut, and then thinned using a window technique by polishing in 20% $HClO_4$, 80% CH_3OH at 21 V, −30°C (243 K). The specimens were examined in an AEI EM6G 100 kV electron microscope equipped with a tilting stage.

Tensile tests were carried out at room temperature and at 400°C (673 K) on extruded rod machined to a standard Hounsfield specimen

size (No. 14). The tests were performed on an Instron tensile-testing machine equipped with a Haddow split furnace for the high-temperature tests.

Macrohardness tests were made on a standard Vickers machine using a 2 kg load. Specimens for hardness testing were prepared by electrolytic polishing and etching and measurements were made on transverse sections at ~1 mm intervals.

Results and Discussion

The results of the experiments conducted are shown in Tables III–VIII.

Load/Displacement Diagrams

A typical output trace from the X–Y recorder is shown in Fig. 2. The diagram can be divided clearly into two regions, the compaction zone and the normal extrusion zone.

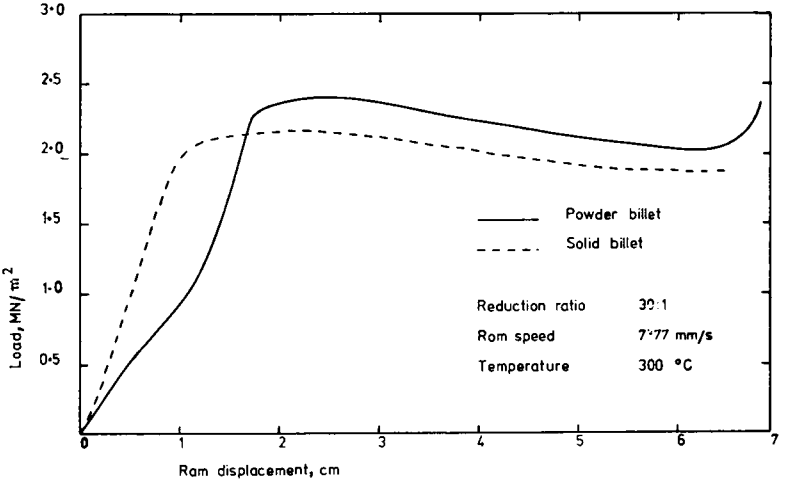

FIG. 2. Load/ram displacement diagram.

In the compaction zone, there is a non-linear increase in load until the billet attains 100% density. This was checked by stopping the extrusion at this point and measuring the density. The loads recorded at

TABLE III

Powder	Extrusion Ratio	Ram Speed, mm/s	Initial Billet Temp., °C	Extrusion Pressure, MN/m²	Hardness, HV	Mechanical Properties					
						Room Temp.			400°C		
						0·2% Proof Stress, MN/m²	Tensile Stress, MN/m²	Elongation, %	0·2% Proof Stress, MN/m²	Tensile Stress, MN/m²	Elongation, %
B	5	6·8	300	407·4	38·8	105·9	115·1	4	—	—	—
	10	7·77	304	527	42·3	102·3	128·5	21·9	29·8	36	18·4
	20	5·16	271	565·7	40·7	89·5	143·9	30·8	31·1	33·3	21·4
	20	7·93	305	584·6	41·8	101·7	126·7	24	28·6	35·3	17·4
	30	6·48	297	596·2	40·6	97	135·4	29·9	30·8	36·2	21·2
	30	7·77	302	564·6	41·7	93·3	129·6	28·4	29·8	39·9	20·7
	40	5·44	285	627	40·8	87·3	133·4	28·6	28·8	34	19·3
	40	7·87	300	648·8	42·6	103·8	136·4	28·8	29·2	34·1	20·2
	50	5·45	300	688	40·7	100·4	138·5	27·5	—	—	—
	50	5·45	300	662	42·4						
B	10	5·26	285	541·6	45·5	136·4	158·2	23·4			
	10	7·77	287	553·6	45·8	130·4	156·8	22·9			
	20	7·77	300	695·3	46·3	127·3	157·5	22·8	44·3	57·2	10
	30	7.77	297	697·5	46·5	125·3	160·7	24·4	45·4	58·5	18·6
	40	7·62	297	721·8	46·5	119·8	153·6	22·1	45·7	55·4	13·4

TABLE IV

Powder	Extrusion Ratio	Ram Speed, mm/s	Initial Billet Temp., °C	Extrusion Pressure, MN/m²	Hardness, HV	Mechanical Properties					
						Room Temp.			400°C		
						0·2% Proof Stress, MN/m²	Tensile Stress, MN/m²	Elongation, %	0·2% Proof Stress, MN/m²	Tensile Stress, MN/m²	Elongation, %
B	30	5·36	150	971·9	48·4	137·3	168·7	16·9	29	38·4	17·1
	30	6·71	150	921·1	48·5	142·7	154	20·6	29·5	37·4	12·8
	30	5·16	203	827·7	45·7	131·1	166·7	22·7	—	—	—
	30	7·62	200	801·6	46·8	128·6	144·8	17·8	29·4	38·4	15·5
	30	5·26	250	659·2	45·6	113·3	158·2	26·3	30·5	37·5	19·2
	30	7·9	250	659·8	45·6	117·3	139·9	23·4	29·8	42·7	20
	30	5·26	277	611·5	40·9	103·1	139·7	28·1	30·2	35·9	23·2
	30	3·91	295	580	42	95·1	131·1	27·8	—	—	—
	30	6·48	297	596·2	40·6	97	135·4	29·9	30·8	36·2	21·2
	30	7·77	300	564·6	41·7	93·3	129·6	28·4	29·8	39·9	20·7
	30	5·36	350	528·5	37·7	88·6	131·9	35·3	31·7	37·8	26
	30	4·24	370	443	37·8	88·6	126·5	34·5	—	—	—
	30	7·77	382	441	37·5	—	—	—	—	—	—

TABLE V

Powder	Extrusion Ratio	Ram Speed, mm/s	Initial Billet Temp., °C	Extrusion Pressure, MN/m^2	Hardness, HV	Mechanical Properties					
						Room Temp.			400°C		
						0·2% Proof Stress, MN/m^2	Tensile Stress, MN/m^2	Elongation, %	0·2% Proof Stress, MN/m^2	Tensile Stress, MN/m^2	Elongation, %
A	30	3·91	200	964	52·8	138·8	169·8	20·9			
	30	7·77	200	978·7	53·7	139·4	178·3	20·8	48·1	61	8·6
	30	5·92	240	921	52·2	134·6	168·4	20·6			
	30	8·38	250	887·9	51	136·8	164·6	20·6	47·9	59·5	7·4
	30	5·92	280	813	48·7	131·2	164·7	20·2			
	30	7·77	297	697·5	46·5	127·3	157·5	22·8	45·4	58·5	18·6
	30	7·48	300	728	46·4	122·7	167·8	22·2			
	30	5·92	310	635	46·2	124·6	163·2	22·9			
	30	7·62	320	588	46·5	124·4	160·2	24·8			
	30	3·91	340	578·5	46	113·3	143·3	24·7			

TABLE VI

Powder	Extrusion Ratio	Ram Speed, mm/s	Initial Billet Temp., °C	Extrusion Pressure, MN/m²	Hardness, HV	Mechanical Properties					
						Room Temp.			400°C		
						0·2% Proof Stress, MN/m²	Tensile Stress, MN/m²	Elongation, %	0·2% Proof Stress, MN/m²	Tensile Stress, MN/m²	Elongation, %
B	30	1·24	285	543·4	40·1	95·6	135·3	29·8	28·1	35·4	17·5
	30	2·54	305	552·8	41·3	98·5	135	27·9	25·6	29·1	22
	30	3·91	295	580	42	95·1	131·1	27·8			
	30	5·26	277	611·5	40·9	103·1	139·7	28·1	30·2	35·9	23·2
	30	6·48	297	596·2	40·6	97	135·4	29·9	30·8	36·2	21·2
	30	7·77	300	564·6	41·7	93·3	129·6	28·4	29·8	39·9	20·7
	30	13·57	289	614·1	41·5	103·3	132·3	25·9	30·5	35·6	19·7
	30	13·57	306	563·7	41·6	98·6	132·4	28·3	32·9	39·4	22·3
	30	13·57	279	681·4	41·6	98·6	134·8	27·3	30·2	35·6	23·6
	30	248	290	669·6	41·5	103·2	124·8	25·3	30·2	37·4	19·8
	40	2·49	297	543·8	40·9	87·5	129	28·7	—	—	—
	40	5·44	285	567	40·1	87·3	133·4	28·6	26·8	34	19·3
	40	7·87	300	648·8	42·6	103·8	136·4	28·8	27·2	34·1	20·2
	40	11	293	749·1	40·7	104·4	142·2	27·4	26·2	34	18·3

TABLE VII

Mean Particle Size, μm	Extrusion Ratio	Ram Speed, mm/s	Initial Billet Temp., °C	Extrusion Pressure, MN/m²	Hardness, HV	Mechanical Properties					
						Room Temp.			400°C		
						0·2% Proof Stress, MN/m²	Tensile Stress, MN/m²	Elongation, %	0·2% Proof Stress, MN/m²	Tensile Stress, MN/m²	Elongation, %
430	30	5·36	300	443	29·5	56·9	88·2	39·7	16·5	23·2	37·8
310	30	5·28	300	460·6	32·6	68·8	104·4	35·4	22·2	28·8	36·4
200	30	5·44	300	504·2	36·1	80·1	119·4	30·4	27·0	33·6	31·6
120	30	5·22	301	497·8	38·5	86·3	124·4	29·3	29·7	37·8	32·2
120	30	8·72	288	594	38·5	95·5	136·7	28·1	—	—	—
90	30	6·15	280	561·3	40·2	98	136·9	27·9	—	—	—
90	30	5·36	301	519·8	39·3	90	136	28·8	27·5	30·8	22·6
69	30	5·54	290	578·8	40·9	95·8	137·6	28·8	27·3	29·7	23·7
69	30	5·83	310	522·2	41·1	95	134·2	27·1	26·2	31·6	19·6
58	30	5·26	280	563·5	41·6	95·8	144·1	29·0	35·4	39·3	22·6
58	30	5·26	280	681·4	41·4	100·6	147	26·7	31·1	36·1	17·1
49	30	5·26	270	605	43·2	104·8	152·5	26·5	—	—	—
49	30	5·26	300	648·2	43·4	106·9	157·7	26·1	33·8	37·8	18·8
25	30	8·76	287	698·9	44·6	129·5	168·4	26·1	—	—	—
25	30	5·36	300	664	44·3	129·1	169	26·5	42·1	45·2	13·9
22	30	7·77	300	697·5	46·5	125·3	166	24·4	—	—	—
22	30	7·48	300	728	46·4	122·7	167·8	22·2	—	—	—

TABLE VIII

Initial Relative Density	Extrusion Ratio	Ram Speed, mm/s	Initial Billet Temp., °C	Extrusion Pressure, MN/m²	Hardness, HV	Mechanical Properties					
						Room Temp.			400°C		
						0·2% Proof Stress, MN/m²	Tensile Stress, MN/m²	Elongation, %	0·2% Proof Stress, MN/m²	Tensile Stress, MN/m²	Elongation, %
0·68	30	5·48	297	566·8	40·4	95·5	139·1	26·9	29·6	36·6	22·4
0·77	30	6·45	300	582·3	40·4	96·8	135·9	27·6	29·8	34	21·6
0·82	30	6·45	299	597·8	40·8	96·7	136·5	29·7			
0·87	30	6·48	297	596·2	40·6	97	153·4	29·9	30·8	36·2	21·2
0·93	30	6·09	301	591·6	40·4	96·4	134·5	30·5			
0·94	30	6·09	299	569·1	40·6	97	135·7	27·3	29·9	35·7	21·3

100% theoretical density are shown in Fig. 3, from which it is seen that the pressure appears to be a linear function of log time. Thus, we may write

$$p = 315 - 250 \log T$$

Although the pressure required for maximum density would appear to be an important parameter in all hot-pressing operations, this is, to the authors' knowledge, the first time a pressure/temperature relationship has been expressed in this form.

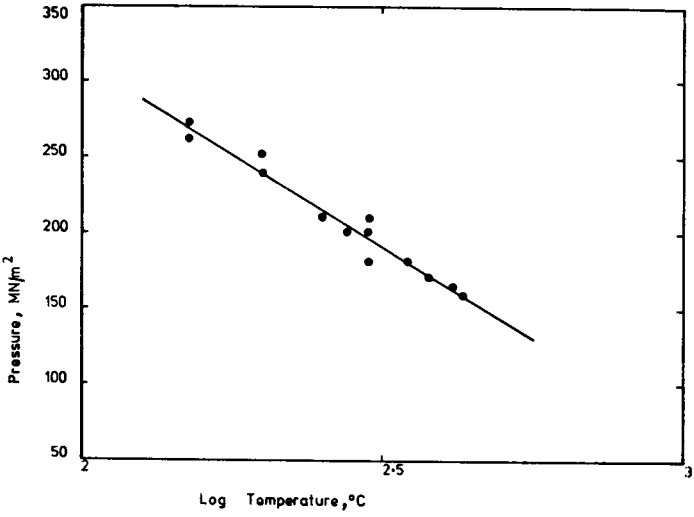

FIG. 3. Compaction pressure as a function of temperature.

Extrusion Load

The maximum load during extrusion is somewhat higher than that recorded when extruding a comparable commercially pure solid billet. It is, however, only some 10% higher, whereas the yield stress of the product may be three times that of the commercial material at an equivalent temperature.

It is thus evident that conventional theories predicting extrusion pressure do not hold for the powder process. The total extrusion pressure will still consist of three components, viz:

(*a*) The homogeneous work of deformation representing the least work required to produce deformation.
(*b*) The redundant work.
(*c*) The work against friction.

It is clear, however, that both the redundant work and the homogeneous term will no longer be properties of the product but will be dependent on both the final properties and the powder properties. This may best be illustrated by referring to an idealized upper-bound solution for plane-strain extrusion. Although the same mathematical analysis does not apply in axisymmetric extrusion, the fundamental principles are not altered. Fig. 4 shows an upper-bound solution of the

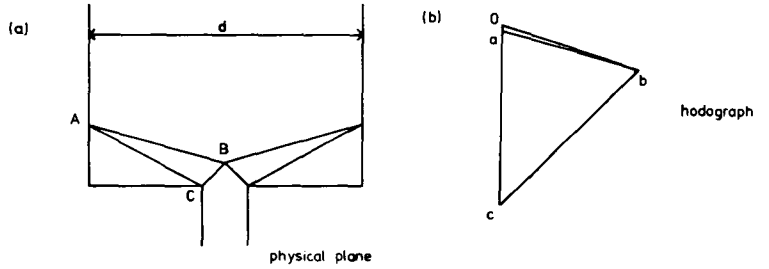

FIG. 4. Simple upper-bound solution for a 30 : 1 reduction ratio. (*a*) Physical plane; (*b*) hodograph.

type obtained by Johnson[4] and supported experimentally by Sheppard and Raybould.[5] The principle of an upper-bound solution is that the extruding material is assumed to consist of a number of rigid blocks of uniform quasi-static zones, bordered by velocity discontinuities. Thus, referring to Fig. 4(*a*), material approaching the velocity discontinuity AB at velocity u_{0a} is forced to move parallel to the dead zone boundary throughout the region ABC. On encountering the discontinuity BC, the material then leaves the extrusion chamber at velocity u_{0c}. It is possible that the diagram could be refined by the addition of further discontinuities. From this diagram a hodograph (Fig. 4(*b*)) can be constructed, which must be kinematically admissible. An upper-bound solution giving the pressure required for homogeneous deformation and redundant work can be obtained by considering the work done at each discontinuity. Thus

$$pd = k_{\text{initial}}\, ab\, AB + k_{\text{final}}\, bc\, BC$$

It is evident that the reason for the lower extrusion pressure is that the yield stress of the material varies considerably in the quasi-static deformation zone. At the first discontinuity the yield stress k_{initial} will be low because the *modus operandi* will be a shearing of the newly formed welds in the powder compact. k_{initial} will therefore be more closely connected with powder properties than with the final material properties. On the other hand, at the discontinuity BC the compact should

have acquired the properties of the final material and one can expect that k_{final} will be related closely to the yield stress of the extrude. Nevertheless, the material does not behave in this discontinuous manner and the process actually occurring is one of continuous breaking and rewelding of the particle contacts. This gradually redistributes the oxide and with each successive breaking increment the process becomes more difficult until the material reaches BC, where the deformation is by shear only as in the conventional extrusion process.

Fig. 5 shows for powder B extruded at 300°C (573 K) that the ex-

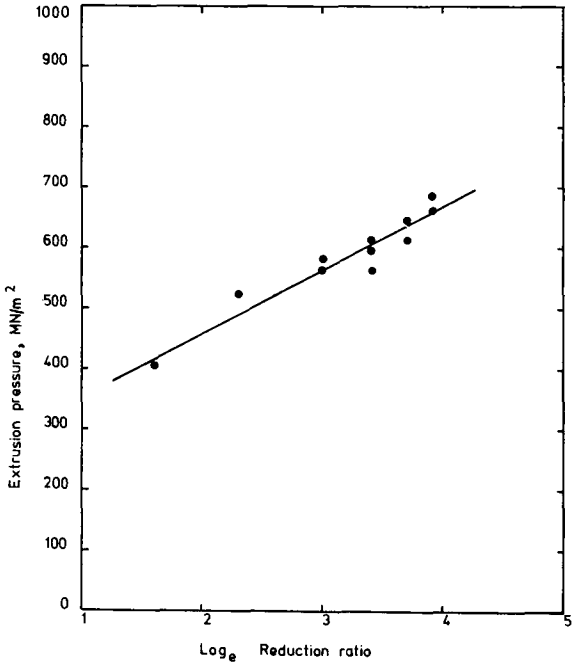

FIG. 5. Extrusion pressure as a function of reduction ratio.

trusion pressure is in fact still a function of ln R as in the conventional extrusion process. From this we may write

$$p = 160 + 70{\cdot}6 \ln R$$

It was also found that the extrusion pressure did not vary with the extrusion punch speed (i.e. strain rate). It is accepted that during conventional mechanical working there exists a relationship which shows that the yield stress of the material (and hence the extrusion

pressure) increases as the strain rate increases. This indicates that the final 'solid' properties must develop at the exit end of the quasi-static zone, for if they did not then the material would exhibit strain-rate-dependence. Table IX shows clearly that for powder B the minimal variation in extrusion pressure is within accepted experimental scatter.

TABLE IX

Powder	Ram Speed, mm/s	Extrusion Pressure, MN/m^2
B	1·24	543
	2·54	553
	5·26	612
	6·48	596
	7·77	565
	13·6	588
	248	602

Figs. 6 and 7 show that the extrusion pressure varies with the extrusion ratio and the extrusion temperature in much the same way as a conventional billet would behave. The main exception is that there is less increase of pressure with increase in extrusion ratio than one would expect. This is in agreement with the model proposed above. Fig. 8 shows that the extrusion pressure is much higher for small particles than for large ones, suggesting that far more redundant work is required. The larger surface area will result inevitably in the formation of a greater number of welds and consequently more work will be required to shear them during the 'powder-properties' phase of extrusion.

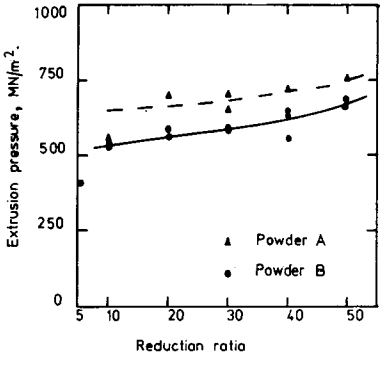

FIG. 6. Variation of extrusion pressure with reduction ratio.

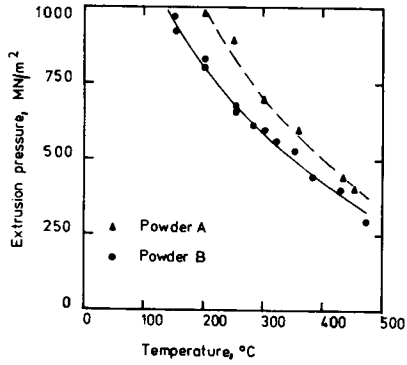

FIG. 7. Variation of extrusion pressure with temperature.

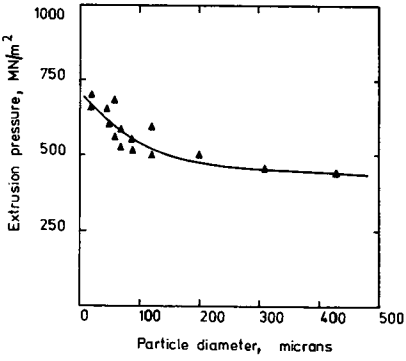

FIG. 8. Variation of extrusion pressure with mean particle dia.

Mechanical Properties of the Extrude

Fig. 9 shows the variation in yield strength at room temperature and 400°C (673 K) with mean particle dia. The results are in agreement with previous work[2,6–8] and show a considerable increase in proof stress and decrease in elongation (Fig. 10) when the particle dia. is decreased and, hence, the oxide content increased. These results were obtained for rods extruded at 300°C (573 K) and 30:1 reduction ratio.

The reduction ratio had little effect on the hardness, elongation, or proof stress (Table III). However, material extruded at a reduction ratio of 5:1 was found to be extremely brittle and a ratio of 10:1 was required for the powder to attain its maximum properties. Thus, it is

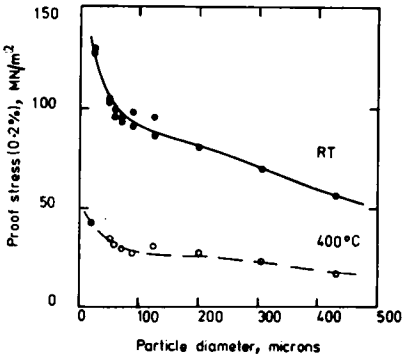

FIG. 9. Variation of proof stress (0·2%) with mean particle dia.

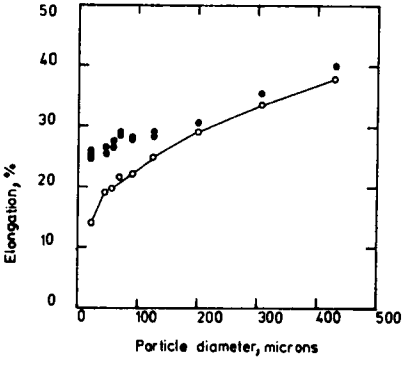

FIG. 10. Variation of elongation with mean particle dia.

clear that there is a transition reduction ratio below which it is impossible to develop full material properties. This ratio must be a function of the deformation zone, which is smaller and has fewer velocity discontinuities for lower reduction ratios. There will be a tendency, therefore, to prolong the 'powder-properties' region and shorten, or annihilate, the 'final-properties' extrusion zone.

Table VI indicates that the ram speed has little effect on the properties of the extrude. This may be an important observation and will be discussed later.

The initial billet temperature plays an important role in the development of final properties. The room-temperature proof stress falls

considerably with increase in the extrusion temperature as shown in Fig. 11, which indicates also that proof stress at 400°C (673 K) is un-

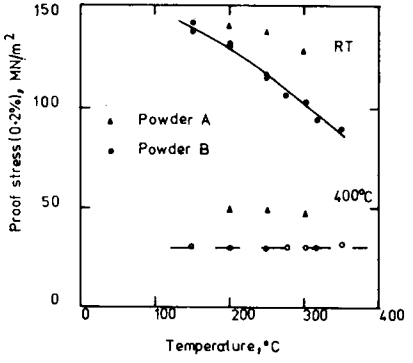

FIG. 11. Variation of proof stress (0·2%) with temperature.

affected by this parameter. This trend has been noted previously[2] and the explanation given was that the subgrain-strengthening was ineffective at 400°C. The elongation at room temperature and at 400°C can, however, be considerably improved by extrusion at higher temperatures (Fig. 12).

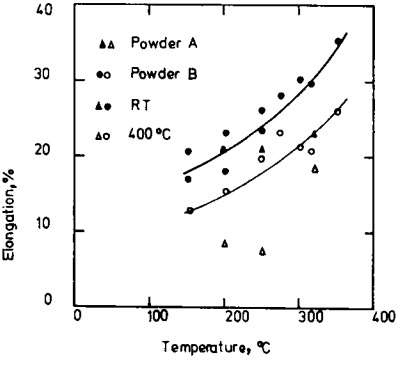

FIG. 12. Variation of elongation with temperature.

Fig. 13 shows a plot of proof stress vs. the square root of the particle dia. at room temperature and at 400°C. From these results it can be

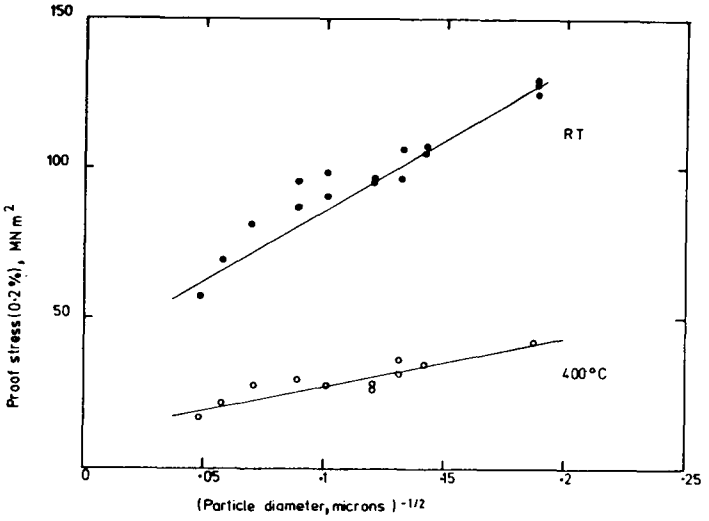

FIG. 13. Proof stress (0·2%) at room temperature and 400°C as a function of particle dia.

seen that there exists a linear relationship and one can write a Petch type equation

$$\sigma = (\sigma_0') + k_1\, dp^{-\frac{1}{2}} \text{ at } 400°C$$

and $$\sigma = (\sigma_0'') + k_2\, dp^{-\frac{1}{2}} \text{ at room temperature}$$

$$k_1 = 14 \qquad k_2 = 44{\cdot}5$$

$$\sigma_0' = 11 \qquad \sigma_0'' = 48$$

where σ_0 is the proof stress (0·2%).

The values for σ_0 were obtained by extrapolation.

Transmission Electron Microscopy

Figs. 14 and 15 show the results of scanning electron microscopy on the original grains and Figs. 16 and 17 show a typical microstructure obtained when extruding at 300°C. The discontinuous nature of the original oxide film resulting from the large thermal stresses on cooling is evident and it can also be seen that the individual particles have had insufficient time to acquire their minimum-energy spherical shape. During extrusion the original oxide envelope can be observed to have broken up and formed a skeleton around each elongated needle-like grain (i.e. A in Fig. 17). The apparent presence of oxide in the middle of grain A is most probably caused by debris from an adjacent grain due to the orientation selected during the thinning operation. Dynamic

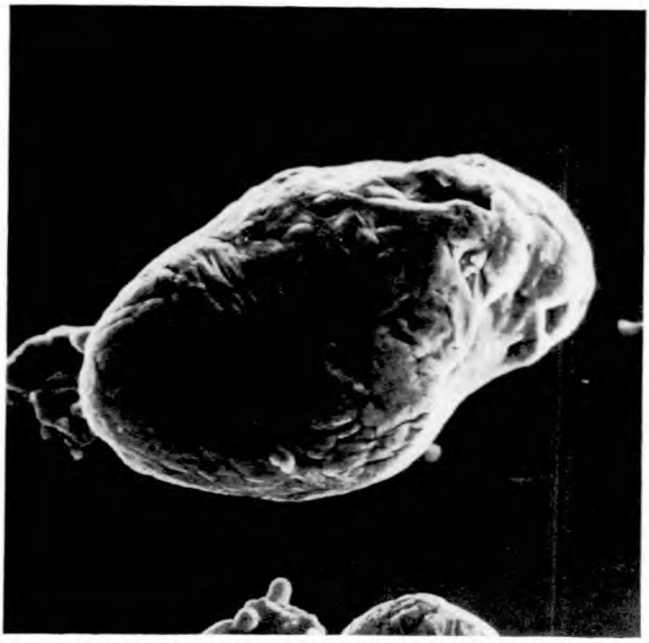

FIG. 14. An aluminium particle of powder A. × 1360.

recovery during extrusion[6,7,10] has occurred, as there is a predominance of subgrains in the structure. However, we can also identify dislocations that have clearly been pinned by the oxide particles. There is also evidence that some static recovery has occurred after the extrusion process (e.g. the forming of subgrains C and D in Fig. 17).

By comparing Figs. 16 and 17 one can clearly see that the effect of decreasing particle size is to thin the oxide skeleton obtained in the extrude. It is also evident that the final grain size is dependent almost entirely on the original powder mesh. In fact, in Fig. 17 the oxide film is only just visible. The transverse section shown in Fig. 18 confirms this cylinder type of deformation and illustrates again the pinning effect of the oxide.

It was found impossible to trace a significant number of dislocation tangles, even in those products extruded at room temperature. In fact, the only dislocations present are clearly those that have been pinned by stray oxide particles. The cold-work structures produced by cold rolling commercially pure aluminium (Fig. 19) differ significantly from those produced by extruding at 150°C (423 K) (Fig. 20). This absence

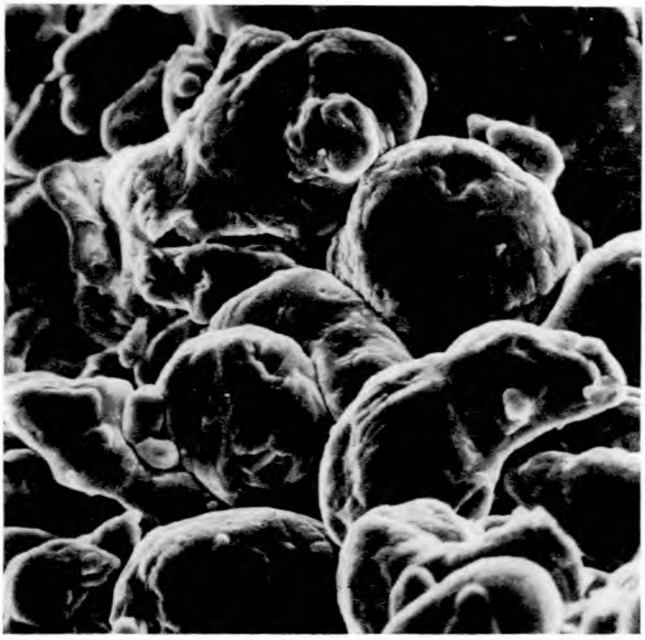

FIG. 15. Section of a cold compact of powder A. × 1825.

FIG. 16. Longitudinal section of an extruded rod manufactured from powder A. Initial billet temperature 300°C, extrusion ratio 30 : 1.

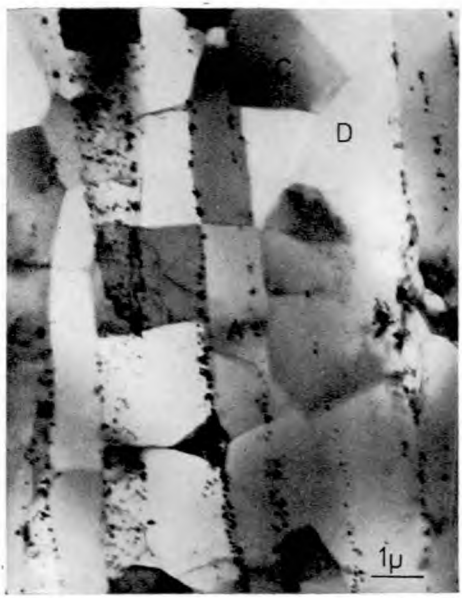

FIG. 17. Longitudinal section of an extruded rod manufactured from powder B. Initial billet temperature 300°C, extrusion ratio 30 : 1.

FIG. 18. Transverse section of an extruded rod manufactured from powder B. Initial billet temperature 300°C, extrusion ratio 30 : 1.

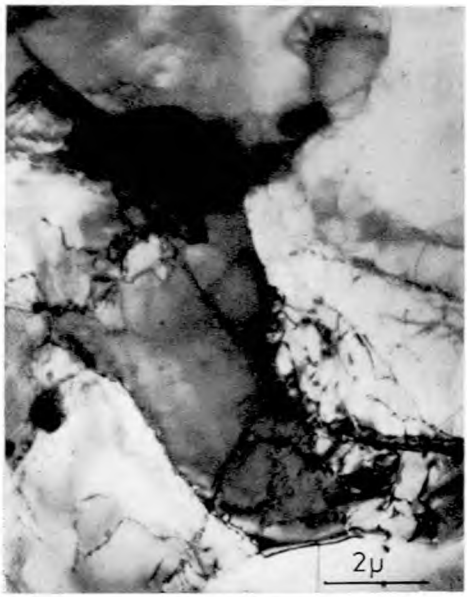

FIG. 19. Section of a cold-worked aluminium structure.

FIG. 20. Transverse section of an extruded rod manufactured from powder B. Initial billet temperature 150°C, extrusion ratio 30 : 1.

of dislocations occurs because of the differing nature of deformation in the two processes.

During powder extrusion, particles in intimate contact must first exhibit welding at the interface; the interface must then extend before theoretical density is reached. The welding must be accompanied by very high local temperatures; this effectively ensures that a powder compact cannot be cold worked in the accepted sense.

Conclusions

(1) The achievement of 100% density during the extrusion process is governed by the relationship

$$p = 314 - 247\ T \quad (T \text{ in } ^\circ\text{C})$$

(2) The deformation during extrusion of metal powders occurs in a quasi-static zone that may be divided into two merging regions--'powder properties' and 'final properties'.

(3) The law giving extrusion pressure required for aluminium powders may be written

$$p = 160 + 70{\cdot}6 \ln R$$

(4) The extrusion pressure required is much less than that for conventional properties and is also independent of strain rate.

(5) There is a transition extrusion ratio below which coherent material may not be obtained.

(6) Materials with a proof stress up to 3 times that of a conventionally produced material at room temperature may be produced by the extrusion process, simply and economically. At 400°C (673 K) this property becomes seven times as great. Elongation may be improved by extrusion at elevated (400–500°C, 673–773 K) temperatures.

(7) There is a relationship between original particle size and final proof stress given by:

$$\sigma = 48 + 44{\cdot}5\ dp^{-\frac{1}{2}} \text{ at room temperature}$$
$$\sigma = 11 + 14\ dp^{-\frac{1}{2}} \quad \text{at } 400^\circ\text{C}$$

(8) During extrusion, welding and rewelding represent a continuous process giving rise to high local temperatures and consequent dynamic recovery.

(9) The oxide skeleton surrounding the final grain structure varies with initial particle dia.; the smaller the particles the thinner is the consequent film.

The fact that the extrusion pressure is largely independent of final

properties has important connotations, especially for those alloys that are stiff and difficult to extrude. Coupled with the observation that extrusion pressure is independent of strain rate, this may well mean that extrudes of such alloys can compete with normal commercially produced solids. Thus, this represents a fertile area for research, which is at present being vigorously pursued at Imperial College.

References

1. N. Hansen, *Powder Met.*, 1967, **10**, 94.
2. N. Hansen, *ibid.*, 1969, **12**, 23.
3. S. Brunauer, P. Emmett, and E. Teller, *J. Amer. Chem. Soc.*, 1938, **60**, 309.
4. W. Johnson and P. B. Mellor, 'Plasticity for Mechanical Engineers'. **1962**: New York (Van Nostrand).
5. T. Sheppard and D. Raybould, to be published.
6. F. V. Lenel, *Trans. Met. Soc. AIME*, 1957, **209**, 124.
7. B. Eastwood and D. Robins, *Powder Met.*, 1966, **9**, 175.
8. C. D. Wiseman *et al.*, *Trans. Amer. Soc. Metals*, 1963, **56**, 717.
9. W. A. Wong, H. McQueen, and J. Jonas, *J. Inst. Metals*, 1967, **95**, 129.
10. R. Leguet, R. Whitwham, and J. Hérenguel, *Mém. Sci. Rev. Mét.*, 1962, **59**, 649.